



BRNO UNIVERSITY OF TECHNOLOGY

VYSOKÉ UČENÍ TECHNICKÉ V BRNĚ

FACULTY OF CHEMISTRY

FAKULTA CHEMICKÁ

**NANOTECHNOLOGY IN
MACROMOLECULAR CHEMISTRY:
POLYMER NANOCOMPOSITES**

HABILITATION THESIS IN THE FIELD MACROMOLECULAR CHEMISTRY

Ing. Milan Kráčalík, Ph.D.

Brno, 2023

Preface

This habilitation thesis summarizes the most important results of my scientific work in the field of polymer-clay nanocomposites. The research presented in this thesis was accomplished in collaboration with coworkers and colleagues as well as academic and industrial partners as indicated in the list of the publications included in this thesis.

I am very grateful to all my former colleagues at Institute of Macromolecular Chemistry, Czech Academy of Sciences and at Department Polymer Engineering and Science, Montanuniversität Leoben, for their contributions to the presented experimental work, their ideas, suggestions and discussions and the great atmosphere and spirit I experienced there.

I would like to thank to my current colleagues at Institute of Polymer Science, Johannes Kepler University Linz, to head of the institute - Prof.ⁱⁿ Sabine Hild, for their support, inputs and the discussions we had about the fundamental research approaches in physical, chemical and processing aspects of multiphase polymeric systems.

I would also like to thank all my bachelor, master and PhD students and guests from all the world I had the pleasure to work with, especially at Brno University of Technology and Tomas Bata University in Zlin for all their contributions and support and the fruitful discussions we had.

Finally, my thanks belong to my family, especially to my daughter Viktoria and stepdaughter Ema, who motivated me for my engagement in teaching young people.

Content

Preface.....	2
1. Introduction.....	5
1.1 Nanotechnology in polymer science.....	5
1.2 Polymer-clay nanocomposites.....	7
1.2.1 Montmorillonite.....	8
1.2.2 Intercalation by ion-exchange method.....	11
1.2.3 Exfoliation methods.....	16
1.3 Characterization of polymer nanocomposites.....	22
1.3.1 Off-line structural characterization.....	23
1.3.2 On-line & in-line structural characterization.....	27
1.4 Viscoelasticity of polymer nanocomposites.....	35
Résumé.....	42
References.....	43
2. Objectives of the conducted research.....	58
2.1 Preparation of polymer nanocomposites.....	58
2.1.1 Manuscript 1.....	58
2.1.2 Manuscript 2.....	66
2.1.3 Manuscript 3.....	79
2.1.6 Manuscript 4.....	89
2.1.7 Manuscript 5.....	97
2.2 Processing of polymer nanocomposites.....	104
2.2.1 Manuscript 6.....	104
2.2.2 Manuscript 7.....	112
2.2.3 Manuscript 8.....	122
2.2.4 Manuscript 9.....	130
2.2.5 Manuscript 10.....	137
2.3 Characterization of polymer nanocomposites.....	147
2.3.1 Manuscript 11.....	147
2.3.2 Manuscript 12.....	155
2.3.3 Manuscript 13.....	163

2.3.4 Manuscript 14	172
2.3.5 Manuscript 15	181
2.3.6 Manuscript 16	188
2.3.7 Manuscript 17	194
3. Summary.....	199

1. Introduction

1.1 Nanotechnology in polymer science

Nanotechnology is continuously expanded area of science, which contains the engineering of nanosized particles of different materials. It is the understanding and control of matter at the nanoscale, at dimensions between approximately 1 and 100 nanometers, where unique phenomena enable novel applications. Matter can exhibit unusual physical, chemical, and biological properties at the nanoscale, differing in important ways from the properties of bulk materials or individual single atoms and molecules. Some nanostructured materials are much stronger or have different magnetic, electric or insulating properties compared to other forms or sizes of the same material. They may become more chemically reactive, reflect light better, or change color as their size or structure is altered. Although modern nanoscience and nanotechnology are relatively new, nanoscaled materials have been already used for centuries. Gold and silver nanoparticles created colors in the stained-glass windows of churches hundreds of years ago (Figure 1). Nanotechnology comprises nanoscale science, engineering and technology in fields such as chemistry, biology, physics, materials science, and engineering. Nanotechnology research and development involves imaging, measuring, modeling, and manipulating matter in particular using special effects on surfaces and interfaces. [1]



Figure 1: stained-glass window [1]

In the polymer science and technology nanotechnology covers a broad range of topics. This includes microelectronics (which could now be referred to as nanoelectronics) as the critical dimension scale for modern devices is now below 100 nm. Other areas include polymer-based biomaterials, nanoparticle drug delivery, miniemulsion particles, fuel cell electrode polymer bound catalysts, layer-by-layer self-assembled polymer films, electrospun nanofibers, imprint lithography, polymer blends and nanocomposites. [2]

Polymer nanocomposite research covers a wide range of nanofillers such as layered silicates (clays), carbon nanotubes/nanofibers, colloidal oxides, double-layered hydroxides, quantum dots, nanocrystalline metals, etc. [3] The majority of the research conducted to date has been performed with layered silicates as this area emerged with the recognition that exfoliated clays could yield significant mechanical property advantages as a modification of macromolecular systems. The achieved results were at least initially viewed as unexpected (“nano-effect”) offering improved properties over that expected from continuum mechanics predictions. More recent results have, however, indicated that while the property profile is interesting, the clay-based nanocomposites often obey continuum mechanics predictions. However, there are situations where nanocomposites can exhibit properties not expected with larger scale particulate reinforcements. Especially for polymer-clay nanocomposites, the surface effects are responsible for significant improvement of barrier, mechanical and rheological properties, dimensional stability, heat, flame and oxidative resistance. In comparison with traditional fillers (20-40 wt. % loading), 2-5 wt. % filling of layered clays is sufficient to achieve analogous or even higher material improvement [2]. Typically, organoclays can replace talc or glass fillers at a 3:1 ratio. For example, 5% of an organoclay can replace 15–50 wt. % of a filler like calcium carbonate reducing material costs and improving mechanical properties. Due to relatively low price, as compared to other nanoparticles, organoclays are the most dominant commercial nanomaterial to prepare polymer nanocomposites, accounting for nearly 70% of the volume used. Applications include adsorbents, rheological control agents, paints, grease, cosmetics, personal care products, oil well drilling fluids, etc. Among the clay minerals, smectites, especially montmorillonite, have been extensively used to prepare organoclays because of its excellent properties, such as high cation exchange capacity, swelling behavior, adsorption properties and large surface area. [2]

1.2 Polymer-clay nanocomposites

In the broad field of nanotechnology, polymer matrix based nanocomposites have become an outstanding area of research and development in last decades.

Nanocomposites are filled polymers with particles, where at least one dimension is in the order of nanometers. The shape of particles used in nanocomposites can be spherical, cylindrical or laminar. Maximal reinforcement is achieved using laminar or cylindrical particles because the reinforcing efficiency is highly dependent on the aspect ratio (the largest dimension divided by the smallest dimension of the particle).

Conventional polymer composites are based on reinforcement of the polymer matrix by micrometer scaled particles. For example, isotactic polypropylene filled with talc, micro-ground calcium carbonate, wood powder, possibly with other suitable filler, or epoxy and polyester resins filled with mineral particles offer an advantageous combination of mechanical properties and price. However, polymeric materials reinforced by nanoscaled particles exhibit significantly higher performance (improvement in processing and application properties) already at low level of filler loading. This advantage comes from immobilisation of polymer chains in close contact with inorganic filler possessing a large surface area [2]. Using this development strategy, polymers can be improved keeping their lightweight and ductile feature. Addition of nanoscaled particles to a broad range of polymers results in significant improvement in their biodegradability. On the other hand, performance of biodegradable and bio-based polymers can be improved in order to increase their application potential [4–30].

Generally, polymer nanocomposites with high dispersion grade reveal significant enhancement of matrix properties: higher elastic modulus, tensile strength, lower gas and liquid permeability, reduced flammability, heat and impact resistance, flame retardancy, electrical conductivity and enhanced rheological properties (higher melt strength and viscosity, which are required for example in foams processing). Metal and ceramic nanoparticles open possibilities to develop unique magnetic, electronic, optical or catalytic properties [2, 31–150].

For example, uniaxial arrangement of inorganic platelets remarkably reduces gas and liquid permeability in perpendicular direction (Figure 2).

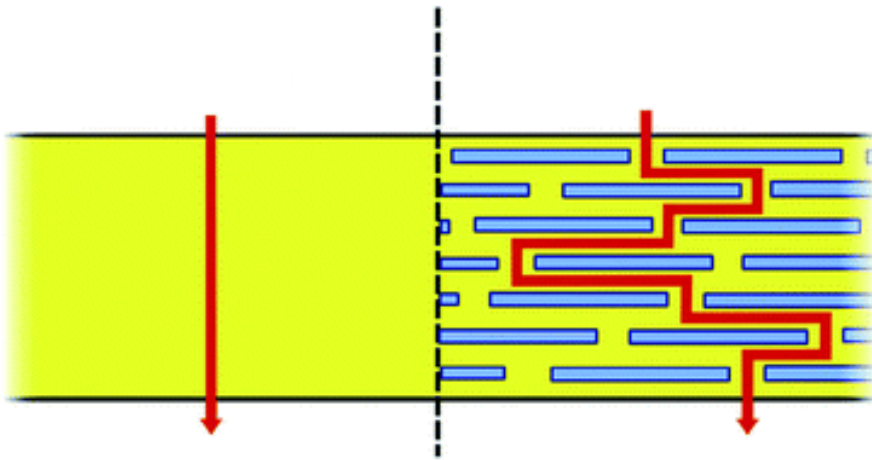


Figure 2: Scheme of liquid and gas permeability decrease [31]

Especially improvements in mechanical properties of nanocomposites can be used in automotive and general industrial applications. There is potential for utilization as mirror housing on different types of cars, door handles, engine covers, or belt covers. General applications include e.g. packaging, fuel cell, solar cell, fuel tank, plastic containers, impellers and blades for vacuum cleaners, power tool housing, or cover for portable electronic equipment like mobile phones and pagers [156].

1.2.1 Montmorillonite

For preparation of polymer nanocomposites, layered silicate clays (especially montmorillonite, MMT) have been the most used nanofillers hitherto due to the financial acceptability and opportunity to achieve aspect ratios ideally up to 1000 (by clay platelet thickness of 1 nm). High reinforcement by addition of the layered silicate clays results from their large active surface area (in the case of montmorillonite 700-800 m²/g) [157].

The structure of MMT agglomerates (tactoids) as well of one primary plate is shown in figure 3.

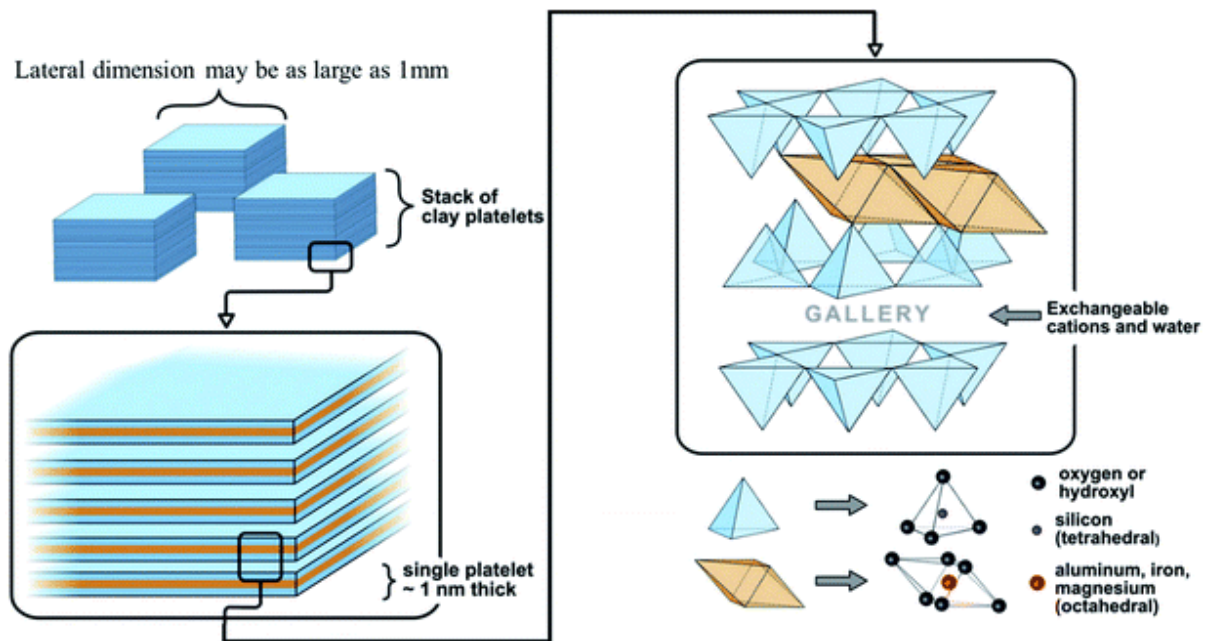


Figure 3: Structure of montmorillonite tactoid and single platelet [32]

MMT primary plate consists of two silica tetrahedral sheets and one aluminium octahedral sheet (Fig. 3, 4), forming one basic platelet. The binding force between the stacked platelets is based on Van Der Waals interactions, which relate to change in the interlayer distance depending on the humidity and the type of possible intercalating agent encountered within the interlayer distance of the clay. Its permanent negative charge is located mainly on the basal plane and the pH-dependent charge is located on the edge surfaces. At $\text{pH} < \text{p.z.c.}$ (the point of zero charge): (a) the positively charged edge surface of MMT may interact attractively with negatively charged basal planes of other particles; and (b) anions may be simultaneously adsorbed by the positively charged edge surface and excluded by the negatively charged basal plane. Therefore, in the mechanisms of anion reactions with clay minerals, surface charge neutralization, quasicrystal formation, and the special heterogeneity of anion exclusion and adsorption should be taken into account. MMT has to be purified and separated from a low-grade natural bentonite. Bentonite is an important impure clay, aluminium phyllosilicate adsorbent, usually contains montmorillonite with structure a gibbsite layer placed between silica layers to produce the structural unit (Fig. 4). The replacements are specially within the octahedral layer (Mg^{2+} , Fe^{2+}) and to a much lesser degree between the silicate layer ($\text{Al}^{3+}/\text{Si}^{4+}$). The constitution of the clay is mainly related to the hydroxyl-

aluminosilicate structure. The alliance between tetrahedral layers of silica and aluminosilicate octahedral sheets makes the crystal framework of clays. In their structure, Mg^{2+} or Fe^{2+} partly exchange Al^{3+} cations, and this replacement is followed by the inclusion of metals, such as Na, K, Mg, or Ca that give charge balance. The studied organoclays are different in the level of cation exchange capacity exchanged using organic counter ions [155].

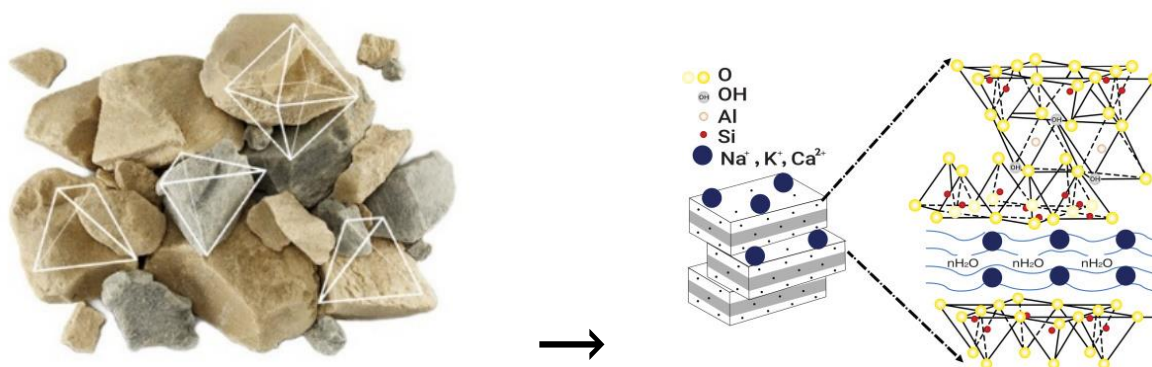


Figure 4: Bentonite mineral [154]

The XRD pattern of natural Na-bentonite is plotted in Fig. 5. It can be seen that the clay is composed primarily of montmorillonite, with the characteristic peaks at $d_{001} = 14.29 \text{ \AA}$ and $d_{020} = 4.49 \text{ \AA}$. The basal spacing, $d_{001} = 14.29 \text{ \AA}$, indicates a predominance of sodium which determines the sample mainly as sodium bentonite (Na-bentonite). The other peaks are impurities related to quartz and feldspar. [153]

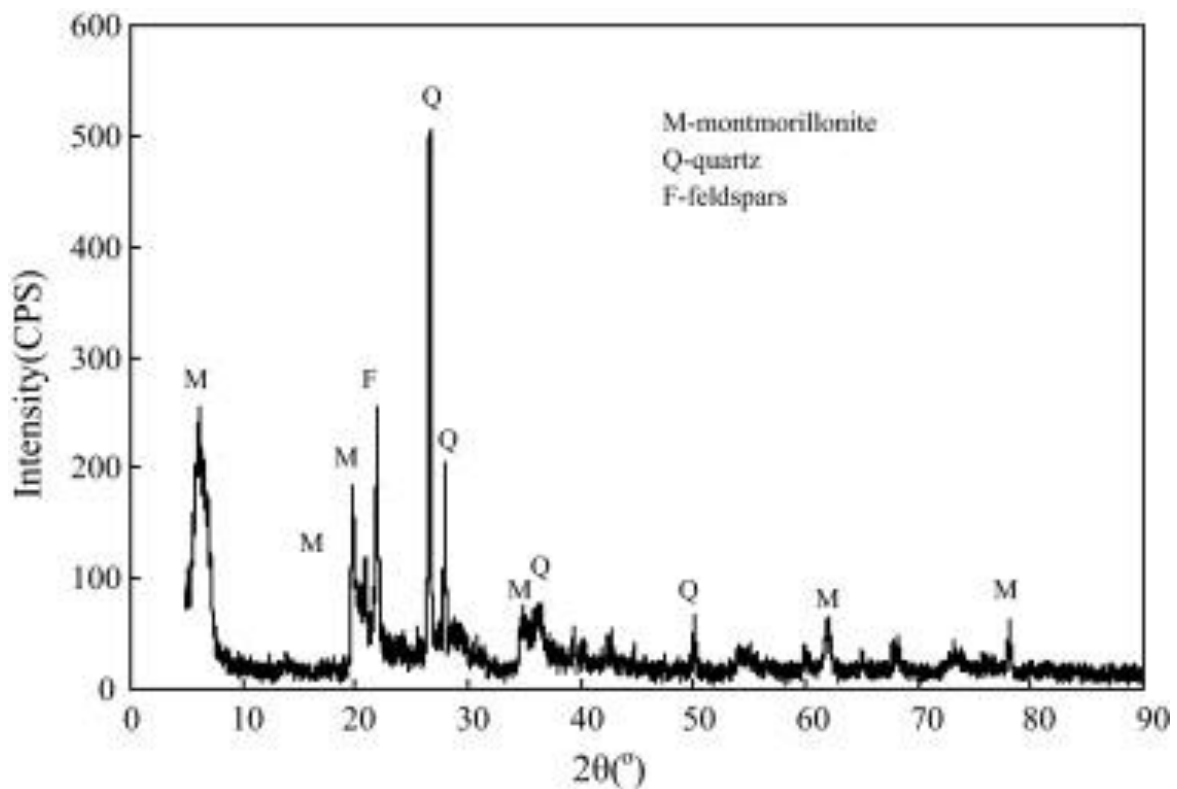


Figure 5: XRD pattern of natural Na-bentonite [153]

1.2.2 Intercalation by ion-exchange method

To achieve high dispersion level and good adhesion with a non-polar polymer, chemical modification (intercalation) of MMT is required. Intercalation of natural Na⁺ type of MMT by organophilic molecules (organophilisation) is usually based on the ion-exchange method (Figure 6), where the sodium cation is generally replaced by organic compound having long alkyl chain. Such organically modified MMT is usually referred to as organoclay.

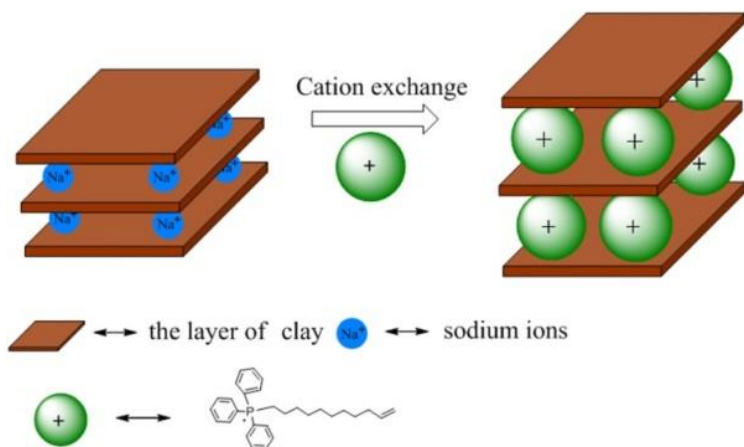


Figure 6: Ion-exchange method for organoclays [33]



Cloisite Na⁺

Cloisite 30B

Figure 7: TEM picture of natural clay (Cloisite Na⁺) and organoclay (Cloisite 30B) [152]

The main advantage of intercalation is increase in interlayer distance (basal spacing, d_{001}) of the clay (Fig. 6, 7). For this purpose, quaternary alkylammonium salts are the most used organic compounds to prepare organoclays. They are synthesized by complete alkylation of ammonia or amines. For practical and industrial uses, quaternary alkylammonium ions are preferred to primary alkylammonium ions because hydrolysis (alkylammonium/alkylamine equilibrium) is absent, and desorption of free alkylamine is strongly reduced. A further advantage is that the large amount of organic material (30–40%) reduces the density of the dispersed particles. Currently, there is a significant

amount of research on modification of clay minerals with several kinds of quaternary alkylammonium salts (bromides or chlorides) in laboratory scale. In the case of the organoclays for polymer nanocomposites the kind of quaternary alkylammonium salt influences the affinity between the clay mineral and the polymer. For apolar polymers as polypropylene and polyethylene the clay minerals are modified with dialkyl dimethylammonium halides, while for polar polymers as polyamide the clay minerals are modified with alkyl benzyl dimethylammonium halides or alkyl hydroxyethylammonium halides. [3] The most used commercial organoclays are listed in Tab 1. [172] Today, the producer of these organo-modified clays is BYK-Chemie Ltd, Wesel, Germany / POLYchem Ltd, Markt Allhau, Austria, respectively. There are sometimes other commercial names or numbering, coming from previous suppliers, US Southern Clay Products, Inc., Gonzales, TX (Cloisite series) or Süd-Chemie AG, Moosburg, Germany (Nanofil series), which have, however, identical chemistry variations as mentioned in Tab. 1.

Table 1: Characteristics of commercial organoclay fillers a

Organoclay	Organic modifier ^b	Modifier concentration [mequiv/100 clay]	g Moisture [%]	Weight loss on ignition [%]
Cloisite 6A	2M2HT	140	< 2	45
Cloisite 15A	2M2HT	125	< 2	43
Cloisite 20A	2M2HT	95	< 2	38
Cloisite 10A	2MBHT	125	< 2	39
Cloisite 25A	2MHTL8	95	< 2	34
Cloisite 30B	MT2EtOH	90	< 2	30

^a according to the manufacturer

^b quaternary ammonium chlorides: dialkyldimethyl- (2M2HT), alkyl(benzyl)dimethyl- (2MBHT), alkyl(2-ethylhexyl)dimethyl- (2MHTL8), alkylbis(2-hydroxyethyl)methyl- (MT2EtOH). Alkyls are a mixture of 65 % C18, 30 % C16 and 5 % C14, derived from hydrogenated tallow.

Results presented in this thesis confirmed improvement of processing properties by addition of commercial organoclays to recycled PET. Nevertheless, a problem occurred with the thermal stability of commercial organic modifiers (quaternary ammonium salts) leading to the matrix degradation during melt mixing. The low thermal stability of

commercial organoclays resulted in chemical decomposition by α , β elimination (Fig. 8) [172].

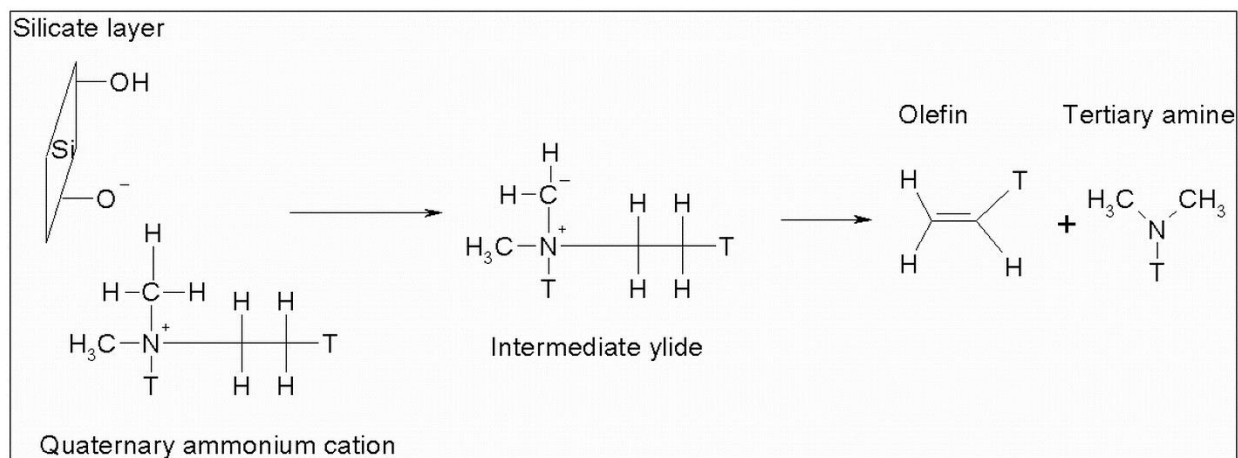


Figure 8: Chemical decomposition by α , β elimination

With a view to reduce degradation processes and to enhance delamination in the system, selected commercial organoclays were modified by silanization with [3-(glycidyloxy)propyl]trimethoxysilane, hexadecyltrimethoxysilane and (3-aminopropyl)trimethoxysilane (Fig. 9). [174]

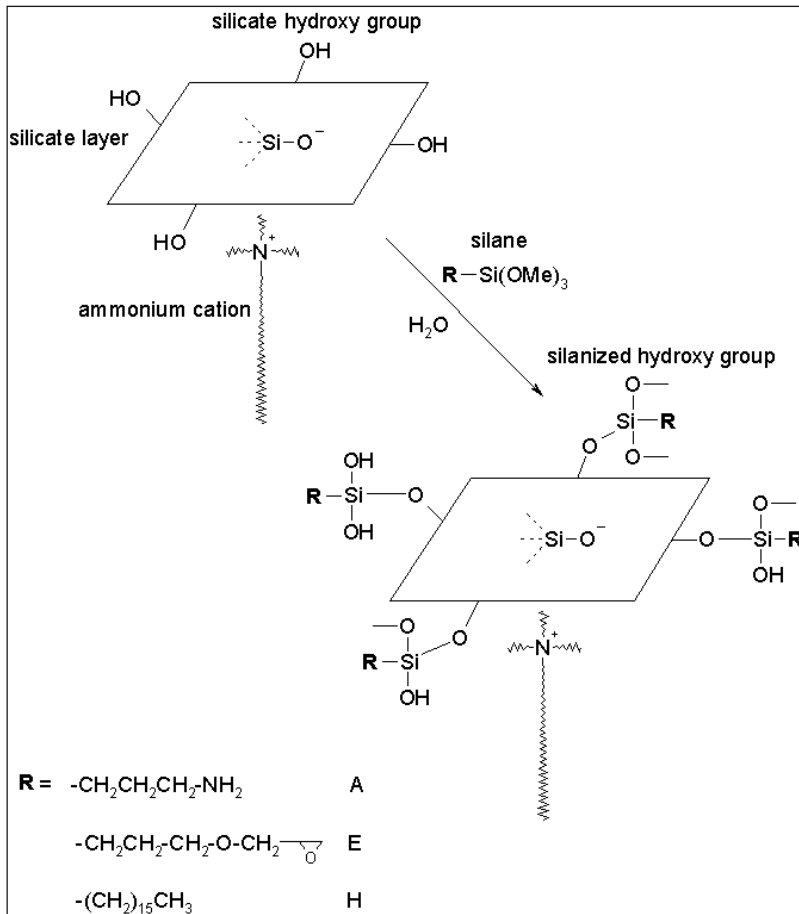


Figure 9: Silanization of commercial organoclays

The epoxy functional groups attached to the silicate surface facilitated interactions between the filler and polymer matrix and reduced the adverse effect of the silicate hydroxyl groups. Moreover, the epoxy-silanized organoclay could be directly bound to polymer chains resulting in higher delamination of silicate platelets (Fig. 10).

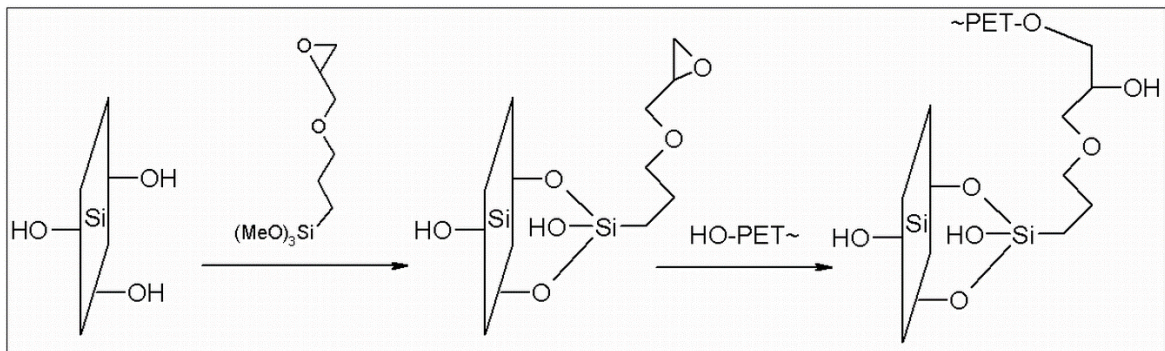


Figure 10: Epoxy-silanization vs. polymer chains

With the view of complete suppression of degradation reactions during compounding, the sodium montmorillonite was modified with spacers based on an imidazolium salt (Fig. 11). The “imidazolium organoclay” was further modified by silanization.

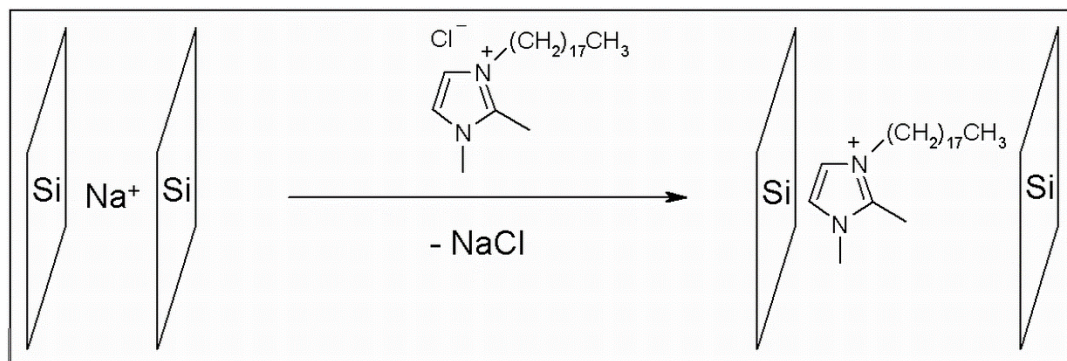


Figure 11: imidazolium organoclay

1.2.3 Exfoliation methods

According to the dispersion of MMT platelets in the polymer matrix, three composite structures can be formed:

- conventional composites,
- intercalated nanocomposites,
- exfoliated nanocomposites.

In the first case, the MMT tactoids are dispersed in the polymer matrix in micrometer scale with the tactoids acting as a micro-filler. On the other hand, intercalated (partially delaminated) systems show penetration of polymer chains into interlayer gallery of silicate platelets. Exfoliated (entirely delaminated) nanocomposite is characterized by homogeneous and uniform dispersion of silicate layers in the polymer (Figure 12).

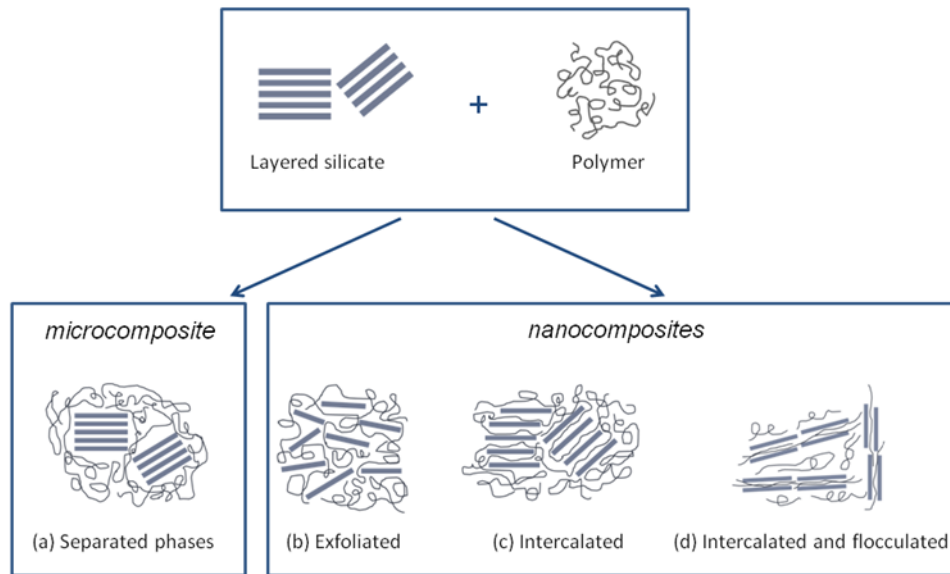


Figure 12: Scheme of composite structures [34]

Polymer/clay nanocomposites can generally be prepared by three methods (Figure 13):

- a) mixing during polymerisation („in situ“),
- b) melt mixing,
- c) mixing in solvent.

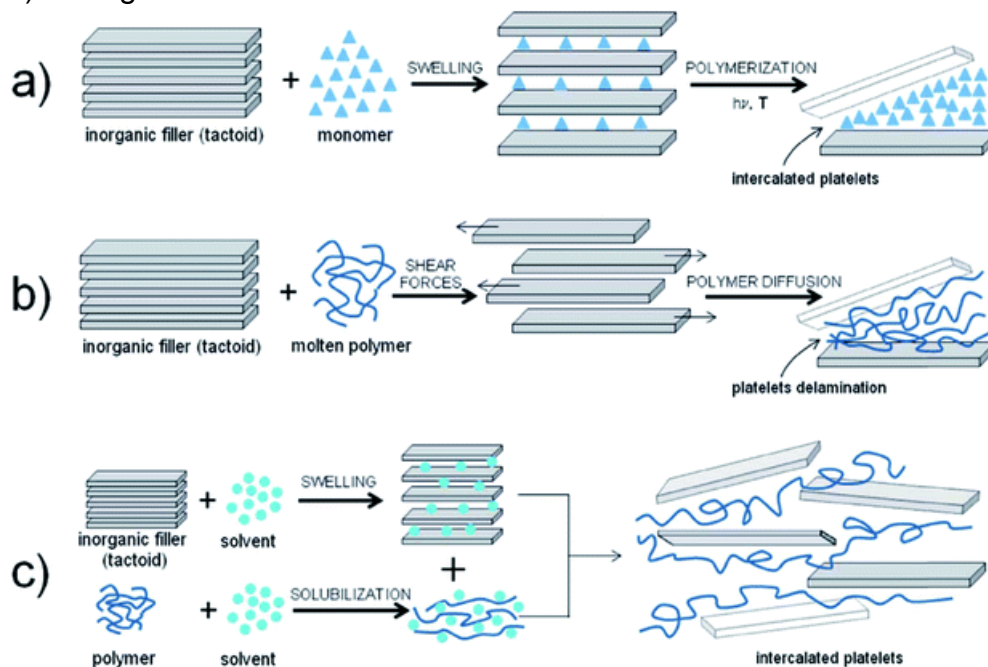


Figure 13: Difference in methods of nanocomposites preparation [32]

Additionally, possibilities of nanoparticle dispersion by application of electric field, by ultrasonic mixing or direct chemical bonding of polymer chains onto the surface of silicate platelets have been studied [158].

Melt mixing (compounding) is the industrially most attractive method due to its technological simplicity (usage of common polymer processing machines in contrast to special equipment and procedures in chemical laboratories). Moreover, it is possible to use various polymers as a matrix (different molecular weight, branching degree, copolymers, etc.). The production efficiency of this method is considerably higher than that of the others (“melt mixing” proceeds in the order of minutes, as compared to several hours characteristic for “in-situ” and “solution” methods) [159, 160].

The principle of the melt mixing method consists in delamination of silicate platelets in the polymer melt by shear forces (in extruder or kneader) and thermodynamical interactions between polymer chains and organoclay (the affinity between clay and polymer is usually increased by modification of silicate with organic compounds, in the case of polypropylene matrix also a compatibilizer is admixed). During compounding, penetration of polymer chains into the silicate gallery (intercalation) facilitates delamination of individual platelets, resulting in better dispersion of silicate layers in the polymer matrix [157]. This procedure is also shown in Figure 13b. The whole process has to be controlled in order to prevent degradation of the polymer or the organic part of organoclay (by high shear forces, temperature, etc.). Knowledge of possible degradation mechanisms is crucial to assess their impact on processing and application properties [161–171]. Therefore, research in this thesis is devoted also to this issue, especially for nanocomposites using polymers with high melt temperature (above 250°C) [172–174]. An example for complexity of melt mixing process using technical polymers is given with recycled PET matrix. On one hand, organoclays with nonpolar surface treatment (Fig. 14) lead to low level of dispersion (delamination) and, consequently, to low improvement of material (typically mechanical) properties.

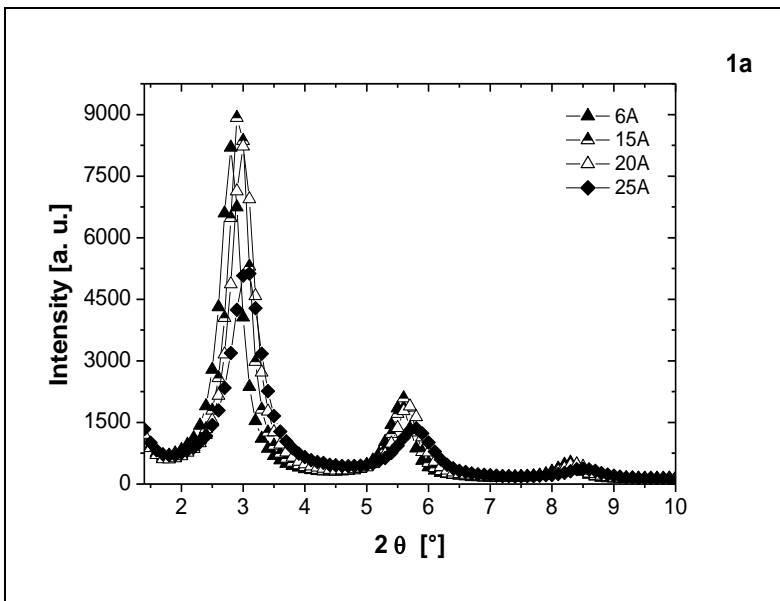


Figure 14: WAXS patterns of the nanocomposites with nonpolar organophilization

On other hand, organoclays with polar surface treatment (Fig. 15) revealed high dispersion grade (which would normally cause improvement in mechanical properties), but due to side reactions the mechanical properties were deteriorated. [172].

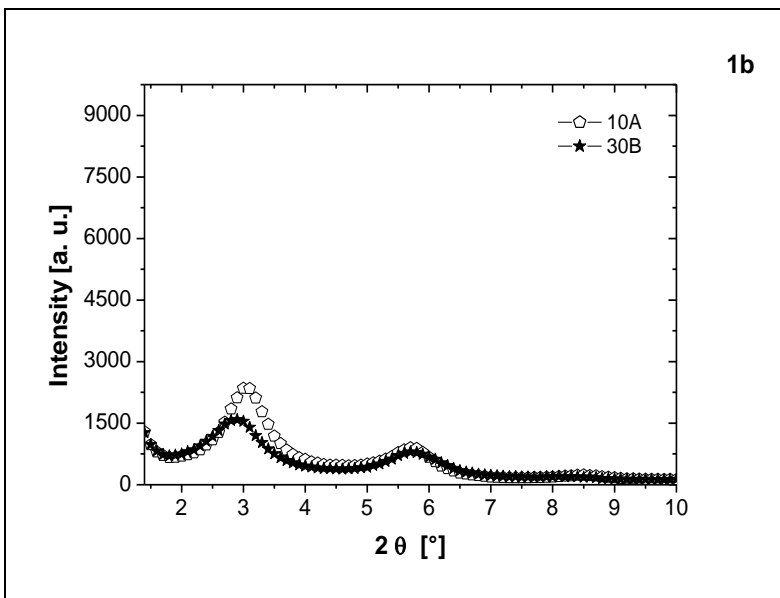


Figure 15: WAXS patterns of the nanocomposites with polar organophilization

Exact data on delamination grade is given in Tab. 2.

Table 2: WAXS analysis of organoclays in PET nanocomposites*

Organoclay	XRD peak position (°)	Basal Spacing (Å)	Δd_{001} (Å)
Cloisite 6A	2.8 (2.64)	31.5 (33.4)	-1.9
Cloisite 15A	2.9 (2.8)	30.4 (31.5)	-1.1
Cloisite 20A	3 (3.65)	29.4 (24.2)	5.2
Cloisite 10A	3 (4.6)	29.4 (19.2)	10.2
Cloisite 25A	3.1 (4.75)	28.5 (18.6)	9.9
Cloisite 30B	2.9 (4.77)	30.4 (18.5)	11.9

* manufacturer's data for neat organoclays are given in parentheses

Using the co-rotating twin-screw extruder as the continuous processing way is industrially preferred to melt mixing in a kneader (discontinuous process). It is obvious that for the successful dispersion of silicate plates in polymer melt by continuous processing the following two requirements have to be fulfilled: sufficient shear energy and enough residence time. However, these two effects are opposite in the extrusion process. With higher shear forces (e.g. usage of kneading blocks generating higher shear rate or increase in screw speed) the residence time is shortened. In this thesis is presented that both high shear rate as well as longer residence time can be matched by implementing a melt pump in front of an twin-screw extruder. The melt pump in extrusion technology is usually applied in order to control the pressure and throughput instability (melt pulsation) in extruder. In this thesis, the melt pump acts as an effective tool to control the residence time during compounding – example on polypropylene nanocomposites. Three different melt pump adjustments have been examined: 1) Δp negative, where the negative pressure difference between the outlet and inlet pressure of the melt pump has been set ($p_{out} - p_{in} = -100$ bar). In this way, a back pressure of polymer melt up to 9th extruder segment (approximately 30-40 cm before the melt pump) has been achieved. 2) Δp neutral, where the inlet and outlet pressure have been

kept at the same level ($p_{out} - p_{in} = 0$ bar) and 3) Δp positive with a positive pressure difference ($p_{out} - p_{in} = 5$ bar) has been set. For a comparison, all the tested compounds have been processed without the melt pump as well. The minimal residence time has been measured using a colour masterbatch as the time between granulat insertion into the hopper and colouring of the outgoing molten string. For characterization of material reinforcement by tensile force value (s. also chapter 1.3), Rheotens 71.97 equipment (Göttfert Ltd., Buchen, Germany) in combination with a capillary rheometer has been used. As extruder torque is important processing parameter (giving information about compounding efficiency), it was involved into analysis of material reinforcement. As can be seen on Fig. 16, the highest effect of the melt pump on increase in residence time and extruder torque occurs by adjustment of melt pump to maximal pressure difference; on the other hand, no significant differences between processing characteristics at neutral and positive melt pump operating modes have been observed.

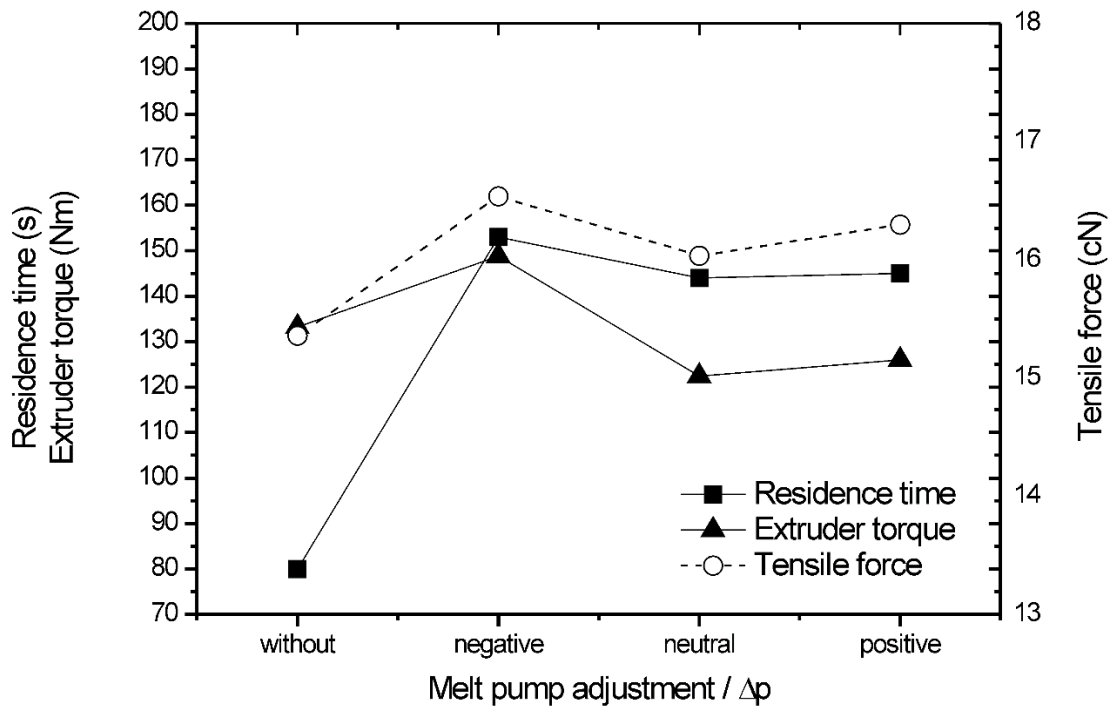


Figure 16: Processing characteristics vs. tensile force

Values of residence time and average torque revealed the same trend, which has an important impact on the processing efficiency. The level of torque in extruder gives information about level of shear forces applied during compounding. It can be clearly seen that both residence time as well as shear forces can be increased at the same time using the melt pump. The applied shear energy can be controlled by the screw speed and the residence time by adjustment of the melt pump. In this way, efficiency of dispersive as well as distributive mixing in continuous compounding can be substantially increased, depending on construction of twin-screw extruder and the melt pump. The main benefit of the melt pump consists in approximately two-times higher residence time achievable. In this way, diffusion process of intercalation and subsequent delamination of silicate platelets in the polymer matrix is substantially prolonged. The residence time is a dominant factor in production of satisfactory nanocomposites in extruders so the implementation of melt pump into compounding process introduces an interesting and technologically accessible method of continuous compounding enhancement employable in the field of polymer composites and blends. It should be mentioned that maximal residence time achieved in this study was limited by melt pump construction and torque limitation in extruder. By the usage of industry-scale processing equipment (allowing higher pressure in the melt pump and higher extruder torque) a further significant increase in residence time can be expected. Concerning the measurement of tensile force (level of melt strength) the same trends have been found as compared with measurements of processing parameters and more detailed description (also regarding effect of different screw geometries and screw speeds) can be seen in relevant paper included in this thesis. [175]

1.3 Characterization of polymer nanocomposites

Characterization of the nanocomposite materials is performed with aim to describe different aspects of polymer nanocomposites:

- a) dispersion grade of filler in the polymer matrix and filler orientation in relation to used processing parameters,
- b) effect of filler surface treatment on filler dispersion and nanocomposite properties,

- c) physical and chemical interactions between modified filler and polymer chains,
- d) application potential of the nanocomposites.

With the introduction of first commercial applications of polymer nanocomposites [176], relevant characterization techniques can be divided to analysis of material performance (mechanical & thermal analysis, barrier properties, flame retardancy, electrical & thermal conductivity, rheological properties, barrier properties, thermal stability, flame retardancy, biodegradation, drug delivery systems) and analysis of material structure. To the structural methods belongs X-ray diffraction (XRD), scanning electron microscopy (SEM), transmission electron microscopy (TEM), infrared spectroscopy (IR) or atomic force microscopy (AFM) [31–155]. Melt rheology describes mechanical response of the material in shear or elongational flow field and, therefore, can be used for structural as well as performance characterization. In order to use rheology for structural characterization, typical structural methods have to be used for establishment of relevant correlations (off-line measuring methods) or calibrations (on-line / in-line measuring methods), respectively.

1.3.1 Off-line structural characterization

The most used method for structural characterization of polymer nanocomposites is X-ray diffraction (XRD), using scattering at different angles: small angle X-ray scattering (SAXS) and wide angle X-ray scattering (WAXS). Classical XRD is used to determine the degree of crystallinity in semi-crystalline polymers, phase composition and crystallographic texture of materials. These method utilities the fact that X-Rays are scattered by regularly arranged atoms to discrete scattering angles according to their average distances [177, 178].

SAXS is a tool for studying structural features of rather large objects in the dimensions between some 100 nm and few nm – where measurable dimensions are strongly depending on the used instrument. “Any scattering or diffraction processes are characterized by a reciprocal law, which gives an inverse relationship between particle size and scattering angle” [179] – that means that large (in relation to used wavelength) objects, generally described as electron density fluctuation scatter to relatively small scattering angles. In condensed mater polymer science important parameters like the

long period, thickness of crystalline and amorphous domains, volume of pores and preferred orientation [180, 181] are determined by SAXS. In polymer nanocomposites the structure of physical network can be determined by using the SAXS method.

SAXS in principle is analysing structural dimensions in the range between a few 100 and 0.5 nm. The range is strongly depending on the equipment used. With laboratory instruments, dimensions between 70 and 0.4 nm are accessible. In semi crystalline polymers and polymer nanoclay composites many structural features are in the size between 10 to 20 nm (long period) and 2 to 5 nm (clay gap), perfectly matching the accessible range of small angle X-Ray scattering equipment. Regular arrangement of the clay platelets in dimensions between 2 and 5 nm leads to a diffraction peak at scattering angles between 1 and 3°. This is the most important feature in nanocomposite characterisation. The position of the peak is shifted from the initial state of the filler to lower scattering angles (= larger spacing) when intercalation occurs. The scattered intensity concentrated in the peak is directly proportional to the amount of scattering planes. When the concentration of clay in the polymer is known, the degree of exfoliation can therefore also be determined. The width of the reflexion is proportional to the “stacking height” of the clay tactoids, i.e. to the number of silicate platelets in one particle.

For data analysis typically the 2D scattering patterns are averaged and corrected for background scatter. The scattering curves can be analysed applying a one-dimensional correlation function method **Fehler! Verweisquelle konnte nicht gefunden werden.** to calculate the interlayer distance d_{001} and thickness of the clay platelets (t) of the filler prior to compounding. The position and magnitude (I) of the clay period (cp) peak in the composite material are determined by peak fitting with a pseudo-Voight function. The clay period is then the sum of plate thickness and interlayer distance ($cp = t + d_{001}$). Because t does not change during composite formation changes in cp are directly caused by changes in interlayer distance. Therefore cp can be used as a measure for intercalation. For comparison purposes a value Δd_{001} is calculated and defined as:

$$\Delta d_{001} = cps - cpN$$

where cp_S is the clay period in nanocomposite sample and cp_N is the clay period in the native state.

The magnitude of the peak arising from the regular arrangement of clay platelets is directly proportional to the amount of scattering planes and therefore to the overall amount of clay stacks, when the distribution of stacks within the probed volume is random (as in powder). When exfoliation occurs, clay platelets are no longer arranged in stacks and do not contribute to the scattered intensity any more. The degree of exfoliation (X_{FS}) is a relative measure to compare series of different compounding procedures. The factor X_{FS} becomes zero when no intercalated material or agglomerates are in the material. Values >1 indicate the existence of additional agglomerates and/or intercalated clay material.

From the peak width the so-called "Scherer size" (d_s) can be calculated, which is a measure for the size of crystalline domains. Although it is only a rough approximation at small scattering angles, it is very useful for comparison of samples. It must be noted that it is a mean value, meaning that the smaller dimensions are favored by this evaluation. The staking number $n_s = d_s/cp_S$ is a measure for the average number of clay platelets stacked in the material.

Whereas the average interlayer distance d_{001} has been widely applied as standard structural measurement concerning polymer nanocomposites at all, degree of exfoliation X_{FS} and staking number n_s have been established in the frame of project work within Austrian nanoinitiative. On example with 2 different screw geometries is visible that changing the screw speed can lead to the same level of average interlayer distance and staking number (in the case using Geometry 2, Fig. 17, 19) but different exfoliation degree (Fig. 18). [151]

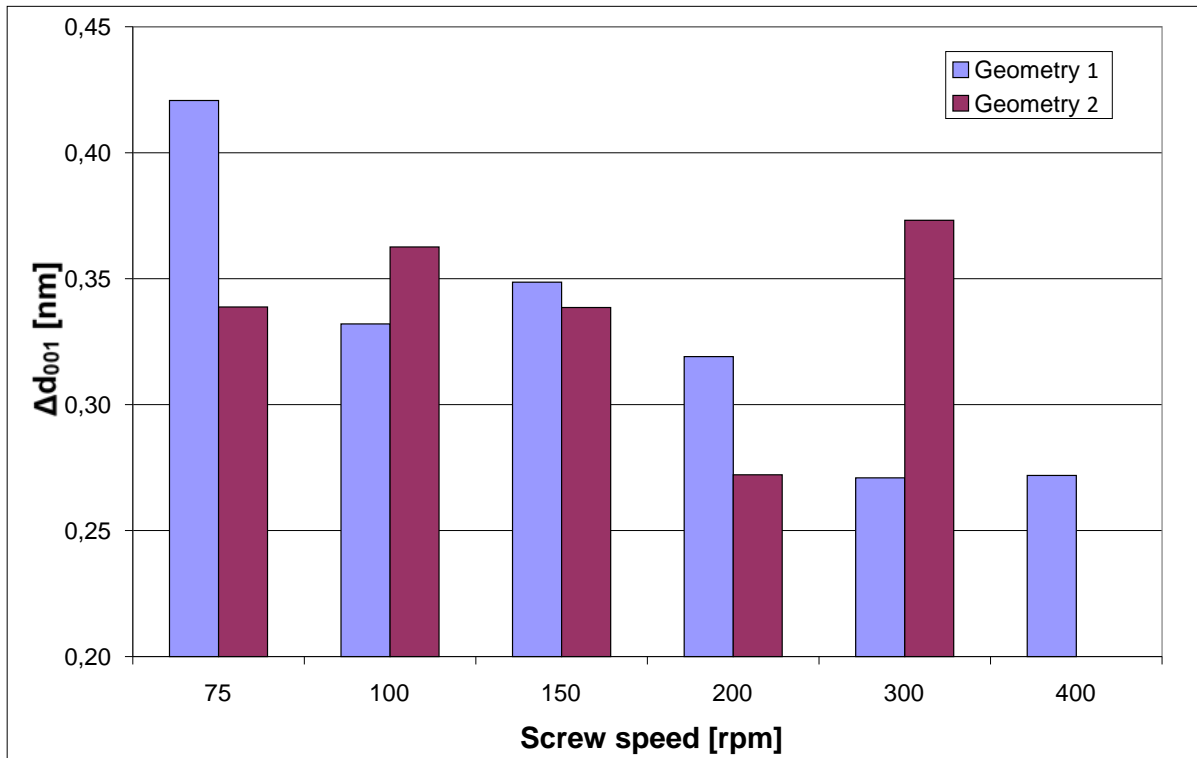


Figure 17: Interlayer distance in dependency on screw geometry and speed

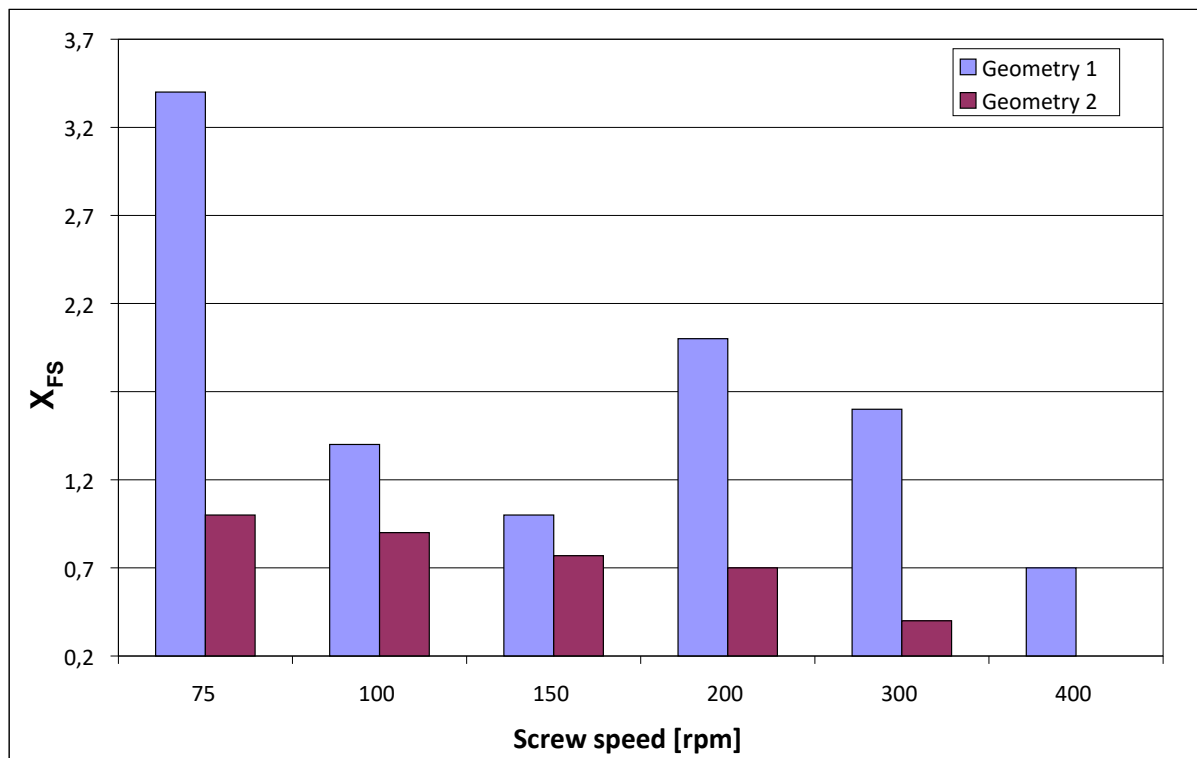


Figure 18: Degree of exfoliation in dependency on screw geometry and speed

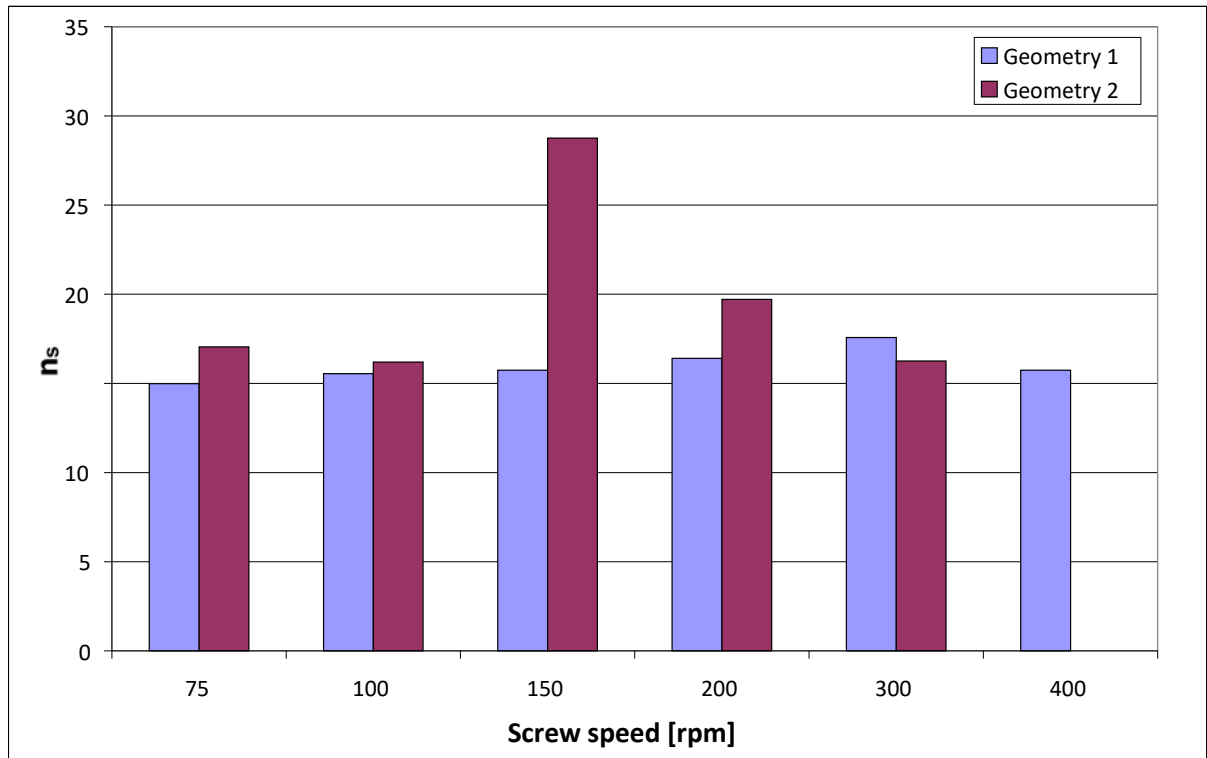


Figure 19: Staking number in dependency on screw geometry and speed

Due to instrumental development during the last few years it is now possible to perform all types of characterizations also in-situ at elevated temperatures and under mechanical load. The in-situ techniques allow for characterization of structural details during melting and recrystallization process in native polymer as well as in composites. Relations between structural and mechanical properties can be determined by in-situ tensile testing. However, these approaches are difficult and expensive to apply in industrial scale manufacturing processes.

1.3.2 On-line & in-line structural characterization

Different spectroscopic techniques have already been tested for real-time monitoring of the extrusion process, such as ultrasound, Raman, UV-VIS (ultra-violet-visible) and NIR (near-infrared) spectroscopy, demonstrating possibility of process control without time consumption for off-line analyses and samples preparation. They work on principle of inserting optical probes in the main (in-line) or by-pass (on-line) polymer stream in

production line [183–191]. For the research in this thesis, in-line NIR spectroscopy in a combination with on-line extensional rheometry was used [192].

1.3.2.1 In-line NIR spectroscopy & chemometrical modelling

Near-infrared (NIR) spectroscopy is a non-destructive, optical method to determine information on the composition of samples. Like mid-infrared (MIR) spectroscopy, the NIR method measures the absorbance of light due to excitation of molecular vibrations of the substance under investigation. However, MIR, which exploits radiation in the wavelength range of 2500 to 25000 nm, measures the fundamental molecular vibrations, whereas NIR, operating in the spectral range between 780 and 2500 nm, detects the overtones and combinations of these vibrations (Figure 20).

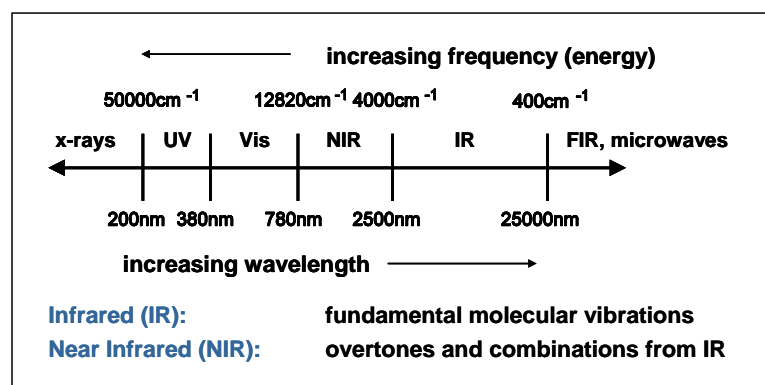


Figure 20: Spectral ranges of spectroscopic techniques [193]

By placing the sample in the light path, the substances present in the sample absorb NIR radiation at specific frequencies according to their molecular structure, resulting in NIR sample spectra (Figure 21).

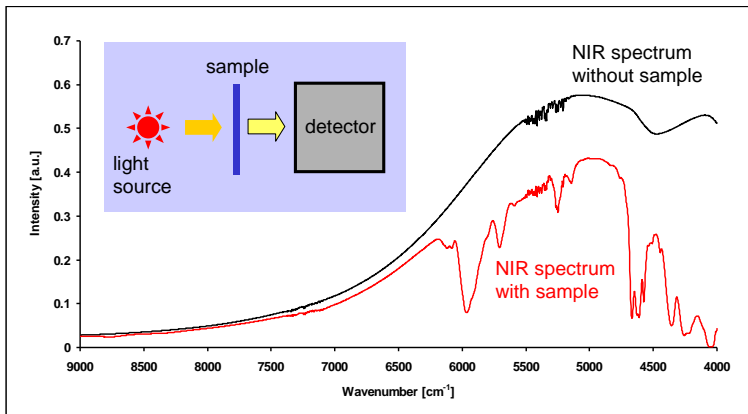


Figure 21: Measurement principle of NIR spectroscopy [193]

As the frequencies, at which the absorbances take place are depending on the energy a molecular structure requires to be stimulated, the position of the absorbance bands in the NIR spectrum provides the information for identification of substances and for the existence of specific chemical functionalities present in the sample. By evaluating the intensity of the features identifying a substance or chemical functionality (Figure 22), the amount/concentration of the respective analyte can be determined [194].

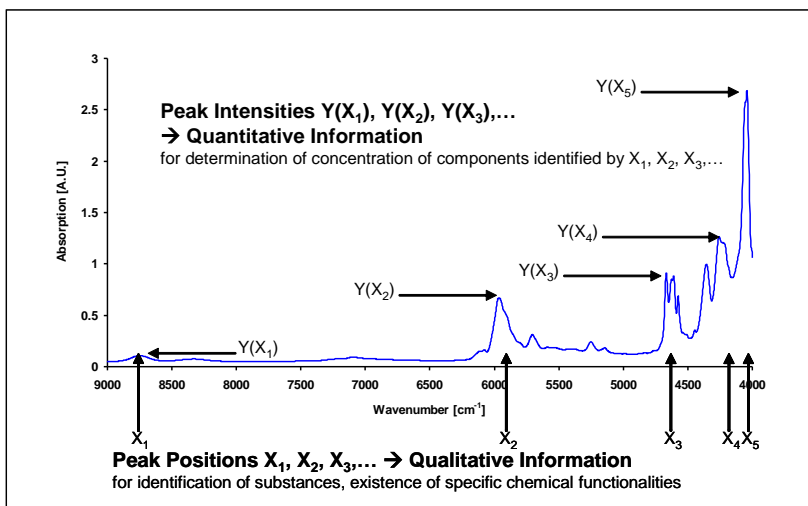


Figure 22: Information content of NIR spectra [193]

Regarding polymer materials, NIR spectroscopy has been tested for detection of different physical-chemical changes like examination of polymerisation or copolymerisation, moisture content, crystallinity, molecular weight, intermolecular interactions, tacticity, orientation, dispersion and alteration of particle size of fillers and density of polyethylenes. As described above, NIR spectroscopy in principle determines the chemical composition of samples. However, it is also capable of providing information on mechanical properties as these properties are generally linked to the chemical state of the sample. For example the strength of coatings often depends on the degree of polymerisation of polymers, which again can be monitored by determining the remaining amount of monomer functionalities which have not been converted by the polymerisation reaction. Furthermore, some parameters can be determined by NIR spectroscopy although neither a chemical conversion is the basis for the phenomenon nor does the analyte show any activity in the NIR. For example, ions dissolved in water can be determined to a certain degree although they are not IR active and do not cause any specific chemical reaction. The reason for this is the fact that the charged ions interact with the water molecules, influencing the strength of the O-H-bond and thereby shifting the water's O-H absorbance peak.

In polymer nanocomposites, the silicate platelets form different levels of 3D physical network. Generally, in the real nanocomposite systems both the intercalated as well as exfoliated structure persists. During the dispersion process, the both structures are formed by the physical bounds between the hydrophilic clay, hydrophobic polymer matrix and possibly compatibilizer. The number and type of interactions between polymer chains and organoclay depend on the experimental conditions and can be monitored with NIR spectroscopy [187–191].

Chemometrical modelling / multivariate data analysis

For NIR spectroscopic applications it is very important to extract process relevant information from the measured NIR spectra. In the MIR range often methods like peak integration are used to evaluate the absorption strength of one specific species and thus to quantify the amount of this species in an unknown mixture. In practice the approach of evaluating single spectral lines can only be applied to MIR spectra where spectral lines of different species are well separated. In the NIR region typically the spectral

features of different species show strong overlapping. This results in the need for more sophisticated evaluation methods [195].

In this thesis, partial least squares (PLS) method is used to extract quantitative information from NIR spectra and to evaluate the data if the desired parameter can be measured using this technology.

For example, NIR spectra are often used to estimate the amount of different compounds in a chemical sample. In this case, the so called “factors” are the wavelength specific measurements that comprise the spectrum. They can number in the hundreds but are likely to be highly collinear. The parameters of interest, the so called “responses” are typically component amounts that the researcher wants to predict in future samples. Such responses of interest can be the mechanical properties of the nanocomposite in dependency on material composition and processing conditions.

PLS is a method for constructing predictive models when the factors are many and highly collinear. The emphasis is on predicting the responses and not necessarily on trying to understand the underlying relationship between the variables. For example, PLS is not usually appropriate for screening out factors that have a negligible effect on the response. However, when prediction is the goal and there is no practical need to limit the number of measured factors, PLS is a very useful tool.

Usually, each spectrum is comprised of measurements at a 1,000 different frequencies; these are the factor levels, and the responses are the sample parameters of interest. Typically the parameters are related to chemical composition of the samples. Indirect effects can lead to models evaluating mechanical or physical parameters like hardness, stiffness or density.

The PLS factors (the NIR spectra) are computed as certain linear combinations of the spectral amplitudes (eigenvectors or loadings), and the responses are predicted linearly based on these extracted factors. Thus, the final predictive function for each response is also a linear combination of the spectral amplitudes. PLS prediction is a function of all of the input factors and can be interpreted as contrasts between broad bands of frequencies [196].

In research concluded in this thesis for evaluating the method of NIR spectroscopy for being able to measure a certain sample attribute (responses: e.g. E-modulus or tensile force) a straight forward approach was applied. NIR spectra of samples with varying but known responses were used. Then PLS was applied to generate a linear predictive model for calculating the responses from the measured NIR data (factors). By looking at special correlation parameters (like R^2 and RMSECV – see below) of the resulting model it was possible to evaluate whether the model shows sufficient predictive ability or not. If the developed model shows sufficient correlation the method can be used to deliver measurement data about correlated properties of the material. Since the NIR method can be easily implemented to the extruder and the measurement time is in the region of seconds this enables a non-destructive real time monitoring of structural and application properties of the produced material.

The correlation coefficient R^2 shows the correlation of the NIR data with the investigated response parameter. Values of R^2 are between 0 and 100. Typically models with R^2 values above 90 enable quantitative calculation of the response parameter of interest. Correlation coefficients above 60 allow qualitative evaluations. If R^2 lies below 60 the response is not well pronounced in the factors (the spectral data) and thus cannot be evaluated with reasonable practical relevance.

The root mean square error of cross validation (RMSECV) is estimated by calculating a predictive model by using all samples expected one. This model is applied to the left out sample for predicting the desired response parameter. RMSECV is calculated by doing this procedure for every sample and by summing up the root mean square errors of the deviations of the calculation results from the real values. This value is a measure for the measurement error of the developed NIR measurement method.

In general the quality of the “real” response values is very important for the quality of the generated models. Outliers are strongly influencing the model generation and, consequently, the model describing parameters like R^2 and RMSECV [195, 196].

1.3.2.2 On-line extensional rheometry

Generally, two methods of reinforcement assessment in polymer nanocomposites in the molten state can be used: analysis of melt elasticity using rotational rheometry or melt strength evaluation by extensional rheometry. In this thesis, commercial extensional rheometer Rheotens 71.97 was used. The advantage of Rheotens measurements consists in their simplicity without need of expensive scientific equipment and additional time for sample preparation. The principle of Rheotens measurement can be seen in Figure 23 and Figure 24. It is based on elongation of an extruded string by two or four rotating wheels connected with force transducer. The rotation speed is linearly increased up to when the molten string breaks. The tensile force applied to the wheels and the draw speed at break allow the calculation of the melt strength (stress at break):

$$\sigma_b = F_b \cdot v_b / A_0 \cdot v_0$$

σ_b ... stress at break [Pa]

F_b ... draw force at break [N]

v_b ... draw speed at break [$\text{mm} \cdot \text{s}^{-1}$]

A_0 ... initial cross section of molten string (at the die outlet) [m^2]

v_0 ... extrusion speed of molten string (piston speed) [$\text{mm} \cdot \text{s}^{-1}$]

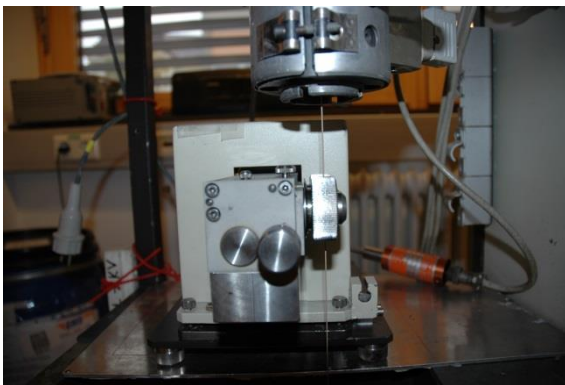


Figure 23: Measurement performed by Rheotens equipment [197]

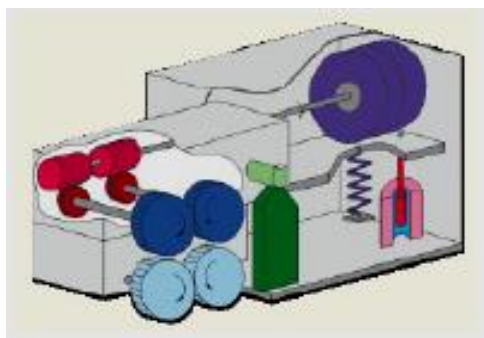


Figure 24: Principle of Rheotens measurement [197]

In order to compare the melt strength level of different nanocomposite systems (revealing different magnitudes of v_b), the tensile force at specific draw speed has been chosen as a comparative value (e.g. figure 25).

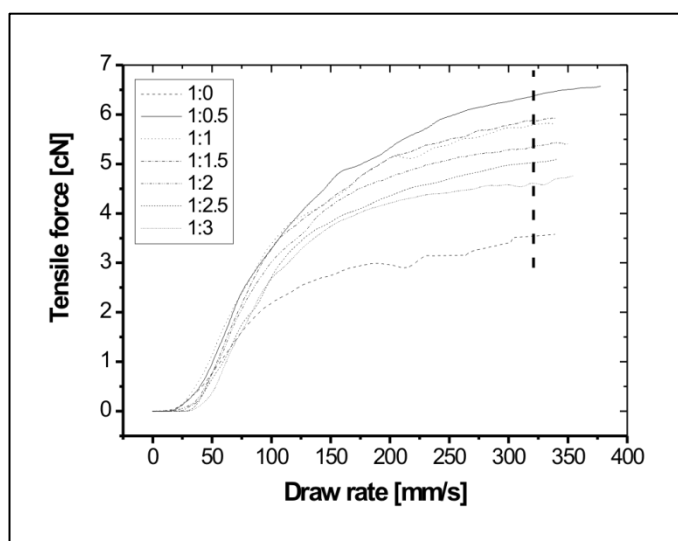


Figure 25: Melt strength level comparison [197]

The silicate platelets form different levels of 3D physical network in the polymer matrix depending on their structure (intercalated or exfoliated, figure 12). The different physical crosslinking and bonding between polymer chains and organoclay results in diversity of viscoelastic response. Individual nanoparticles act as entanglement- or crosslinking-sites and raise the extensional stiffness of the composite, measured by the melt strength level. Depending on the degree of dispersion, this change is more or less pronounced compared to the unfilled polymer. Research in this thesis shows how the

extensional rheometry can be used for fast determination of material reinforcement for both off-line as well as on-line measuring principles [175, 192, 194, 197–203].

1.4 Viscoelasticity of polymer nanocomposites

Comparing to typical characterization of individual polymer nanocomposite properties (like mechanical & thermal analysis, microscopy, X-ray diffractometry, barrier properties, electrical & thermal conductivity) [31–155], melt rheology has been established as a powerful tool to analyse dispersion of nanofiller in polymer matrix and to correlate it with processing and application properties [160, 173, 200, 201, 204–255]. Especially usage of rotational rheometry is very interesting, because knowledge of viscoelasticity enables assessment of nanocomposite structure, which is responsible for material performance.

In the case of highly dispersed systems, a 3D physical network formed by nanofiller and polymer chains is achieved. This phenomenon can be investigated by the analysis of the melt elasticity in the system using rotational rheometry [160, 173, 200, 201, 204–255].

The magnitude of storage modulus (real part of complex modulus, G') reflects level of elasticity (entanglement of polymer chains) in material during oscillating flow and is directly related to imaginary part of complex viscosity. The G' modulus is increasing with the filler loading. The G' *secondary plateau*, which occurs at low frequencies and high concentration of the filler, reflects structures with much longer relaxation times than those of neat matrix. The curve of this plateau is dependent on filler concentration, particles size and rheological history of material. The G' secondary plateau seems to be in relation to yield stress because both phenomena reflect level of physical network stability in the system [253].

The loss (viscous) modulus G'' (imaginary part of complex modulus) reflects energy dissipation to heat (the level of viscous properties resulting from slippage of polymer chains) and is directly related to real part of complex viscosity. The ratio of the loss modulus to the storage modulus $\tan \delta$ (loss factor, $\tan \delta = G'' / G'$) provides information about damping ability of the material. The complex viscosity η^* gives information about overall material resistance (complex modulus) to flow as a function of frequency in terms of $\eta^* = G^* / \omega$.

Using rotational rheometry, the physical network in polymer nanocomposites has been characterized by dynamic measurements in oscillatory shear flow concomitant with G' and G'' secondary plateau formation (pseudo-solid-like behavior) with the silicate loading in the range of 3 - 5 wt. % [160, 173, 200, 201, 204–255], (Figure 26).

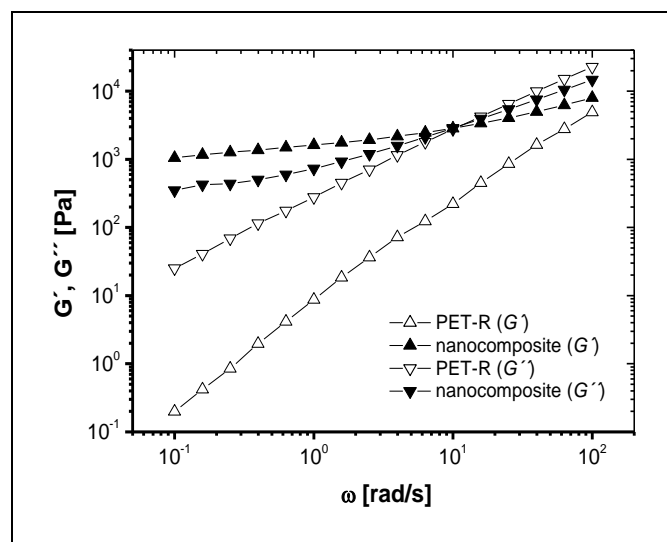


Figure 26: Comparison of viscoelastic properties of the matrix and the nanocomposite with Cloisite 6A [172]

Rheological properties of polymer nanocomposites (poly- ϵ -caprolactone, PA-6) prepared by “in situ” method (polymer chains were chemically bonded on the surface of silicate) were firstly described by Krishnamoorti and Giannelis [211]. “Solid-like” response has been observed also in conventional polymer composites, where the “yielding” phenomenon reflected very strong interactions between the polymer and filler [239]. In this thesis, “rubber-like” behavior typical for well dispersed polymer nanocomposites was also detected for complex polymer composites, where synergic effect of different fillers on formation of 3D physical network was revealed [213, 249] (Figure 27).

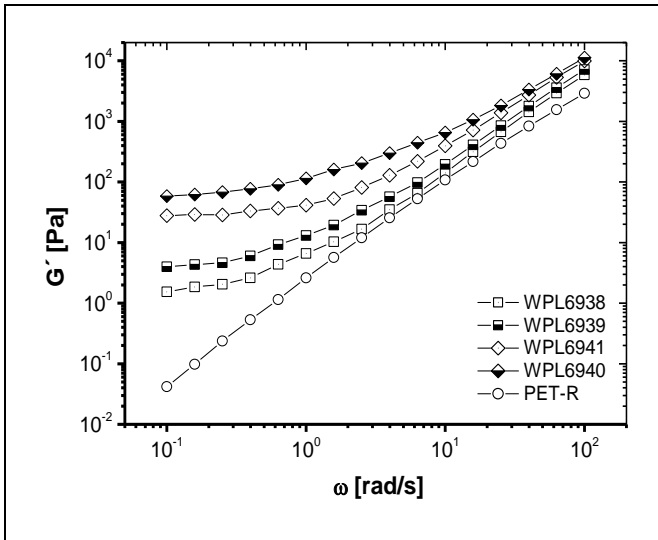


Figure 27: Storage modulus of the PET matrix and composites [213]

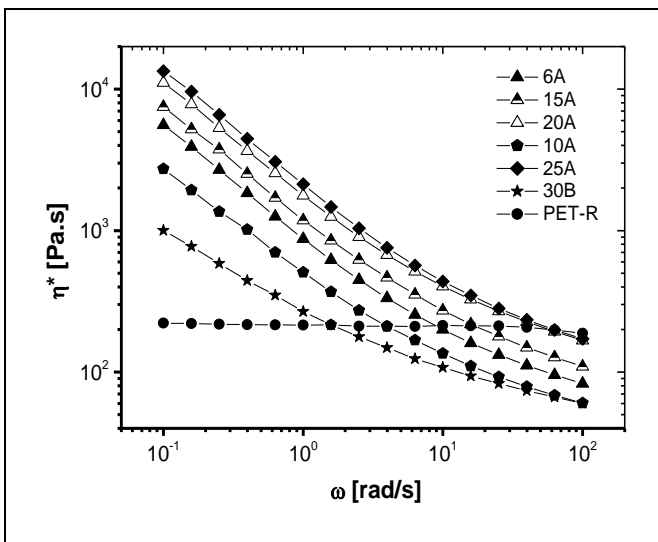


Figure 28: The viscosity curves of the PET matrix and nanocomposites [172]

The melt viscosity trend of nanocomposites is similar to other filled polymer systems: a significant increase (comparing to neat matrix) in the range of low shear rates and a subsequent decrease with shear rate rise (Figure 28). This “shear thinning” (yielding) phenomenon is attributed to destruction of physical network and re-arrangement of silicate platelets in flow direction with raising shear rate.

One of unconventional rheological approaches presented in this thesis is usage of the van Gorp-Palmen (vGP) plot (dependency of loss angle δ on complex modulus $|G^*|$) for analysis of spatial structures in polymer nanocomposites [200, 201, 250, 256]. In original work [225, 230], polymer samples with rather linear chain structure exhibited a continuous shaped curve. On the contrary, long chain branched (LCB) polymers showed a developed bump between the $|G^*|$ minimum and the 90° plateau.

For example, in polyethylene nanocomposite blend, systems prepared with Cloisite20 organoclay and Cloisite20/nanoscaled ZnO showed spatial structure similar to mentioned LCB polymers with even two bumps or peaks (in the case of mixture with Cloisite20), indicating complex 3D structure made of filler and polymer chains. On the other hand, the polyethylene (CA9150) matrix and nanocomposite blend with only nanoscaled ZnO exhibited behaviour similar to linear chain structure (Figure 29).

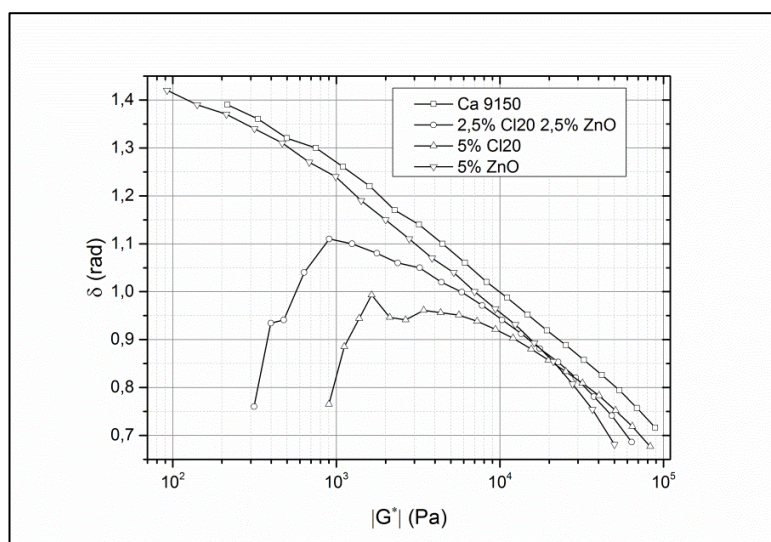


Figure 29: The van Gorp-Palmen plot of PE nanocomposite blends [256]

Another approach for description of viscoelastic damping behaviour is so called “Cole-Cole” figure, in which imaginary part of complex viscosity over the real part is plotted. This figure has been widely used to assess miscibility/homogeneity of polymer blends and composites in the way that a smooth, semi-circular shape can be interpreted by better compatibility and homogeneity, respectively [229, 235]. Usage of this analysis for a polyethylene nanocomposite blend is shown in figure 30.

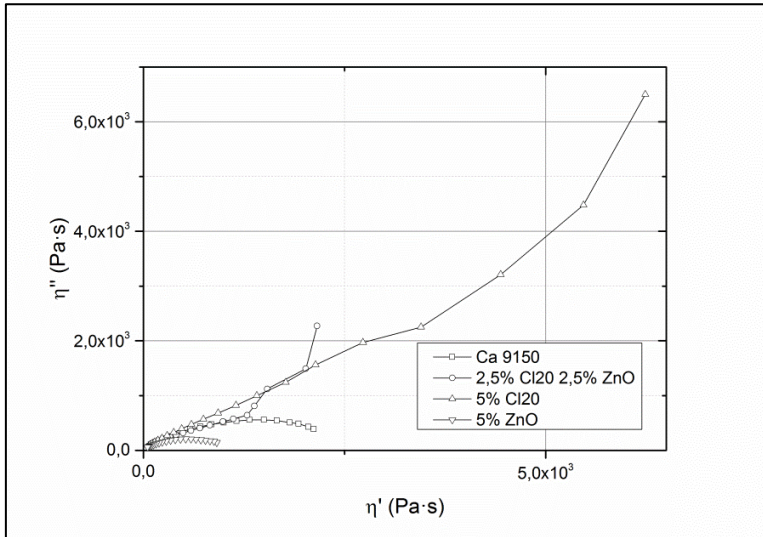


Figure 30: The Cole-Cole plot of PE nanocomposite blends [256]

The polyethylene CA9150 matrix and nanocomposite with ZnO showed semi-circle shapes, reflecting rather high homogeneity of the system. However, for the analysis of polymer nanocomposites performance, not only homogeneity but also reinforcement effect should be addressed. Using Cole-Cole plot, it can be said, that systems prepared with Cloisite20 and Cloisite 20/ZnO revealed deviation from semi-circle shape and, therefore, are rather not homogeneous. Nevertheless, no information about reinforcement level can be obtained from this figure and this problem is actually concomitant with each previously described rheological analysis based on damping behaviour. Therefore, new rheological approach based on rigidity behaviour is presented in this thesis. This approach uses evaluation of new rheological parameter ($\cotg \delta$), which was called as storage factor (analogically to loss factor $\tan \delta$). In order to reduce the values of storage factor to one representative magnitude (cumulative storage factor, CSF) for one nanocomposite sample, G' as well as G'' values of each sample were integrated over the measured frequency range according following equation:

$$CSF = \frac{\int_{0.1 \text{ rad/s}}^{628 \text{ rad/s}} G' / \int_{0.1 \text{ rad/s}}^{628 \text{ rad/s}} G''$$

It was proved that cumulative storage factor reflects reinforcement in polymer nanocomposites in the shear flow, similarly to melt strength parameter in the elongational flow. Moreover, calculation of further cumulative rheological parameters (in the same principle as calculation of CSF) enables new opportunities of using rheological data from shear flow for structural analysis of complex multiphase polymer systems [200, 250, 256].

An example of using CSF value is given concerning nanocomposites with recycled PET. According to typical rheological evaluation (viscosity and storage modulus curves, respectively) it would be difficult to recognize what organoclays led to the real reinforcement of the polymer matrix (Fig. 31, 32).

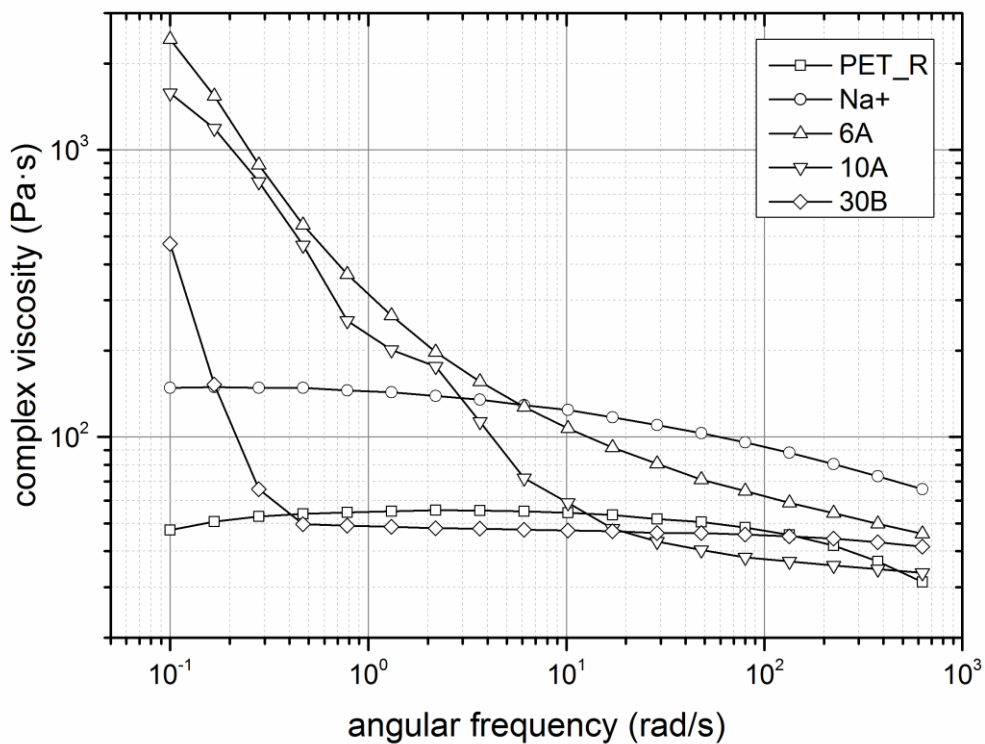


Figure 31: Complex viscosity of PET-R nanocomposites

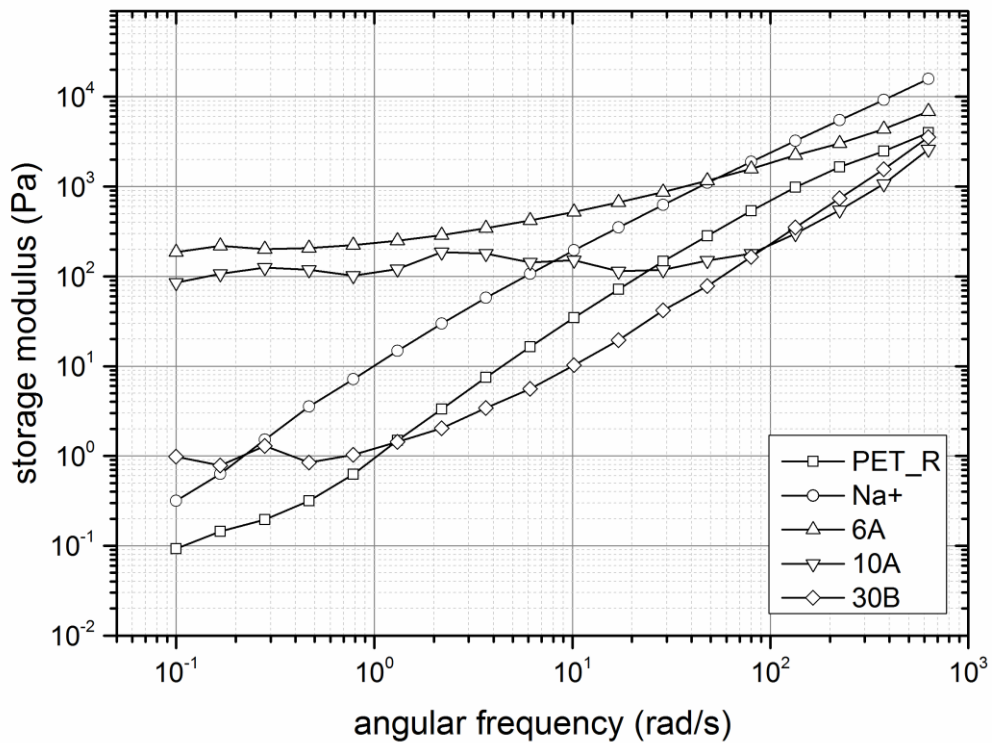


Figure 32: Storage modulus of PET-R nanocomposites

However, the CSF plotted over CCV in Fig. 33 shows clearly differences in material reinforcement between various CPNs. It can be seen that CSF values can be divided into three groups: CSF of the neat polymer matrix, CPNs with lower CSF values (10A, 30B) and CPNs with higher CSF values (6A, Na+). It means that effective material reinforcement was reached only in CPN systems using 6A and Na+.

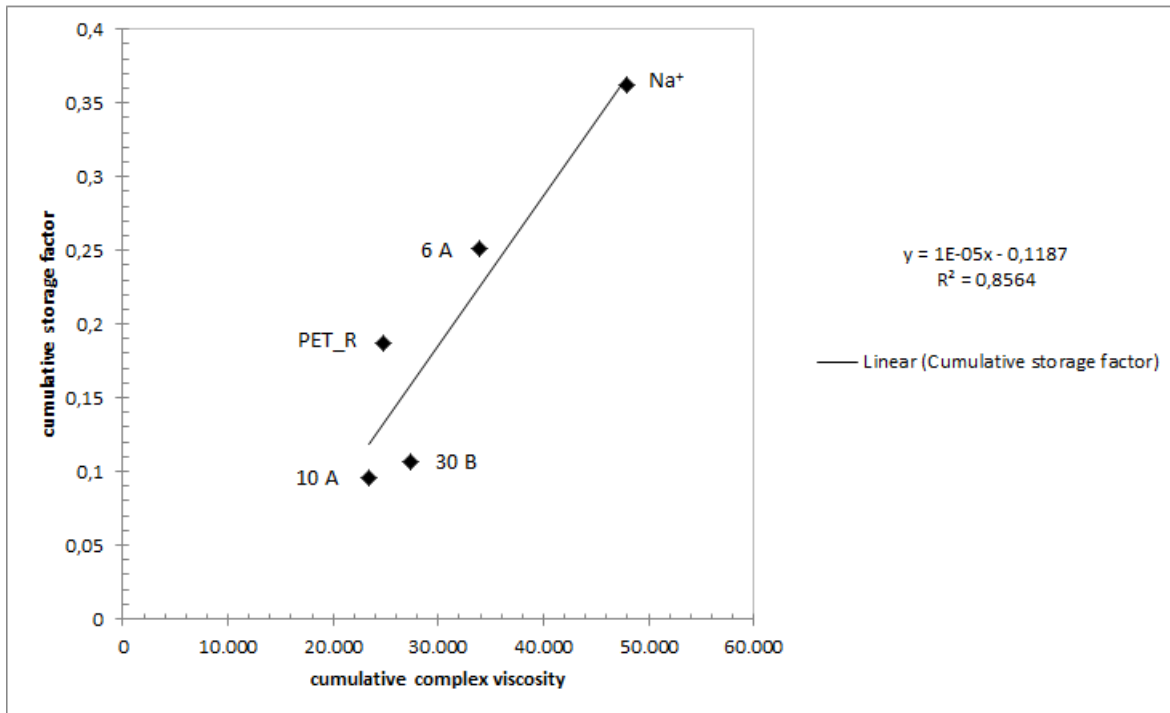


Figure 33: CSF plotted over CCV

This is result of complex physical and chemical reactions, which occur during the processing. On one side, physical interactions based on electrostatic forces between polymer and clay mineral result into formation of differently organized structures (combination of agglomerated, delaminated and exfoliated structure) depending on achieved 3D network. On the other side, processing of PET CPNs is concomitant with different chemical reactions (e.g. chain scission, Hofmann elimination) that lower CPN mechanical performance. Using cumulative storage factor, it can be clearly said which organoclays leads to effective material reinforcement (effect of 3D physical network is higher than effect of chemical degradation) and vice versa.

Résumé

Research in this thesis shows contribution to preparation, processing and characterization of polymer nanocomposites. Concerning preparation, organoclays with increased temperature stability and interlayer distance (modification by silanization and imidazole salt) have been developed. In the field of processing, advanced compounding was established, using specific adjustment of melt pump in combination with twin-screw

extruder. Addressing characterization of polymer nanocomposites, in-line NIR spectroscopy as well as novel rheological parameter (cumulative storage factor) have been successfully tested in combination with advanced evaluation of small angle X-ray scattering (additional parameters for description of clay delamination). Incorporation of new results into broad research in the field of polymer nanocomposites can be found more in detail in the following scientific papers, being the part of this thesis.

References

- [1] Official website of the United States government, <http://nano.gov>.
- [2] LeBaron P. 1999. Polymer-layered silicate nanocomposites: an overview. 15(1-2):11-29. [https://doi.org/10.1016/s0169-1317\(99\)00017-4](https://doi.org/10.1016/s0169-1317(99)00017-4)
- [3] Lucilene Betega de Paiva, Ana Rita Morales, Francisco R. Valenzuela Díaz Applied Clay Science Volume 42, Issues 1–2, December 2008, Pages 8-24
- [4] Y. Shieh, Y. Twu, C. Su, R. Lin, G. Liu, Crystallization Kinetics Study of Poly(L-lactic acid)/Carbon Nanotubes Nanocomposites, Journal of Polymer Science Part B: Polymer Physics 48 (2010) 983–989.
- [5] S.S. Ray, K. Yamada, A. Ogami, M. Okamoto, K. Ueda, New Poly(lactide)/Layered Silicate Nanocomposite: Nanoscale Control Over Multiple Properties, Macromolecular Rapid Communicates 23 (2002) 943–947.
- [6] S. Ouchiar, G. Stoclet, C. Cabaret, A. Addad, V. Gloaguen, Effect of biaxial stretching on thermomechanical properties of poly(lactide) based nanocomposites, Polymer 99 (2016) 358–367.
- [7] M. Pluta, Melt Compounding of Poly(lactide)/Organoclay: Structure and Properties of Nanocomposites, Journal of Polymer Science: Part B: Polymer Physics 44 (2006) 3392–3405.
- [8] E. Pollet, C. Delcourt, M. Alexandre, P. Dubois, Transesterification catalysts to improve clay exfoliation in synthetic biodegradable polyester nanocomposites, European Polymer Journal 2006 1330–1341.
- [9] H. Wang, Z. Qiu, Crystallization kinetics and morphology of biodegradable poly(l-lactic acid)/graphene oxide nanocomposites: Influences of graphene oxide loading and crystallization temperature, Thermochimica Acta 527 (2012) 40–46.
- [10] K.M. Zia, M. Zuber, M. Barikani, R. Hussain, T. Jamil, S. Anjum, Cytotoxicity and mechanical behavior of chitin-bentonite clay based polyurethane bio-nanocomposites, International Journal of Biological Macromolecules 49 (2011) 1131–1136.
- [11] M. Zuber, K.M. Zia, S. Mahboob, M. Hassan, I.A. Bhatti, Synthesis of chitin-bentonite clay based polyurethane bio-nanocomposites, International Journal of Biological Macromolecules 47 (2010) 196–200.
- [12] M. Vestena, I.P. Gross, C.M.O. Müller, A.T. Pires, Nanocomposite of Poly(Lactic Acid)/Cellulose Nanocrystals: Effect of CNC Content on the Polymer Crystallization Kinetics, Langmuir 27 (2015) 905–911.
- [13] K. Sownthari, S. Suthanthiraraj, Preparation and properties of biodegradable polymer-layered silicate nanocomposite electrolytes for zinc based batteries, Electrochimica Acta 174 (2015) 885–892.
- [14] P. Stloukal, S. Pekařová, A. Kalendova, H. Mattausch, S. Laske, C. Holzer, L. Chitu, S. Bodner, G. Maier, M. Slouf, M. Koutny, Kinetics and mechanism of the biodegradation of PLA/clay during nanocomposites during thermophilic phase of composting process, Waste Management 42 (2015) 31–40.

- [15] M. Tesfaye, R. Patwa, R. Kommadath, P. Kotecha, V. Katiyar, Silk nanocrystals stabilized melt extruded poly (lactic acid)nanocomposite films: Effect of recycling on thermal degradation kinetics and optimization studies, *Thermochimica Acta* 643 (2016) 41–52.
- [16] N. Najafi, M.C. Heuzey, P.J. Carreau, Poly(lactide (PLA)-clay nanocomposites prepared by melt compounding in the presence of a chain extender, *Composites Science and Technology* 72 (2012) 608–615.
- [17] C.H.C. Flaker, R.V. Lourenço, Bittante, Ana M. Q. B., P.J.A. Sobral, Gelatin-based nanocomposite films: A study on montmorillonite dispersion methods and concentration, *Journal of Food Engineering* 2015 65–70.
- [18] K. Fukushima, D. Tabuani, G. Camino, Poly(lactic acid)/clay nanocomposites: effect of nature and content of clay on morphology, thermal and thermo-mechanical properties, *Materials Science and Engineering C* 32 (2012) 1790–1795.
- [19] S.T. Lim, Y.H. Hyun, C.H. Lee, H.J. Choi, Preparation and characterization of microbial biodegradable poly(3-hydroxybutyrate)/organoclay nanocomposite, *Journal of Materials Science Letters* 22 (2003) 299–302.
- [20] J.H. Chang, Y.U. An, G.S. Sur, Poly(lactic acid); Nanocomposites with Various Organoclays. I. Thermomechanical Properties, Morphology, and Gas Permeability, *Journal of Polymer Science: Part B: Polymer Physics* 41 (2003) 94–103.
- [21] D.S. Achilias, E. Panayotidou, I. Zuburtikudis, Thermal degradation kinetics and isoconversional analysis of biodegradable poly(3-hydroxybutyrate)/organomodified montmorillonite nanocomposites, *Thermochimica Acta* 514 (2011) 58–66.
- [22] Y. Ando, H. Sato, H. Shinzawa, M. Okamoto, I. Noda, Y. Ozaki, Isothermal melt crystallization behavior of neat poly(L-lactide)(PLLA) and PLLA/organically modified layered silicate (OMLS) nanocomposite studied by two-dimensional (2D) correlation spectroscopy, *Vibrational Spectroscopy* 60 (2012) 158–162.
- [23] F. Carrasco, J. Gámez-Pérez, O.O. Santana, M. Maspoch, Processing of poly(lactic acid)/organomontmorillonite nanocomposites: Microstructure, thermal stability and kinetics of the thermal decomposition, *Chemical Engineering Journal* 178 (2011) 451–460.
- [24] H. Miyagawa, M. Misra, L.T. Drzal, A.K. Mohanty, Novel biobased nanocomposites from functionalized vegetable oil and organically- modified layered silicate clay, *Polymer* 46 (2005) 445–453.
- [25] A.K. Mohapatra, S. Mohanty, S.K. Nayak, Study of Thermo-Mechanical and Morphological Behaviour of Biodegradable PLA/PBAT/Layered Silicate Blend Nanocomposites, *J Polym Environ* 22 (2014) 398–408.
- [26] M. Naffakh, C. Marco, Isothermal crystallization kinetics and melting behavior of poly (L-lactic acid)/WS2 inorganic nanotube nanocomposites, *Journal of Materials Science* 50 (2015) 6066–6074.
- [27] S.I. Marras, I. Zuburtikudis, C. Panayiotou, Solution casting versus melt compounding: effect of fabrication route on the structure and thermal behavior of poly(L-lactic acid) clay nanocomposites, *J Mater Sci* 45 (2010) 6474–6480.
- [28] C. Liza, B. Soegijono, E. Budianto, J. Alinasiri, Jayatin, Effect of Pretreatment of Oregon Layer Silicate with Surfactant Using Sonication to the Gallery of Silicate Layer for Biodegradable Nanocomposite Preparation, *Procedia Chemistry* 4 (2012) 47–52.
- [29] P. Manafi, I. Ghasemi, M. Karrabi, H. Azizi, M. Manafi, P. Ehsaninamin, Thermal stability and thermal degradation kinetics (model-free kinetics) of nanocomposites based on poly (lactic acid)/graphene: the influence of functionalization, *Polymer Bulletin* 72 (2015) 1095–1112.
- [30] S.I. Marras, K.P. Kladi, I. Tsivintzelis, I. Zuburtikudis, C. Panayiotou, Biodegradable polymer nanocomposites: The role of nanoclays on the thermomechanical characteristics and the electrospun fibrous structure, *Acta Biomaterialia* 4 (2008) 756–765.

- [31] D. Enescu, A. Frache, F. Geobaldo, Formation and oxygen diffusion barrier properties of fish gelatin/natural sodium montmorillonite clay self-assembled multilayers onto the biopolyester surface, *RSC Adv.* 5 (2015) 61465–61480.
- [32] Y. Cui, S. Kumar, B. Rao Kona, D. van Houcke, Gas barrier properties of polymer/clay nanocomposites, *RSC Adv.* 5 (2015) 63669–63690.
- [33] D. Xiao, Z. Li, X. Zhao, U. Gohs, U. Wagenknecht, B. Voit, D.-Y. Wang, Functional organoclay with high thermal stability and its synergistic effect on intumescent flame retardant polypropylene, *Applied Clay Science* 143 (2017) 192–198.
- [34] K. Friedrich, S. Fakirov, Z. Zhang, *Polymer Composites*, Springer US, Boston, MA, 2005.
- [35] D. Acierno, E. Amendola, P. Russo, Dynamic-mechanical Investigation of Melt Compounded Poly(butylterephthalate)/ organoclay Nanocomposites, *Macromol. Symp.* 247 (2007) 156–161.
- [36] T. Ahn, H.J. Suk, J. Won, M.H. Yi, Extended lifetime of pentacene thin-film transistor with polyvinyl alcohol (PVA)/layered silicate nanocomposite passivation layer, *Microelectronic Engineering* 86 (2009) 41–46.
- [37] H.M. Akil, M.F. Rasyid, J. Sharif, Effect of Compatibilizer on Properties of Polypropylene Layered Silicate Nanocomposite, *Procedia Chemistry* 4 (2012) 65–72.
- [38] S. Anandhan, H.G. Patil, R.R. Babu, Characterization of poly(ethylene-co-vinyl acetate-co-carbon monoxide)/layered silicate clay hybrids obtained by melt mixing, *J. Mater. Sci.* 46 (2011) 7423–7430.
- [39] M. Arroyo, R.V. Suárez, B. Herrero, M.A. López-Manchado, Optimisation of nanocomposites based on polypropylene/polyethylene blends and organo-bentonite, *Journal of Materials Science* 13 (2003) 2915–2921.
- [40] L. As'habi, S.H. Jafari, H.A. Khonakdar, R. Boldt, U. Wagenknecht, G. Heinrich, Tuning the processability, morphology and biodegradability of clay incorporated PLA/LLDPE blends via selective localization of nanoclay induced by melt mixing sequence, *eXPRESS Polymer Letters* 7 (2013) 21–39.
- [41] E. Ayres, R.L. Oréface, D. Sousa, Influence of Bentonite Type in Waterborne Polyurethane Nanocomposite Mechanical Properties, *Macromol. Symp.* 245-246 (2006) 330–336.
- [42] A.R. Bahramian, M. Kokabi, Ablation mechanism of polymer layered silicate nanocomposite heat shield, *Journal of Hazardous Materials* 166 (2009) 445–454.
- [43] A.R. Bahramian, M. Kokabi, M.H.N. Famili, M.H. Beheshty, High temperature ablation of kaolinite layered silicate/phenolic resin/asbestos cloth nanocomposite, *Journal of Hazardous Materials* 150 (2008) 136–145.
- [44] A.K. Barick, D.K. Tripathy, Thermal and dynamic mechanical characterization of thermoplastic polyurethane/organoclay nanocomposites prepared by melt compounding, *Materials Science and Engineering A* 527 (2010) 812–823.
- [45] S.-T. Bee, A. Hassan, C.T. Ratnam, T.-T. Tee, L.T. Sin, D. Hui, Dispersion and roles of montmorillonite on structural, flammability, thermal and mechanical behaviours of electron beam irradiated flame retarded nanocomposite, *Composites: Part B* 2014 41–48.
- [46] N.N. Bhiwankar, R.A. Weiss, Melt intercalation/exfoliation of polystyrenesodium-montmorillonite nanocomposites using sulfonated polystyrene ionomer compatibilizers, *Polymer* 2006 6684–6691.
- [47] G.L. Bohnhoff, C.D. Shackelford, Improving membrane performance via bentonite polymer nanocomposite, *Applied Clay Science* 86 (2013) 83–98.
- [48] J. Cai, Q. Yu, Y. Han, X. Zhang, L. Jiang, Thermal stability, crystallization, structure and morphology of syndiotactic 1,2-polybutadiene/organoclay nanocomposite, *European Polymer Journal* 43 (2007) 2866–2881.
- [49] J.H. Chang, Y.U. An, Nanocomposites of Polyurethane with Various Organoclays: Thermomechanical Properties, Morphology, and Gas Permeability, *Journal of Polymer Science: Part B: Polymer Physics* 40 (2002) 670–677.

- [50] J.H. Chang, S.J. Kim, Y.L. Joo, S. Im, Poly(ethylene terephthalate) nanocomposites by in situ interlayer polymerization: the thermo-mechanical properties and morphology of the hybrid fibers, *Polymer* 45 (2004) 919–926.
- [51] J.H. Chang, B.S. Seo, S.H. Kim, Blends of a Thermotropic Liquid-Crystalline Polymer and a Poly(butylene terephthalate)/Organoclay Nanocomposite, *Journal of Polymer Science: Part B: Polymer Physics* 42 (2004) 3667–3676.
- [52] J.-H. Chang, B.-S. Seo, D.-H. Hwang, An exfoliation of organoclay in thermotropic liquid crystalline polyester nanocomposites, *Polymer* 2002 2969–2974.
- [53] J.H. Chen, M.C. Yang, Preparation and characterization of nanocomposite of maleated poly(butylene adipate-co-terephthalate) with organoclay, *Materials Science and Engineering C* 46 (2015) 301–308.
- [54] F.-c. Chiu, S.-M. Lai, J.-W. Chen, P.-H. Chu, Combined Effects of Clay Modifications and Compatibilizers on the Formation and Physical Properties of Melt-Mixed Polypropylene/Clay Nanocomposites, *Journal of Polymer Science: Part B: Polymer Physics*, 42 (2004) 4139–4150.
- [55] S. Choudhary, R.J. Sengwa, Dielectric properties and structural dynamics of melt compounded hot-pressed poly(ethylene oxide)–organophilic montmorillonite clay nanocomposite films, *Bull. Mater. Sci.* 35 (2012) 19–25.
- [56] S. Choudhary, R.J. Sengwa, Dielectric dispersion and relaxation studies of melt compounded poly(ethylene oxide)/silicon dioxide nanocomposites, *Polymer Bulletin* 72 (2015) 2591–2604.
- [57] C. Chozhan, M. Alagar, R.J. Sharmila, P. Gnanasundaram, Thermo mechanical behaviour of unsaturated polyester toughened epoxy–clay hybrid nanocomposites, *J Polym Res* 14 (2007) 319–328.
- [58] L.-L. Chu, S.K. Anderson, J.D. Harris, M.W. Beach, A.B. Morgan, Styrene-acrylonitrile (SAN) layered silicate nanocomposites prepared by melt compounding, *Polymer* 45 (2004) 4051–4061.
- [59] H. Chul Koha, J.S. Park, M.A. Jeong, H.Y. Hwang, Y.T. Hongc, S.Y. Ha, S.Y. Nam, Preparation and gas permeation properties of biodegradable polymer/layered silicate nanocomposite membranes, *Desalination* 233 (2008) 201–209.
- [60] L. Cui, D.L. Hunter, P.J. Yoon, D.R. Paul, Effect of organoclay purity and degradation on nanocomposite performance, Part 2: Morphology and properties of nanocomposites, *Polymer* 49 (2008) 3762–3769.
- [61] S.A. Dadfar, I. Alemzadeh, S.R. Dadfar, M. Vosoughi, Studies on the oxygen barrier and mechanical properties of low density polyethylene/organoclay nanocomposite films in the presence of ethylene vinyl acetate copolymer as a new type of compatibilizer, *Materials and Design* 32 (2011) 1806–1813.
- [62] A. Dasari, Z.-Z. Yu, Y.-W. Mai, G.-H. Hu, J. Varlet, Clay exfoliation and organic modification on wear of nylon 6 nanocomposites processed by different routes, *Composites Science and Technology* 2005 2314–2328.
- [63] W.E. Dondero, R.E. Gorga, Morphological and Mechanical Properties of Carbon Nanotube/Polymer Composites via Melt Compounding, *Journal of Polymer Science: Part B: Polymer Physics* 44 (2006) 864–878.
- [64] Y. Dong, D. Bhattacharyya, Effects of clay type, clay/compatibiliser content and matrix viscosity on the mechanical properties of polypropylene/organoclay nanocomposites, *Composites: Part A* (2008) 1177–1191.
- [65] Y. Dong, D. Bhattacharyya, Investigation on the competing effects of clay dispersion and matrix plasticisation for polypropylene/clay nanocomposites. Part II: crystalline structure and thermo-mechanical behaviour, *J Mater Sci* 47 (2012) 4127–4137.
- [66] A. Dorigato, A. Pegoretti, M. Quaresimin, Thermo-mechanical characterization of epoxy/clay nanocomposites as matrices for carbon/nanoclay/epoxy laminates, *Materials Science and Engineering A* 528 (2011) 6324–6333.
- [67] L. Du, B. Qu, Y. Meng, Q. Zhu, Structural characterization and thermal mechanical properties of poly(propylene carbonate)/MgAl-LDH exfoliation nanocomposite via solution intercalation, *Composites Science and Technology* 2006 913–918.

- [68] M.J. Fernández, M.D. Fernández, I. Aranburu, Poly(L-lactic acid)/organically modified vermiculite nanocomposites prepared by melt compounding: Effect of clay modification on microstructure and thermal properties, *European Polymer Journal* 49 (2013) 1257–1267.
- [69] J.D. Fidelus, E. Wiesel, F.H. Gojny, K. Schulte, H.D. Wagner, Thermo-mechanical properties of randomly oriented carbon/epoxy nanocomposites, J. D. Fidelus et al. / *Composites: Part A* 36 (2005) 1555–1561.
- [70] T.D. Fornes, P.J. Yoon, D.L. Hunter, H. Keskkula, D.R. Paul, Effect of organoclay structure on nylon 6 nanocomposite morphology and properties, *Polymer* 43 (2002) 5915–5933.
- [71] D. García-López, I. Gobernado-Mitre, J.F. Fernández, J.C. Merino, J.M. Pastor, Properties of polyamide 6/clay nanocomposites processed by low cost benonite and different organic modifiers, *Polymer Bulletin* 62 (2009) 791–800.
- [72] I. Goitisoló, J.I. Eguiazábal, J. Nazabal, Structure and properties of an hybrid system based on bisphenol A polycarbonate modified by A polyamide 6/organoclay nanocomposite, *European Polymer Journal* 44 (2008) 1978–1987.
- [73] M. Hasan, A.N. Banerjee, M. Lee, Enhanced thermo-mechanical performance and strain-induced band gap reduction of TiO₂@PVC nanocomposite films, *Bull. Mater. Sci.* 38 (2015) 283–290.
- [74] M. Hasan, M. Lee, Enhancement of the thermo-mechanical properties and efficiency of mixing technique in the preparation of graphene/PVC nanocomposites compared to carbon nanotubes/PVC, *Progress in Natural Science: Materials International* 24 (2014) 579–587.
- [75] R. Jan, A. Habib, M.A. Akram, T.-u.-H. Zia, N. Khan, Uniaxial Drawing of Graphene-PVA Nanocomposites: Improvement in Mechanical Characteristics via Strain-Induced Exfoliation of Graphene, Jan et al. *Nanoscale Research Letters* 2016 1–9.
- [76] D. Kaempfer, R. Thomann, R. Mülhaupt, Melt compounding of syndiotactic polypropylene nanocomposites containing organophilic layered silicates and in situ formed core/shell nanoparticles, *Polymer* 43 (2002) 2909–2916.
- [77] A.K. Kalkar, V.D. Deshpande, B.S. Vatsaraj, Poly(butylene terephthalate)/montmorillonite nanocomposites: Effect of montmorillonite on the morphology, crystalline structure, isothermal crystallization kinetics and mechanical properties, *Thermochimica Acta* 568 (2013) 74–94.
- [78] A. Kaushik, D. Ahuja, V. Salwani, Synthesis and characterization of organically modified clay/castor oil based chain extended polyurethane nanocomposites, *Composites: Part A* 42 (2011) 1534–1541.
- [79] J.-H. Ko, C.S. Yoon, J.H. Chang, Polypropylene Nanocomposites with Various Functionalized-Multiwalled Nanotubes: Thermomechanical Properties, Morphology, Gas Permeation, and Optical Transparency, *Journal of Polymer Science: Part B: Polymer Physics* 49 (2011) 244–254.
- [80] T. Kongkhlang, Y. Kousaka, T. Umemura, D. Nakaya, W. Thuamthong, Y. Pattamamongkolchai, S. Chirachanchai, Role of primary amine in polyoxymethylene (POM)/bentonite nanocomposite formation, *Polymer* 49 (2008) 1676–1684.
- [81] E. Kontou, M. Niaounakis, Thermo-mechanical properties of LLDPE/SiO₂ nanocomposites, *Polymer* 47 (2006) 1267–1280.
- [82] M.H.A. Kudus, H.M. Akil, M.F.A. Rasyid, Muscovite-MWCNT hybrid as a potential filler for layered silicate nanocomposite, *Materials Letters* 79 (2012) 92–95.
- [83] A. Kumar, P.K. Ghosh, K.L. Yadav, K. Kumar, Thermo-mechanical and anti-corrosive properties of MWCNT/epoxy nanocomposite fabricated by innovative dispersion technique, *Composites Part B* 113 (2017) 291–299.

- [84] S.-M. Lai, W.-C. Chen, X.S. Zhu, Melt mixed compatibilized polypropylene/clay nanocomposites: Part 1 – the effect of compatibilizers on optical transmittance and mechanical properties, *Composites: Part A* 40 (2009) 754–765.
- [85] H.-C. Lee, T.-W. Lee, Y.T. Lim, O.O. Park, Improved environmental stability in poly(p-phenylene vinylene)/layered silicate nanocomposite, *Applied Clay Science* 21 (2002) 287–293.
- [86] T.-W. Lee, O.O. Park, J. Yoon, J.-J. Kim, Enhanced quantum efficiency in polymer/layered silicate nanocomposite light-emitting devices, *Synthetic Metals* 121 (2001) 1737–1738.
- [87] T.-W. Lee, O.O. Park, J. Yoon, J.-J. Kim, Polymer-Layered Silicate Nanocomposite Light-Emitting Devices, *Advanced Materials* 13 (2001).
- [88] W. Loyens, P. Jannasch, F.H.J. Maurer, Effect of clay modifier and matrix molar mass on the structure and properties of poly(ethylene oxide)/Cloisite nanocomposites via melt-compounding, *Polymer* 46 (2005) 903–914.
- [89] S. Maiti, K. Shrivastava, S. Suin, B.B. Khatua, A strategy for achieving low percolation and high electrical conductivity in melt-blended polycarbonate (PC)/multiwall carbon nanotube (MWCNT) nanocomposites: Electrical and thermo-mechanical properties, *eXPRESS Polymer Letters* 7 (2013) 505–518.
- [90] Y.P. Mamunya, V.V. Levchenko, A. Rybak, G. Boiteux, E.V. Lebedev, J. Ulanski, G. Seytre, Electrical and thermomechanical properties of segregated nanocomposites based on PVC and multiwalled carbon nanotubes, *Journal of Non-Crystalline Solids* 356 (2010) 635–641.
- [91] M. McCrary-Dennis, M.J. Uddin, O.I. Okoli, Synthesis and characterization of polystyrene carbon nanotube nanocomposite for utilization in the displaced foam dispersion methodology, *Composites Part B* 2016 484–495.
- [92] K.D. Min, M.Y. Kim, K.Y. Choi, J.H. Lee, S.-G. Lee, Effect of Layered Silicates on the Crystallinity and Mechanical Properties of HDPE/MMT Nanocomposite Blown Films, *Polymer Bulletin* 57 (2006) 101–108.
- [93] S.M. Mirabedini, M. Behzadnasab, K. Kabiri, Effect of various combinations of zirconia and organoclay nanoparticles on mechanical and thermal properties of an epoxy nanocomposite coating, *Composites: Part A* 43 (2012) 2095–2106.
- [94] J.K. Mishra, G.H. Kim, I. Kim, I.J. CHung, C.S. Ha, A new Thermoplastic Vulcanizate (TPV)/Organoclay Nanocomposite: Preparation, Characterization, and Properties, *Journal of Polymer Science: Part B: Polymer Physics* 42 (2004) 2900–2908.
- [95] J.K. Mishra, I. Kim, C.S. Ha, New Millable Polyurethane/Organoclay Nanocomposite: Preparation, Characterization and Properties, *Macromolecular Rapid Communicates* 24 (2003) 671–675.
- [96] S.C. Motshekga, S.S. Ray, M.S. Onyango, M.N. Momba, Preparation and antibacterial activity of chitosan-based nanocomposites containing bentonite-supported silver and zinc oxide nanoparticles for water disinfection, *Applied Clay Science* 114 (2015) 330–339.
- [97] S. Nam, H. Woo Cho, T. Kim, D. Kim, B. June Sung, S. Lim, H. Kim, Effects of silica particles on the electrical percolation threshold and thermomechanical properties of epoxy/silver nanocomposite, *Applied Physics Letters* 99 (2011).
- [98] S. Nguyen, D. Rouxel, B. Vincent, L. Badie, F.D.D. Santos, E. Lamouroux, Y. Fort, Influence of cluster size and surface functionalization of ZnO nanoparticles on the morphology, thermomechanical and piezoelectric properties of P(VDF-TrFE) nanocomposite films, *Applied Surface Science* 279 (2013) 204–211.
- [99] E. Onder, N. Sarier, M. Ersoy, The manufacturing of polyamide- and polypropylene-organoclay nanocomposite filaments and their suitability for textile applications, *Thermochimica Acta* 543 (2012) 37–58.
- [100] M.A. Osman, V. Mittal, U.W. Suter, Poly(propylene)-Layered Silicate Nanocomposites: Gas Permeation Properties and Clay Exfoliation, *Macromolecular Chemistry and Physics* (2007) 68–75.

- [101] M.A. Osman, J.E.P. Pupp, U.W. Suter, Effect of non-ionic surfactants on the exfoliation and properties of polyethylene-layered silicate nanocomposites, *Polymer* 2005 8202–8209.
- [102] C. Özdilek, B. Norder, S.J. Picken, A study of the thermo-mechanical behavior of Boehmite-polyamide-6 nanocomposites, *Thermochimica Acta* 472 (2008) 31–37.
- [103] C.M. Paranhos, K. Dahmouche, S. Zaioncz, B.G. Soares, L.A. Pessan, Relationships between Nanostructure and Thermomechanical Properties in Poly(vinyl alcohol)/Montmorillonite Nanocomposite with Entrapped Polyelectrolyte, *Journal of Polymer Science: Part B: Polymer Physics* 46 (2008) 2618–2629.
- [104] C.I. Park, O.O. Park, J.G. Lim, H.J. Kim, The fabrication of syndiotactic polystyrene/organophilic clay nanocomposites and their properties, *Polymer* 42 (2001) 7465–7475.
- [105] D.R. Paul, L.M. Robeson, Polymer nanotechnology: Nanocomposites, *Polymer* 49 (2008) 3187–3204.
- [106] R.A. Paz, E.M. Araujo, L.A. Pessan, T.J.A. Melo, A.D. Leite, V.d.N. Medeiros, Evaluation of Impact Strength of Polyamide 6/Bentonite Clay Nanocomposites, *Materials Research* 15 (2012) 506–509.
- [107] R.A.d. Paz, A.M.D. Leite, E.M. Araújo, V.d.N. Medeiros, Melo, Tomás Jeferson Alves de, L.A. Pessan, Mechanical and thermomechanical properties of polyamide 6/Brazilian organoclay nanocomposites, *Polímeros* 26 (2016) 52–60.
- [108] P. Pokharel, B. Pant, K. Pokhrel, H.R. Pant, J.-g. Lim, D.S. Lee, H.-Y. Kim, S. Choi, Effects of functional groups on the graphene sheet for improving the thermomechanical properties of polyurethane nanocomposites, *Composites Part B* 78 (2015) 192–201.
- [109] S. Ponnuvel, T.V. Moorthy, Investigation on the influence of multi walled carbon nanotubes on delamination in drilling epoxy/glass fabric polymeric nanocomposite, *Procedia Engineering* 2013 735–744.
- [110] M. Preghenella, A. Pegoretti, C. Migliaresi, Thermo-mechanical characterization of fumed silica-epoxy nanocomposites, *Polymer* 46 (2005) 12065–12072.
- [111] A. Rapacz-Kmita, N. Moskala, M. Dudek, M. Gajek, Mandecka-Kamień, INFLUENCE OF THE ORGANOPHILISATION PROCESS ON PROPERTIES OF THE BENTONITE FILLER AND MECHANICAL PROPERTIES OF THE CLAY/EPOXY NANOCOMPOSITE S, *Arch. Metall. Mater.* 61 (2016) 875–880.
- [112] Rath, Sangram, K., M. Patri, D.V. Khakhar, Structure–thermomechanical property correlation of moisture cured poly(urethane-urea)/clay nanocomposite coatings, *Progress in Organic Coatings* 75 (2012) 264–273.
- [113] D. Ratna, S. Divekar, A.B. Samui, B.C. Chakraborty, A.K. Banthia, Poly(ethylene oxide)/clay nanocomposite: Thermomechanical properties and morphology, *Polymer* 47 (2006) 4068–4074.
- [114] S.S. Ray, J. Bandyopadhyay, M. Bousmina, Thermal and thermomechanical properties of poly[(butylene succinate)-co-adipate] nanocomposite, *Polymer Degradation and Stability* 92 (2007) 802–812.
- [115] S.S. Ray, K. Okamoto, P. Maiti, M. Okamotoa, New Poly(butylene succinate)/Layered Silicate Nanocomposites: Preparation and Mechanical Properties, *J nanosci nanotechnol* 2 (2002) 171–176.
- [116] P. Reichert, H. Nitz, S. Klinke, R. Brandsch, R. Thomann, R. Mülhaupt, Poly(propylene)/organoclay nanocomposite formation: Influence of compatibilizer functionality and organoclay modification, *Macromolecular Materials and Engineering* 275 (2000) 8–17.
- [117] S.A. Sadrani, S.A.A. Ramazani, S.E. Khorshidiyeh, N.J. Esfad, Preparation of UHMWPE/carbon black nanocomposites by in situ Ziegler–Natta catalyst and investigation of product thermo-mechanical properties, *Polymer Bulletin* 73 (2016) 1085–1101.
- [118] P. Sanguansat, T. Amornsakchai, Effect of matrix morphology on mechanical and barrier properties of polypropylene nanocomposite films containing preferentially aligned organoclay platelets, *J Polym Res* 22 (2015) 30.

- [119] R.J. Sengwa, S. Clouthary, Dielectric properties and structural dynamics of melt compounded hot-pressed poly(ethylene oxide)-organophilic montmorillonite clay nanocomposite films, *Bull. Mater. Sci.* 35 (2012) 19–25.
- [120] M. Shabanian, Z. Mirzakhani, N. Basaki, H.A. Khonakdar, K. Faghihi, F. Hoshyargar, U. Wagenknecht, Flammability and thermal properties of novel semi aromatic polyamide/organoclay nanocomposite, *Thermochimica Acta* 585 (2014) 63–70.
- [121] M. Shafiee, S.A. Ramazani, Investigation of Barrier Properties of Poly(ethylene vinyl acetate)/Organoclay Nanocomposite Films Prepared by Phase Inversion Method, *Macromolecular Symposia* 274 (2008) 1–5.
- [122] F. Shiravand, J.M. Hutchinson, Y. Calventus, A novel comparative study of different layered silicate clay types on exfoliation process and final nanostructure of trifunctional epoxy nanocomposites, *Polymer Testing* 2016 148–155.
- [123] S. Siengchin, J. Karger-Kocsis, R. Thomann, Nanofilled and/or toughened POM composites produced by water-mediated melt compounding: Structure and mechanical properties, *eXPRESS Polymer Letters* 2 (2008) 746–756.
- [124] L. Song, Y. Hu, Z. Lin, S. Xuan, S. Wang, Z. Chen, W. Fan, Preparation and properties of halogen-free flame-retarded polyamide 6/organoclay nanocomposite, *Polymer Degradation and Stability* 86 (2004) 535–540.
- [125] L. Song, Y. Hu, Y. Tang, R. Zhang, Z. Chen, W. Fan, Study of the properties of flame retardant polyurethane/organoclay nanocomposite, *Polymer Degradation and Stability* 87 (2005) 111–116.
- [126] M. Song, H.S. Xia, K.J. Yao, D.J. Hourston, A study on phase morphology and surface properties of polyurethane/organoclay nanocomposite, *European Polymer Journal* 41 (2005) 259–266.
- [127] M.-K. Song, S.-B. Park, Y.-T. Kim, K.-H. Kim, S.-K. Min, H.-W. Rhee, Characterization of polymer-layered silicate nanocomposite membranes for direct methanol fuel cells, *Electrochimica Acta* 50 (2004) 639–643.
- [128] M.A. Soto-Oviedo, O.A. Araújo, R. Faez, M.C. Rezende, M.A. de Paoli, Antistatic coating and electromagnetic shielding properties of a hybrid material based on polyaniline/organoclay nanocomposite and EPDM rubber, *Synthetic Metals* 156 (2006) 1249–1255.
- [129] V.S. Souza, O. Bianchi, M.F.S. Lima, R.S. Mauler, Morphological, thermomechanical and thermal behavior of epoxy/MMT nanocomposites, *Journal of Non-Crystalline Solids* 400 (2014) 58–66.
- [130] J. Tan, X. Wang, Y. Luo, D. Jia, Rubber/clay nanocomposites by combined latex compounding and melt mixing: A masterbatch process, *Materials and Design* 34 (2012) 825–831.
- [131] P.L. Teh, Z.A.M. Ishak, A.S. Hashim, J. Karger-Kocsis, U.S. Ishiaku, Effects of epoxidized natural rubber as a compatibilizer in melt compounded natural rubber–organoclay nanocomposites, *European Polymer Journal* 40 (2004) 2513–2521.
- [132] R. Tessier, E. Lafranche, P. Krawczak, Development of novel melt-compounded starch-grafted polypropylene/polypropylene-grafted maleic anhydride/organoclay ternary hybrids, *eXPRESS Polymer Letters* 6 (2011) 937–952.
- [133] Y. Turhan, Z.G. Alp, M. Alkan, M. Doğan, Preparation and characterization of poly(vinylalcohol)/modified bentonite nanocomposites, *Microporous and Mesoporous Materials* 174 (2013) 144–153.
- [134] S. Varghese, J. Karger-Kocsis, K.G. Gatos, Melt compounded epoxidized natural rubber/layered silicate nanocomposites: structure-properties relationships, *Polymer* 44 (2003) 3977–3983.
- [135] D. Vennerberg, R. Hall, M.R. Kessler, Supercritical carbon dioxide-assisted silanization of multi-walled carbon nanotubes and their effect on the thermo-mechanical properties of epoxy nanocomposites, *Polymer* 55 (2014) 4156–4163.

- [136] M. Vlacha, A. Giannakas, P. Katapodis, H. Stamatis, A. Ladavos, N.-M. Barkoula, On the efficiency of oleic acid as plasticizer of chitosan/clay nanocomposites and its role on thermo-mechanical, barrier and antimicrobial properties - Comparison with glycerol, *Food Hydrocolloids* 57 (2016) 10–19.
- [137] K. Wang, S. Liang, Q. Zhang, R. Du, Q. Fu, An Observation of Accelerated Exfoliation in iPP/Organoclay Nanocomposite as Induced by Repeated Shear during Melt Solidification, *Journal of Polymer Science: Part B: Polymer Physics* 2005 2005–2012.
- [138] L. Wang, Y.-B. Yan, Q.-Q. Yang, J. Yu, Z.-X. Guo, Polyamide 66/organoclay nanocomposite fibers prepared by electrospinning, *J Mater Sci* 47 (2012) 1702–1709.
- [139] X. Wang, L. Yang, J. Zhang, C. Wang, Q. Li, Preparation and characterization of chitosan-poly(vinyl alcohol)/bentonite nanocomposites for adsorption of Hg(II) ions, *Chemical Engineering Journal* 251 (2014) 404–412.
- [140] Y.-P. Wu, Y. Ma, Y.-Q. Wang, L.-Q. Zhang, Effects of Characteristics of Rubber, Mixing and Vulcanization on the Structure and Properties of Rubber/Clay Nanocomposites by Melt Blending, *Macromolecular Materials and Engineering* 289 (2004) 890–894.
- [141] S. Xie, S. Zhang, F. Wang, M. Yang, R. Séguéla, J.-M. Lefebvre, Preparation, structure and thermomechanical properties of nylon-6 nanocomposites with lamella-type and fiber-type sepiolite, *Composites Science and Technology* 67 (2007) 2334–2341.
- [142] B. Xu, Y.Q. Fu, M. Ahmad, J.K. Luo, W.M. Huang, A. Kraft, R. Reuben, Y.T. Pei, Z.G. Chen, De Hosson, J. Th. M., Thermo-mechanical properties of polystyrene-based shape memory nanocomposites, *Journal of Materials Chemistry* 20 (2010) 3442–3448.
- [143] D. Xu, J. Karger-Kocsis, Dry rolling and sliding friction and wear of organophilic layered silicate/hydrogenated nitrile rubber nanocomposite, *J Mater Sci* 45 (2010) 1293–1298.
- [144] K. Xu, G. Chen, J. Shen, Exfoliation and dispersion of micrometer-sized LDH particles in poly(ethylene terephthalate) and their nanocomposite thermal stability, *Applied Clay Science* 2013 114–119.
- [145] S. Xu, W. Yu, X. Yao, Q. Zhang, Q. Fu, Nanocellulose-assisted dispersion of graphene to fabricate poly(vinyl alcohol)/graphene nanocomposite for humidity sensing, *Composites Science and Technology* 2016 67–76.
- [146] J.-M. Yeh, K.-C. Chang, Polymer/layered silicate nanocomposite anticorrosive coatings, *Journal of Industrial and Engineering Chemistry* 14 (2008) 275–291.
- [147] J.-M. Yeh, K.-C. Chang, C.-W. Peng, M.-C. Lai, Effect of dispersion capability of organoclay on cellular structure and physical properties of PMMA/clay nanocomposite foams, *Materials Chemistry and Physics* 115 (2009) 744–750.
- [148] B.-S. Yim, J.-M. Kim, Effect of multi-walled carbon nanotube (MWCNT) concentration on thermomechanical reliability of MWCNT-reinforced solderable isotropic polymer nanocomposites, *J Mater Sci: Mater Electron* 27 (2016) 9159–9171.
- [149] Z. Ying, L. Xianggao, C. Bin, C. Fei, F. Jing, Highly exfoliated epoxy/clay nanocomposites: Mechanism of exfoliation and thermal/mechanical properties, *Composite Structures* 2015 44–49.
- [150] O. Yucel, E. Unsal, J. Harvey, M. Graham, D.H. Jones, M. Cakmak, Enhanced gas barrier and mechanical properties in organoclay reinforced multi-layer poly(amide-imide) nanocomposite film, *Polymer* 55 (2014) 4091–4101.
- [151] M. Kracalik, S. Laske, M. Feuchter, G. Pinter, G. Maier, W. Märzinger, M. Haberkorn, G. R. Langecker: FT-NIR as a new determination method for polymer nanocomposites, report for Austrian NANO Initiative, Project NanoComp – 0901 PlaComp
- [152] Faculty of technology, Tomas Bata University in Zlin, Czech Republic

- [153] Liu Zhirong, Md. Azhar Uddin, Sun Zhanxue FT-IR and XRD analysis of natural Na-bentonite and Cu(II)-loaded Na-bentonite *Spectrochimica Acta Part A: Molecular and Biomolecular Spectroscopy* Volume 79, Issue 5, September 2011, Pages 1013-1016
- [154] www.clariant.com.
- [155] A. Dimirkou, A. Ioannou, M. Doula: Preparation, characterization and sorption properties for phosphates of hematite, bentonite and bentonite–hematite systems, *Advances in Colloid and Interface Science*, Volume 97, Issues 1–3, 29 March 2002, Pages 37-61
- [156] J. Cuppoletti (Ed.), *Nanocomposites and Polymers with Analytical Methods*, InTech, 2011.
- [157] S. Sinha Ray, M. Okamoto, *Polymer/layered silicate nanocomposites: A review from preparation to processing*, *Progress in Polymer Science* 28 (2003) 1539–1641.
- [158] *Clay-Containing Polymer Nanocomposites*, Elsevier, 2013.
- [159] C.H. Davis, L.J. Mathias, J.W. Gilman, D.A. Schiraldi, J.R. Shields, P. Trulove, T.E. Sutto, H.C. Delong, Effects of melt-processing conditions on the quality of poly(ethylene terephthalate) montmorillonite clay nanocomposites, *J. Polym. Sci. B Polym. Phys.* 40 (2002) 2661–2666.
- [160] R. Krishnamoorti, R.A. Vaia, E.P. Giannelis, *Structure and Dynamics of Polymer-Layered Silicate Nanocomposites*, *Chem. Mater.* 8 (1996) 1728–1734.
- [161] M. Al-Samhan, J. Samuel, F. Al-Attar, G. Abraham, *Comparative Effects of MMT Clay Modified with Two Different Cationic Surfactants on the Thermal and Rheological Properties of Polypropylene Nanocomposites*, Hindawi (2017).
- [162] S. Bocchini, H.A. Patel, A. Frache, One-pot synthesis of hexadecyl modified layered magnesium silicate and polyethylene based nanocomposite preparation, *Applied Clay Science* 80-81 (2013) 320–325.
- [163] L. Cui, D.M. Khrarov, C.W. Bielawski, D.L. Hunter, P.J. Yoon, D.R. Paul, Effect of organoclay purity and degradation on nanocomposite performance, Part1: Surfactant degradation, *Polymer* 49 (2008) 3751–3761.
- [164] N.T. Dintcheva, F.P. La Mantia, *Thermo-Mechanical Degradation of LDPE-Based Nanocomposites*, *Macromolecular Materials and Engineering* 292 (2007) 855–862.
- [165] A. Ghanbari, M.C. Heuzey, P.J. Carreau, M.T. Ton-That, A novel approach to control thermal degradation of PET/organoclay nanocomposites and improve clay exfoliation, *Polymer* 2013 1361–1369.
- [166] A. Ghanbari, M.-C. Heuzey, P.J. Carreau, M.-T. Ton-That, Morphological and rheological properties of PET/clay nanocomposites, *Rheol Acta* (2013) 59–74.
- [167] P. Liborio, V.A. Oliveira, Marques, Maria de Fatima V., New chemical treatment of bentonite for the preparation of polypropylene nanocomposites by melt intercalation, *Applied Clay Science* 111 (2015) 44–49.
- [168] M.K. Mun, J.-C. Kim, J.H. Chang, Preparation of poly(ethylene terephthalate) nanocomposite fibers incorporating a thermally stable organoclay, *Polymer Bulletin* 57 (2006) 797–804.
- [169] H. Wang, T. Zhao, L. Zhi, Y. Yan, Y. Yu, Synthesis of Novolac/Layered Silicate Nanocomposites by Reaction Exfoliation Using Acid-Modified Montmorillonite, *Macromol. Rapid Commun.* (2002) 44–48.
- [170] M. Wang, J.H. Yu, A.J. Hsieh, G.C. Rutledge, Effect of tethering chemistry of cationic surfactants on clay exfoliation, electrospinning and diameter of PMMA/clay nanocomposite fibers, *Polymer* 2010 6295–6302.
- [171] S. Zulfiqar, M.I. Sarwar, Synthesis and Characterization of Aromatic-Aliphatic Polyamide Nanocomposite Films Incorporating a Thermally Stable Organoclay, *Nanoscale Res. Lett.* 4 (2009) 391–399.
- [172] M. Kráčalík, J. Mikešová, R. Puffr, J. Baldrian, R. Thomann, C. Friedrich, Effect of 3D structures on recycled PET/organoclay nanocomposites, *Polym. Bull.* 58 (2007) 313–319.

- [173] M. Kráčalík, M. Studenovský, J. Mikešová, J. Kovářová, A. Sikora, R. Thomann, C. Friedrich, Recycled PET-organoclay nanocomposites with enhanced processing properties and thermal stability, *J. Appl. Polym. Sci.* 106 (2007) 2092–2100.
- [174] M. Kráčalík, M. Studenovský, J. Mikešová, A. Sikora, R. Thomann, C. Friedrich, I. Fortelný, J. Šimoník, Recycled PET nanocomposites improved by silanization of organoclays, *J. Appl. Polym. Sci.* 106 (2007) 926–937.
- [175] M. Kracalik, S. Laske, M. Gschweidl, W. Friesenbichler, G.R. Langecker, Advanced compounding: Extrusion of polypropylene nanocomposites using the melt pump, *J. Appl. Polym. Sci.* 113 (2009) 1422–1428.
- [176] F. Gao, Clay/polymer composites: The story, *Materials Today* 7 (2004) 50–55.
- [177] F.J. Baltá Calleja, C.G. Vonk, X-ray scattering of synthetic polymers, Elsevier, Amsterdam, 1989.
- [178] C.A. Taylor, X-ray diffraction methods in polymer science by L. E. Alexander, *Acta Cryst A* 26 (1970) 700–701.
- [179] O. Glatter, Small angle x-ray scattering, second. print, Academic Press, London, New York, 1983.
- [180] P. Fratzl, Small-angle scattering in materials science - a short review of applications in alloys, ceramics and composite materials, *J Appl Crystallogr* 36 (2003) 397–404.
- [181] N. Stribeck, W. Ruland, B. Smarsly, Scattering methods and the properties of polymer materials, Springer, Berlin, New York, 2005.
- [182] R.A. Vaia, W. Liu, H. Koerner, Analysis of small-angle scattering of suspensions of organically modified montmorillonite: Implications to phase behavior of polymer nanocomposites, *J. Polym. Sci. B Polym. Phys.* 41 (2003) 3214–3236.
- [183] R.D. Davis, A.J. Bur, M. McBrearty, Y.-H. Lee, J.W. Gilman, P.R. Start, Dielectric spectroscopy during extrusion processing of polymer nanocomposites: a high throughput processing/characterization method to measure layered silicate content and exfoliation, *Polymer* 2004 6487–6493.
- [184] R. Casini, G. Papari, A. Andreone, D. Marrazzo, A. Patti, P. Russo, Dispersion of carbon nanotubes in melt compounded polypropylene based composites investigated by THz spectroscopy, *Optics Express* 23 (2015).
- [185] A.J. Bur, Y.-H. Lee, S.C. Roth, P.R. Start, Measuring the extent of exfoliation in polymer/clay nanocomposites using real-time process monitoring methods*, *Polymer* 2005 10908–10918.
- [186] J.M. Barbas, A.V. Machado, J.A. Covas, In-line near-infrared spectroscopy for the characterization of dispersion in polymer-clay nanocomposites, *Polymer Testing* 31 (2012) 527–536.
- [187] I. Alig, D. Fischer, D. Lellinger, B. Steinhoff, Combination of NIR, Raman, Ultrasonic and Dielectric Spectroscopy for In-Line Monitoring of the Extrusion Process, *Macromol. Symp.* 230 (2005) 51–58.
- [188] S.E. Barnes, E.C. Brown, M.G. Sibley, H.G.M. Edwards, I.J. Scowen, P.D. Coates, Vibrational spectroscopic and ultrasound analysis for in-process characterization of high-density polyethylene/polypropylene blends during melt extrusion, *Applied spectroscopy* 59 (2005) 611–619.
- [189] E. Bugnicourt, T. Kehoe, M. Latorre, C. Serrano, S. Philippe, M. Schmid, Recent Prospects in the Inline Monitoring of Nanocomposites and Nanocoatings by Optical Technologies, *Nanomaterials (Basel, Switzerland)* 6 (2016).
- [190] M.G. Hansen, S. Vedula, In-line fiber-optic near-infrared spectroscopy: Monitoring of rheological properties in an extrusion process. Part I, *J. Appl. Polym. Sci.* 68 (1998) 859–872.
- [191] M. Watari, A Review of Online Real-Time Process Analyses of Melt-State Polymer Using the Near-Infrared Spectroscopy and Chemometrics, *Applied Spectroscopy Reviews* 49 (2013) 462–491.

- [192] S. Laske, A. Witschnig, M. Kracalik, M. Feuchter, G. Pinter, G. Maier, G.R. Langecker, C. Holzer, IN-LINE QUALITY CONTROL OF POLYMER NANOCOMPOSITES USING NEAR-INFRARED SPECTROSCOPY, NANOCON 2009, CONFERENCE PROCEEDINGS (2009) 120+.
- [193] i-RED Infrarot Systeme GmbH.
- [194] S. Laske, M. Kracalik, M. Feuchter, G. Pinter, G. Maier, W. Märzinger, M. Haberkorn, G.R. Langecker, FT-NIR as a determination method for reinforcement of polymer nanocomposites, *J. Appl. Polym. Sci.* 114 (2009) 2488–2496.
- [195] R.G. Brereton, *Chemometrics: Data analysis for the laboratory and chemical plant*, Repr, Wiley, Chichester, 2006.
- [196] I. Cox, *Discovering partial least squares with JMP*, SAS Institute, Cary, NC, 2013.
- [197] S. Laske, M. Kracalik, M. Gschweilt, M. Feuchter, G. Maier, G. Pinter, R. Thomann, W. Friesenbichler, G.R. Langecker, Estimation of reinforcement in compatibilized polypropylene nanocomposites by extensional rheology, *J. Appl. Polym. Sci.* 111 (2009) 2253–2259.
- [198] M. Kracalik, S. Laske, C. Holzer, FROM MICRO TO ADVANCED COMPOUNDING: THE WAY FOR APPLICATIONS OF POLYMER NANOCOMPOSITES, NANOCON 2009, CONFERENCE PROCEEDINGS (2009) 113–119.
- [199] M. Kracalik, S. Laske, C. Holzer, Extensional Rheology as Effective Tool for Characterization of Polymer Nanocomposites, *Novel Trends in Rheology IV* 1375 (2011).
- [200] M. Kracalik, S. Laske, A. Witschnigg, C. Holzer, Elongational and shear flow in polymer-clay nanocomposites measured by on-line extensional and off-line shear rheometry, *Rheol Acta* 50 (2011) 937–944.
- [201] M. Kracalik, S. Laske, A. Witschnigg, C. Holzer, Effect of the Mixture Composition on Shear and Extensional Rheology of Recycled PET and ABS Nanocomposites, *Macromol. Symp.* 311 (2012) 33–40.
- [202] A. Witschnigg, S. Laske, M. Kracalik, M. Feuchter, G. Pinter, G. Maier, W. Märzinger, M. Haberkorn, G.R. Langecker, C. Holzer, In-line characterization of polypropylene nanocomposites using FT-NIR, *J. Appl. Polym. Sci.* 8 (2010) n/a-n/a.
- [203] A. Witschnigg, S. Laske, M. Kracalik, C. Holzer, Influence of induced shear work on the properties of polyolefine nanocomposite pipes, *Polym. Eng. Sci.* 52 (2012) 1155–1160.
- [204] P. Pötschke, T.D. Fornes, D.R. Paul, Rheological behavior of multiwalled carbon nanotube/polycarbonate composites, *Polymer* 43 (2002) 3247–3255.
- [205] M.R. Nobile, G.P. Simon, O. Valentino, M. Morcom, Rheological and Structure Investigation of Melt Mixed Multi-Walled Carbon Nanotube/PE Composites, *Macromol. Symp.* 247 (2007) 78–87.
- [206] J.K. Mishra, K.-J. Hwang, C.-S. Ha, Preparation, mechanical and rheological properties of a thermoplastic polyolefin (TPO)/organoclay nanocomposite with reference to the effect of maleic anhydride modified polypropylene as a compatibilizer, *Polymer* 46 (2005) 1995–2002.
- [207] F. Samyn, S. Bourbigot, C. Jama, S. Bellayer, S. Nazare, R. Hull, A. Castrovinci, A. Fina, G. Camino, Crossed characterisation of polymer-layered silicate (PLS) nanocomposite morphology: TEM, X-ray diffraction, rheology and solid-state nuclear magnetic resonance measurements, *European Polymer Journal* 44 (2008) 1642–1653.
- [208] A. Samakande, R.D. Sanderson, P.C. Hartmann, Rheological properties of RAFT-mediated poly(styrene-co-butyl acrylate)–clay nanocomposites [P(S-co-BA)-PCNs]: Emphasis on the effect of structural parameters on thermo-mechanical and melt flow behaviors, *Polymer* 50 (2009) 42–49.

- [209] H. Sadeghipour, H. Ebadi-Dehaghani, D. Ashouri, S. Mousavian, M. Hashemi-Fesharaki, M.S. Gahrouei, Effects of modified and non-modified clay on the rheological of high density polyethylene, *Composites: Part B* (2013) 164–171.
- [210] Q. Liu, D. Chen, Viscoelastic behaviors of poly(ϵ -caprolactone)/attapulgite nanocomposites, *European Polymer Journal* 44 (2008) 2046–2050.
- [211] R. Krishnamoorti, E.P. Giannelis, Rheology of End-Tethered Polymer Layered Silicate Nanocomposites, *Macromolecules* 30 (1997) 4097–4102.
- [212] R. Krishnamoorti, I. Banik, L. Xu, Rheology and processing of polymer nanocomposites, *Reviews in Chemical Engineering* 26 (2010) 354.
- [213] M. Kráčalík, L. Pospíšil, M. Šlouf, J. Mikešová, A. Sikora, J. Šimoník, I. Fortelný, Recycled poly(ethylene terephthalate) reinforced with basalt fibres: Rheology, structure, and utility properties, *Polym. Compos.* 29 (2008) 437–442.
- [214] J. Li, C. Zhou, G. Wang, D. Zhao, Study on rheological behavior of polypropylene/clay nanocomposites, *J. Appl. Polym. Sci.* 89 (2003) 3609–3617.
- [215] M.H. Lee, C.H. Dan, J.H. Kim, J. Cha, S. Kim, Y. Hwang, C.H. Lee, Effect of clay on the morphology and properties of PMMA/poly (styrene-co-acrylonitrile)/clay nanocomposites prepared by melt mixing, *Polymer* 47 (2006) 4359–4369.
- [216] C.H. Lee, S.T. Lim, Y.H. Hyun, H.J. Choi, M.S. Jhon, Fabrication and viscoelastic properties of biodegradable polymer/organophilic clay nanocomposites, *Journal of Materials Science Letters* 22 (2003) 53–55.
- [217] K.S. Santos, S.A. Liberman, R.S. Mauler, Polyolefin-Based Nanocomposite: The Effect of Organoclay Modifier, *Journal of Polymer Science: Part B: Polymer Physics* 46 (2008) 2519–2531.
- [218] X. Zhang, G. Yang, J. Lin, Synthesis, Rheology, and Morphology of Nylon-11/Layered Silicate Nanocomposite, *Journal of Polymer Science: Part B: Polymer Physics* 44 (2006) 2161–2172.
- [219] D. Wu, L. Wu, Y. Sun, M. Zhang, Rheological properties and crystallization behavior of multi-walled carbon nanotube/poly(ϵ -caprolactone) composites, *J. Polym. Sci. B Polym. Phys.* 45 (2007) 3137–3147.
- [220] M. Wang, X. Fan, Thitsartarn W., He C., Rheological and mechanical properties of epoxy/clay nanocomposites with enhanced tensile and fracture toughnesses, *Polymer* (2014) 43–52.
- [221] Y. Zhong, Z. Zhu, S.-Q. Wang, Synthesis and rheological properties of polystyrene/layered silicate nanocomposite, *Polymer* 46 (2005).
- [222] Y. Zhao, H.-X. Huang, Dynamic rheology and microstructure of polypropylene/clay nanocomposites prepared under Sc-CO₂ by melt compounding, *Polymer Testing* 27 (2008) 129–134.
- [223] J. Zhao, A.B. Morgan, J.D. Harris, Rheological characterization of polystyrene-clay nanocomposites to compare the degree of exfoliation and dispersion, *Polymer* 2005 8641–8660.
- [224] R. Wagener, T.J.G. Reisinger, A rheological method to compare the degree of exfoliation of nanocomposites, *Polymer* 2003 7513–7518.
- [225] S. Trinkle, C. Friedrich, Van Gorp-Palmen-plot: A way to characterize polydispersity of linear polymers, *Rheologica Acta* 40 (2001) 322–328.
- [226] M.R. Thompson, K.K. Yeung, Recyclability of a layered silicate - thermoplastic olefin elastomer nanocomposite, *Polymer Degradation and Stability* 91 (2006) 2396–2407.
- [227] S. Thomas, R. Muller, J. Abraham, *Rheology and Processing of Polymer Nanocomposites*, John Wiley & Sons, Inc, Hoboken, NJ, USA, 2016.

- [228] J. Vermant, S. Ceccia, M.K. Dolgovskij, P.L. Maffettone, C.W. Macosko, Quantifying dispersion of layered nanocomposites via melt rheology, *Journal of Rheology* 51 (2007) 429–450.
- [229] L.A. Utracki, C.A. Wilkie, *Polymer blends handbook*, second. ed., Springer, Dordrecht, 2014.
- [230] S. Trinkle, P. Walter, C. Friedrich, Van Gorp-Palmen Plot II - classification of long chain branched polymers by their topology, *Rheologica Acta* 41 (2002) 103–113.
- [231] J.S. Choi, S.T. Lim, H.J. Choi, A. Pozsgay, L. Százdi, B. Pukanszky, Viscoelastic properties of exfoliated polyamide-6/layered silicate nanocomposite, *J. Mater. Sci.* 41 (2006) 1843–1846.
- [232] W. Chen, H. Lu, S.R. Nutt, The influence of functionalized MWCNT reinforcement on the thermomechanical properties and morphology of epoxy nanocomposites, *Composites Science and Technology* 68 (2008) 2535–2542.
- [233] P. Cassagnau, Melt rheology of organoclay and fumed silica nanocomposites, *Polymer* 49 (2008) 2183–2196.
- [234] J.W. Chung, K.S. Oh, S.-Y. Kwak, Evaluation of the Degree of Exfoliation in Poly(ϵ -caprolactone)/Organoclay Nanocomposites Based on Viscoelastic Relaxation, *Macromol. Mater. Eng.* 2007 627–633.
- [235] J.D. Ferry, *Introduction to polymer viscoelasticity*, John J. Aklonis and William J. MacKnight, Wiley-Interscience, New York, 1983, 295 pp. Price: \$39.95, *J. Polym. Sci. B Polym. Lett. Ed.* 21 (1983) 958–959.
- [236] M. Faghihi, A. Shojaei, R. Bagheri, Characterization of polyamide 6/carbon nanotube composites prepared by melt mixing-effect of matrix molecular weight and structure, *Composites: Part B* 78 (2015) 50–64.
- [237] Drozdov A.D., Høg Lejre A.-L., Christiansen J. deC., Viscoelasticity, viscoplasticity, and creep failure of polypropylene/clay nanocomposites, *Composites Science and Technology* (2009) 2596–2603.
- [238] J. Ahmed, R. Auras, T. Kijchavengkul, S.K. Varshney, Rheological, thermal and structural behavior of poly(ϵ -caprolactone) and nanoclay blended films, *Journal of Food Engineering* (2012) 580–589.
- [239] S. Agarwal, R. Salovey, Model filled polymers. XV: The effects of chemical interactions and matrix molecular weight on rheology, *Polym. Eng. Sci.* 35 (1995) 1241–1251.
- [240] M. Abdel-Goad, Rheological characterization of melt compounded polypropylene/clay nanocomposites, *Composites Part B* 42 (2011) 1044–1047.
- [241] R.K. Ayyer, A.I. Leonov, Comparative rheological studies of polyamide-6 and its low loaded nanocomposite based on layered silicates, *Rheol. Acta* 43 (2004) 283–292.
- [242] F.J. Carrión, A. Arribas, M.-D. Bermúdez, A. Guillamon, Physical and tribological properties of a new polycarbonate-organoclay nanocomposite, *European Polymer Journal* 44 (2008) 968–977.
- [243] D.J. Carastan, N.R. Demarquette, A. Vermogen, K. Masenelli-Varlot, Linear viscoelasticity of styrenic block copolymers–clay nanocomposites, *Rheol. Acta* (2008) 521–536.
- [244] E. Burgaz, Poly(ethylene-oxide)/clay/silica nanocomposites: Morphology and thermomechanical properties, *Polymer* 52 (2011) 5118–5126.
- [245] X. Fu, S. Qutubuddin, Polymer–clay nanocomposites: exfoliation of organophilic montmorillonite nanolayers in polystyrene, *Polymer* 42 (2001) 807–813.
- [246] K. Ke, Y. Wang, X.-Q. Liu, J. Cao, Y. Luo, W. Yang, B.-H. Xie, M.-B. Yang, A comparison of melt and solution mixing on the dispersion of carbon nanotubes in a poly(vinylidene fluoride) matrix, *Composites: Part B* 43 (2012) 1425–1432.
- [247] Y.-H. Hu, C.-Y. Chen, C.-C. Wang, Viscoelastic properties and thermal degradation kinetics of silica/PMMA nanocomposites, *Polymer Degradation and Stability* 84 (2004) 545–553.

- [248] H.B. Kim, J.S. Choi, C.H. Lee, S.T. Lim, M.S. Jhon, H.J. Choi, Polymer blend/organoclay nanocomposite with poly(ethylene oxide) and poly(methyl methacrylate), *European Polymer Journal* 41 (2005) 679–685.
- [249] M. Kráčalik, L. Pospíšil, M. Šlouf, J. Mikešová, A. Sikora, J. Šimoník, I. Fortelný, Effect of glass fibers on rheology, thermal and mechanical properties of recycled PET, *Polym. Compos.* 29 (2008) 915–921.
- [250] M. Kracalik, Rheology of multiphase polymer systems using novel “melt rigidity” evaluation approach, *AIP Conference Proceedings* (2015).
- [251] A.-L. Goffin, J.M. Raquez, E. Duquesne, G. Siqueria, Y. Habibi, A. Dufresne, P. Dubois, Poly(ϵ -caprolactone) based nanocomposites reinforced by surface-grafted cellulose nanowhiskers via extrusion processing: Morphology, rheology, and thermo-mechanical properties, *Polymer* 52 (2011) 1532–1538.
- [252] M. Galimberti, M. Coombs, S. Pandini, T. Riccò, V. Cipolletti, L. Conzatti, G. Guerra, Delamination of organically modified montmorillonite for reducing the filler networking with carbon black in poly(1,4-cis-isoprene) based nanocomposites, *Applied Clay Science* 2015 8–17.
- [253] C.D. Han, T. van den Weghe, P. Shete, J.R. Haw, Effects of coupling agents on the rheological properties, processability, and mechanical properties of filled polypropylene, *Polym. Eng. Sci.* 21 (1981) 196–204.
- [254] B. Hoffmann, C. Dietrich, R. Thomann, C. Friedrich, R. Mülhaupt, Morphology and rheology of polystyrene nanocomposites based upon organoclay, *Macromol. Rapid Commun.* 21 (2000) 57–61.
- [255] B. Hoffmann, J. Kressler, G. Stöppelmann, C. Friedrich, G.-M. Kim, Rheology of nanocomposites based on layered silicates and polyamide-12, *Colloid & Polymer Science* 278 (2000) 629–636.
- [256] M. Kracalik, Assessment of reinforcement in polymer nanocomposites using cumulative rheological parameters, *Epitoanyag - JSBCM* 69 (2017) 116–120.

2. Objectives of the conducted research

Research concluded in this thesis is divided into 3 chapters:

2.1 Preparation of polymer nanocomposites

In this chapter (manuscripts 1 – 5), conventional analysis approaches based on rotational rheometry have been used for correlations with structural and application properties of nanocomposites. The main effort was focused on evaluation of melt viscosity and melt elasticity (rubber-like behaviour) for better understanding of thermal and structural changes during the processing and consequent application of polymer nanocomposites. For this reason, new approaches for increase of thermal stability of organoclays, fillers combinations and structural parameters were developed.

2.1.1 Manuscript 1

“Effect of 3D structures on recycled PET/organoclay nanocomposites”

Kráčalík, Milan; Mikešová, Jana; Puffr, Rudolf; Baldrian, Josef; Thomann, Ralf; Friedrich, Christian (2007): In: Polym. Bull. 58 (1), S. 313–319. DOI: 10.1007/s00289-006-0592-5.

In this manuscript, evaluation of melt viscosity and elasticity revealed reinforcing effect of different commercial organoclays on recycled polyethyleneterephthalate, which was concomitant with degradation reactions during the processing. Relevant degradation mechanisms and their association with nanofiller dispersion were discussed. Structural evaluation has been done using wide-angle X-ray scattering and transmission electron microscopy. According to structural analysis, the highest level of dispersion revealed system filled with Cloisite 30B. However, this nanocomposite showed the lowest level of melt elasticity as compared with mixtures filled with other commercial organoclays. With this discovery, a broad discussion in relevant scientific community has been started with the view to develop new kinds of organoclays with enhanced thermal stability, which could be used not only for obtaining high dispersion grade, but also for improvement of material performance, especially for technical thermoplastic polymers with high melt temperature (above 250°C).

Effect of 3D structures on recycled PET/organoclay nanocomposites

Milan Kráčalík^{1,2} (✉), Jana Mikešová¹, Rudolf Puffr¹, Josef Baldrian¹,
Ralf Thomann², Christian Friedrich²

¹ Institute of Macromolecular Chemistry, Academy of Sciences of the Czech Republic,
Heyrovský Sq. 2, 162 06 Prague, Czech Republic

² Freiburger Materialforschungszentrum, Albert-Ludwigs-Universität Freiburg,
Stefan-Meier-Straße 21, 79104 Freiburg, Germany
E-mail: kracalik@imc.cas.cz

Received: 25 August 2005 / Revised version: 16 February 2006 / Accepted: 1 March 2006
Published online: 16 June 2006 – © Springer-Verlag 2006

Summary

Formation of physical network in PET/organoclay nanocomposites leads to significant improvement of processing and utility properties. The state of dispersion of silicate platelets in PET by melt mixing depends on shear forces as well on surface chemical treatment of the filler. The level of dispersion was determined by X-ray diffraction analysis and transmission electron microscopy. Melt rheology was used to examine the presence of network particles. It was shown that the addition of 5 wt. % of organo-modified montmorillonite into recycle leads to a 3D network structure with secondary plateau of G' at lowest frequencies. XRD and TEM experiments supported the conclusion.

Introduction

Investigation of relationship between the structure and processing properties has an important impact on various branches of materials science. Understanding the influence of processing parameters on final properties is the key to preparation of new materials for specific purposes.

Polymer/clay nanocomposites with a relatively low loading of the filler are interesting in terms of improvement of barrier, mechanical and rheological properties, dimensional stability, heat, flame and oxidative resistance [1]. Melt mixing as the most industrially attractive method for nanocomposite production requires study of rheological properties during compounding and their effect on the state of dispersion (delamination level) in the resulting polymer system. Up to now, a few papers have dealt with this topic for some polymer matrices [2, 3, 4, 5], but no mention for recycled PET (which is interesting particularly from the environmental point of view) was found in available literature. The difficulties that accompany processing of PET

Presented at 44th P.M.M. Microsymposium “Polymer Gels and Networks”,
Prague, 10–14 July 2005

with commercial organoclays arise from thermally limited stability of the quaternary ammonium salts used for modification of montmorillonite (MMT). Davis et al. [6] reported black, brittle and tarlike nanocomposites prepared from PET and ammonium-salt-based organoclay. In our work, transparent nanocomposites with improved processing, mechanical and barrier properties from recycled PET and commercially modified MMT were prepared, although moderate degradation of the matrix was observed in rheological measurements. Thus prepared nanocomposites could find applications in industry on account of continuously decreasing price of commercial organoclays. Description of physical as well as chemical phenomena which occur during compounding and their effect on the material structure are investigated by rheological and morphological testing.

Experimental

Materials

Organo-modified clays were supplied by Southern Clay Products, Inc., Gonzales, TX, U.S.A.

Table 1. Characteristics of organoclay fillers ^a

Organoclay	Organic modifier ^b	Modifier concentration [mequiv/100 g clay]	Moisture [%]	Weight loss on ignition [%]
Cloisite 6A	2M2HT	140	< 2	45
Cloisite 15A	2M2HT	125	< 2	43
Cloisite 20A	2M2HT	95	< 2	38
Cloisite 10A	2MBHT	125	< 2	39
Cloisite 25A	2MHTL8	95	< 2	34
Cloisite 30B	MT2EtOH	90	< 2	30

^a according to the manufacturer

^b quaternary ammonium chlorides: dialkyldimethyl- (2M2HT), alkyl(benzyl)dimethyl- (2MBHT), alkyl(2-ethylhexyl)dimethyl- (2MHTL8), alkylbis(2-hydroxyethyl)methyl- (MT2EtOH). Alkyls are a mixture of 65 % C18, 30 % C16 and 5 % C14, derived from hydrogenated tallow.

Recycled poly(ethylene terephthalate) from colour-selected beverage bottles (PET-R), with the intrinsic viscosity 0.73 dl/g was delivered by Polymer Institute Brno, Ltd., Czech Republic.

Preparation of nanocomposites

Organoclays were dried at 80 °C and PET regranulate at 110 °C in an oven at least for 12 h. PET-R was compounded with 5 wt. % of organoclay in a co-rotating twin-screw micro-extruder (DSM Research, Netherlands) under nitrogen environment. The mixing temperature 255 °C was set in order to exert maximal shear stress and minimal thermal degradation on the modified MMT during processing. The blending time was 10 min at the speed 200 rpm.

Structure of nanocomposites

WAXS (wide-angle x ray scattering) analysis was performed with a HZG 4/4A diffractometer (Präzisionsmechanik Freiburg, Ltd., Germany) at room temperature at a scanning rate of 1.5°/min. The Ni-filtered Cu K α radiation generator was operated at 30 kV accelerating voltage and 30 mA current. The TEM measurements were carried out with a Zeiss LEO 912 Omega transmission electron microscope using an acceleration voltage of 120 keV. The samples were prepared using a Leica Ultracut UCT ultramicrotome equipped with a cryo-chamber. Thin sections of about 50 nm were cut with a Diatome diamond knife at -120 °C.

Melt rheology

An ARES 3 Rheometer (Advanced Rheometric Expanded System, Rheometric Scientific, Inc., U.S.A.) with 25 mm parallel plate geometry was employed for rheological characterization. Dynamic frequency sweep measurements (at the strain level 2 % for the nanocomposites and 30 % for the matrix) as well as time sweep tests were performed at 270 °C under nitrogen.

Results and discussion

As seen in Table 1, the difference between various types of the Cloisite nanofillers comes from the ammonium cations located in the gallery of silicate layers. With two long alkyl groups, the ammonium cations in Cloisite 6A, 15A and 20A are non-polar, while those in Cloisite 30B (two 2-hydroxyethyl groups), 10 A (one hydrogenated alkyl replaced by benzyl group) and 25 A (one hydrogenated alkyl group replaced by a short 2-ethylhexyl group) are more polar. To obtain well-intercalated and exfoliated structure, the surface polarities of polymer matrix and organoclay must be matched [7]. Polar interactions are also crucial for the formation of well-dispersed systems via polymer melt intercalation [8]. These assumptions are confirmed by the results obtained.

Nanofillers Cloisite 6A, 15A and 20 A show a large initial gallery spacing, allowing an easier penetration of polymer chains, but they are exceedingly hydrophobic and do not match the polarity of PET. Subsequently, the weak interactions between the ammonium cations of fillers Cloisite 6A, 15A, 20 A and chains of PET resulted in inferior PET intercalation (Figure 1a, Table 2). On the other hand, due to the moderate surface polarity of Cloisite 30B and 10A, highly delaminated structures of recycled PET nanocomposites were obtained (Figure 1b, Table 2).

The WAXS diffractograms of nanocomposites (Figure 1a, 1b) showed that the first peaks of the pure fillers Cloisite 6A and Cloisite 15A as well as of composites PET-R/Cloisite 6A and PET-R/Cloisite 15A occur in similar positions (Table 2), indicating only very low interactions of the matrix with these organoclays. For PET-R/Cloisite 30B, PET-R/Cloisite 10A, PET-R/Cloisite 25A and PET-R/Cloisite 20A systems, the peaks of fillers were shifted to lower angular values. The increased basal spacing d_{001} showed that the polymer chains were intercalated in the gallery of silicate layers (Table 2). The obviously larger interlayer distance of Cloisite 30B, 10A and 25A in recycled PET nanocomposites demonstrates the efficiency of filling. The highest

decrease in the first peak in WAXS patterns (Figure 1b) corresponds with partial exfoliation (exfoliation of a certain number of tactoids) in the systems mixed with Cloisite 30B and 10A. Cloisite 25A exhibits also a high level of intercalation, which is attributed to the hydrophobicity decrease resulting from the loss of one hydrogenated alkyl group (Figure 1a, Table 2).

Table 2. WAXS analysis of organoclays in nanocomposites*

Organoclay	XRD peak position (°)	Basal Spacing (Å)	Δd_{001} (Å)
Cloisite 6A	2.8 (2.64)	31.5 (33.4)	-1.9
Cloisite 15A	2.9 (2.8)	30.4 (31.5)	-1.1
Cloisite 20A	3 (3.65)	29.4 (24.2)	5.2
Cloisite 10A	3 (4.6)	29.4 (19.2)	10.2
Cloisite 25A	3.1 (4.75)	28.5 (18.6)	9.9
Cloisite 30B	2.9 (4.77)	30.4 (18.5)	11.9

* manufacturer's data for neat organoclays are given in parentheses

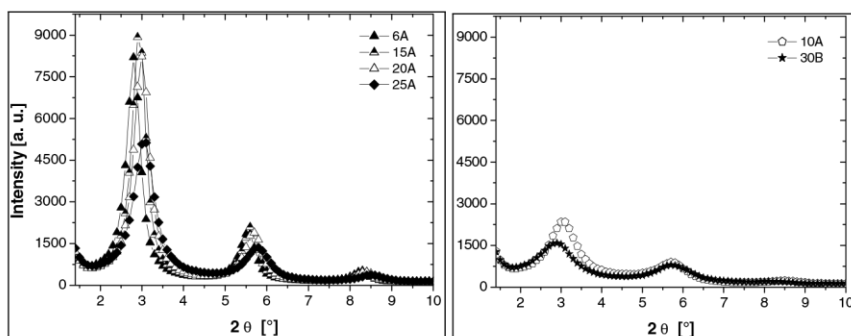


Figure 1a, 1b. WAXS patterns of the matrix and nanocomposites.

According to TEM micrographs, the highest level of homogeneity and delamination was found in the system filled with Cloisite 25A (Figure 2A). The nanocomposites with Cloisite 30B and 10A showed heterogeneous structure, which manifested itself by both exfoliated platelets and their stacks (Figure 2B, C). On the other hand, materials containing Cloisite 6A, 15A and 20A exhibited poor dispersion due to highly hydrophobic nature of these organoclays (Figure 2D, Table 2).

Processing properties of nanocomposites are characterized by rheological measurements. The flow curves (Figure 3) indicate the efficiency of the organoclay filling which manifests itself as a significant increase in melt viscosity in the range of low shear rates. At higher frequencies, the complex viscosity of nanocomposites decreased below the value of the unfilled matrix with the same processing history as the nanocomposites. The wall slip of filled melts between the parallel plates and matrix degradation during the rheological measurements were disproved by the time sweep tests, performed at various frequencies and plotted in Figure 4. The reason for the observed phenomenon could then be a slip between the polymer matrix and filler particles or a decrease in the complex viscosity of PET-R matrix in nanocomposites.

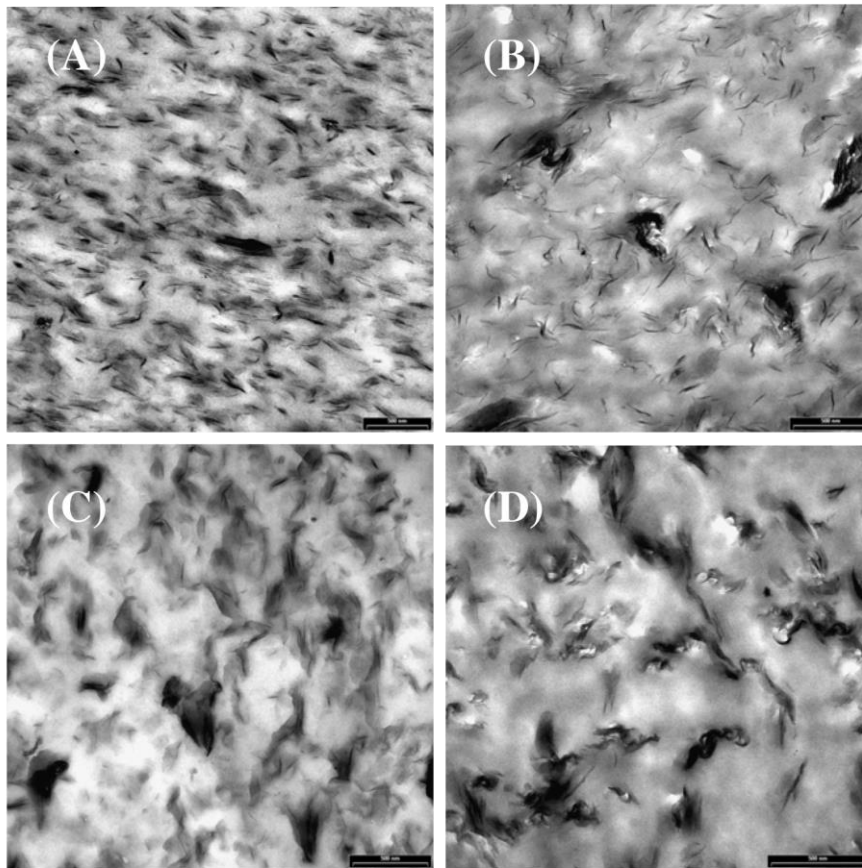


Figure 2. TEM photomicrographs of PET-R/organoclay nanocomposites; (A) Cloisite 25A, (B) Cloisite 30B, (C) Cloisite 10A, (D) Cloisite 6A.

Monitoring the melt compounding process, it was found that the most significant degradation during the processing of recycled PET and organoclay is attributed to chemical reactions between the functional groups of organic modifiers, free water of silicate and the polymer chains. These reactions lead to a decrease in molecular weight, which is indicated by decreasing values of load force (F_L) during mixing in microextruder (Figure 5). For a constant volume of the compounded material and the same processing speed, the F_L magnitude is proportional to the viscosity of the material. The sharpest decrease in F_L with time was observed for the system containing Cloisite 30B, which is attributed to the presence of hydroxyl groups in the nanofiller. The clays treated with organic compounds, which show a higher reactivity to PET (Cloisite 30B, 10A) manifesting itself by a decrease in F_L (Figure 5), support a much higher level of delamination (changes in the intensity and shape of basal reflections) than the other nanocomposites (Figure 1a, b). This phenomenon could be explained by easier penetration of shorter, degraded polymer chains into the gallery of silicate layers. The melt viscosity decrease of nanocomposites at higher frequencies compared with PET-R matrix is caused by inert low-molecular-weight compounds formed by thermal

degradation of alkylammonium tethers as well as by chain scission due to water and hydroxyl groups of silicate and especially due to the hydroxyalkyl groups of Cloisite 30B. Thermal decomposition of quaternary ammonium tethers proceeds by Hofmann elimination. The silicate anion abstracts hydrogen from the β -carbon of an alkyl, yielding an olefin, tertiary amine and acid, a protonated site of silicate. An excess surfactant chloride over the montmorillonite cation exchange capacity which is in Cloisite 6A, 15A and 10A, decomposes also by S_N2 nucleophilic substitution yielding alkyl chloride and tertiary amine [9].

Although organoclays are conventionally considered hydrophobic, water absorption still proceeds on the outer surface of particles, along the hydrophilic layer edges and on polar groups of alkylammonium tethers. The water content in dried, mostly hydrophobic Cloisites 6A, 15A and 20A is up to 0.6–0.7 wt. % [9]. Hydrolytic degradation of PET proceeds under the catalysis with Bronsted and Lewis acid sites of silicate. The nanocomposite with 5 wt. % of Cloisite 30B contains an amount of 2-hydroxyethyl groups comparable with that of PET, whose M_n is ca. 10000. This means that every PET molecule can be split once on average due to transacylation during the melt mixing process. This is the main cause of significant viscosity and storage modulus decrease in the nanocomposite mentioned.

Except the composites containing Cloisite 30B and 10A (due to the degradation mentioned above), a relationship between rheological properties and structure of

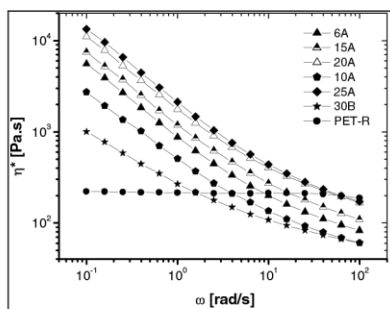


Figure 3. The dynamic flow curves of the matrix and nanocomposites.

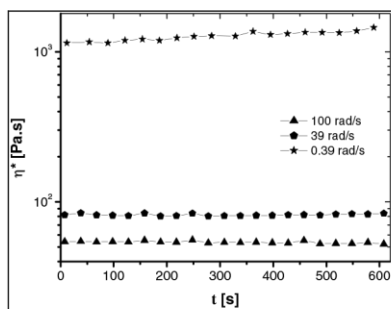


Figure 4. Time sweep test of the nanocomposite with Cloisite 10A.

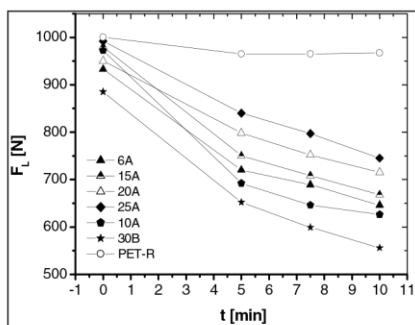


Figure 5. Time dependence of the load force during melt mixing of the matrix and nanocomposites.

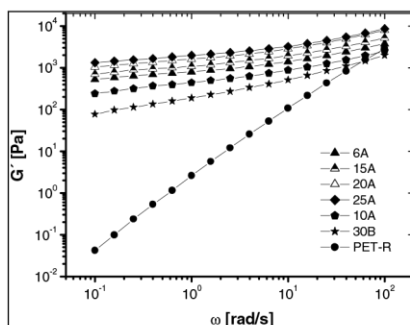


Figure 6. Dependence of storage modulus on frequency for the matrix and nanocomposites.

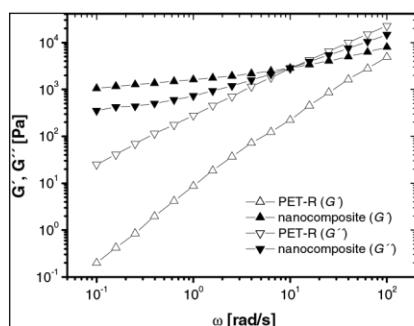


Figure 7. Comparison of viscoelastic properties of the matrix and the nanocomposite with Cloisite 6A.

prepared nanocomposites was revealed. The higher increase in interlayer distance Δd_{001} (level of intercalation of the silicate platelets, Figure 1a, b; Table 2) resulted in an enhancement of the complex viscosity and storage modulus (dispersion of clay particles forms stronger physical network in the polymer matrix, Figure 3, 6).

Compared with the unfilled polymer, all nanocomposites show rubber-like behaviour which is indicated as G' secondary plateau in the range of low frequencies. This phenomenon is especially distinct in Figure 7, where the viscoelastic liquid of recycled PET ($G'' > G'$) is transformed into rubber-like nanocomposite ($G' > G''$). These properties are attributed to physical network structures in nanocomposites.

Conclusions

Morphological investigations (WAXS and TEM) revealed partial exfoliation in nanocomposites prepared from recycled PET and commercial organoclays Cloisite 25A, 30B and 10A. The dynamic flow properties of the prepared composites related to structural changes associated both with the reinforcing effect (formation of physical network with organoclay loading) and degrading aspect (chain scission of PET and organoclay decomposition tendency). Moderate matrix degradation caused by some organoclays did not affect visual properties (transparency) of composites.

Acknowledgement. This research was supported by the Ministry of Environment of the Czech Republic (project VaV-1C/7/48/04).

References

1. Ray SS, Okamoto M (2003) Prog Polym Sci 28:1539
2. Hoffmann B, Dietrich C, Thomann R, Friedrich C, Mülhaupt R (2000) Macromol Rapid Commun 21:57
3. Reichert P, Hoffmann B, Bock T, Thomann R, Mülhaupt R, Friedrich C (2001) Macromol Rapid Commun 22:519
4. Lim YT, Park OO (2001) Rheol Acta 40:220
5. Incarnato L, Scarfato P, Scatteia L, Acierno D (2004) Polymer 45:3487
6. Davis CH, Mathias LJ, Gilman JW, Schiraldi DA, Shields JR, Trulove P, Sutto TE, Delong HC (2002) J Polym Sci, Part B Polym Phys 40:2661
7. Lebaron PC, Wang Z, Pinnavaia TJ (1999) Appl Clay Sci 15:11
8. Khan SA, Prud'homme RK (1987) Rev Chem Eng 4:205
9. Xie W, Gao Z, Pan WP, Hunter D, Singh A, Vaia R (2001) Chem Mater 13:2979

2.1.2 Manuscript 2

“Recycled PET nanocomposites improved by silanization of organoclays”

Kráčalík, Milan; Studenovský, Martin; Mikešová, Jana; Sikora, Antonín; Thomann, Ralf; Friedrich, Christian et al. (2007): In: J. Appl. Polym. Sci. 106 (2), S. 926–937. DOI: 10.1002/app.26690.

This is the first manuscript describing new approach for thermal stability improvement of commercial organoclays for application in polymers with high melt temperature (above 250°C). Based on the knowledge from manuscript 1, the most suitable commercial organoclays were modified with different functional groups ([3-(glycidyoxy)propyl]trimethoxysilane, hexadecyltrimethoxysilane and (3-aminopropyl)trimethoxysilane). This modification was based on silanization of hydroxyl groups on the edge of silicate platelets. Thermogravimetical measurements confirmed significant enhancement of thermal stability of silanized organoclays compared to their commercial versions. Using rotational rheometry, it was possible to compare the effect of organoclay stability improvement on degradation mechanisms during the processing and on final structure & application properties, which were analysed by X-ray diffraction, TEM, DSC and mechanical testing. According to rheological measurements, usage of Cloisite 25A modified with ([3-(glycidyoxy)propyl]trimethoxysilane led to high thermal stability during processing with recycled PET, as the values of melt viscosity were higher than those of pure PET matrix in the whole range of measured frequencies. For all other nanocomposites, starting at specific frequency, values of melt viscosity were lower than those of pure PET matrix, indicating presence of degradation mechanisms (e.g. hydrolytic degradation of PET, thermal decomposition of quaternary ammonium tethers by Hofmann elimination) during the processing.

Recycled PET Nanocomposites Improved by Silanization of Organoclays

Milan Kráčalík,¹ Martin Studenovský,² Jana Mikešová,² Antonín Sikora,^{2,3} Ralf Thomann,⁴ Christian Friedrich,⁴ Ivan Fortelný,^{2,3} Josef Šimoník^{3†}

¹Institute of Plastics Processing, University of Leoben, 8700 Leoben, Austria

²Institute of Macromolecular Chemistry, Academy of Sciences of the Czech Republic, 162 06 Prague 6, Czech Republic

³Faculty of Technology, Tomas Bata University in Zlín, 762 72 Zlín, Czech Republic

⁴Freiburg Materials Research Center, University of Freiburg, 79104 Freiburg, Germany

Received 6 April 2006; accepted 12 March 2007

DOI 10.1002/app.26690

Published online 3 July 2007 in Wiley InterScience (www.interscience.wiley.com).

ABSTRACT: Recycled PET/organo-modified montmorillonite nanocomposites were prepared via melt compounding as a promising possibility of the used beverage bottles recovery. According to our previous work, the three suitable commercial organoclays Cloisite 25A, 10A, and 30B were additionally modified with [3-(glycidyoxy)propyl]trimethoxysilane, hexadecyltrimethoxysilane and (3-aminopropyl)trimethoxysilane. The selected organoclays were compounded in the concentration 5 wt % and their degree of intercalation/delamination was determined by wide-angle X-ray scattering and transmission electron microscopy. Modification of Cloisite 25A with [3-(glycidyoxy)propyl]trimethoxysilane increased homogeneity of silicate layers in recycled PET. Additional modification of Cloisite 10A and Cloisite 30B led to lower level of delamination concomitant with melt viscosity reduction. However, flow characteristics of all studied organoclay nanocomposites

showed solid-like behavior at low frequencies. Silanization of commercial organoclays had remarkable impact on crystallinity and melt temperature decrease accompanied by faster formation of crystalline nuclei during injection molding. Thermogravimetric analysis showed enhancement of thermal stability of modified organoclays. The tensile tests confirmed significant increase of PET-R stiffness with organoclays loading and the system containing Cloisite 25A treated with [3-(glycidyoxy)propyl]trimethoxysilane revealed combination of high stiffness and extensibility, which could be utilized for production of high-performance materials by spinning, extrusion, and blow molding technologies. © 2007 Wiley Periodicals, Inc. *J Appl Polym Sci* 106: 926–937, 2007

Key words: recycled PET; organoclay; silanization

INTRODUCTION

Poly(ethylene)terephthalate (PET) is a semicrystalline polymer with high chemical resistance, thermal stability, melt mobility, spinnability, and low permeability to gases. Applications of PET are directed to different industrial branches, such as packaging, textile, automotive, electro-technical, construction, and other industries.^{1–3} Industrial production of PET bottles started in the USA in the 80s, using advantageous properties of PET, such as low weight, high impact resistance, nontoxic nature, and high transparency.⁴ Due to the growing amount of PET used in plastics industry (especially for beverage bottles),

finding various proper methods of recycling is an emergent challenge from the ecological and economical points of view.⁵ The amount of recycled PET bottles in PET-reprocessing countries is usually only 20–30 wt %. The rest of the used bottles ends in energy recovery or in deposits.⁶

At present, two PET recovery methods are used: chemical and physical recycling. Chemical depolymerization⁷ is economical only for high amounts of waste. On the other hand, physical (mechanical, material) recycling is a convenient way for economical and environmental purposes.^{6,8,9} Some high-tech pilot projects with recycled PET bottles have been tested^{4,5,10,11}; nevertheless, PET staple fibers with limited application still occupy the market. In particular, no study of PET recovery for the purpose of nanocomposite materials with improved processing and utility properties has been found in available literature.

In our previous work, the viscosity decrease of recycled PET during processing was investigated.¹² The study showed that reprocessing of PET waste with the intrinsic viscosity value below 0.7 dL/g is

Correspondence to: M. Kráčalík (Milan.Kracalik@unileoben.at)

Contract grant sponsor: Ministry of Environment of the Czech Republic; contract grant number: VaV-1C/7/48/04.

Contract grant sponsor: Academy of Sciences of the Czech Republic; contract grant number: AVOZ 40500505.

†Diseased.

Journal of Applied Polymer Science, Vol. 106, 926–937 (2007)

© 2007 Wiley Periodicals, Inc.



not possible.⁶ However, viscosity of the recycled polymer can be increased by filler addition. In the effort not to deteriorate mechanical properties of the material, nanofillers seem interesting.

Nanotechnology was introduced as a new method of improvement of polymer properties in 1995. The technology involves not only incorporation of nano-sized particles into the polymer but, more importantly, investigation of interactions between the polymer matrix and the enormously large nanofiller surface.¹³ Especially for polymer/clay nanocomposites, the surface effects are responsible for improvement of barrier, mechanical and rheological properties, dimensional stability, heat, flame, and oxidative resistance. In comparison with traditional fillers (20–40 wt % loading), 2–5 wt % filling of layered clays is sufficient to achieve analogous material improvement.^{14,15} Generally, three methods of the polymer/clay nanocomposites preparation are used: *in situ* polymerization, solution mixing, and melt mixing.^{16,17} In the case of PET/clay systems, the first two techniques were successfully tested.^{18–28} The melt mixing process is technologically much more interesting; nevertheless, satisfactory results with PET have not been achieved.^{29,30,31}

Despite sensitivity of melt rheology to changes in structure of the dispersed nanoparticles in the matrix, rheological experiments have been so far rarely used in investigation and characterization of polymer nanocomposites. A few rheological studies of polymer/clay systems, usually concerning nanocomposites with polyamides, confirm the enormous viscosity increase associated with clay loading in the region of low shear rates. The connection between the level of delamination of silicate platelets and formation of a physical network, indicated by secondary G' and G'' plateaus,^{13,30–45} was also published. For the PET/clay systems, Sanchez-Solis et al.^{30,31} reported the reduction of the shear viscosity and storage modulus explained by a decrease in particle-matrix interactions.

According to our work, addition of organoclays to recycled PET led to transparent nanocomposites with enhanced rheological, thermal, and mechanical properties. For the extrusion technology, the loss of melt strength causes an incohesion of material after leaving the extrusion die and, consequently, makes impossible the production of sheets or precise profiles. On the other hand, injection molding requires sufficient flow of polymer melts, which is carried out by alignment of silicate platelets in the flow direction at a high shear rates. Therefore, both processing technologies can be applied to recycled PET nanocomposites production. Possible applications of the recycled polymer/clay systems could be found in various industry fields, which would utilize enhancement of strength, thermal, barrier, and other

material properties, such as in car components (combination of barrier and strength characteristics), building industry, etc.

Our previous results confirmed improvement of processing properties by addition of commercial organoclays to recycled PET. Nevertheless, moderate degrading reactions were detected during the mixing in micro-extruder.⁴⁶ With a view to reduce the mentioned degradation and to increase delamination in the system, the selected commercial organoclays were additionally modified. The principle of the treatment consists in silanization of clay hydroxy groups by the selected silanes in aqueous-methanolic environment. The bonded functional groups can facilitate chemical or physical interaction of the filler with the polymer matrix and eliminate the degrading nature of the silicate hydroxyl groups (hydrolysis of PET).

The aim of the study was to investigate effects of additionally modified organoclays on rheological properties of recycled PET with the goal to enhance PET bottles recovery and to test utility properties of the prepared nanocomposites.

EXPERIMENTAL

Materials

The commercial organoclays were produced by Southern Clay Products, Gonzales, TX. The specifications of the organoclays are summarized in Table I. Nine new organoclays were prepared by additional modification (Fig. 1, Table II).

Color-sorted recycled poly(ethylene)terephthalate (PET-R), with the intrinsic viscosity 0.73 dL/g (dilution in phenol/tetrachloroethane 1 : 3), supplied by Polymer Institute Brno, was used as matrix. As can be seen in Figure 2, PET-R exhibits usual thermal behavior (similar to virgin bottle grade PET) because no remarkable decrease in T_g (T_m) magnitude occurred.

TABLE I
Specification of Commercial Organoclays^a

Organoclay	Organic modifier ^b	Modifier concentration (mequiv/100 g clay)	Moisture (%)	Weight loss on ignition (%)
Cloisite 25A	2MHTL8	95	<2	34
Cloisite 10A	2MBHT	125	<2	39
Cloisite 30B	MT2EtOH	90	<2	30

^a According to the manufacturer.

^b Quaternary ammonium chlorides: alkyl(2-ethylhexyl)-dimethyl (2MHTL8), alkyl(benzyl)dimethyl (2MBHT), alkylbis(2-hydroxyethyl)methyl (MT2EtOH). Alkyls are a mixture of 65% C18, 30% C16, and 5% C14, derived from hydrogenated tallow.

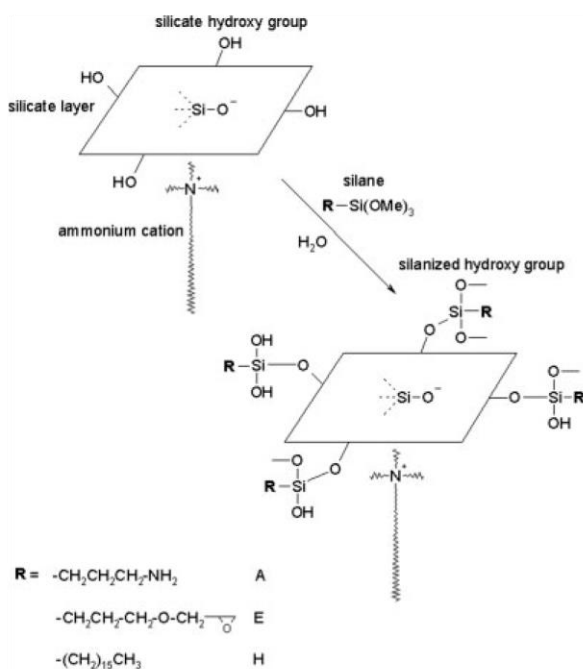


Figure 1 Chemical modification of commercial organoclays.

Preparation of silanized organoclays

The commercial organoclay (1 g) was suspended in 50 mL of methanol–water mixture (10 : 1) with subsequent addition of silane (0.3 g). The mixture was stirred for 2 days at room temperature and the precipitate was filtered off and rigorously washed with methanol. The solid was dried under vacuum at 50°C for 4 h.

Preparation of recycled PET/organoclay nanocomposites

Organically modified clays (om-MMT) were dried at 80°C and PET regranelated at 110°C in oven at least for 12 h. The recycled polymer was mixed with 5 wt % (relative to the anorganic part of organoclays) of

TABLE II
Indication of Silanized Organoclays

Commercial organoclay	Modifier/prepared organoclay		
	E ^a	H ^b	A ^c
Cloisite 25A	C 25AE	C 25AH	C 25AA
Cloisite 10A	C 10AE	C 10AH	C 10AA
Cloisite 30B	C 30BE	C 30BH	C 30BA

^a [3-(glycidyoxy)propyl]trimethoxysilane.

^b Hexadecyltrimethoxysilane.

^c (3-Aminopropyl)trimethoxysilane.

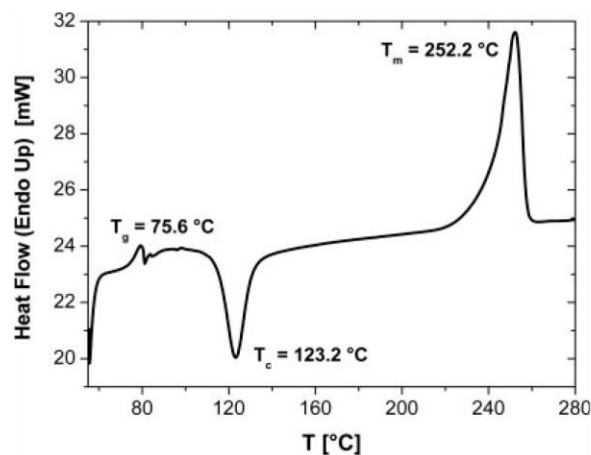


Figure 2 DSC thermograph of the recycled PET matrix.

om-MMT in a corotating twin-screw micro-extruder (DSM Research, Netherlands) under nitrogen atmosphere. The compounding temperature was 255°C to exert maximal shear stress and minimal thermal degradation on the modified montmorillonite during processing. The mixing time of PET granules and organoclay powder was 10 min at the speed 200 rpm. The time dependences of load force were measured in the micro-extruder during mixing. Recycled PET nanocomposites were injection-molded (micro-injection system; DSM Research) to specimens for mechanical, rheological, thermal, and wide-angle X-ray scattering (WAXS) testing at 260–265°C. The duration of injection cycle was ca. 10 s. The samples for TEM measurements were vacuum-compression molded at 260°C for 5 min (hydraulic laboratory plate press machine Collin 200P) due to higher isotropy of silicate platelets in polymer matrix.

Melt rheology

Rheological properties were studied using an ARES 3 Rheometer (Advanced Rheometric Expanded System; Rheometric Scientific, Piscataway, NJ) with a parallel-plate geometry of 25-mm-diameter plates. All measurements were performed with two automatically switched force transducers with a torque range of 0.02–2000 g cm. The samples thickness ranged from 0.9 to 1.1 mm. Experiments were performed at 270°C under nitrogen (liquid N₂ source) to prevent degradation of samples. The following types of rheological measurements were carried out: (1) dynamic strain sweep test (at 6.28 rad/s) to confirm the linearity of viscoelastic region, (2) dynamic frequency sweep test over a frequency range of

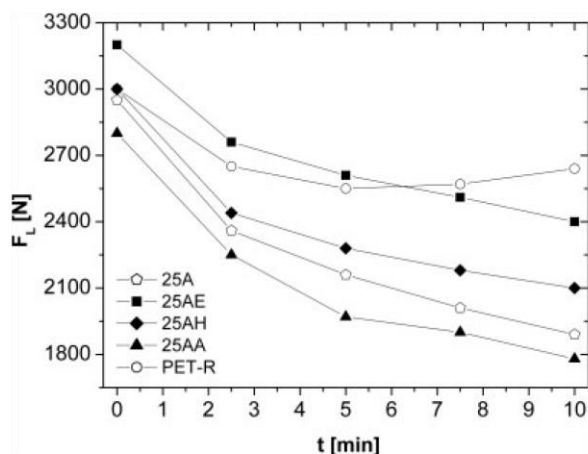


Figure 3 Load force of PET-R melt and nanocomposites filled with Cloisite 25A and additionally modified organoclays (the “zero” time is presented as the moment shortly after the start of mixing, when the values of load force can be measured).

0.01–100 rad/s, at the strains 2% for the nanocomposites, 30% for the matrix.

For an estimative investigation of viscosity during compounding, a load force generated by melt inside the mixing barrel was monitored.

Wide-angle X-ray scattering

The intensities of WAXS reflections were recorded at room temperature with a HZG 4/4A diffractometer (Präzisionsmechanik Freiburg, Germany). The Ni-filtered Cu K α radiation generator was operated at 30 kV accelerating voltage and 30 mA current (wavelength $\lambda = 1.54$ Å). Patterns were recorded by monitoring those diffractions that appeared during angular scan from 1.4 to 10° (2 θ) at a scanning rate of 1.5°/min.

Transmission electron microscopy

The TEM experiments were performed with a Zeiss LEO 912 Omega transmission electron microscope using an acceleration voltage of 120 keV. The samples were prepared using a Leica Ultracut UCT ultramicrotome equipped with a cryochamber. Thin sections of about 50 nm were cut with a Diatome diamond knife at -120°C .

Thermal characteristics

Thermal characterization of the polymer matrix and nanocomposites was carried out by differential scanning calorimetry (Pyris 1 DSC; Perkin Elmer, Waltham, MA) using a standard mode: (1) holding at 30°C for 3 min, (2) heating from 30 to 280°C at 10°C/min,

(3) holding at 280°C for 2 min. The thermal parameters, glass transition temperature (T_g), cold crystallization temperature (T_c), melting temperature (T_m), enthalpy of cold crystallization (ΔH_c), and enthalpy of melting (ΔH_m) were calculated. The relative crystalline content (X_c) in nanocomposites was evaluated by assuming the ΔH_m for a hypothetical 100% crystalline PET to be 117.6 J/g.⁴⁷ Thermal stability of organoclays was tested using Perkin Elmer TGA 7 instrument equipped with a software Pyris 1. The samples were heated from 40 to 750°C at 10°C/min with a nitrogen purge of 20 mL/min.

Mechanical properties

For tensile tests an Instron 5800 R was employed. Experiments were measured according to ISO 527 and ISO 1873-2 standards. The crosshead speeds for tensile modulus measurements at 1 mm/min and for all other characteristics at 50 mm/min were adjusted.

RESULTS AND DISCUSSION

Melt rheology

Monitoring of viscosity during compounding

The load sensor of micro-extruder enables to monitor the downward force F_L that is generated by the pressure of transported melt. For a constant volume of the mixed material and constant processing speed, the F_L magnitude is proportional to the viscosity of the material. It is evident that all nanocomposite systems exhibit a decrease in F_L during mixing (Figs. 3–5) caused by degradation reactions.⁴⁶ However, the systems filled with organoclay modified with [3-(glycidioxy)propyl]trimethoxysilane or hexadecyltri-

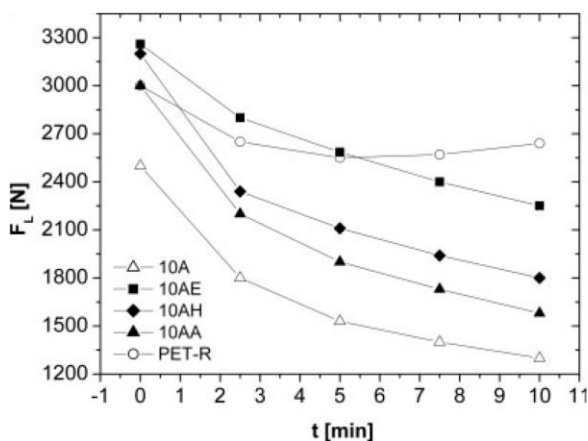


Figure 4 Load force of PET-R melt and nanocomposites filled with Cloisite 10A and additionally modified organoclays.

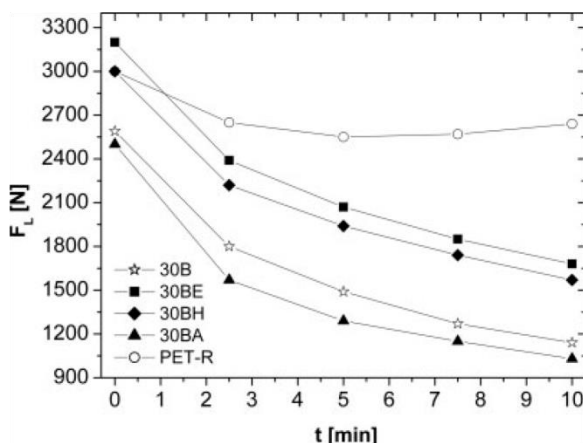


Figure 5 Load force of PET-R melt and nanocomposites filled with Cloisite 30B and additionally modified organoclays.

thoxysilane show a significantly lower degradation tendency than the corresponding materials containing unmodified commercial nanofillers. Using the fillers C25AE, 10AE, and 30BE led to the lowest degradation (Figs. 3–5). Therefore, the effects of these modified organoclays on processing and utility properties of nanocomposites were compared with those of the best dispersed commercial nanofillers Cloisite 25A, 10A, and 30B.⁴⁶

Complex rheological behavior

Dynamic shear flow properties of PET-R/organoclay nanocomposites were investigated in the region of linear viscoelasticity. The dynamic strain sweep test ($G'(\gamma)$) confirmed the linearity region in the range 1–100% strain for the matrix and 1–5% strain for the nanocomposites. According to our previous results, the color-selected recycled PET matrices and their blends exhibited a Newtonian behavior in the dependences $\eta^*(\omega)$ up to 100 rad/s and their complex viscosity decreased with increasing number of processing steps.¹²

In comparison with the matrix, complex viscosity of nanocomposites significantly increased in the range of low frequencies (more than 2 orders), as is shown in Figure 6. All the prepared nanocomposites show a shear thinning phenomenon, which is caused first by disruption of network structures and later on by orientation of filler particles in flow.

The results in Figure 6 demonstrate the highest filling effect of organoclay C 25AE. Moreover, the magnitude of complex viscosity of appropriate nanocomposite exceeded the value of matrix in the whole range of shear rates. That means significant reduction of degradation during the processing (visible

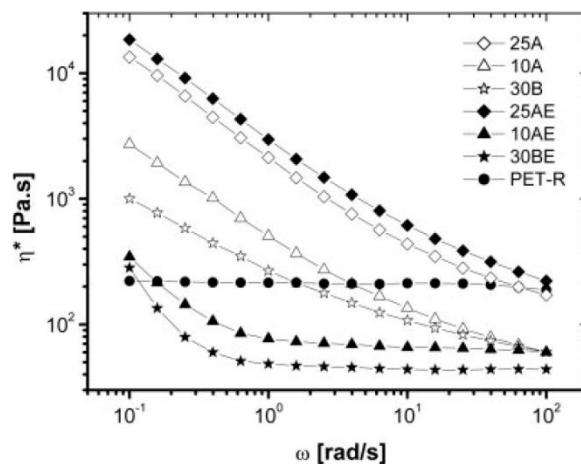


Figure 6 The complex viscosity versus frequency of the recycled PET matrix and nanocomposites.

also in Fig. 3). On the other hand, filling with C 10AE and 30BE exhibited adverse effect on viscosity (degradation tendency, described in Ref. 46). In this case, the complex viscosity decreased (comparing to systems with Cloisite 10A and 30B) together with very fast destruction of physical network (manifested itself by sharp viscosity decrease in the range of low shear rates). Generally, thermal stability of quaternary ammonium salts containing benzyl group⁴⁸ and resulting nanocomposites⁴⁹ is lower than that of systems with alkyl-based components. The several percent decade mass loss of quaternary ammonium chlorides containing benzyl and long alkyl groups during the heating up to 200°C has been observed from TGA measurements due to cleavage of benzyl group.⁵⁰ The details dealing with

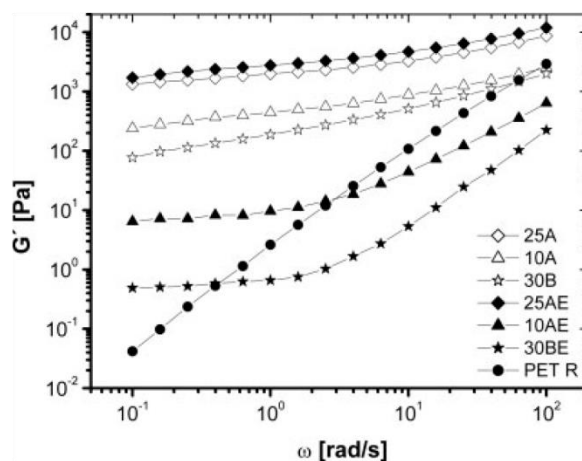


Figure 7 The storage modulus versus frequency of the recycled PET matrix and nanocomposites.

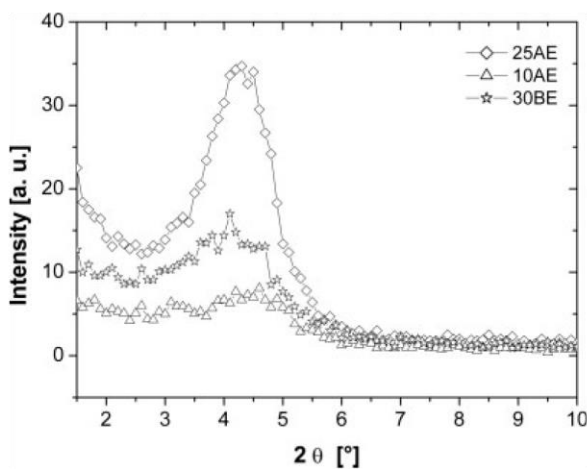


Figure 8 XRD patterns of pure fillers.

adverse effect of Cloisite 30B on PET melt have been published in our previous work.⁴⁶

The internal structural changes in nanocomposites during shear flow can be analyzed from frequency dependences of the storage (G') and loss (G'') moduli. Addition of clay to the PET-R melt causes an increase in the dynamic moduli, particularly in G' (Fig. 7). The pure matrix behaves as a viscoelastic liquid ($G'' > G'$). The higher value of G' than G'' for nanocomposites shows a change in viscoelastic behavior, i.e. a liquid-solid transformation. Moreover, the power-law dependence of the dynamic moduli at low frequencies, which is characteristic of the neat PET, is absent in the nanocomposites. The dependence of $G'(\omega)$ becomes nearly invariable. This "secondary" plateau indicates the formation of a network structure (exfoliation) of silicate layers in nanocomposites.^{41,51,52}

An increase of G' in the mixture with C 25AE (comparing to system filled with Cloisite 25A and pure matrix) exhibits an enhancement of melt strength (Fig. 7). Nevertheless, an opposite effect of C 10AE and C 30BE fillers on elasticity in the melt

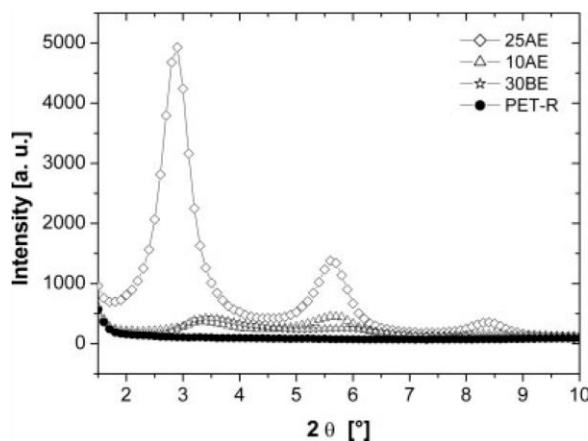


Figure 9 XRD patterns of matrix and nanocomposites.

state was observed as compared to Cloisite 10A and 30B. Therefore, the most remarkable G' "secondary" plateau was obtained in nanocomposites containing Cloisite 25A and C 25AE.

Morphology of organoclays in recycled PET

The prepared nanocomposites were analyzed by X-ray diffraction in the solid state to determine changes in the om-MMT interlayer distance caused by the insertion of PET between silicate layers. The effects of variations of their hydrophobicity and polar interactions on the structure in recycled PET were investigated and the results are shown in Figures 8 and 9. The influence of polymer intercalation on the arrangement of silicate layers is indicated by changes in the intensity, shape and peak positions of basal reflections. The basal spacings, d_{001} , were calculated from the observed peaks of the angular position 2θ according to Bragg's formula, $\lambda = 2d \sin \theta$. The level of intercalation is evaluated as Δd_{001} , which refer to the difference between the initial and final values of interlayer distance of organoclay (Table III).

TABLE III
XRD Analysis of Pure Organoclays and PET-R/Organoclay Nanocomposites

Organoclay	XRD peak position (°)		Basal spacing (Å)		Δd_{001} (Å)
	Pure	Nanocomposite	Pure	Nanocomposite	
Cloisite 25A	4.75 ^a	3.1	18.6 ^a	28.5	9.9
Cloisite 10A	4.6 ^a	3	19.2 ^a	29.4	10.2
Cloisite 30B	4.77 ^a	2.9	18.5 ^a	30.4	11.9
C 25AE	4.3	2.9	20.5	30.4	9.9
C 10AE	4.6	3.3	19.2	26.8	7.6
C 30BE	4.1	3.4	21.5	26	4.5

^a Manufacturer's specification.

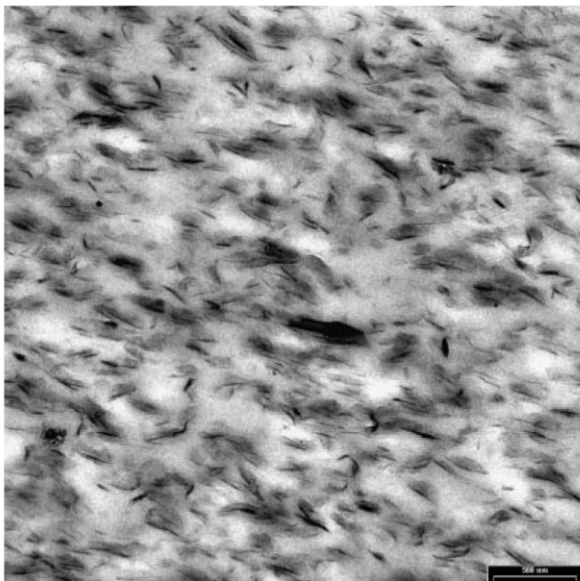


Figure 10 PET-R/Cloisite 25A (500 nm).

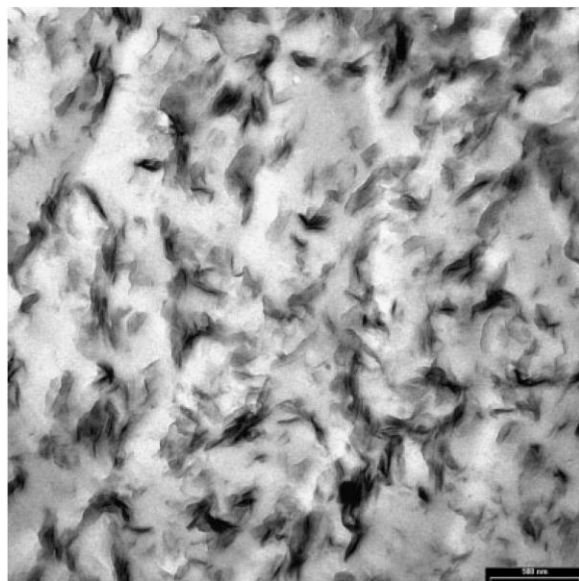


Figure 12 PET-R/Cloisite 25AE (500 nm).

The first peak of pure silanized organoclays C 25AE and C 30BE (Fig. 8, Table III) showed an increase of interlayer distance compared to Cloisite 25A and Cloisite 30B. Modification of Cloisite 10A resulted to equal intercalation (first peak at 4.6°). For the neat PET-R matrix the typical absence of peaks was found (Fig. 9). Concerning nanocomposite systems, silanization of Cloisite 25A led to similar increase of interlayer distance after melt mixing. The

negative effect of C 30BE and C 10AE fillers (manifested itself by melt viscosity reduction, Fig. 6) exhibited also on significant decrease of Δd_{001} in appropriate nanocomposites (Table III).

The level of delamination/homogeneity is observable in TEM micrographs (Figs. 10–21) and is in good agreement with WAXS measurements. The systems filled with Cloisite 25A and C 25AE revealed similar partial exfoliation of silicate layers

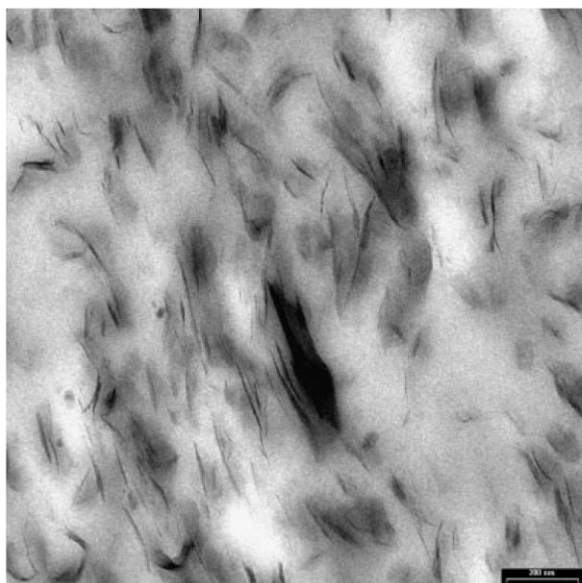


Figure 11 PET-R/Cloisite 25A (200 nm).

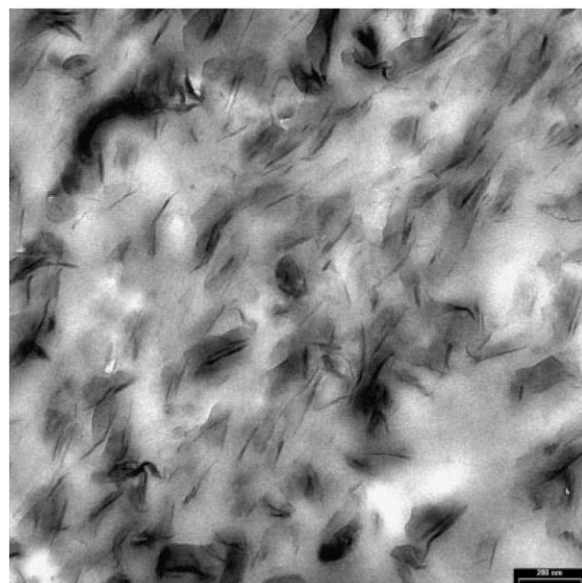


Figure 13 PET-R/Cloisite 25AE (200 nm).

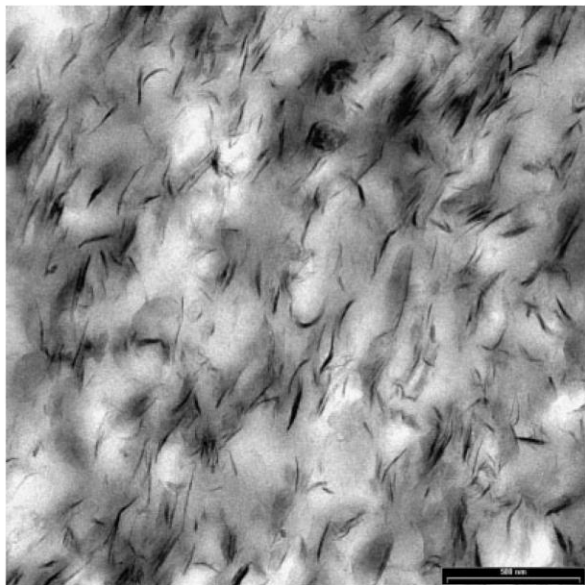


Figure 14 PET-R/Cloisite 10A (500 nm).

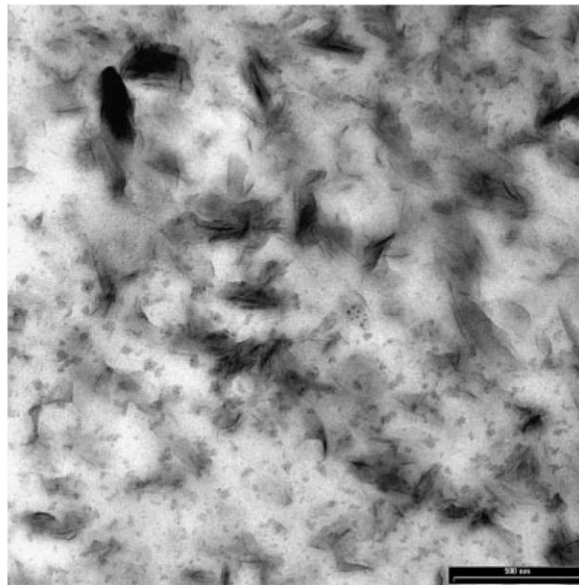


Figure 16 PET-R/Cloisite 10AE (500 nm).

(Figs. 10 and 12). From the 200-nm scale pictures (Figs. 11 and 13), a slightly higher homogeneity of nanocomposite containing C 25AE can be found. On the other hand, dispersion of C 30BE and C 10AE platelets in PET-R had a deteriorative impact on both exfoliation as well as homogeneity (Figs. 14–21). Pictures with resolution of 200 nm clearly show exfoliated structures as well as tactoids with lateral dimensions between 100 and 300 nm. Micrographs

at the 500-nm scale show rather overall level of dispersion.

It is assumed that delamination decrease of C 30BE and C 10AE fillers in PET-R matrix arise from chemical reactions between the quaternary ammonium cations of commercial organoclays and [3-(glycidyoxy)propyl]trimethoxysilane. In the case of Cloisite 30B and Cloisite 10A, the organic modifiers are enabled to react directly with polymer chains and

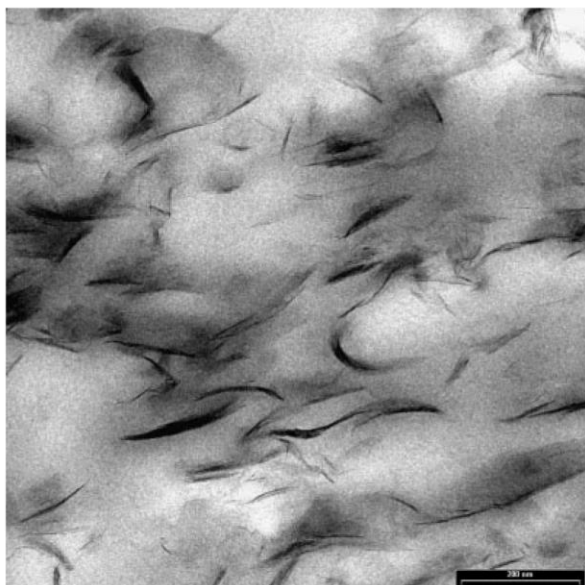


Figure 15 PET-R/Cloisite 10A (200 nm).

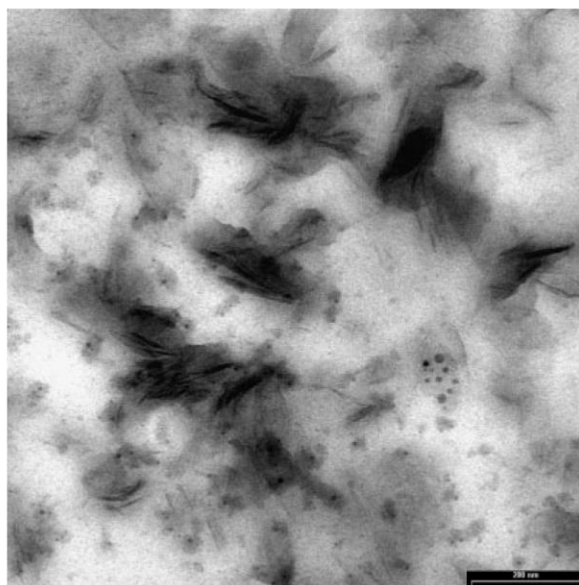


Figure 17 PET-R/Cloisite 10AE (200 nm).

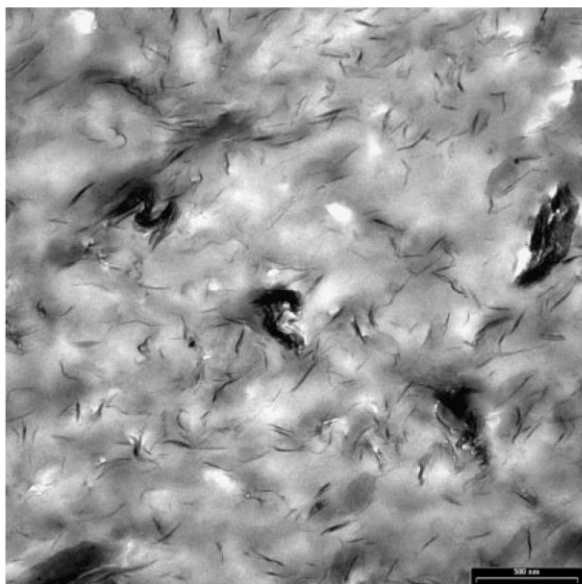


Figure 18 PET-R/Cloisite 30B (500 nm).

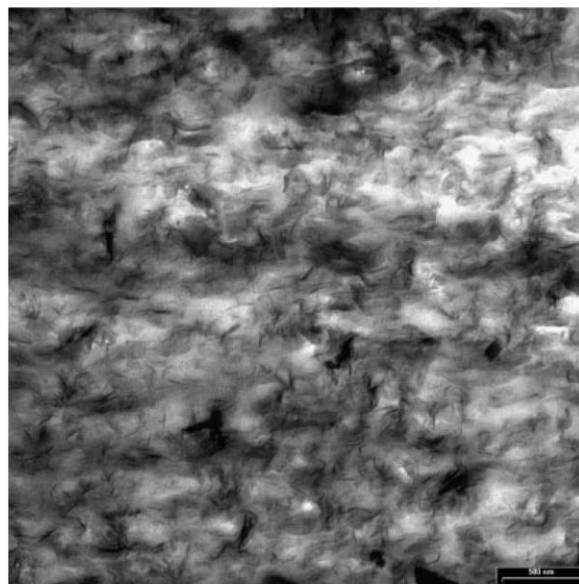


Figure 20 PET-R/Cloisite 30BE (500 nm).

thereby to facilitate increase of interlayer distance. This possibility of delamination in C 30BE and C 10AE silicates is considerably reduced by mechanism described.

Thermal characteristics

Thermal properties of nanocomposites were studied by DSC and TGA methods (Table IV). The systems filled with silanized organoclays (compared to com-

posites containing commercial fillers) revealed decrease in total crystallinity and melting temperature together with faster formation of crystalline nuclei (decline in enthalpy of cold crystallization ΔH_c) during cooling in injection mould. In comparison with commercial organoclays, an effect on decrease in T_g and T_c temperature with C 25AE loading and opposite tendency with C 10AE and C 30BE usage was observed. This phenomenon can be explained as an increase of free volume (decrease of

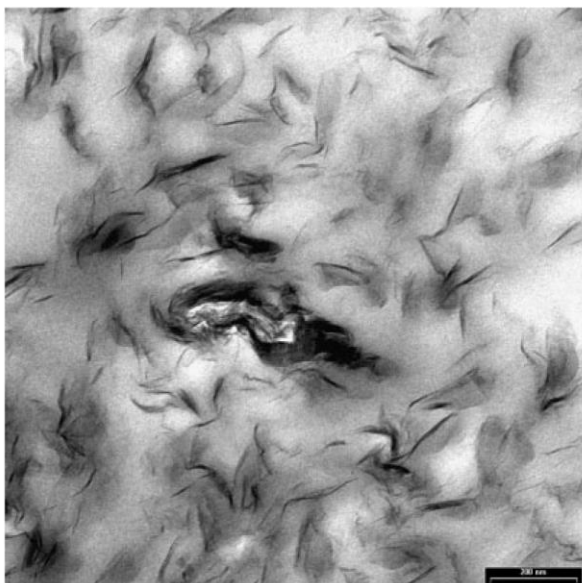


Figure 19 PET-R/Cloisite 30B (200 nm).

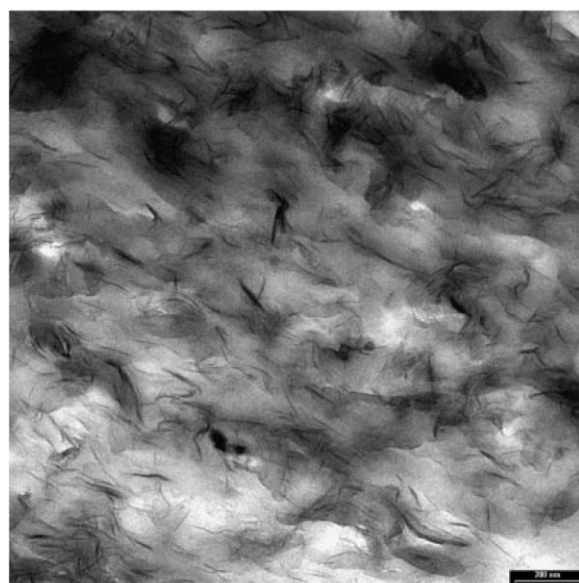


Figure 21 PET-R/Cloisite 30BE (200 nm).

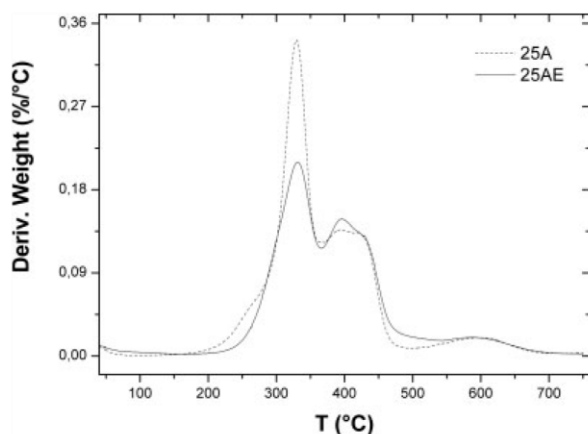


Figure 22 Thermogravimetric decomposition curves of Cloisite 25A and additionally modified organoclay.

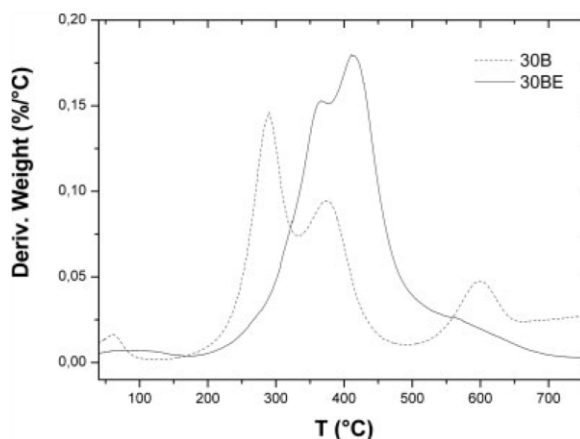


Figure 24 Thermogravimetric decomposition curves of Cloisite 30B and additionally modified organoclay.

T_g) with a higher delamination of silicate layers (Figs. 11 and 13). On the contrary, smaller surface area of tactoids causes weak interactions with polymer matrix resulting in decrease in free volume and increase in T_g (Figs. 15 vs. 17, 19 vs. 21). This relation is in accordance with WAXS and TEM analysis (Table III, Figs. 10–21). It is assumed that delaminated silicate platelets reduce mobility and consequently crystallization ability of polymer chains. This phenomenon is possible to observe as a crystallinity decline of nanocomposites compared to neat matrix, except the system with Cloisite 30B. The crystallinity growth in this composite implies that hydroxyl groups of Cloisite 30B modifier and the presence of undispersed silicate tactoids facilitate formation of crystalline nuclei.

The thermal stability of modified organoclays was increased, as evaluated in Figures 22–24 and Table

V. Compared with commercial silicates, the significant enhancement was achieved in organoclays C 10AE and C 30BE, where the first decomposition peak was shifted from 242 to 319°C (Fig. 23) and from 290 to 366°C, respectively (Fig. 24). However, the strong effect of these organoclays on free water retention (evaporation peaks shifted approximately from 60 to 80°C) was observed. TGA patterns of Cloisite 25A and its silanized version were nearly unchanged.

The mass loss at 500°C was considerably decreased by silanization of Cloisite 10A and Cloisite 25A, while organoclay C 30BE exhibited opposite tendency. Nevertheless, all the modified versions of commercial clays manifested significant growth of temperature at both 5% as well as 10% mass loss (Table V).

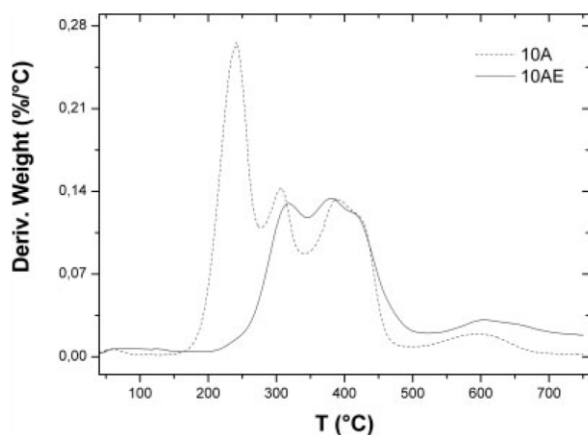


Figure 23 Thermogravimetric decomposition curves of Cloisite 10A and additionally modified organoclay.

TABLE IV
Thermal Properties of Nanocomposites and Neat Matrix

Sample	T_g^a (°C)	T_c^b (°C)	T_m^c (°C)	ΔH_c^d (J/g)	ΔH_m^e (J/g)	X_c^f (%)
PET-R/Cloisite 25A	72.6	122.3	254	25.3	41.4	35.2
PET-R/C 25AE	65.3	116.4	251.8	5.9	37.2	31.6
PET-R/Cloisite 10A	67.4	114.5	254.4	23.7	42.4	36.1
PET-R/C 10AE	75.6	118.8	250.8	13.5	38.3	32.6
PET-R/Cloisite 30B	72.8	118.1	254.6	25.5	46	39.1
PET-R/C 30BE	78.2	121.9	251.9	17.3	40.6	34.5
PET-R	75.6	123.2	252.2	24.9	43.2	36.7

^a Glass transition temperature.

^b Cold crystallization temperature.

^c Melting point.

^d Enthalpy of cold crystallization.

^e Enthalpy of melting.

^f Relative crystalline content.

Tensile characteristics

The mechanical properties of PET-R and appropriate nanocomposites are listed in Table VI. The systems containing fillers C 10AE and C 30BE were not measured due to their deteriorative effect on rheological properties (Figs. 6 and 7). In comparison to recycled polymer, the stiffness of all the composite systems was substantially increased. On the contrary, the tensile strength and extensibility were decreased. However, nanocomposite filled with C 25AE revealed interesting combination of high stiffness and satisfactory level of extensibility. The large elongation of PET-R/25AE nanocomposite results from high interfacial adhesion (increased polarity of Cloisite 25A by modification with [3-(glycidylxy)propyl]trimethoxysilane match more the polar feature of PET) and from the lowest degradation (compared to other systems filled with silanized organoclays) during the processing (proved in Fig. 6).

CONCLUSIONS

Recycled PET/organoclay nanocomposites were prepared by a melt intercalation method. According morphological analysis, C 25AE (from the group of modified organoclays) and Cloisite 25A (from the group of commercial fillers) were shown to be the most dispersed organoclays in the recycled PET matrix. The highest level of intercalation Δd_{001} was obtained using the filler Cloisite 30B. However, some bigger stacks of these clay platelets were found in TEM micrographs. Rheological study showed the complex flow behavior of the nanocomposites and melt behavior during compounding. The significant increase in the complex viscosity and storage modulus with organoclay loading was observed at low frequencies, where the viscoelastic liquid of recycled PET changed into nanocomposites with a solid-like behavior. The filling with C 25AE exhibited enhancing effect on rheological properties of nanocomposite. On the other hand, silanization of Cloisite 10A and 30B led to significant loss of melt strength, which is attributed to higher water retention of silicates together with chemical reactions between the

TABLE V
Thermogravimetric Decomposition
Characteristics of Organoclays

Organoclay	5% Mass loss (°C)	10% Mass loss (°C)	500°C mass loss (%)
Cloisite 30B	279.1	324.2	17.7
Cloisite 30BE	327.2	366.1	25
Cloisite 25A	298.5	321.0	30.6
Cloisite 25AE	304.6	331.3	27
Cloisite 10A	224.6	244.1	34.3
Cloisite 10AE	303.6	343.6	23.3

TABLE VI
Mechanical Properties of the Neat
Matrix and Nanocomposites

Sample	Tensile modulus (MPa)	Tensile strength (MPa)	Elongation at break (%)
PET-R	2170	57.1	316.5
PET-R/Cloisite 30B	2905	42.3	5.1
PET-R/Cloisite 10A	2523	33.7	19.2
PET-R/Cloisite 25A	2984	26.6	30.6
PET-R/C 25AE	2810	22	244.6

organic groups of organoclays and [3-(glycidylxy)propyl]trimethoxysilane modifier. The moderate "secondary" plateau on the G' frequency dependence confirmed the network formation in the nanocomposites, qualitatively explained by polymer–filler and particle–particle interactions. A correlation between commercial and silanized organoclays effect on linear viscoelastic flow characteristics and dispersion level (TEM and WAXS) of the prepared nanocomposites was found. Thermal characterization of nanocomposites filled with additionally modified organoclays compared with that of containing commercial organoclays revealed reduction of crystalline content and melt temperature together with higher crystallization rate during injection molding. The change of glass transition and cold crystallization temperature depending on delamination level was observed. Thermal stability of commercial organoclays was enhanced by silanization. The mechanical testing confirmed growth of stiffness up to 38% with organoclay loading and for system containing C 25AE also sufficient extensibility was reached. This property can be interesting for applications in fiber and film industry (combination of high stiffness with extensibility).

The authors gratefully appreciate the work of Dr. Jana Kovářová (TGA measurements) and Dr. Josef Baldrian (WAXS measurements) from Institute of Macromolecular Chemistry.

References

- Rwei, S. P. *Polym Eng Sci* 1999, 39, 12.
- Wang, C. S.; Sun, Y. M. *J Polym Sci Part A: Polym Chem* 1994, 32, 1295.
- Stewart, M. E.; Cox, A. J.; Naylor, D. M. *Polymer* 1993, 34, 4060.
- Gargiulo, C.; Belletti, G. *Chem Fibres Int* 1997, 47, 28.
- PETCORE Association (PET Containers Recycling Europe), <http://www.petcore.org>.
- Kráčalík, M.; Pospíšil, L.; Šimoník, J.; Kimmer, J.; Hrnčířík, J. *Plasty Kauc* 2003, 40, 356.
- Paszun, D.; Sychaj, T. *Ind Eng Chem Res* 1997, 36, 1373.
- Mankosa, M. J.; Carver, R.; Venkatraman, P. *Miner Eng* 1997, 49, 46.
- Lin, C. C. *Macromol Symp* 1998, 135, 129.

10. Koester, E. *Mater World* 1997, 9, 525.
11. Pegoretti, A.; Kolarik, J.; Peroni, C.; Migliaresi, C. *Polymer* 2004, 45, 2751.
12. Kráčalík, M.; Hrnčířík, J.; Pospíšil, L.; Šimoník, J. In *Proceedings of PPS-18 International Conference*, Guimaraes, Portugal, June 16–20, 2002, p 139.
13. Lee, K. M.; Han, C. D. *Macromolecules* 2003, 36, 7165.
14. Ray, S. S.; Okamoto, M. *Prog Polym Sci* 2003, 28, 1539.
15. Olphen, H. *Clay Colloid Chemistry*; Wiley: New York, 1977.
16. Lee, J. F.; Mortland, M. M.; Chiou, C. T.; Kile, D. E.; Boyd, S. A. *Clays Clay Miner* 1990, 38, 113.
17. Gilman, J. W.; Morgan, A. B.; Harris, R. H., Jr.; Trulove, P. C.; DeLong, H. C.; Sutto, T. E. *Polym Mater Sci Eng* 2000, 83, 59.
18. Imai, Y.; Nishimura, S.; Abe, E.; Tateyama, H.; Abiko, A.; Yamaguchi, A.; Aoyama, T.; Taguchi, H. *Chem Mater* 2002, 14, 477.
19. Maxfield, M.; Shacklette, L. W.; Baughman, R. H.; Christiani, B. R.; Eberly, D. E. *Int. Pat. WO 93/04118* (1993).
20. Lee, S. S.; Kim, J. *Polym Mater Sci Eng* 2003, 89, 370.
21. Takekoshi, T.; Khouri, F. F.; Campbell, J. R.; Jordan, T. C.; Dai, K. H. *U.S. Pat. 5,530,052* (1996).
22. Ke, Y. C.; Long, C.; Qi, Z. *J Appl Polym Sci* 1999, 71, 1139.
23. Sekelik, D. J.; Stepanov, E. S.; Schiraldi, D.; Hiltner, A.; Baer, E. *J Polym Sci Part B: Polym Phys* 1999, 37, 847.
24. Matayabas, J. C., Jr.; Turner, S. R.; Sublett, B. J.; Connell, G. W.; Barbee, R. B. *Int. Pat. WO 98/29499* (1998).
25. Pinnavaia, T. J.; Beall, G. W. *Polymer-Clay Nanocomposites*; Wiley: Chichester, 2000.
26. Imai, Y.; Inukai, Y.; Tateyama, H. *Polym J* 2003, 35, 230.
27. Barber, G. D.; Moore, R. B. *Abstr Pap Am Chem Soc* 2000, 219, 131-PMSE Part 2, 241.
28. Ou, C. F.; Ho, M. T.; Lin, J. R. *J Polym Res* 2003, 10, 127.
29. Davis, C. H.; Mathias, L. J.; Gilman, J. W.; Schiraldi, D. A.; Shields, J. R.; Trulove, P.; Sutto, T. E.; Delong, H. C. *J Polym Sci Part B: Polym Phys* 2002, 40, 2661.
30. Sanchez-Solis, A.; Garcia-Rejon, A.; Manero, O. *Macromol Symp* 2003, 192, 281.
31. Sanchez-Solis, A.; Romero-Ibarra, I.; Estrada, M. R.; Calderas, F.; Manero, O. *Polym Eng Sci* 2004, 44, 1094.
32. Hoffmann, B.; Dietrich, C.; Thomann, R.; Friedrich, C.; Mülhaupt, R. *Macromol Rapid Commun* 2000, 21, 57.
33. Hoffmann, B.; Kressler, J.; Stöppelmann, G.; Friedrich, C.; Kim, G. M. *Colloid Polym Sci* 2000, 278, 629.
34. Solomon, M. J.; Almusallam, A. S.; Seefeldt, K. F.; Somwangth-anaroj, A.; Varadan, P. *Macromolecules* 2001, 34, 1864.
35. Hyun, Y. H.; Lim, S. T.; Choi, H. J.; Jhon, M. S. *Macromolecules* 2001, 34, 8084.
36. Ray, S. S.; Yamada, K.; Okamoto, M.; Ueda, K. *Polymer* 2003, 44, 857.
37. Incarnato, L.; Scarfato, P.; Scatteia, L.; Acierno, D. *Polymer* 2004, 45, 3487.
38. Lepoittevin, B.; Devalckenaere, M.; Pantoustier, N.; Alexandre, M.; Kubies, D.; Calberg, C.; Jérôme, R.; Dubois, P. *Polymer* 2002, 43, 4017.
39. Lee, K. M.; Han, C. D. *Polymer* 2003, 44, 4573.
40. Kotsilkova, R. *Mech Time-Dependent Mater* 2002, 6, 283.
41. Krishnamoorti, R.; Giannelis, E. P. *Macromolecules* 1997, 30, 4097.
42. Kim, T. H.; Jang, L. W.; Lee, D. C.; Choi, H. J.; Jhon, M. W. *Macromol Rapid Commun* 2002, 23, 191.
43. Gelfer, M.; Song, H. H.; Liu, L.; Avila-Orta, C.; Yang, L.; Si, M.; Hsiao, B. S.; Chu, B.; Rafailovich, M.; Tsou, A. H. *Polym Eng Sci* 2002, 42, 1841.
44. Wagener, R.; Reisinger, T. J. G. *Polymer* 2003, 44, 7513.
45. Lim, S. T.; Hyun, Y. H.; Choi, H. J.; Jhon, M. S. *Polym Prepr* 2001, 42, 640.
46. Kráčalík, M.; Mikešová, J.; Puffr, R.; Baldrian, J.; Thomann, R.; Friedrich, C. *Polym Bull* 2007, 58, 313.
47. Metha, A.; Wunderlich, B. *J Polym Sci Polym Phys Ed* 1978, 16, 289.
48. Busi, S.; Lahtinen, M.; Kaernae, M.; Valkonen, J.; Kolehmainen, E.; Rissanen, K. *J Mol Struct* 2006, 787, 18.
49. Su, S.; Jiang, D. D.; Wilkie, Ch. A. *Polym Degrad Stab* 2004, 84, 269.
50. Avram, E. *Rev Romaine de Chim* 2001, 46, 49.
51. Khan, S. A.; Prud'homme, R. K. *Rev Chem Eng* 1987, 4, 205.
52. Krishnamoorti, R.; Vaia, R. A.; Giannelis, E. P. *Chem Mater* 1996, 8, 1728.

2.1.3 Manuscript 3

“Recycled PET-organoclay nanocomposites with enhanced processing properties and thermal stability”

Kráčalík, Milan; Studenovský, Martin; Mikešová, Jana; Kovářová, Jana; Sikora, Antonín; Thomann, Ralf; Friedrich, Christian (2007): In: J. Appl. Polym. Sci. 106 (3), S. 2092–2100. DOI: 10.1002/app.26858.

This is the first manuscript describing new approach for surface modification of natural clays for application in polymers with high melt temperature (above 250°C). For this purpose, recycled as well as virgin PET matrix was used. New thermally stable modifier based on imidazole was synthesized and used for surface treatment of sodium montmorillonite. This thermally stable organoclay was then additionally modified by silanization using knowledge from manuscript 2. Using rotational rheometry it was proved that nanocomposites with novel organoclays revealed no degradation mechanisms during the processing. This was confirmed as the viscosity values of nanocomposites using recycled as well as virgin PET matrix were higher than the pure matrix in the whole measured frequency range. The silanized version of imidazole organoclay revealed further improvement of processing stability for recycled PET. Rheological investigation was supported by structural (X-ray diffraction, TEM) as well as mechanical and thermal (DSC) testing. Especially mechanical testing revealed interesting stiffness/toughness combination, which was not possible to achieve in PET nanocomposites using commercial organoclays.

Recycled PET-Organoclay Nanocomposites with Enhanced Processing Properties and Thermal Stability

Milan Kráčalík,¹ Martin Studenovský,² Jana Mikešová,² Jana Kovářová,² Antonín Sikora,² Ralf Thomann,³ Christian Friedrich³

¹Institute of Plastics Processing, University of Leoben, 8700 Leoben, Austria

²Institute of Macromolecular Chemistry, Academy of Sciences of the Czech Republic, 162 06 Prague 6, Czech Republic

³Freiburg Materials Research Center, University of Freiburg, 79104 Freiburg, Germany

Received 19 March 2007; accepted 2 May 2007

DOI 10.1002/app.26858

Published online 23 July 2007 in Wiley InterScience (www.interscience.wiley.com).

ABSTRACT: Preparation of thermally stable recycled PET-organoclay nanocomposites with improved processing and mechanical properties is a challenging task from the environmental as well as industrial and commercial point of view. In this work, both modification of sodium-type montmorillonite with 1,2-dimethyl-3-octadecyl-1H-imidazol-3-ium chloride and additional treatment with [3-(glycidylloxy)propyl]trimethoxysilane was performed. Thermal stability of the organoclays and nanocomposites prepared by melt compounding was tested by thermogravimetric analysis, differential scanning calorimetry, and melt rheology. In comparison with the organoclays modified with quaternary ammonium compounds, the prepared clays showed substantial suppression of matrix degradation during melt mixing. The increase in inter-

layer distance of silicate platelets and homogeneity of dispersions in the recycled and virgin PET matrices have been evaluated by transmission electron microscopy and wide-angle X-ray scattering. The higher degree of delamination in the nanocomposites filled with imidazole organoclays was in a good agreement with improved rheological characteristics and led to significant enhancement in mechanical properties and thermal stability. A difference in structure (besides the level of delamination and homogeneity of silicate platelets) of recycled versus virgin PET nanocomposites was detected by X-ray diffraction patterns. © 2007 Wiley Periodicals, Inc. *J Appl Polym Sci* 106: 2092–2100, 2007

Key words: recycled PET; organoclay; melt compounding

INTRODUCTION

Recycling of poly(ethylene terephthalate) (PET), in particular beverage bottles, is not yet satisfactorily solved. The European average of PET recovery is approximately 30% and in the United States 20% only.^{1,2} During the recycling procedure and each processing step of thermoplastic materials, the melt viscosity decreases as a result of chain scission. As a key parameter in processing of recycled materials, their melt strength has to be held at a sufficient level. The low viscosity of recycled PET causes problems in the employment of some technologies (e.g. flat-die extrusion, blow molding) for reprocessing. Hence, only limited applications of this high-tech material (mostly staple fibers, packaging, films, and strips) have appeared on the market.³ The addition of highly dispersed silicate particles to recycled PET increases melt consistence, leading to more opportu-

nities of further processing. Nanocomposites prepared by melt mixing introduce an interesting method of polymer recycling especially with regard to the properties enhancement via intercalation/exfoliation of silicate platelets. To our knowledge, only few papers dealing with recycled PET-organoclay nanocomposites have been published so far. The presented materials exhibited poor processing as well as utility characteristics (deterioration of mechanical properties, melt viscosity decrease, etc.).^{4–6}

In our previous work, we studied the nanocomposites of recycled PET with commercial organoclays and we obtained an increase in melt viscosity due to the formation of a physical network between polymer and organoclay.⁷ However, a problem occurred with the thermal stability of commercial organic modifiers (quaternary ammonium salts), leading to the matrix degradation during melt mixing. The low thermal stability of commercial organoclays resulted in chemical decomposition by α , β elimination (Fig. 1).^{8–12} To reduce degradation processes and to enhance delamination in the system, we modified the selected commercial organoclays by silanization with [3-(glycidylloxy)propyl]trimethoxysilane, hexadecyltrimethoxysilane and (3-aminopropyl)trimethoxysilane.¹³ The epoxy functional groups attached to

Correspondence to: M. Kráčalík (milan.kracalik@mu-leoben.at).

Contract grant sponsor: Ministry of Environment of the Czech Republic; contract grant number: V-1C/7/48/04.

Journal of Applied Polymer Science, Vol. 106, 2092–2100 (2007)
© 2007 Wiley Periodicals, Inc.



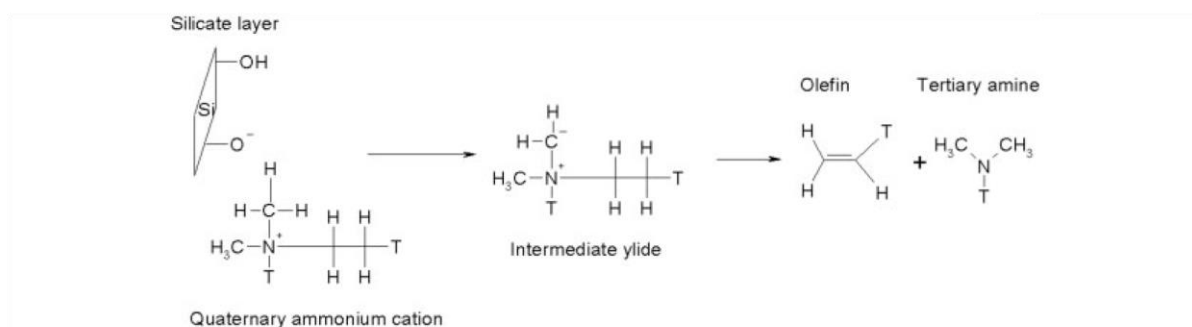


Figure 1 Scheme of α , β elimination. Where T is a hydrogenated tallow (mixture of 65% C18, 30% C16, and 5% C14).

the silicate surface facilitated interactions between the filler and polymer matrix and reduced the adverse effect of the silicate hydroxyl groups. Moreover, the epoxy-silanized organoclay could be directly bound to polymer chains, resulting in higher delamination of silicate platelets (Fig. 2). With the view of complete suppression of degradation reactions during compounding, the sodium montmorillonite was modified with spacers based on an imidazolium salt (Fig. 3). The "imidazolium organoclay" was further modified by silanization. The effect of various organoclay surface modifications on the processing and utility properties of recycled and virgin PET was the main object of interest in this work.

EXPERIMENTAL

Materials and methods

All chemical compounds were purchased from Fluka or Aldrich in sufficient purity. The synthesized compounds were characterized by elemental analysis, and melting point, if possible. The MMT-IM and MMT-IME organoclays have been synthesized using the molar excess of modifiers in order to achieve maximal modification efficiency.

Recycled poly(ethylene terephthalate) from color-sorted beverage bottles (PET-R), with the intrinsic viscosity 0.73 dL/g, was supplied by Polymer Institute Brno, Czech Republic. Virgin bottle grade PET Elixir (PET-V) with the intrinsic viscosity 0.8 dL/g was delivered by EKO PET, Czech Republic.

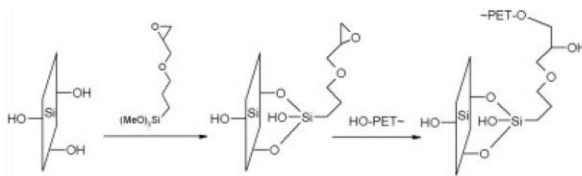


Figure 2 The scheme of epoxy-silanization and subsequent bonding of polymer chain to the silicate layer.

Synthesis of 1,2-dimethyl-3-octadecyl-1H-imidazol-3-ium chloride¹⁴

1,2-Dimethyl-1H-imidazole (18 g, 0.188 mol) was suspended in 1-chlorooctadecane (65 g, 0.225 mol) and the mixture was homogenized by stirring at 100°C for 12 h. The reaction mixture was cooled to 50°C and shaken with 200 mL of benzene. Precipitated crystals were filtered off, washed with a small amount of benzene and dried under vacuum [Fig. 4(a)].

The yield was 49.3 g (68%) and the melting point 93–95°C.

Preparation of organoclay with 1,2-dimethyl-3-octadecyl-1H-imidazol-3-ium (MMT-IM)

Cloisite Na⁺ (20.6 g of dry matter) was stirred in 1000 mL of deionized water and the suspension was kept at room temperature for 12 h. The suspension was heated at 80°C under vigorous stirring and the warm (60°C) solution of 1,2-dimethyl-3-octadecyl-1H-imidazol-3-ium chloride (7.85 g, 20.38 mmol) in 200 mL water was slowly added. The thick suspension was stirred for 90 min at 80°C, filtered off while hot, and washed with a high amount of boiling water. The filtration cake was suspended in 1000 mL of hot water (80°C) and vigorously stirred for 1 h. The final suspension was filtered off, washed, and the described procedure was repeated. The properly washed organoclay was air-dried and then dried under vacuum at 110°C [Fig. 4(b)]. The yield of the product was 25.6 g.

Elemental analysis (Perkin Elmer CHNSO Analyzer Series II 2400): Found C 20.70%, H 3.83%, N

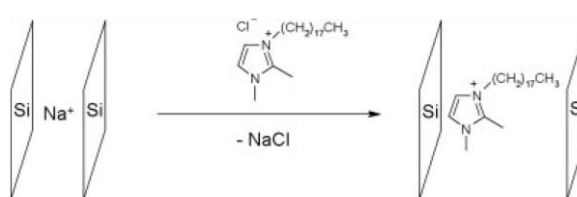


Figure 3 The scheme of ion exchange.

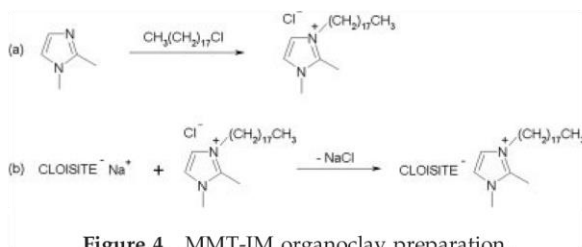


Figure 4 MMT-IM organoclay preparation.

1.60%, ash 68.39%. The 23% fraction of organic phase was calculated from TGA measurement.

Epoxy-silanization of 1,2-dimethyl-3-octadecyl-1H-imidazol-3-ium organoclay (MMT-IME)

The MMT-IM organoclay (1 g) was suspended in 50 mL of a methanol–water mixture (10:1) and [3-(glycidyloxy)propyl]trimethoxysilane (0.3 g) was added. The mixture was stirred at room temperature for 2 days and the precipitate was filtered off and thoroughly washed with methanol. The solid was dried under vacuum at 50°C for 4 h. This procedure has been performed according to scheme in Figure 2.

Preparation of nanocomposites

Organoclay powder was dried at 80°C and PET pellets at 110°C in an oven overnight. Polymer was compounded with 5 wt % of organoclay in a co-rotating twin-screw microextruder (DSM Research, Netherlands) at 255°C under nitrogen. The mixing time was 10 min at a speed of 200 rpm. Immediately after blending cycle, the nanocomposite melt was injected into a form at 260°C using DSM micro-injection equipment.

Structure of nanocomposites

Wide-angle X-ray scattering (WAXS) was measured with a HZG 4/4A diffractometer (Prazisionsmechanik Freiburg, Germany) at room temperature at the scanning rate 1.5°/min. The Ni-filtered Cu K α radiation generator operated on the accelerating voltage 30 kV and 30 mA current. Morphological analysis was made with a Zeiss LEO 912 Omega transmission electron microscope using an acceleration voltage of 120 keV. The samples were prepared using a Leica Ultracut UCT ultramicrotome equipped with a cryo-chamber. Thin sections of about 50 nm were cut with a Diatome diamond knife at –120°C.

Melt rheology

An ARES 3 Rheometer (Advanced Rheometric Expanded System, from Rheometric Scientific, USA) with the 25-mm parallel-plate geometry was

employed for rheological characterization. Dynamic frequency sweep measurements were performed at 270°C under nitrogen at the strain level of 2% (nanocomposites) or 30% (neat matrices), respectively.

Thermal properties

Thermal characterization of the polymer matrices and nanocomposites was carried out by a differential scanning calorimetry (Perkin Elmer, Pyris 1 DSC) using a common mode: (1) holding at 30°C for 3 min; (2) heating from 30 to 280°C at 10°C/min; (3) holding at 280°C for 2 min.

The glass transition temperature (T_g), cold crystallization temperature (T_c), melting temperature (T_m), enthalpy of cold crystallization (ΔH_c), and enthalpy of melting (ΔH_m) were recorded. The relative crystalline content (X_c) in nanocomposites was calculated by taking the value 117.6 J/g as ΔH_m of a hypothetical 100% crystalline poly(ethylene terephthalate).¹⁵

Thermal stability of organoclays was evaluated using Perkin Elmer TGA 7 instrument equipped with the software Pyris 1. The samples were heated from 40°C up to 750°C at 10°C/min under a nitrogen flow of 20 mL/min.

Mechanical testing

Mechanical properties of the prepared materials were measured on an Instron 5800 R test instrument. The experiments were carried out according to ISO 527 and ISO 1873-2 standards. The crosshead speed was set to 1 mm/min (tensile modulus) or to 50 mm/min (other characteristics).

RESULTS AND DISCUSSION

Dispersibility of organo-clays in recycled PET

The morphological analysis revealed a similar level of dispersion and homogeneity of silicate platelets in PET/MMT-IM and PET/MMT-IME nanocomposites. According to Table I and Figure 5(A,B), a slight increase in intercalation, expressed by the difference in basal spacing Δd_{001} , was achieved in the systems containing the filler treated with [3-(glycidyloxy)pro-

TABLE I
WAXS Analysis of Organoclays in PET Nanocomposites^a

Nanocomposite	XRD peak position (°)	Basal spacing (Å)	Δd_{001} (Å)
PET-R/IM	3.1 (4.3)	28.5 (20.5)	8
PET-R/IME	3 (4.6)	29.4 (19.3)	10.1
PET-V/IM	3 (4.3)	29.4 (20.5)	8.9
PET-V/IME	3.1 (4.6)	28.5 (19.3)	9.2

^a Data of neat organoclays are given in parentheses.

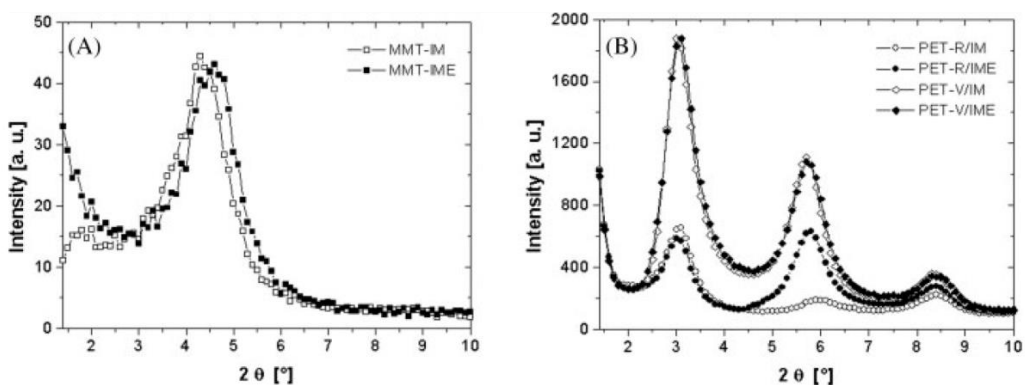


Figure 5 WAXS patterns of the neat organoclays (A) and nanocomposites (B).

pyl]trimethoxysilane. However, TEM micrographs (Figs. 6 and 7) showed a moderate delamination decrease in the MMT-IME-filled nanocomposites observable both on 500 and on 1000 nm scale (Figs. 6 and 7: A, C). At the 100 nm scale (Figs. 6 and 7: B, D), individual sheets of silicate and a slightly higher delamination level in the systems containing MMT-

IME organoclay can be seen. Concerning the neat organoclays, a higher interlayer distance was achieved in MMT-IM silicate (20.5 Å) than in MMT-IME, whose intercalation reached 19.3 Å. Nevertheless, the MMT-IM organoclay resulted in a higher final interlayer distance only in the virgin PET.

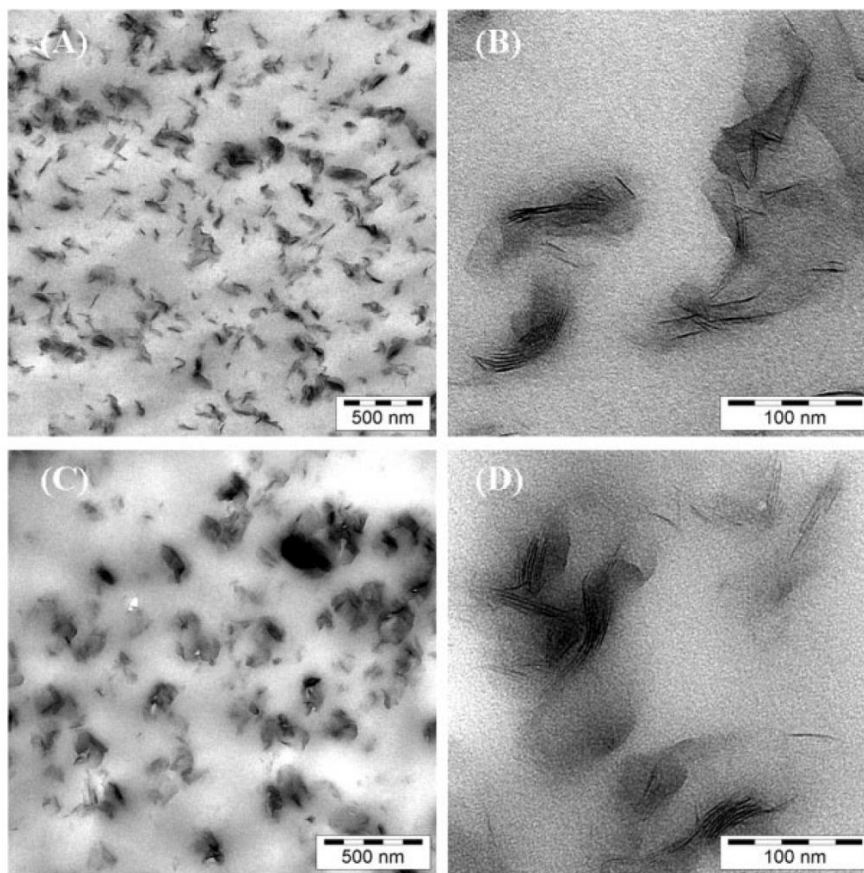


Figure 6 TEM micrographs of PET-R/organoclay nanocomposites: (A, B) MMT-IM; (C, D) MMT-IME.

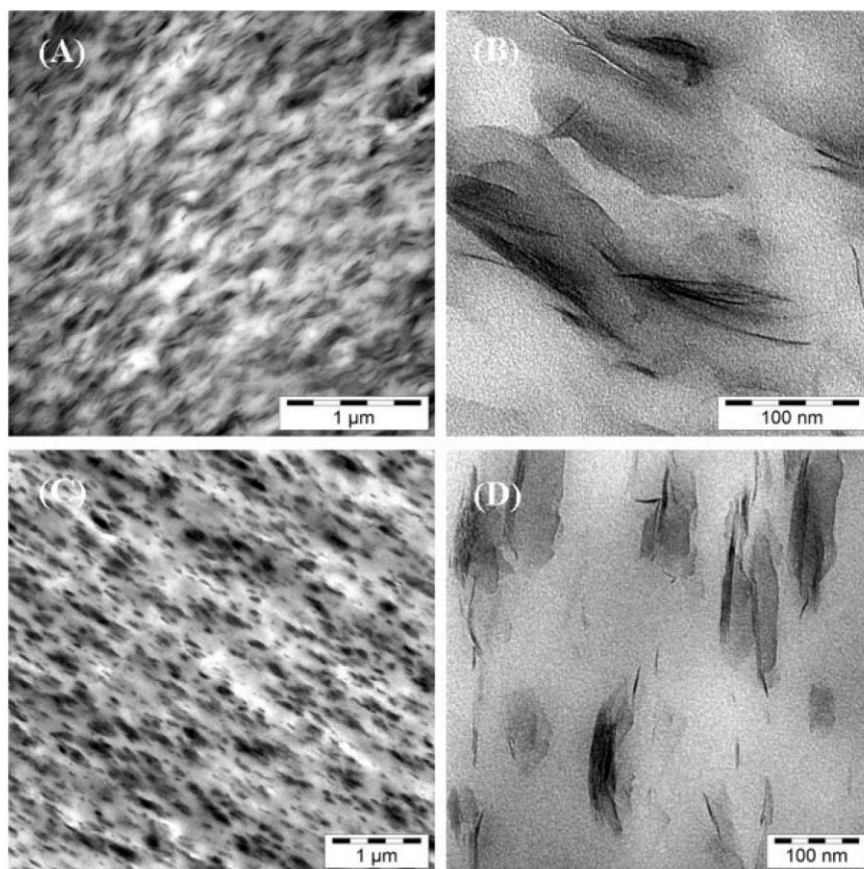


Figure 7 TEM photomicrographs of PET-V/organoclay nanocomposites: (A, B) MMT-IM; (C, D) MMT-IME.

Results of XRD measurements [Fig. 5(B)] indicate an organized structure of silicate platelets in nanocomposites based on the virgin PET matrix (manifested by the regularity of XRD patterns). On the other hand, the same organoclays mixed with recycled PET exhibited a rather disordered structure of clay layers, manifesting itself by specific XRD peaks [Fig. 5(B)]. This observation is in a good agreement with transmission microscopy measurements (Figs. 6 and 7). In our previous work,¹³ a rather low level of delamination was observed using commercial fillers silanized with [3-(glycidyoxy)propyl]trimethoxysilane. A similar adverse effect of epoxy-silanization on the overall dispersion of silicate platelets was observed in this study (Figs. 6 and 7; A, C), although the average interlayer distance was slightly increased with MMT-IME loading (Table I, Figs. 6 and 7; B, D).

Melt rheology

Dynamic rheological behavior of the prepared nanocomposites was investigated in the region of linear

viscoelasticity. The dynamic strain sweep test ($G'(\gamma)$) revealed the linearity region of 1–100% strain (the matrices) or 1–15% strain (the composites), respectively. The processing properties of the prepared materials are characterized by flow curves (Figs. 8 and 9). In comparison with neat matrices (showing a Newtonian behavior within the frequency dependence $\eta^*(\omega)$ nearly in the whole range of tested shear rates), filling with imidazole organoclays led to an increase of an order of magnitude in complex viscosity at low shear rates. A typical shear thinning effect can be observed as a result of physical network destruction and particle orientation in flow direction.

In the case of systems based on recycled PET matrix, the epoxy-silanization of MMT-IM silicate had a remarkable impact on the melt viscosity increase of resultant nanocomposite (Fig. 8). On the other hand, the virgin PET filled with MMT-IME organoclay showed a lower melt viscosity than the system containing the MMT-IM silicate in the range of low shear rates (Fig. 9).

The G' secondary plateau at low frequencies (Figs. 10 and 11), observable for all nanocomposites,

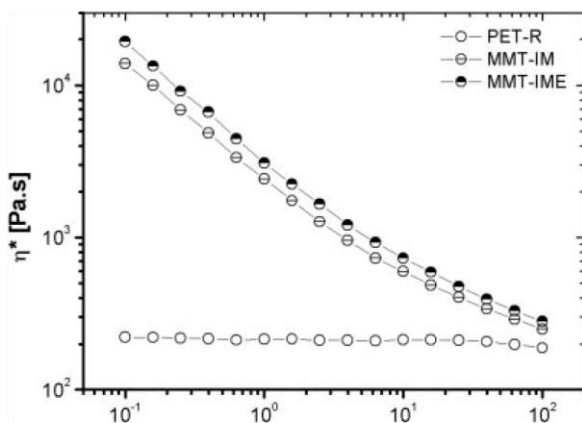


Figure 8 The dynamic flow curves of the PET-R matrix and nanocomposites.

reflects highly delaminated structure of clay platelets in the polymer matrix. According to previous studies,^{16–18} the structural changes in nanocomposites in the molten state can be evaluated from frequency dependences of the storage (G') and loss (G'') moduli. Addition of silicate platelets to the polymer melt causes an increase in the dynamic moduli, particularly in G' (Figs. 10 and 11). The unfilled PET behaves as a viscoelastic liquid ($G'' > G'$). The higher value of G' than that of G'' in nanocomposites indicates a different viscoelastic behavior, i.e. a liquid–solid transformation through filling with clay.⁷ This pseudo-rubber response in the range of low shear rates (up to 10^0 s^{-1}) reflects a strong rigidity of a 3D structure, where the action of moderate shear forces on delaminated silicate platelets results in entirely elastic response (without viscous factor) of the whole physical network. Furthermore, the power-law dependence of dynamic moduli at low shear rates

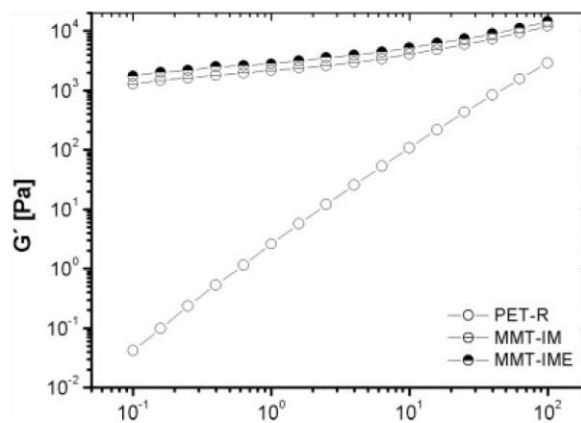


Figure 10 The storage modulus of the PET-R matrix and nanocomposites.

(characteristic of neat PET) was not observed in the nanocomposite systems. The G' becomes nearly frequency-independent. In comparison with other physical methods, the evaluation of dynamic moduli gives information about network structure associated with the level of delamination in the molten state. Moreover, the substantial storage modulus increase of the filled systems in comparison with neat matrices proves an enhancement of melt strength that plays an important role in processing of recycled materials.

In our previous work,^{7,13} incorporation of commercial or silanized commercial organoclays into recycled PET led to certain degradation during compounding process. This degradation was indicated by a decrease in the complex viscosity and the storage modulus in the region of higher shear rates. Overall rheological characteristics in this work confirmed the nondegrading effect of imidazole organo-

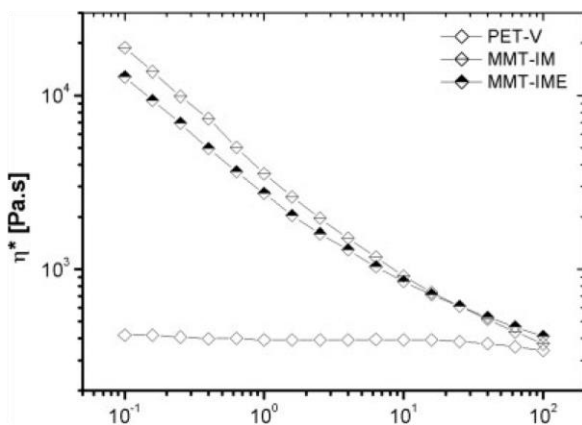


Figure 9 The dynamic flow curves of the PET-V matrix and nanocomposites.

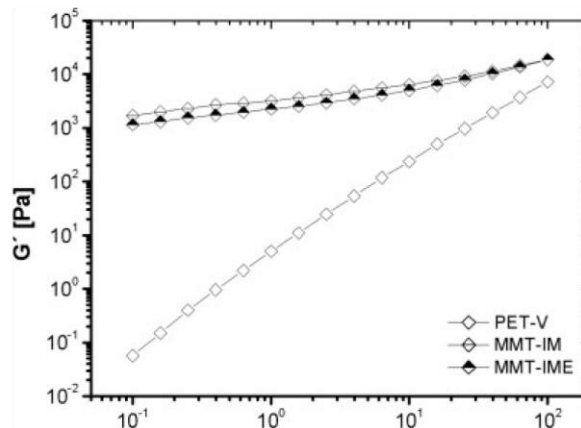


Figure 11 The storage modulus of the PET-V matrix and nanocomposites.

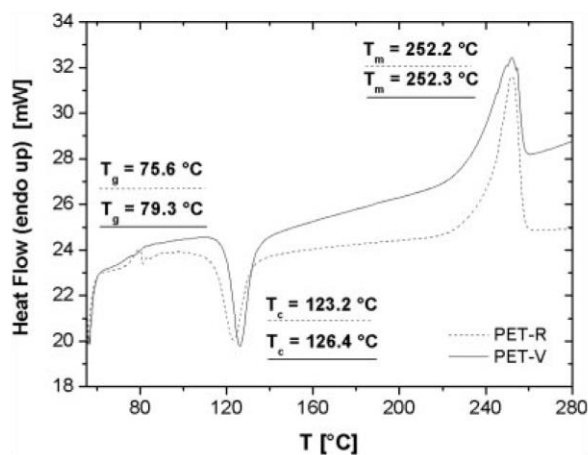


Figure 12 DSC thermograms of the recycled and virgin PET matrix.

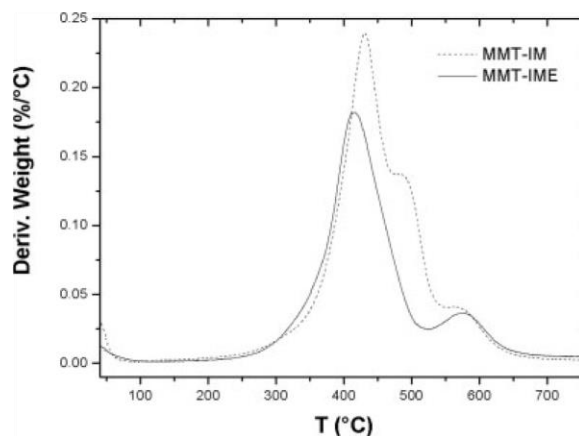


Figure 13 Thermogravimetric decomposition curves of organoclays.

clays on recycled and virgin PET matrix, manifesting itself by higher η^* and G' values compared with unfilled matrices in the whole range of applied shear rates. The obtained frequency dependences of the measured rheological characteristics indicate that the enhanced melt viscosity and elasticity of the recycled PET nanocomposites should persist also at higher shear rates applied in processing technologies (extrusion, injection molding, blow molding).

Thermal characterization

Judging from differential scanning calorimetry experiments, PET-R exhibits usual thermal behavior (similar to PET-V) because no remarkable decrease in T_g and T_m values was observed (Fig. 12).

The DSC spectra of nanocomposites (Table II) based on recycled and virgin PET matrix show no fundamental differences. Nanocomposites prepared from recycled PET revealed a decrease in total crystallinity and melt temperature, a faster formation of

crystalline nuclei, an increase in glass transition and cold crystallization temperature compared with the neat matrix. The systems containing virgin PET showed similar level of total crystallinity, a higher crystallization rate, and a lower glass transition temperature compared with the unfilled matrix. The recycled PET exhibited lower values of T_g and T_c temperatures, a higher crystallization rate, and a higher total crystallinity than virgin PET. The faster formation of crystalline nuclei in recycled PET in relation to virgin polymer could be attributed to the lower value of melt viscosity (Figs. 8 and 9) associated with a faster translation of polymer chains and easier arrangement into lamellar structure. The higher crystallization rate of nanocomposites when compared with neat matrices is explained by the nucleating effect of silicate particles on heterogeneous crystallization of PET chains.

Results of thermogravimetric measurements (Fig. 13, Table III) revealed the first decomposition peak of MMT-IM at 430 °C and MMT-IME at 416 °C. Surprisingly, the second decomposition peak at 500 °C is

TABLE II
Thermal Properties of the Matrices and Nanocomposites

Nanocomposite/matrix	T_g^a (°C)	T_c^b (°C)	T_m^c (°C)	ΔH_c^d (J/g)	ΔH_m^e (J/g)	X_c^f (%)
PET-R/IM	75.8	124.7	250.3	20.7	40.2	34.2
PET-R/IME	75.4	122.9	253.9	17.4	42.9	36.5
ET-V/IM	76.3	124.7	250.9	17.8	37.5	31.9
PET-V/IME	75.6	131.5	252.1	21.9	36.5	31.1
PET-R	72.8	118.1	254.6	25.5	46	39.1
PET-V	79.3	126.4	252.3	27.9	37.1	31.6

^a Glass transition temperature.

^b Cold crystallization temperature.

^c Melting point.

^d Enthalpy of cold crystallization.

^e Enthalpy of melting.

^f Relative crystalline content.

absent in the MMT-IME organoclay. This evidence suggests that more rigid structure of silanized groups leads to a higher clustering tendency of particles and, consequently, to the uniform main decomposition peak. A higher level of clustering of nanocomposites containing MMT-IME silicate than that filled with MMT-IM clay is also obvious in TEM micrographs (Figs. 6 and 7: A, C). The different shape of MMT-IME main decomposition peak will be further investigated. Comparing to commercially available organoclays, the thermal stability of prepared imidazole organoclays has been substantially enhanced (Table III).¹³

Mechanical properties

According to tensile tests (Table IV), a higher stiffness and extensibility of the PET-V matrix than that of recycled PET was revealed. Filling of MMT-IM and MMT-IME organoclays into the recycled as well as virgin matrix led to a substantial increase in the Young modulus and to satisfactory values of extensibility, which could be used in the spinning technology (e.g. preparation of fibers with quite a high stiffness). The nanocomposite with the best mechanical properties was prepared by the addition of MMT-IME organosilicate to the virgin PET. On the other hand, the highest stiffness combined with an acceptable level of tensile strength and extensibility was achieved in the PET-V/MMT-IM system. Therefore, various materials for specific purposes could be prepared using different organoclays. The higher tensile strength of nanocomposites containing the MMT-IME filler than those filled with MMT-IM organoclay could result from the presence of polar epoxy functional groups, leading to lower interfacial stress accumulation in a hydrophilic PET matrix. This explanation is in a good accordance with rheological measurements, where the PET-R/MMT-IME system revealed higher melt viscosity and storage modulus than that filled with MMT-IM organoclay. The higher level of melt strength in PET-R/MMT-IME nanocomposite resulted in high interfacial shear strength also in solid state.

TABLE III
Thermogravimetric Decomposition Characteristics of Organoclays

Organoclay	5% mass loss (°C)	10% mass loss (°C)	500°C mass loss (%)
Cloisite 10A	224.6	244.1	34.3
Cloisite 30B	279.1	324.2	17.7
Cloisite 25A	298.5	321.0	30.6
MMT-IME	379.4	412.4	18.8
MMT-IM	381.5	416.6	23.7

TABLE IV
Mechanical Properties of the Matrices and Nanocomposites

Nanocomposite/matrix	Tensile modulus (MPa)	Tensile strength (MPa)	Elongation at break (%)
PET-R/IM	2628	20.6	210.4
PET-R/IME	2743	37.7	192.3
PET-V/IM	2898	30.4	227
PET-V/IME	2460	51.9	253.1
PET-R	2170	54.7	316.5
PET-V	2286	57.1	327.2

CONCLUSIONS

Nanocomposites using both recycled and virgin bottle-grade PET with improved thermal stability and processability were prepared. Rheological investigations revealed a typical shear thinning behavior with organoclay addition and a higher melt viscosity of nanosystems in the whole measured range of shear rates compared with unfilled matrices. These nondegrading organoclays could be used for the preparation of multilayer beverage bottles without admixture of polyamide and, consequently, the recycling of multilayer bottles would be simplified. In comparison with the unfilled matrix, the melt strength of all the nanocomposite systems was significantly enhanced by the formation of a 3D physical network made of silicate platelets. Therefore, more processing technologies for recycled PET can be employed. Differential scanning calorimetry and thermogravimetric analysis supported the evaluation of thermal behavior from rheological experiments. According to transmission electron microscopy, addition of MMT-IM organoclay to recycled or virgin PET led to a better dispersion of silicate platelets than in the MMT-IME filled systems. However, the average increase in interlayer distance determined by WAXS showed a slightly higher level of intercalation in PET/MMT-IME systems. The results of tensile testing showed that specific materials can be prepared by organoclay variation, which leads to different values of tensile strength, Young modulus, and extensibility.

References

1. The Container Recycling Institute; <http://www.container-recycling.org>.
2. PETCORE association (PET containers recycling Europe); <http://www.petcore.org>.
3. PET recycling association; <http://www.petrecycling.cz>.
4. Pegoretti, A.; Kolarik, J.; Peroni, C.; Migliaresi, C. *Polymer* 2004, 45, 2751.
5. Sanchez-Solis, A.; Romero-Ibarra, I.; Estrada, M. R.; Calderas, F.; Manero, O. *Polym Eng Sci* 2004, 44, 1094.
6. Sanchez-Solis, A.; Garcia-Rejon, A.; Manero, O. *Macromol Symp* 2003, 192, 281.

7. Kráčalík, M.; Mikešová, J.; Puffr, R.; Baldrian, J.; Thomann, R.; Friedrich, C. *Polym Bull* 2007, 58, 313.
8. Weygand, F.; Daniel, H.; Simon, H. *Chemische Berichte* 1958, 91, 1691.
9. Bach, R. D.; Andrzejewski, D.; Bair, K. W. *J Chem Soc: Chem Commun* 1974, 20, 820.
10. Bach, R. D.; Knight, J. W. *Tetrahedron Lett* 1979, 40, 3815.
11. Wittig, G.; Polster, R. *Ann* 1957, 612, 102.
12. Wittig, G.; Burger, T. F. *Ann* 1960, 632, 85.
13. Kráčalík, M.; Studenovský, M.; Mikešová, J.; Sikora, A.; Thomann, R.; Friedrich, C.; Fortelný, I.; Šimoník, J. Recycled PET nanocomposites improved by silanization of organoclays. *J Appl Polym Sci*, to appear.
14. Webb, P. B.; Sellin, M. F.; Kunene, T. E.; Williamson, S.; Slawin, A. M. Z.; Cole-Hamilton, D. J. *J Am Chem Soc* 2003, 125, 15577.
15. Metha, A.; Wunderlich, B. *J Polym Sci Polym Phys Ed* 1978, 16, 289.
16. Krishnamoorti, R.; Giannelis, E. P. *Macromolecules* 1997, 30, 4097.
17. Krishnamoorti, R.; Vaia, R. A.; Giannelis, E. P. *Chem Mater* 1996, 8, 1728.
18. Khan, S. A.; Pru'homme, R. K. *Rev Chem Eng* 1987, 4, 205.

2.1.6 Manuscript 4

“Effect of glass fibers on rheology, thermal and mechanical properties of recycled PET”

Kráčalík, Milan; Pospíšil, Ladislav; Šlouf, Miroslav; Mikešová, Jana; Sikora, Antonín; Šimoník, Josef; Fortelný, Ivan (2008): In: Polym. Compos. 29 (8), S. 915–921. DOI: 10.1002/pc.20467.

In this paper, synergic effects of two fillers in recycled PET matrix were investigated. It was revealed that interface interactions between glass fibers, talc and PET matrix lead to strong physical 3D network demonstrated by rheological measurements (existence of rubber-like behaviour as in the case of well dispersed polymer nanocomposites). The highest level of fiber-matrix interfacial adhesion was obtained with the fiber filling 20 %. According to rheological study, the highest melt strength was achieved at the 30 % loading of fibers. A significant increase in the complex viscosity and storage modulus with glass fibers and talc loading was observed at low frequencies, where the viscoelastic liquid of recycled PET changed into a solid-like behaviour. In all the mixtures, filling with fibers and talc exhibited an enhancing effect on rheological properties of the composites. On the contrary, processing under production-scale conditions led to formation of air bubbles together with the moderate loss of melt strength and viscosity, compared with analogous system processed on the pilot-plant scale. A correlation between the fiber content on linear viscoelastic flow characteristics and dispersion level (SEM) of the prepared composites was found. Mechanical characterization of composites filled with 20 % of glass fibers revealed the highest toughness, while the 30 % fiber loading resulted in the highest level of stiffness, tensile strength and flexural modulus. Thermal characterization of composites revealed an increase in glass transition temperature and decrease in total crystallinity with fibers loading. Unusual thermal behaviour of composites prepared under lab-scale conditions was attributed to crystallization of PET chains on the surface of glass fibers.

Effect of Glass Fibers on Rheology, Thermal and Mechanical Properties of Recycled PET

Milan Kráčalík,¹ Ladislav Pospíšil,² Miroslav Šlouf,³ Jana Mikešová,³ Antonín Sikora,^{3,4}
Josef Šimoník,⁴ Ivan Fortelný^{3,4}

¹*Institute of Plastics Processing, University of Leoben, Franz-Josef Str. 18, 8700 Leoben, Austria*

²*Polymer Institute Brno Ltd., Tkalcovská 2, 656 49 Brno, Czech Republic*

³*Institute of Macromolecular Chemistry, Academy of Sciences of the Czech Republic, Heyrovský Sq. 2, 162 06 Prague, Czech Republic*

⁴*Faculty of Technology, Tomas Bata University in Zlín, T.G.M. Sq. 275, 762 72 Zlín, Czech Republic*

PET-glass fiber composites were prepared by melt mixing of recycled PET with chopped glass fibers (15, 20, and 30 wt%) and their degree of dispersion was assessed by scanning electron microscopy. Rotational rheometry was employed to analyze the interfacial shear strength between the fibers and polymer matrix in the molten state. The composite containing 30 wt% of glass fibers revealed a moderate G' secondary plateau; hence strong fiber-matrix interactions were confirmed. Results of mechanical testing were in a good accordance with structural and rheological measurements. The higher rate of mixing under production-scale conditions resulted in lower fiber-matrix adhesion and in a similar level of fiber dispersion as compared to the same mixture compounded on pilot-plant scale. Thermal characterization of the composites was performed by differential scanning calorimetry and total crystalline fraction was analyzed. POLYM. COMPOS., 29:915–921, 2008. © 2008 Society of Plastics Engineers

INTRODUCTION

Preparation of composites using recycled polymers is an important issue both from the technological and environmental points of view. The amount of poly(ethylene terephthalate) (PET) used in plastics industry (especially for beverage bottles) has been significantly increasing [1], hence the problem of sufficient recycling is more and more challenging. The volume of recycled PET bottles in

PET-reprocessing countries varies usually around 20 wt%. The rest of the used bottles are incinerated or dumped [2, 3]. A further problem consists in limited applications of recycled PET (mostly staple fibers, packaging, films, and strips) [2]. The limitation is due to processing properties of the recycle (viscosity, melt strength), which are deteriorated during recycling process. This problem can be solved by incorporation of proper particles into recycled polymer by melt compounding. Consequently, melt viscosity increases in the range of low shear rates and enhanced melt strength makes reprocessing possible. The use of glass fibers involves interesting combination of high reinforcement with a rather low price. However, enhancement of processing and utility properties of recycled polymers requires high interfacial adhesion between glass fiber and polymer matrix. Sufficient fiber-matrix interactions are essential to transfer the stresses from the matrix to the reinforcing fibers. Therefore, analysis of interfacial shear strength from rheological measurements in the linear viscoelasticity region gives necessary information on the effect of reinforcing particles on processing behavior. Moreover, material characteristics in the melt state reflect structural changes, which have a strong impact on the final performance of dispersive polymeric system. The recycled PET-glass fiber composites have been studied so far; however, no study dealing with processing properties (exact analysis of elastic and viscous part of melt viscosity) and their correlation with structure and utility performance has been found in literature. The current papers focus mostly on thermal and mechanical (possibly flammability) characterization [4–10] and rarely on degradation analysis or processing/structural changes in recycled PET-glass fiber systems [11, 12]. Neverthe-

Correspondence to: M. Kráčalík; e-mail: milan.kracalik@mu-leoben.at

Contract grant sponsor: Ministry of Industry and Trade of the Czech Republic, Polymer Institute Brno, Ltd; contract grant number: 1H-PK2/67. DOI 10.1002/pc.20467

Published online in Wiley InterScience (www.interscience.wiley.com).

© 2008 Society of Plastics Engineers

less, understanding rheological properties and structural changes and, consequently, material end-properties belongs to the needs of applied polymeric engineering.

EXPERIMENTAL

Materials

Color-sorted recycled poly(ethylene terephthalate) (PET-R), with the intrinsic viscosity 0.93 dl/g (phenol/tetrachloroethane 1:3) as well as ECTA ES2001EF chopped glass fibers (original fiber length 4 mm, diameter 10 μm) were supplied by Polymer Institute Brno. According to characteristics in Table 2, PET-R exhibits usual thermal behavior (similar to virgin bottle grade PET) because no remarkable decrease in T_g (T_m) magnitude occurred indicating quite a low level of impurity. To improve processing and utility properties (higher interfacial adhesion, dispersion, stability of the mixture), 10% of Naintsch A-3 talc, 1% of Licowax OP flow modifier, and 0.2% of Ultrinox 626 stabilizer were admixed before compounding (Table 1).

Preparation of Composites

The recycled PET flakes were dried at 120°C in an oven for 6 h. The polymer was mixed with glass fibers, talc, flow agent, and stabilizer in a corotating twin-screw extruder (Werner & Pfleiderer ZSK 25, $d = 25$ mm, pilot-scale output 10 kg/h; for comparison, production-scale output conditions at 250–400 kg/h were tested). The compounding temperature was 260–275°C and the screw speed 200 rpm. For characterization, recycled PET composites were injection-molded (Battenfeld BA750/200) to specimens at 260–275°C, (mould temperature 40–120°C).

Melt Rheology

Rheological properties were studied using an ARES 3 Rheometer (Advanced Rheometric Expanded System, Rheometric Scientific) with parallel-plate geometry and 25-mm diameter plates. All measurements were performed with two automatically switched force transducers with a torque range of 0.02–2,000 g cm. The sample thickness ranged from 0.9 to 1.1 mm. Experiments were performed at 270°C under nitrogen to prevent degradation of samples. The following types of rheological measurements were carried out: (1) dynamic strain sweep test (at 6.28 rad/s) to confirm the linearity of viscoelastic region, (2) dynamic frequency sweep test over a frequency range of 0.1–100 rad/s, at the strain 2% for the composites, 30% for the matrix.

TABLE 1. Specification of mixtures.

Composition (wt%)	W 5167	W 6187	W 5455	GF20T10
PET-R	73.8	68.8	58.8	68.8
ECTA ES2001EF	15	20	30	20

Scanning Electron Microscopy

The scanning electron microscopy (SEM) micrographs were obtained with JSM 6400 (Jeol). The specimens for SEM observations were prepared in two ways. The first series of specimens was cut with microtome at room temperature and the other series was fractured in liquid nitrogen. The cut and fracture surfaces of the specimens from the first and second series were examined by SEM microscopy. Before microscopic investigations, all specimens were sputtered with thin platinum layer (ca. 4 nm) in a vacuum sputter coater SCD 050 (Balzers) to prevent charging and decrease the sample damage by the electron beam. All micrographs were secondary electron images taken at an acceleration voltage 30 V.

Thermal Characteristics

Thermal characterization of the polymer matrix and nanocomposites was carried out by differential scanning calorimetry (Perkin Elmer, Pyris 1 DSC) using the standard mode: 1, 30°C for 3 min; 2, heating from 30°C to 280°C at 10°C/min; 3, 280°C for 2 min. The thermal parameters, glass transition temperature (T_g), cold crystallization temperature (T_c), melting temperature (T_m), enthalpy of cold crystallization (ΔH_c), and enthalpy of melting (ΔH_m) were calculated for the matrix and polymer fraction in the composites. The crystalline content (X_c) was evaluated by assuming the ΔH_m of hypothetical 100% crystalline poly(ethylene terephthalate) to be 117.6 J/g [13].

Mechanical Properties

For tensile tests an Instron 5800 R was employed. Experiments were performed according to the ISO 527-2 standard. The crosshead speeds were 1 mm/min for tensile modulus measurements and for all other characteristics 50 mm/min. The toughness characterized as Charpy impact strength was measured according to the CSN EN ISO 179-1 standard at room temperature.

RESULTS AND DISCUSSION

Morphology of Glass Fibers in Recycled PET

The prepared composites were analyzed by scanning electron microscopy in the solid state to determine changes in the structure caused by the introduction of glass fibers into recycled PET. The effects of variations in fiber concentration and compounding conditions on the structure of polymer matrix were investigated and the results are shown in Figs. 1–3.

The influence of the fiber content and processing conditions on the structural changes is indicated in Figs. 1 and 2. With increasing fiber concentration, the homogeneity of fiber distribution in polymer matrix remains almost constant. The remarkable change in structure was detected

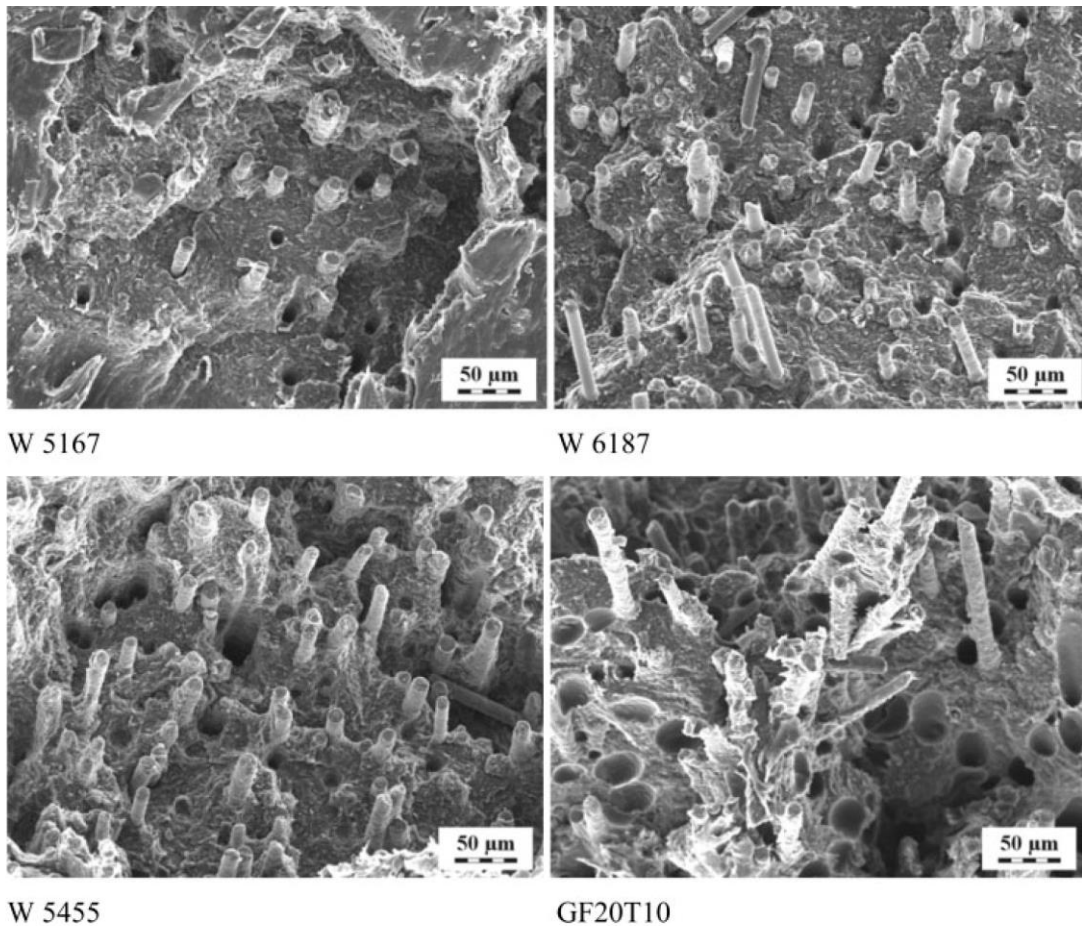


FIG. 1. SEM micrographs of fracture surfaces of composites.

in the GF20T10 system, where air bubbles were observed in both fracture (Fig. 1) and cut surfaces (Fig. 2). The average diameter of the bubbles varies around $30\ \mu\text{m}$ so that confusion of air bubbles with fiber cavities can be excluded. This structural inhomogeneity (remarkable in Fig. 2) is attributed to higher processing speed under production-scale conditions.

According to Fig. 3, a similar level of fiber-matrix interfacial adhesion in all composite systems was achieved. It is obvious from our previous work [14] that talc particles in PET/glass fibers composite systems act as a coupling agent and, consequently, facilitates interfacial interactions resulting in high interfacial shear strength.

Melt Rheology

Dynamic rheological properties of PET-R/glass fiber composites were investigated in the region of linear viscoelasticity. The dynamic strain sweep test [$G'(\gamma)$] revealed the linearity region ranging at 1–100% strain for the matrix and 1–15% strain for the composites. As can

be seen in Fig. 4, the recycled PET matrix showed Newtonian behavior in the frequency dependence $\eta^*(\omega)$ within the investigated range of shear rates.

Compared with the unfilled matrix, a significant growth of the complex viscosity of composites in the range of low frequencies (more than one order) occurred. All the prepared composites show a shear thinning phenomenon, which is caused by orientation of fibers in the flow direction.

The highest filling effect was achieved with 30% loading of glass fibers. A lower content of the filler in the polymer matrix manifested itself by lower melt viscosity in the whole range of shear rates. The flow curves of the W 6187 and GF20T10 systems revealed similar tendency, whereas the composite prepared under production-scale conditions showed slightly lower melt viscosity.

The internal structural changes in composite systems under shear flow can be analyzed using frequency dependences of the storage (G') and loss (G'') moduli. Addition of a filler to the PET-R melt causes an increase in the dynamic moduli, particularly in G' (Fig. 5). The unfilled matrix behaves like viscoelastic liquid ($G'' > G'$).

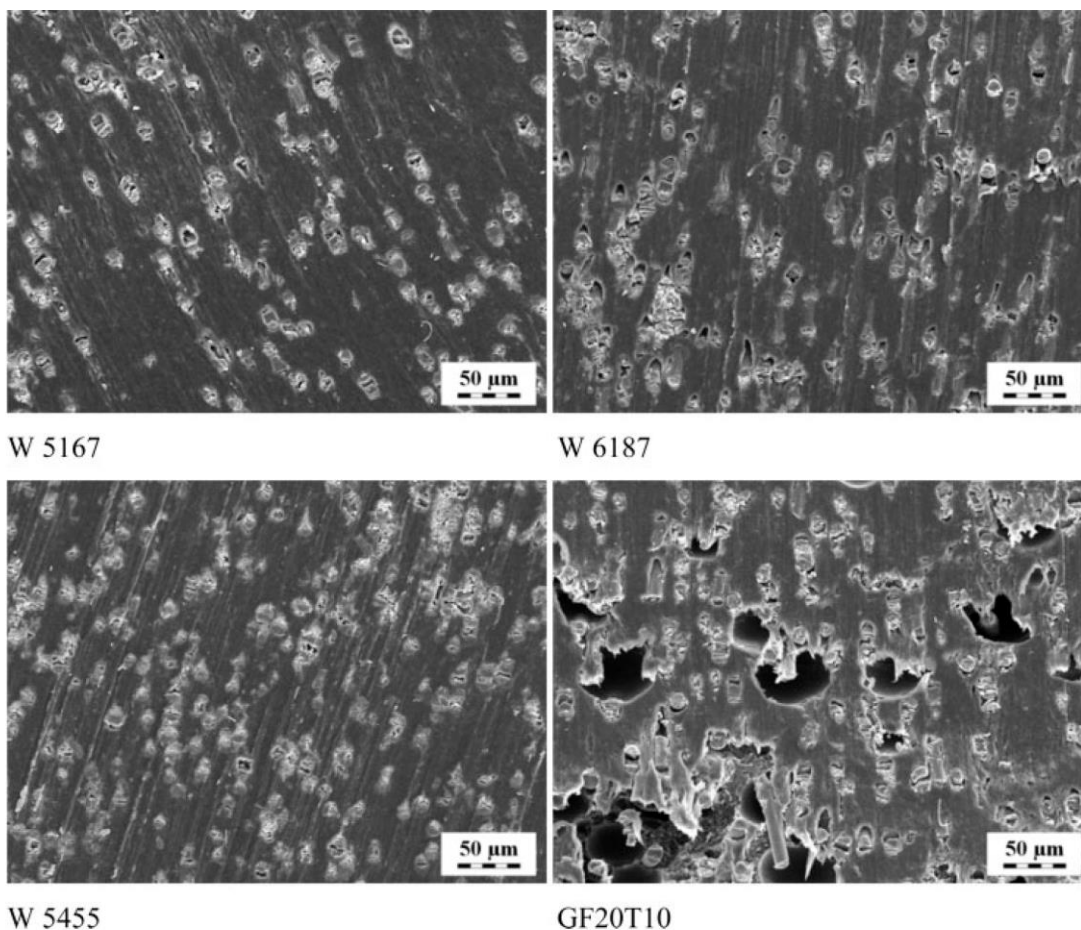


FIG. 2. SEM micrographs of cut surfaces of composites.

The higher value of G' than G'' for the composites shows a change in rheological behavior, the “liquid-solid” transformation. Furthermore, the power-law dependence of the dynamic moduli at low frequencies, which is typical of neat PET, is absent in the composites. The dependence of $G'(\omega)$ at low shear rates is nearly invariable. This indication of a $G'(\omega)$ secondary plateau can be associated with similar behavior of well-dispersed structures in polymer nanocomposites, where high interfacial shear strength is parallel with the formation of network structure (exfoliation) of silicate layers [15–18].

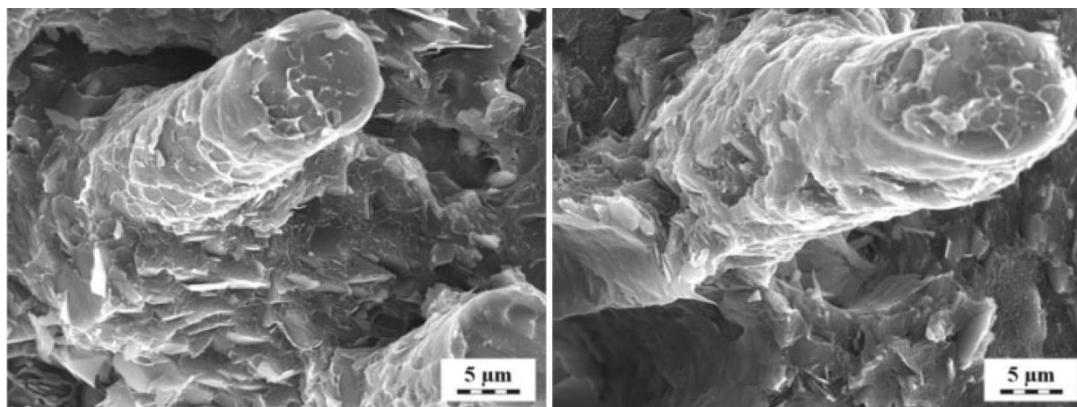
Usually, fiber-filled polymer dispersions exhibit a frequency dependence of storage modulus similar to matrix increasing with the filler content [19]. The composites prepared in our study showed a moderate G' secondary plateau and, thereby, confirmed high fiber-matrix adhesion in the molten state, whereas number of surface interactions rise with glass fiber loading. This increase in melt strength facilitates further processing of material in such cases, where the loss of melt cohesion causes process difficulties (e.g. during flat-die extrusion or blow moulding).

Moreover, the flow and melt strength curves are in good agreement with structure determined by scanning electron microscopy (a higher fiber content in polymer matrix results in higher melt strength and viscosity of composites, while a lower fiber-matrix interfacial adhesion together with porosity of GF20T10 system manifests itself by worse rheological properties compared with the corresponding W 6187 composite).

Thermal Characteristics

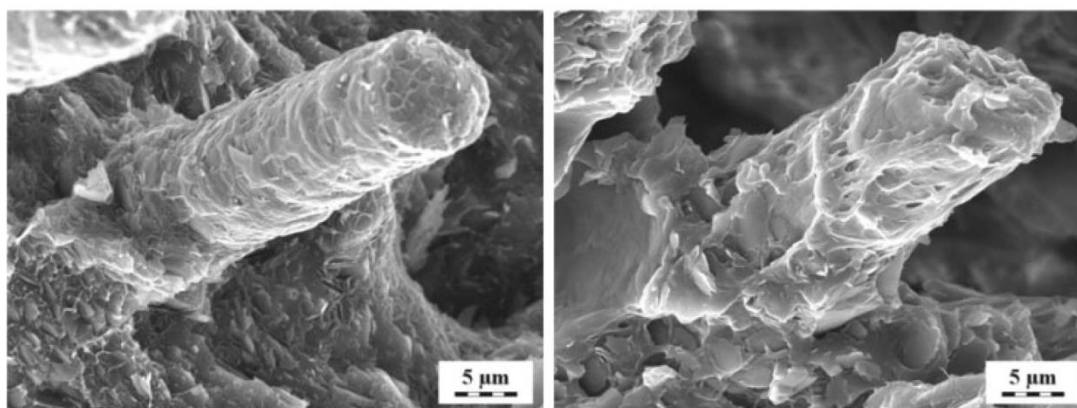
Thermal properties of composites were studied by differential scanning calorimetry. The values of thermal parameters are listed in Table 2. A moderate increase in glass transition temperature with glass fibers loading was observed. This phenomenon can be explained by strong polymer-fiber interactions, which cause higher fixation of polymer chains surrounded by glass fibers. This explanation of high interfacial adhesion is in a good agreement with results of other testing methods.

In comparison to the GF20T10 system (Fig. 6), all the composites from the W series exhibited unusual thermal



W 5167

W 6187



W 5455

GF20T10

FIG. 3. SEM micrographs of fracture surfaces of composites at higher magnification.

behavior characterized by first endothermic melting peak T_{mf} at 183–192°C and by the absence of exothermic peak of cold crystallization. This difference reflects variation in

processing history where crystallization on the fiber surface occurred during lab-scale extrusion. The amount of first crystalline fraction decreased with fiber loading,

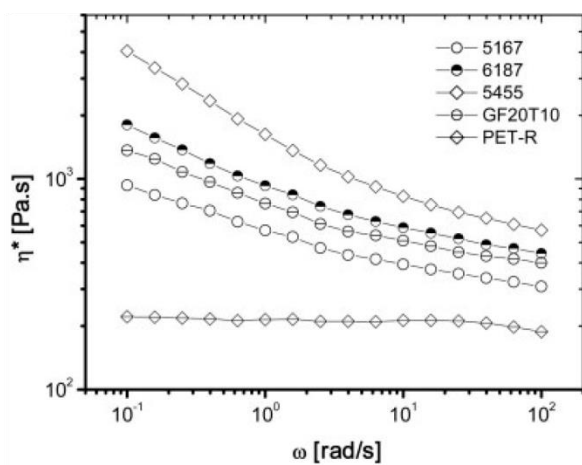


FIG. 4. The complex viscosity vs. frequency for the recycled PET matrix and composites.

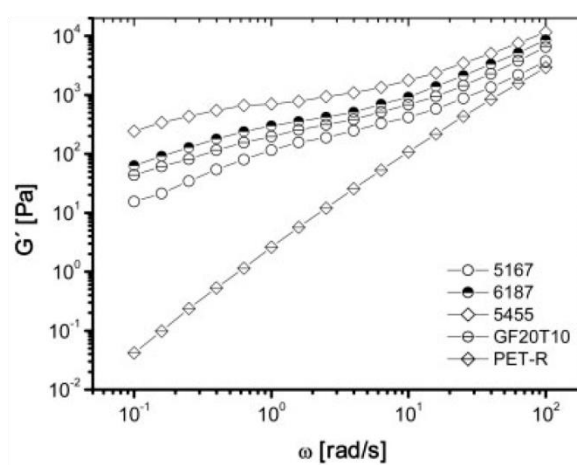


FIG. 5. The storage modulus vs. frequency for the recycled PET matrix and composites.

TABLE 2. Thermal properties of composites and neat matrix.

Composite	T_g^a (°C)	T_{mf}^b (°C)	ΔH_{mf}^c (J/g)	T_m^d (°C)	ΔH_m^e (J/g)	X_c^f (%)
W 5167	74.0	183.4	3.1	252.9	36.9	31.4
W 6187	75.2	187.8	2.69	253.7	29.4	25
W 5455	76.8	191.9	1.7	247.5	25.3	21.5
GF20T10	75.6	—	—	253.2	32.3	27.5
PET-R	75.6	—	—	252.2	43.2	36.7

^a Glass transition temperature.

^b First endothermic melting peak.

^c Enthalpy of first melting (first crystalline fraction).

^d Melting point.

^e Enthalpy of melting.

^f Crystalline fraction content.

which can be associated with increase in melt shear rate resulting in higher degradation of macromolecular chains; consequently, the number of spherulites during heterogeneous crystallization is restricted. This explanation is supported by the lowest melt temperature and total crystallinity of W 5455 composite containing the highest loading of glass fibers. The relative crystalline content of all the composites was lower compared with that of the neat PET-R matrix.

Mechanical Characteristics

Mechanical properties of composites are listed in Table 3. The values of tensile strength, stiffness, flexural modulus, and toughness increased with fiber loading. The processing under production-scale conditions (employed for GF20T10 composite preparation) led to slight deterioration of mechanical properties in comparison to analogous system W 6187. However, W 6187 and GF20T10 systems revealed the highest toughness, probably due to optimal concentration of glass fibers (see chapter Morphology) and coupling effect of talc particles. The extensibility was

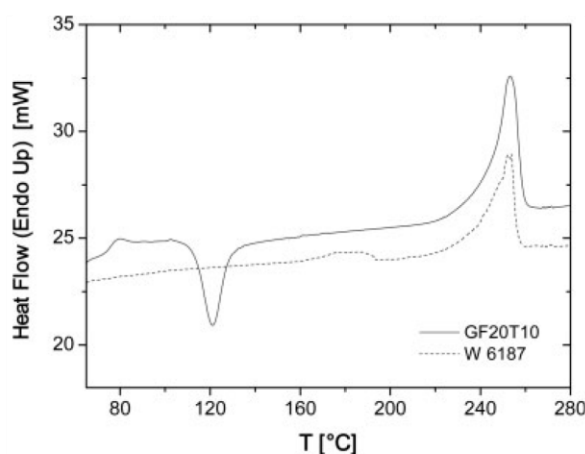


FIG. 6. DSC thermogram of composites filled with 20 wt% of glass fibers.

TABLE 3. Mechanical properties of the composites.

Properties	W 5167	W 6187	W 5455	GF20T10
Tensile strength (MPa)	110	113	121.7	111
s_x	1.2	1.3	1.5	1.1
Elongation at break (%)	2.6	2.2	2.2	2.4
s_x	0.1	0.1	0.1	0.1
Tensile modulus (MPa)	8,200	10,290	13,900	10,111
s_x	52	162	170	138
Flexural modulus (MPa)	7,900	9,377	12,650	9,204
s_x	47	57	151	48
Impact strength (kJ/m ²)	32	43.3	36.6	37.0
s_x	3.1	4.2	3.7	3.5
Notch impact strength (kJ/m ²)	4.6	6.6	6.6	4.8
s_x	2.1	3.3	3.3	32.4

not significantly influenced by different content of added fibers. The highest stiffness, tensile strength, and flexural modulus exhibited the system filled with 30% of glass fibers.

CONCLUSIONS

Recycled PET-glass fiber composites were prepared by melt compounding. According to analysis of SEM micrographs, all the composite systems revealed a high level of fiber dispersion and homogeneity in the recycled PET matrix. The highest level of fiber-matrix interfacial adhesion was obtained with the fiber filling 20%. According to rheological study, the highest melt strength was achieved at the 30% loading of fibers. A significant increase in the complex viscosity and storage modulus with glass fibers and talc loading was observed at low frequencies, where the viscoelastic liquid of recycled PET changed into a solid-like behaviour. In all the mixtures, filling with fibers and talc exhibited an enhancing effect on rheological properties of the composites. On the contrary, processing under production-scale conditions led to formation of air bubbles together with the moderate loss of melt strength and viscosity, compared with analogous system processed on the pilot-plant scale. A correlation between the fiber content on linear viscoelastic flow characteristics and dispersion level (SEM) of the prepared composites was found. Mechanical characterization of composites filled with 20% of glass fibers revealed the highest toughness, while the 30% fiber loading resulted in the highest level of stiffness, tensile strength and flexural modulus. Thermal characterization of composites revealed an increase in glass transition temperature and decrease in total crystallinity with fibers loading. Unusual thermal behaviour of composites prepared under lab-scale conditions was attributed to crystallization of PET chains on the surface of glass fibers.

REFERENCES

1. PETCORE Association (PET containers recycling Europe); <http://www.petcore.org>.

2. PET Recycling Server, <http://www.petrecycling.cz>.
3. M. Kráčalík, L. Pospíšil, J. Šimoník, J. Kimmer, and J. Hrnčířník, *Plasty Kauc.*, **40**, 356 (2003).
4. A.L.F. de M. Giraldi, J.R. Bartoli, J.I. Velasco, and L.H.I. Mei, *Polym. Test.*, **24**, 507 (2005).
5. A.L.F. de M. Giraldi, R. Cardoso de Jesus, and L.H.I. Mei, *J. Mater. Process. Technol.*, **162/163**, 90 (2005).
6. A. Pegoretti and A. Penati, *Polymer*, **45**, 7995 (2004).
7. A. Pegoretti and A. Penati, *Polym. Degrad. Stab.*, **86**, 233 (2004).
8. M.L. MasPOCH, H.E. Ferrando, D. Vega, A. Gordillo, J.I. Velasco, and A.B. Martínez, *Macromol. Symp.*, **221**, 175 (2005).
9. F. Laoutid, L. Ferry, J.M. Lopez-Cuesta, and A. Crespy, *Polym. Degrad. Stab.*, **82**, 357 (2003).
10. K. Tóth, T. Czvikovszky, and M. Abd-Elhamid, *Radiat. Phys. Chem.*, **69**, 143 (2004).
11. M.P. Foulc, A. Bergeret, L. Ferry, P. Ienny, and A. Crespy, *Polym. Degrad. Stab.*, **89**, 461 (2005).
12. R. Assadi, X. Colin, and J. Verdu, *Polymer*, **45**, 4403 (2004).
13. A. Metha and B. Wunderlich, *J. Polym. Sci.: Polym. Phys. Ed.*, **16**, 289 (1978).
14. M. Kráčalík, L. Pospíšil, M. Šlouf, J. Mikešová, A. Sikora, J. Šimoník, and I. Fortelný, *Polym. Compos.*, accepted for publication.
15. R. Krishnamoorti and E.P. Giannelis, *Macromolecules*, **30**, 4097 (1997).
16. S.A. Khan and R.K. Prudhomme, *Rev. Chem. Eng.*, **4**, 205 (1987).
17. R. Krishnamoorti, R.A. Vaia, and E.P. Giannelis, *Chem. Mater.*, **8**, 1728 (1996).
18. M. Kráčalík, J. Mikešová, R. Puffr, J. Baldrian, R. Thomann, and C. Friedrich, *Polym. Bull.*, **58**, 313 (2007).
19. R. Guo, J. Azaiez, and C. Celine Bellehumeur, *Polym. Eng. Sci.*, **45**, 385 (2005).

2.1.7 Manuscript 5

“Recycled poly(ethylene terephthalate) reinforced with basalt fibres. Rheology, structure, and utility properties”

Kráčalík, Milan; Pospíšil, Ladislav; Šlouf, Miroslav; Mikešová, Jana; Sikora, Antonín; Šimoník, Josef; Fortelný, Ivan (2008): In: Polym. Compos. 29 (4), S. 437–442. DOI: 10.1002/pc.20425.

Using know-how from manuscript 4, synergic effect of talc on performance of recycled PET/basalt fibers composite was tested. It was proved that multiphase systems with talc addition revealed enhanced melt viscosity and melt elasticity (existence of rubber-like behaviour as in the case of well dispersed polymer nanocomposites) comparing to typical composites. In the systems containing talc, the recycled PET matrix adhered significantly more to the surface of the reinforcing fibers. Their linear viscoelastic properties reflected structural changes (variations of basalt concentration and talc addition) in composites. Higher values of the complex viscosity and storage modulus confirmed an increase in interfacial filler-matrix adhesion. Addition of talc and higher concentration of basalt fibers in composites resulted in better mechanical performance, manifesting itself mostly by tensile strength, stiffness, flexural modulus and toughness. The values of extensibility were independent of talc and fiber loading. The system filled with talc and 30 % of fibers showed the highest reinforcement. Concerning thermal properties, the results of differential scanning calorimetry revealed interesting thermodynamical behaviour unusual for recycled PET-glass fiber composites or recycled PET-organoclay nanocomposites. The composites without talc addition showed a decrease in the first crystalline fraction (ΔH_{mf}) with higher fiber content. This behaviour can be associated with steric hindrance of fiber excess to the growth of crystalline nuclei during heterogeneous crystallization.

Recycled Poly(ethylene terephthalate) Reinforced With Basalt Fibres: Rheology, Structure, and Utility Properties

Milan Kráčalík,¹ Ladislav Pospíšil,² Miroslav Šlouf,³ Jana Mikešová,³ Antonín Sikora,^{3,4}
Josef Šimoník,⁴ Ivan Fortelný^{3,4}

¹Institute of Plastics Processing, University of Leoben, 8700 Leoben, Austria

²Polymer Institute Brno Ltd., Tkalcovská 2, 656 49 Brno, Czech Republic

³Institute of Macromolecular Chemistry, Academy of Sciences of the Czech Republic, 162 06 Prague, Czech Republic

⁴Faculty of Technology, Tomas Bata University in Zlín, 762 72 Zlín, Czech Republic

Utilization of recycled poly(ethylene terephthalate) (PET) as a matrix for composite materials prepared by continuous compounding is challenging from the environmental as well as industrial point of view. In our work, cut basalt fibers and talc powder of various compositions were used and their reinforcing effect on recycled PET was tested by rheology (Advanced Rheometric Expansion System), differential scanning calorimetry, and tensile experiments. The quality of filler dispersion in recycled PET matrix was investigated by scanning electron microscopy (SEM) and melt rheology. Processing and utility properties of composites were enhanced as compared with those of unfilled matrix. Higher melt elasticity, interfacial adhesion, and better mechanical performance of the composites were in a good agreement with the structure observed from SEM micrographs. POLYM. COMPOS., 29:437–442, 2008. © 2008 Society of Plastics Engineers

INTRODUCTION

The use of polymer materials has been increasing worldwide every year. Replacement of classical (metals, glass, ceramics) materials by plastics requires a good recycling strategy. Poly(ethylene terephthalate) (PET) as the leading synthetic polymer for beverage bottles production is recycled of 30% on average in the European Union and

20% in the United States only [1, 2]. Problems with PET recycling arise also from limited applications of recycle (mostly staple fibers, packaging, films, and strapping bands) [3]. Up to now, glass fibers as a reinforcement of recycled PET have been studied [4–10]. However, some disadvantages associated with glass fibers limit their applications. For example, skin irritation avoids applications, in which released fibers might have contact with the human skin [11]. Moreover, basalt fibers form a better surface as compared to glass fibers [12]. Concerning technological and economical evaluation, filling of basalt fibers affords reinforcement within the range of glass and carbon filaments. High heat resistance, high stability in aggressive media, substantial sound absorption, and enormous physical durability of basalt fibers results in glass fiber replacement in various industrial applications and hereby opens new fields of application [13, 14]. Basalt fibers spun from melted basalt stone possess a higher tensile modulus (at least 16%), equivalent strength, and higher alkaline resistance [15] compared with glass fibers [16], enhanced interfacial adhesion [15] and are available commercially [17]. It is also useful to mention, that basalt is the most current igneous rock on the Earth. According to Czigány [18] the cheap basalt fibers can be efficiently applied in hybrid composite systems. He found out that basalt fiber hybridization of polypropylene-hemp fiber composites increased mechanical properties only moderately while significant enhancement of PP-carbon fiber and PP-glass fiber systems with basalt fibers loading was reached. So far, no mention about recycled PET-basalt fibres systems appeared in available literature. In this work, also relationship between melt rheology, structure, thermal, and mechanical characteristics of composites containing recycled PET matrix is discussed.

Correspondence to: Milan Kráčalík; e-mail: Milan.Kracalik@mu-leoben.at
Contract grant sponsor: Ministry of Industry and Trade of the Czech Republic; contract grant number: IH-PK2/67; contract grant sponsor: Polymer Institute Brno, Ltd., Brno, Czech Republic.
DOI 10.1002/pc.20425
Published online in Wiley InterScience (www.interscience.wiley.com).
© 2008 Society of Plastics Engineers

TABLE 1. Specification of composites.

Composition (%)	WPL 6938	WPL 6939	WPL 6941	WPL 6940
PET-R	78.8	68.8	68.8	58.8
Basalt fibers	20	30	20	30
Talc	0	0	10	10

The effect of talc admixture on basalt fibers-PET interfacial adhesion is investigated. From the industrial point of view, the recycling of PET by continuous melt compounding using good performance and low cost basalt fibers can be interesting.

EXPERIMENTAL PROCEDURES

Materials

Color-sorted recycled poly(ethylene terephthalate) (PET-R), with the intrinsic viscosity 0.95 dl/g (phenol/tetrachloroethane 1:3) as well as cut basalt fibers (average length 4 mm,

diameter 15 μm) were supplied by the Polymer Institute Brno, Ltd. To improve processing and utility properties (higher interfacial adhesion, dispersion, stability), Naintsch A-3 talc, Lico-wax OP flow modifier (1%), and Ultrinox 626 antioxidant (0.2%) were added before compounding (Table 1).

Preparation of Composites

The recycled PET flakes were dried at 120°C in oven for 6 h. The polymer was compounded with basalt fibers, talc, flow modifier, and antioxidant in a corotating twin-screw extruder (Werner & Pfleiderer ZSK 25, $d = 25$ mm). The compounding process proceeded at 260–275°C and the screw speed about 200 rpm. Recycled PET composites were injection-molded (injection moulding machine Battenfeld BA750/200) to specimens at 260–275°C, the mould temperature ranged from 40 to 120°C.

Structure of Composites

The scanning electron microscopy (SEM) measurements were performed with a JEOL JSM 6400 scanning electron

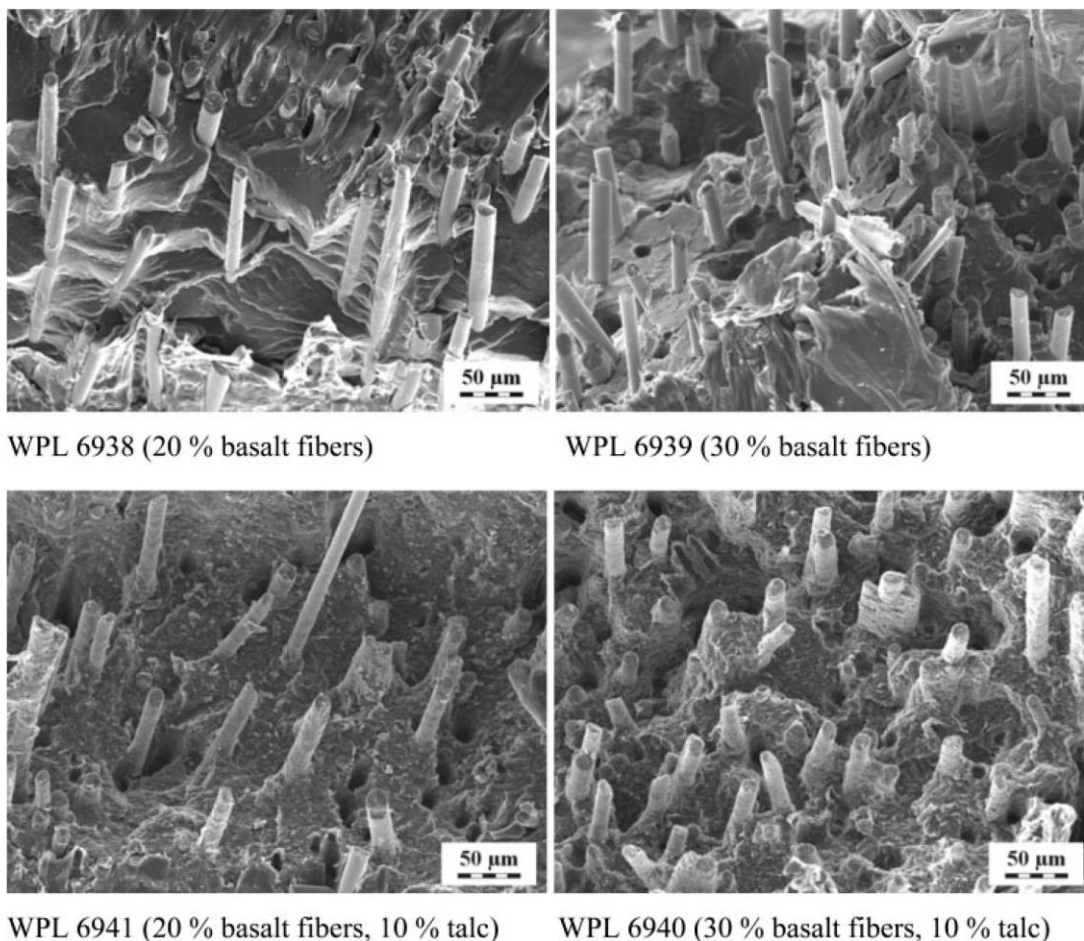
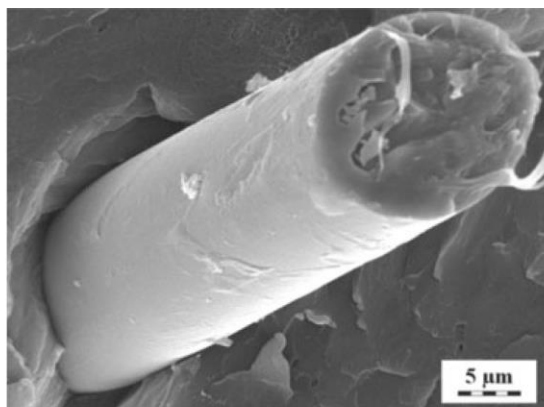
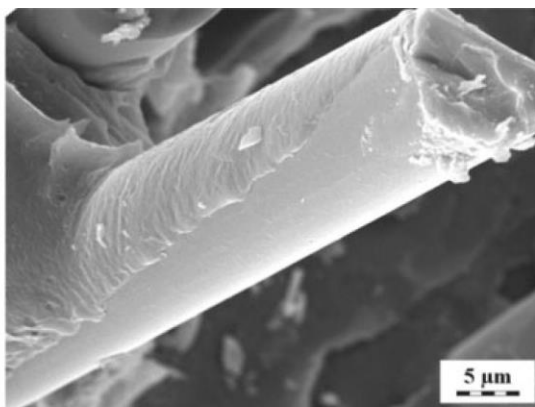


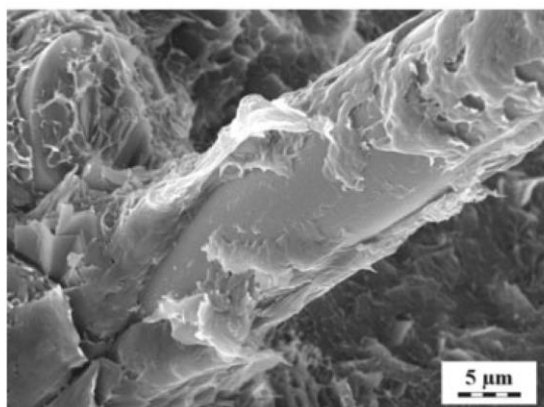
FIG. 1. SEM micrographs of composites (dispersion).



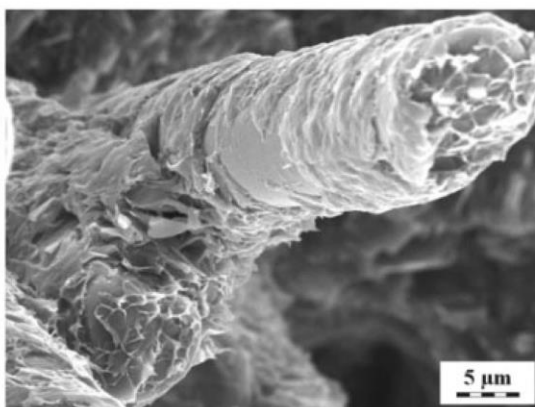
WPL 6938 (20 % basalt fibers)



WPL 6939 (30 % basalt fibers)



WPL 6941 (20 % basalt fibers, 10 % talc)



WPL 6940 (30 % basalt fibers, 10 % talc)

FIG. 2. SEM micrographs of composites (interfacial adhesion).

microscope. The samples were fractured in liquid nitrogen and SEM microphotographs of surface area were obtained. Before experiments, the samples were sputtered with platinum using a vacuum sputter coater (SCD, Balzers). All SEM pictures were secondary electron images taken at an acceleration voltage of 30 kV.

Melt Rheology

Rheological properties were studied using an ARES 3 Rheometer (Advanced Rheometric Expanded System, Rheometric Scientific, USA) with parallel-plate geometry of 25-mm diameter plates. All measurements were performed with two automatically switched force transducers with a torque range of 0.02 (2,000 gcm). The samples thickness ranged from 0.9 to 1.1 mm. Experiments were performed at 270°C under nitrogen to prevent degradation of samples. The following types of rheological measurements were carried out: (1) dynamic strain sweep test (at 6.28 rad/s) to confirm the linearity of viscoelastic region, (2) dynamic frequency sweep test over a frequency range of 0.1 (100 rad/s, at the strain 2% for the composites and 30% for the matrix).

Thermal Properties

Thermal characterization of the polymer matrix and composites was carried out by differential scanning calorimetry (Perkin Elmer, Pyris 1 DSC) using a standard mode: 30°C for 3 min, heating from 30°C to 280°C at 10°C/min, 280°C for 2 min. The thermal parameters, glass transition temperature (T_g), cold crystallization temperature (T_c), melting temperature (T_m), enthalpy of cold crystallization (ΔH_c), and enthalpy of melting (ΔH_m) were calculated. The crystalline content (X_c) in composites was evaluated by assuming the ΔH_m for hypothetical 100% crystalline PET to be 117.6 J/g [19].

Mechanical Testing

Tensile properties were tested using an Instron 5800 R instrument. Experiments were performed according to ISO 527-2 standard. The crosshead speeds were for tensile modulus measurements 1 mm/min and for all other characteristics 50 mm/min. The toughness was measured according to ČSN EN ISO 179-1 standard.

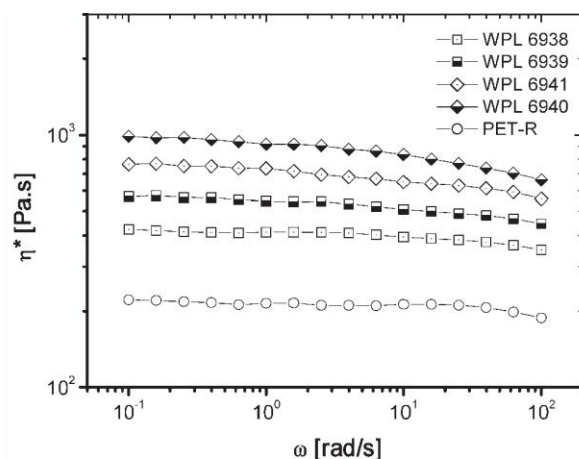


FIG. 3. Dynamic flow curves of the matrix and composites.

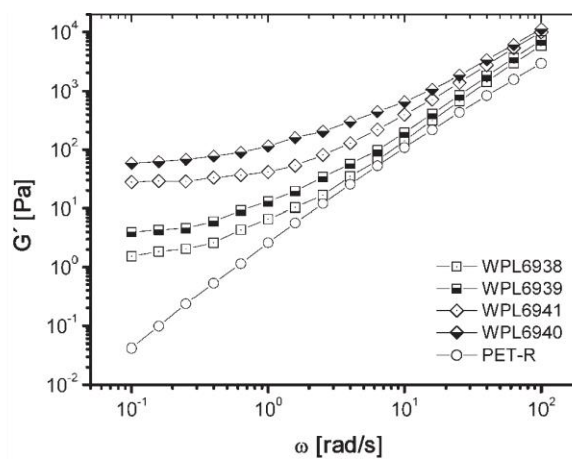


FIG. 4. Storage modulus of the matrix and composites.

RESULTS AND DISCUSSION

Two different concentrations of cut basalt fibers (20 and 30%) and variations with and without talc as a coupling agent have been chosen for this study. As the importance of processing parameters has been increasing in plastics industry, rheological properties of composite melts were discussed with the structure (analyzed from high magnification SEM micrographs) and utility (thermal and mechanical) characteristics.

Morphological analysis examined the level of dispersion and interfacial adhesion of basalt fibers in recycled PET (Figs. 1 and 2). According to Fig. 1, all the composite systems exhibited a high level of dispersion and homogeneity of fiber distribution in polymer matrix. The difference in filler concentration is also remarkable. Addition of talc into the composites did not result in lower separation and clustering of fibers. Furthermore, the presence of talc particles in composite system substantially facilitates fiber-matrix adhesion, as shown in Fig. 2. The growth of filler content in composite did not cause clustering of fibers and highly dispersed structure was maintained.

In Fig. 2, interfacial adhesion of the filler to the matrix can be observed. The composites containing only basalt fibers and PET matrix revealed poor fiber-matrix adhesion. Addition of talc to the mixtures resulted in remarkable higher interfacial interactions, as indicated by cover of fibers with the polymer. This structural change is reflected in rheological, thermal, and mechanical properties described later. The gap between the matrix and fiber in WPL 6938 composite can be caused by displacement of some fibers applying impact forces during fracturing. However, Fig. 1 shows most of the fibers tightly held by the matrix.

Dynamic rheological characteristics of the composites are in a good accordance with the observed structures. From the flow curves (Fig. 3), the 20 and 30% additions of reinforcing fibers led to a considerable increase in complex viscosity. Filling the systems with talc particles resulted in

further growth of melt viscosity, where the 30% addition was concomitant with a high viscosity increase. The nearly Newtonian behavior of all the composites and the matrix would suggest that fillers particles are well incorporated in polymer structure. Usually, addition of a filler to polymer melt shows the “yielding” phenomenon, described as viscosity increase in the range of low shear rates with subsequent viscosity decline during a shear rate increase. The absence of this behavior can be associated with high filler-matrix interactions and high level of dispergation. This conclusion is supported by Fig. 4, where the storage modulus (elastic part of the complex viscosity) is plotted as a function of the shear rate. The G' secondary plateau, observable for composites at low shear rates, is the indication of strong filler-matrix interactions. Formation of this plateau is also associated with physical network between filler particles and polymer chains in a composite system [20]. However, the composites described in this article did not show the “yielding” effect; therefore, the mentioned G' plateau is reflecting rather high interfacial fiber-matrix adhesion.

Concerning thermal properties (Table 2), the results of differential scanning calorimetry revealed interesting ther-

TABLE 2. Thermal properties of matrix and composites.

Composite	T_g^a (°C)	T_{mf}^b (°C)	ΔH_{mf}^c (J/g)	T_m^d (°C)	ΔH_m^e (J/g)	X_c^f (%)
WPL 6938	74.3	171.7	2.9	252.0	35.0	29.8
WPL 6939	76.6	174.5	2.3	256.0	34.5	29.3
WPL 6941	75.9	168.7	2.2	252.9	32.6	27.7
WPL 6940	76.2	—	—	252.5	25.3	21.5
PET-R	75.6	—	—	252.2	43.2	36.7

^a Glass transition temperature.

^b First melting point.

^c Enthalpy of first melting (first crystalline fraction).

^d Melting point.

^e Enthalpy of melting.

^f Relative crystalline content.

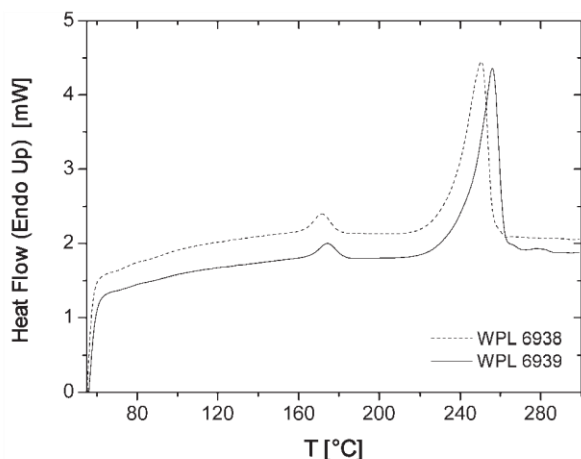


FIG. 5. DSC characterization of composites filled with basalt fibers.

modynamical behavior unusual for recycled PET-glass fiber composites or recycled PET-organoclay nanocomposites [6, 20]. Composites WPL 6938, WPL 6939, and WPL 6941 showed the first endothermic melting peak T_{mf} at about 170°C related to crystalline fraction on the surface of fibers (Figs. 5 and 6). The composites without talc addition show a decrease in the first crystalline fraction (ΔH_{mf}) with higher fiber content. This behavior can be associated with steric hindrance of fiber excess to the growth of crystalline nuclei during heterogeneous crystallization. Can be also observed in talc-containing systems, where the higher amount of fibers resulted in disappearance of the first melting peak (Fig. 6). Addition of talc to the 20% composite led to a remarkable decrease in the first crystalline fraction. The values of glass transition temperature and melt temperature were similar compared with the neat matrix. The level of total crystallinity of composites was lower than that of the unfilled matrix. Similarly to the first crystalline fraction, a higher content of fibers resulted in a lower total crystallin-

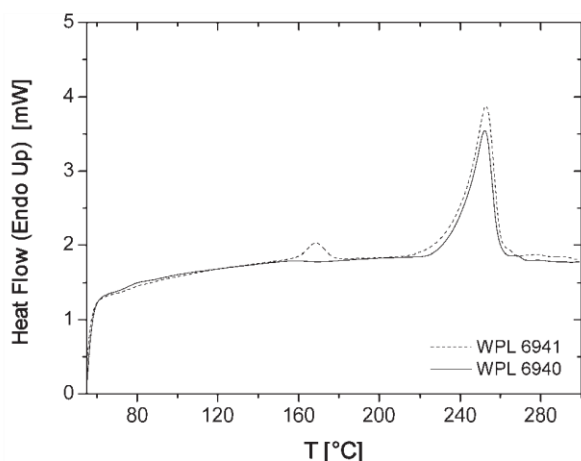


FIG. 6. DSC characterization of composites filled with basalt fibers and talc.

TABLE 3. Mechanical properties of composites.

Properties	WPL 6938	WPL 6939	WPL 6941	WPL 6940
Tensile strength (MPa)	95	112.9	100.7	122.8
Elongation at break (%)	2.9	2.9	2.1	2.2
Tensile modulus (MPa)	6,418	8,655	9,693	12,770
Flexural modulus (MPa)	5,639	7,739	8,817	11,750
Impact strength (kJ/m ²)	32.2	43.5	40.9	41.7
Notch impact strength (kJ/m ²)	5.7	8.1	5.4	5.7

ity, while a remarkable difference in talc-enriched mixtures was observed.

Mechanical properties of the composites are listed in Table 3. The results of tensile, flexural, and impact tests are in good agreement with structural changes, as well as rheological and thermal behavior. Addition of talc and higher concentration of basalt fibers in composites resulted in better mechanical performance, manifesting itself mostly by tensile strength, stiffness, flexural modulus, and toughness. The values of extensibility were independent of talc and fiber loading. The system filled with talc and 30% of fibers showed the highest reinforcement.

CONCLUSIONS

Highly dispersed uniform structures of short basalt fibers in recycled PET were achieved by continuous compounding in a co-rotating twin-screw extruder. In the systems containing talc, the recycled PET matrix adhered significantly more to the surface of the reinforcing fibers. Their linear viscoelastic properties reflected structural changes (variations of basalt concentration and talc addition) in composites. Higher values of the complex viscosity and storage modulus confirmed an increase in interfacial filler-matrix adhesion. Utility properties of recycled PET were significantly enhanced by the 20% and 30% filling with basalt fibers.

REFERENCES

1. PETCORE association, <http://www.petcore.org>.
2. The Container Recycling Institute, <http://www.container-recycling.org>.
3. PET recycling server, <http://www.petrecycling.cz>.
4. A. Pegoretti and A. Penati, *Polym. Degrad. Stabil.*, **86**, 233 (2004).
5. A. Pegoretti and A. Penati, *Polymer*, **45**, 7995 (2004).
6. A.L.F. de M. Giraldo, J.R. Bartoli, J.I. Velasco, and L.H.I. Mei, *Polym. Test.*, **24**, 507 (2005).
7. A.L.F. de M. Giraldo, R. Cardoso de Jesus, and L.H.I. Mei, *J. Mater. Process. Technol.*, **162/163**, 90 (2005).
8. M.L. MasPOCH, H.E. Ferrando, D. Vega, A. Gordillo, J.I. Velasco, and A.B. Martínez, *Macromol. Symp.*, **221**, 175 (2005).

9. F. Laoutid, L. Ferry, J.M. Lopez-Cuesta, and A. Crespy, *Polym. Degrad. Stabil.*, **82**, 357 (2003).
10. K. Tóth, T. Czvikovszky, and M. Abd-Elhamid, *Radiat. Phys. Chem.*, **69**, 143 (2004).
11. J.S. Szabó and T. Czigány, *Polym. Test.*, **22**, 711 (2003).
12. Intrec Polymers Ltd., *Addit. Polym.*, **12**, 3 (2003).
13. Mendex Ltd., <http://www.mendex.de>.
14. J. Militky and V. Kovacic, in *Proceedings of the International Textil, Clothing and Design Conference*, Dubrovnik, Croatia, October 6–9, 100 (2002).
15. A.N. Lisakovski, Y.L. Tsybulya, and A.A. Medvedyev, in *Fiber Society Spring 2001 Meeting*, Raleigh, NC, May 23–25 (2001).
16. Albarrie Ltd., <http://www.albarrie.com>.
17. Plant of Insulation Materials LLC, <http://www.basaltfibre.com>.
18. T. Czigány, *Compos. Sci. Technol.*, **66**, 3210 (2006).
19. A. Metha and B. Wunderlich, *J. Polym. Sci.: Polym. Phys. Ed.*, **16**, 289 (1978).
20. M. Kráčalík, J. Mikešová, R. Puffr, J. Baldrian, R. Thomann, and C. Friedrich, *Polym. Bull.*, **58**, 313 (2007).

2.2 Processing of polymer nanocomposites

In this chapter (manuscripts 6 – 10), the research is focused mainly on investigation of processing of polymer nanocomposites and usage of in-line characterization methods for structural and performance assessment directly during the processing. New technological approaches for processing and new evaluation methods for characterization of polymer nanocomposites are introduced.

2.2.1 Manuscript 6

“Advanced compounding. Extrusion of polypropylene nanocomposites using the melt pump”

Kracalik, Milan; Laske, Stephan; Gschweidl, Michael; Friesenbichler, Walter; Langecker, Günter Rüdiger (2009): In: J. Appl. Polym. Sci. 113 (3), S. 1422–1428. DOI: 10.1002/app.29888.

This is the first manuscript describing possibility to increase the shear rate as well as residence time simultaneously in continuous processing of polymer nanocomposites. This was reached by specific arrangement of the melt pump in compounding process, so that the in-line pressure of the melt pump was higher than the outlet pressure. It was shown that assembling the melt pump in front of an open compounder the residence time was prolonged nearly two-times applying a negative pressure difference of -100 bar in the melt pump. This additional melt shearing led to significant increase in material reinforcement, investigated by extensional rheology. Higher shear screw geometry and screw speed led to higher melt reinforcement as compared to lower shear screw configuration and screw speed, respectively. This novel technological approach opened new research field to study effects of shear force and residence time on processing and application properties of polymer nanocomposites. Different processing parameters (screw geometry, screw speed, melt pump adjustment, extruder torque, extruder pressure profile) were analysed and correlated with melt strength level. The level of melt strength was compared by magnitudes of tensile force measured by extensional rheometer.

Advanced Compounding: Extrusion of Polypropylene Nanocomposites Using the Melt Pump

Milan Kracalik, Stephan Laske, Michael Gschweidl, Walter Friesenbichler, Günter Rüdiger Langecker

Institute of Plastics Processing, University of Leoben, 8700 Leoben, Austria

Received 5 September 2008; accepted 14 December 2008

DOI 10.1002/app.29888

Published online 14 April 2009 in Wiley InterScience (www.interscience.wiley.com).

ABSTRACT: A melt pump was assembled into the compounding line to ensure both sufficient time for diffusion process of polymer chains into the silicate gallery and sufficient mechanical shear energy for exfoliation of clay layers. The melt pump in front of the open co-rotating twin-screw extruder controls the throughput rate and the residence time, whereas the screw speed and screw geometry in the extruder determine the mechanical shear energy applied on the compound. Due to melt pump employment, the melt in metering zone can be accumulated, which results in higher mixing efficiency. It was

found that using the melt pump leads to up to two times higher residence time and, consequently, higher level of material reinforcement as investigated by extensional rheology. Different melt pump adjustments, screw geometries, and screw speeds were tested and their effect on processing characteristics and material reinforcement was investigated. © 2009 Wiley Periodicals, Inc. *J Appl Polym Sci* 113: 1422–1428, 2009

Key words: polypropylene; organoclay; melt compounding; gear pump

INTRODUCTION

“Melt mixing” (compounding) is industrially the most attractive method for polymer nanocomposites preparation due to its technological simplicity (usage of common polymer processing machines in contrast to special equipment and procedures in chemical laboratories, which are required for “in situ” or “solution” method). Moreover, it is possible to use various matrix polymers (different molecular weights, grafting grades, copolymers, etc.) or even recycled polymer materials.^{1–5} The production efficiency of this method is considerably higher than other techniques employed for nanocomposites preparation (“melt mixing” proceeds in order of minutes, as compared to several hours for “in situ” and “solution” methods).^{6,7}

From the economical point of view, using the co-rotating twin-screw extruder as a continuous processing technology is industrially preferred to melt mixing in a discontinuous kneader. It is obvious that for the successful dispersion of silicate plates in polymer melt by continuous processing, the follow-

ing two requirements have to be fulfilled: sufficient high shear energy and enough long residence time.⁸ However, these two effects are opposite in the extrusion process. With higher shear forces (e.g., usage of kneading blocks generating higher shear rate or increase in screw speed), the residence time is shortened. To our knowledge, we presented for the first time⁹ both high shear rate and longer residence time that can be matched by implementing a melt pump in front of an open twin-screw extruder. The melt pump in extrusion technology is usually applied to reduce the pressure and throughput instability (melt pulsation) in the extruder. In the present study, the melt pump acts as an effective tool to control the residence time during compounding of polypropylene nanocomposites.

Only a few articles dealing with processing analysis of nanocomposites preparation in a twin-screw extruder have been published hitherto.^{10–19} The main goal was usually focused on variation in screw geometry, screw speed, or throughput rate. Wang et al.²⁰ studied dependency of compounding quality on feeding sequence and grafting grade of compatibilizer (MA grafting degree of 0.5 up to 4 wt %). Variation in feeding sequence (i.e., feeding of the premixed PP-g-MA and clay by a hopper and usage of side feeder for PP matrix) led only to a moderate increase in residence time. Drawbacks of this concept are reduced throughput rate and the necessity of premixing PP-g-MA with clay. In this article, a substantial prolongation of residence time is

Correspondence to: M. Kracalik (milan.kracalik@mu-leoben.at).

Contract grant sponsors: PlaComp1 Project (part of the NanoComp Research Project Cluster Founded by the Austrian NANO Initiative).

Journal of Applied Polymer Science, Vol. 113, 1422–1428 (2009)
© 2009 Wiley Periodicals, Inc.

reported by using standard industrial feeding sequence without additional premixing. It is obvious that two-step compounding gives superior results as compared with that of one-step mixing.¹¹ Hence, successful preparation of nanocomposite masterbatch is essential to reach a delaminated system in the second processing step (dilution of masterbatch to final clay concentration). As the residence time is the dominant factor in production of nanocomposites in extruders,¹¹ the interest of this work is focused on the possibilities of melt pump application for polymer nanocomposites masterbatch preparation along with deeper analysis of processing conditions.

MATERIALS AND METHODS

Materials

The isotactic polypropylene (PP) homopolymer HC600TF (MFI 2.8 g/10 min; 230°C/2.16 kg) used for the preparation of nanocomposite masterbatches was supplied by Borealis (Linz, Austria). The used nanofiller (montmorillonite intercalated with dimethyl distearyl ammonium chloride) with commercial name Nanofil 5 was supplied by Süd-Chemie (Munich, Germany). The compatibilizer Scona TPPP 2112 FA (PP grafted with 1 wt % of maleic acid anhydride, PP-g-MA, MFI 14.8 g/10 min) was supplied by Kometra (Schkopau, Germany).

Compounding process

For the compounding process, an intermeshing, co-rotating twin-screw extruder Theysohn TSK30/40D (Theysohn Extrusionstechnik, Korneuburg, Austria) using 10 barrel segments and a string die was employed. The PP and compatibilizer were fed upstream through the main hopper and the organoclay downstream at the 4th extruder barrel. All the

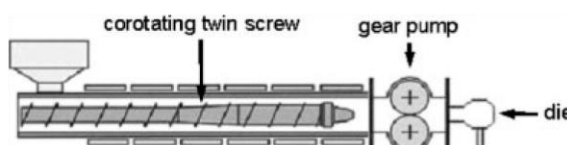


Figure 1 Scheme of setup for the compounding process.

components were fed by separately controlled gravimetric dosage units at an overall throughput rate of 10 kg/h. The screw geometry and speed were varied according to Table I to observe the influence of melt pump on compounding quality at different processing conditions. The Extrex SP gear pump was purchased from Maag Pump Systems Textron (Oberglatt, Switzerland). Three different melt pump adjustments were examined: (1) Δp negative, where the negative pressure difference between the outlet and inlet pressure of the melt pump has been set ($p_{\text{out}} - p_{\text{in}} = -100$ bar). In this way, a back pressure of polymer melt up to 9th extruder segment (approximately 30–40 cm before the melt pump) has been achieved. (2) Δp neutral, where the inlet and outlet pressure have been kept at the same level ($p_{\text{out}} - p_{\text{in}} = 0$ bar) and (3) Δp positive, with a positive pressure difference ($p_{\text{out}} - p_{\text{in}} = 5$ bar) was set. For a comparison, all the tested compounds were processed without the melt pump as well. The setup for the compounding process is schematically illustrated in Figure 1. Specifications of screw geometries (low and high shear configuration, indicated as G1 and G2, respectively) are described in Figures 2 and 3. The high shear configuration (G2) was assembled by insertion of kneading blocks with 90° discs arrangement in the 7th cylinder element and mixing screw elements into 9th cylinder element, as compared with G1 configuration. Extruder temperature profile has been set at 160–200°C from hopper up to die. The melt pump temperature was kept at 200°C. The values of residence time and extruder torque for different adjustments of the melt pump are plotted in Figures 4–7; the radial pressure profile in the extruder was monitored from 5th up to 10th segment (Figs. 8–11). The minimal residence time was measured by using a color masterbatch as the time between granulate insertion into the hopper and coloring of the outgoing molten string. The compatibilizer admixture related to organoclay content (20 wt %) was chosen in a ratio (Clay : Compatibilizer) of 1 : 1 according to our previous investigations.^{21–25}

Extensional melt rheology

We have already presented the advantages of polymer nanocomposites reinforcement assessment by melt strength evaluation using Rheotens

Journal of Applied Polymer Science DOI 10.1002/app

TABLE I
Indication of the Prepared Nanocomposites

Melt pump adjustment	Screw speed (rpm)	Geometry
Without melt pump	100	1
Δp negative		
Δp neutral		
Δp positive		
Without melt pump	75	1
Δp negative		
Δp neutral		
Δp positive		
Without melt pump	100	2
Δp negative		
Δp neutral		
Δp positive		
Without melt pump	75	2
Δp negative		
Δp neutral		
Δp positive		

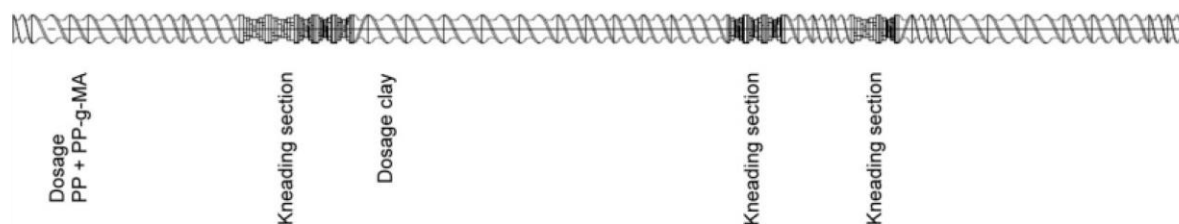


Figure 2 G1 screw configuration.

equipment.^{21–25} The main benefit of the Rheotens measurement consists in its simplicity without need of expensive scientific equipment and additional time for specimens preparation (primary granulate obtained from the extrusion process can be used). The principle of this measurement is illustrated in Figure 12. It is based on elongation of an extruded string by two or four rotating wheels connected with a force transducer. The rotation speed is linearly increased up to when the molten string breaks. The tensile force applied to the wheels along with the draw rate at break allows calculation of the melt strength (stress at break) according to

$$\sigma_b = F_b \times v_b / A_0 \times v_0 \quad (1)$$

where σ_b is the stress at break [Pa], F_b is the tensile force at break [N], v_b is the draw rate at break (mm/s), A_0 is the initial cross-section of molten string (at the die outlet) (m²), v_0 is the extrusion speed of molten string (piston speed) (mm/s).

In our work, the Rheotens 71.97 equipment (Göttfert, Buchen, Germany) in combination with a capillary rheometer was used. The following measuring conditions for capillary rheometer were set: cylinder diameter, 12 mm; die (length/diameter), 30/2 mm; temperature, 210°C; piston speed, 1.9 mm/s; shear rate, 273.6 s⁻¹. The Rheotens equipment was set by applying wheel acceleration of 60 mm/s² and gap between wheels of 0.6 mm.

To compare the melt strength level of different nanocomposites (revealing different magnitudes of v_b), the tensile force at a draw rate of 300 mm/s was chosen as a comparative value. The data were evaluated from at least three measurements for each sample with a measurement error of 2%.

RESULTS AND DISCUSSION

Advanced compounding using the melt pump

The effect of melt pump on processing characteristics during compounding at different screw geometries and speeds is plotted in Figures 4–11. It is obvious that the pressure profile as well as torque and residence time in the extruder are strongly affected by melt pump adjustments. According to the expectations, the highest effect of the melt pump on increase in residence time and extruder torque occurs by adjustment of melt pump to negative pressure difference; on the other hand, no significant differences between processing characteristics at neutral and positive melt pump operating modes were observed. As can be seen from Figures 4–7, values of residence time and average torque revealed the same trend, which has an important impact on the processing efficiency. The level of torque in the extruder gives information about level of shear forces applied during compounding. It can be clearly seen that both residence time as well as shear forces can be increased at the same time by use of the melt pump. The applied shear energy can be controlled by the screw speed and the residence time by adjustment of the melt pump. In this way, efficiency of dispersive as well as distributive mixing in continuous compounding can be substantially increased, depending on construction of twin-screw extruder and the melt pump. The main benefit of the melt pump consists in approximately two times higher residence time achievable. In this way, the diffusion process of intercalation and subsequent delamination of silicate platelets in the polymer matrix are substantially prolonged. The residence time

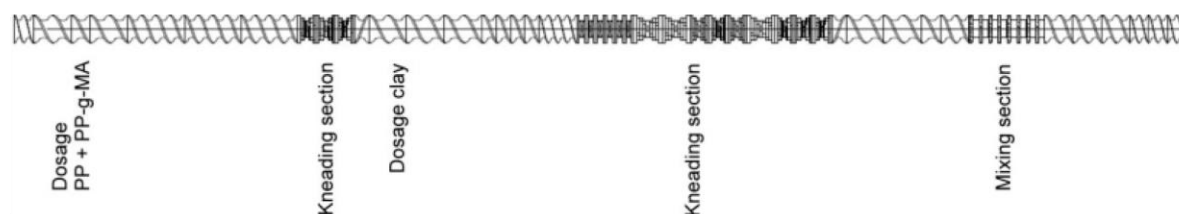


Figure 3 G2 screw configuration.

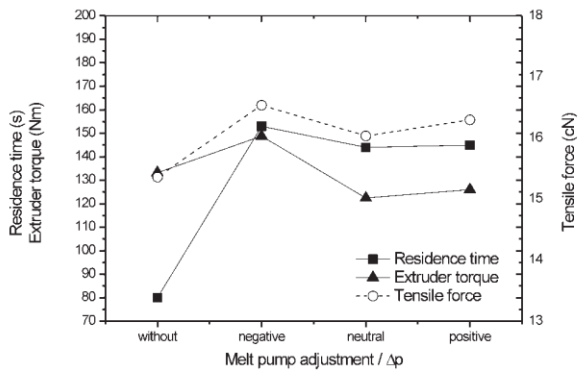


Figure 4 Residence time and extruder torque vs. tensile force (G1, 100 rpm).

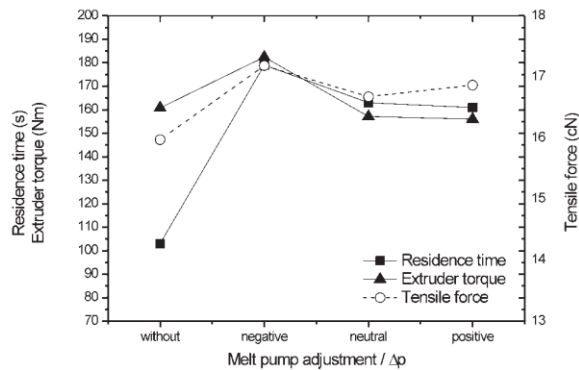


Figure 6 Residence time and extruder torque vs. tensile force (G2, 100 rpm).

is a dominant factor in production of satisfactory nanocomposites in extruders¹¹ so the implementation of melt pump into compounding process introduces an interesting and technologically accessible method of continuous compounding enhancement employable in the field of polymer composites and blends. It should be mentioned that maximal residence time achieved in this study was limited by melt pump construction and torque limitation in extruder. By the usage of larger processing equipment (allowing higher pressure in the melt pump and higher extruder torque), a further significant increase in residence time can be expected.

Evaluation of melt pump effect using extensional rheology

According to our previous investigations,^{9,21–25} the level of reinforcement in PP nanocomposites can be estimated by using extensional rheology with analysis of the melt strength. The silicate platelets form different levels of 3D physical network in the polymer matrix depending on their level of delamina-

tion.^{1–3} Higher delamination results in higher extent of physical network (higher material reinforcement) and therefore in an increase in melt strength. Different particle–particle and polymer–particle physical interactions result in variations in viscoelastic response. It is possible to use extensional rheometry to identify changes in the melt elongational behavior. Individual silicate platelets form a nanoscale network (cardhouse structure)²⁷ and raise the melt strength of the composite.

The level of melt strength, manifested itself by magnitude of tensile force detected at a draw rate of 300 mm/s, is plotted in Figure 13. Nanocomposite systems prepared with the usage of melt pump possess considerably higher levels of melt strength (higher value of tensile force) as those processed without the melt pump. However, at the Δp neutral melt pump operating mode a deterioration in elongational properties occurred. This phenomenon can be assigned to differences in residence time and shear rate applied by the melt pump. At the Δp maximal mode, the residence time was substantially prolonged (Figs. 4–7) and, consequently, diffusion of

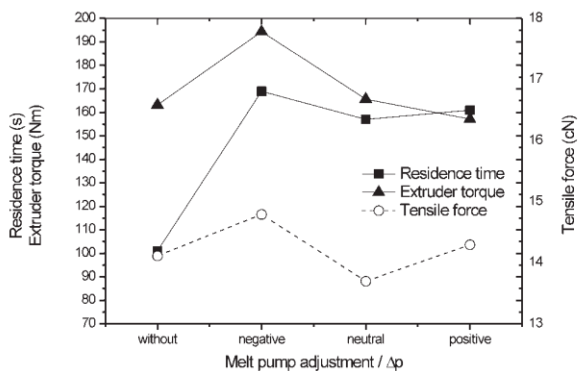


Figure 5 Residence time and extruder torque vs. tensile force (G1, 75 rpm).

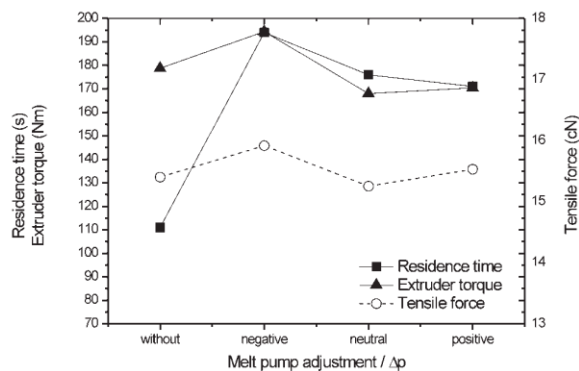


Figure 7 Residence time and extruder torque vs. tensile force (G2, 75 rpm).

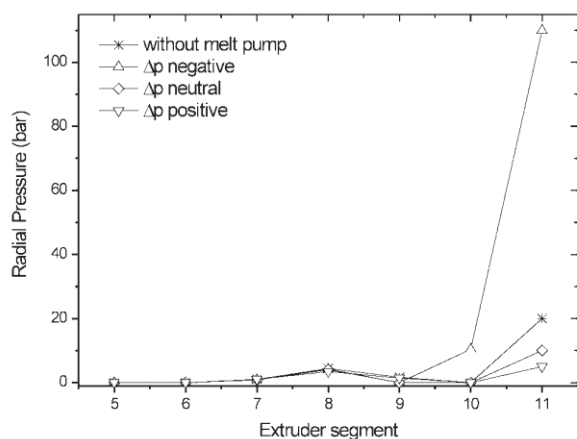


Figure 8 Pressure profile during compounding (G1, 100 rpm, 11 = melt pump inlet).

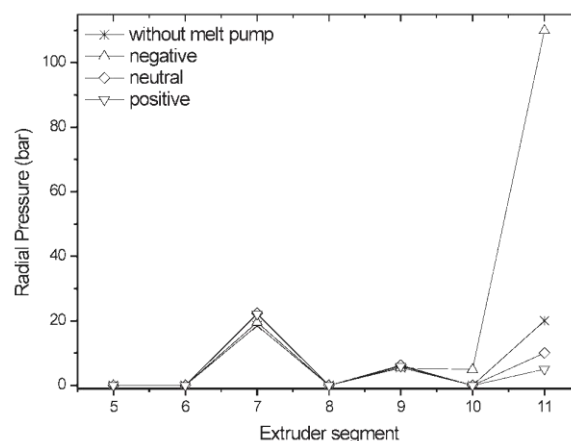


Figure 10 Pressure profile during compounding (G2, 100 rpm, 11 = melt pump inlet).

polymer chains into the silicate interlayer gallery was favored. At the Δp positive mode, the increase in residence time was not so high as in Δp maximal mode, but the outlet pressure in the melt pump was approximately two times higher than the inlet pressure, resulting in additional “melt stretching” inside the melt pump. This additional melt elongation could support higher material reinforcement due to higher orientation of silicate platelets in the flow direction. Subsequently, higher magnitude of melt strength as in the system applying Δp neutral melt pump mode could be reached.

Processing at higher screw speed resulted in the higher reinforcement of polymer matrix. The higher screw speed generates higher shear rate and, subsequently, facilitates clay dispersion during compounding. The high shear screw geometry possesses significantly higher radial pressure along the screws,

considerably higher average torque and residence time, as compared to the low-shear configuration (Figs. 4–11). The significant increase in radial pressure in the 9th cylinder element at G2 configuration was caused by the insertion of mixing screw elements into appropriate screw position. Similarly, employment of kneading blocks with 90° discs arrangement resulted in substantial pressure increase in the 7th cylinder element (Figs. 2, 3, and 8–11) as compared with G1 configuration. Generally, kneading blocks with 90° discs arrangement (as compared to other angles) enable the highest efficiency of dispersive mixing and facilitate delamination of silicate layers during compounding.

It can be clearly seen that the level of attainable material reinforcement is generally proportional to the residence time and torque in the extruder (Figs. 4–7). Therefore, the extent of reinforcement in the

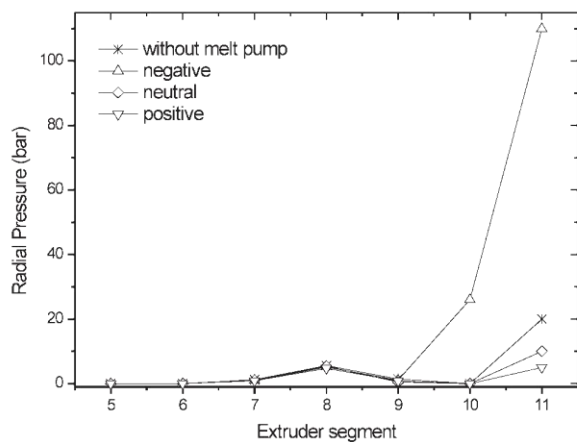


Figure 9 Pressure profile during compounding (G1, 75 rpm, 11 = melt pump inlet).

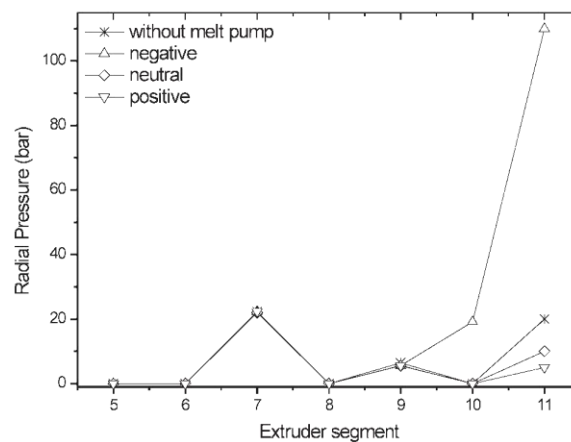


Figure 11 Pressure profile during compounding (G2, 75 rpm, 11 = melt pump inlet).

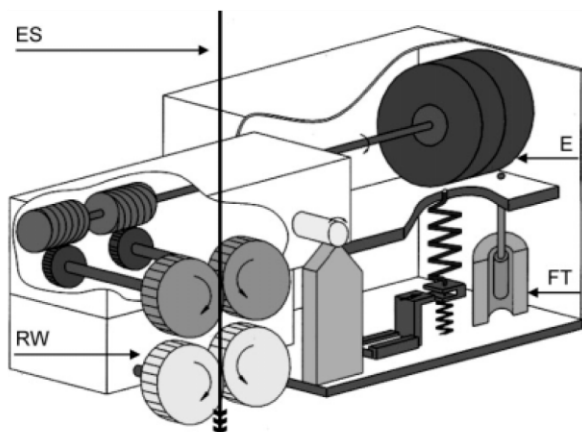


Figure 12 Principle of Rheotens measurement (ES = extruded string, RW = rotating wheels, E = engine, FT = force transducer).²⁶

nanocomposites investigated is dependent on both residence time as well as shear energy simultaneously within all melt pump operating modes. The described method to increase both shear rate as well as residence time simultaneously can be applied for different-scale processing machines and in this way transfer current know-how in the field of polymer nanocomposites from basic to applied research. Comparing the relevance of screw speed and geometry with regard to material enhancement, the higher screw speed using the low-shear configuration is preferable to lower screw speed with high-shear geometry (Fig. 13). That means, within the screw speeds and configurations tested, that higher screw speed is more important than increasing amount of kneading blocks to achieve higher shear rate and, consequently, maximal improvement in material properties. This relation will be further investigated

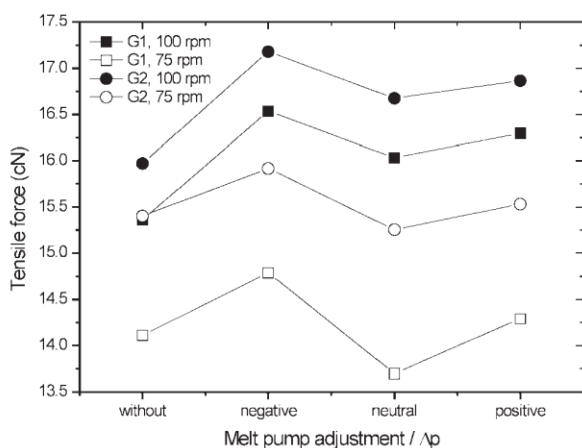


Figure 13 Melt strength level comparison of nanocomposite masterbatches.

to be confirmed applying broader range of screw speeds and geometries.

CONCLUSION

Advanced compounding by using a co-rotating twin-screw extruder in a combination with the melt pump has been presented. This configuration makes it possible to apply high shear forces and long residence time simultaneously within a continuous processing technique. It was shown that assembling the melt pump in front of an open compounder prolonged the residence time nearly two times, applying a negative pressure difference of -100 bar in the melt pump. This additional melt shearing led to a significant increase in material reinforcement, investigated by extensional rheology. Higher shear screw geometry and screw speed led to higher melt reinforcement as compared to lower shear screw configuration and screw speed, respectively. By use of a larger scale melt pump allowing higher pressure difference, a further increase in the residence time can be assumed. Generally, the mentioned technique of advanced compounding can be employed in the field of polymer composites and blends, where sufficient shear energy together with long enough residence time is required.

The authors thank Dr. Tung Pham, Borealis, Linz, for cooperation within the Nanocomp cluster.

References

- Kracalik, M.; Mikesova, J.; Puffr, R.; Baldrian, J.; Thomann, R.; Friedrich, C. *Polym Bull* 2007, 58, 313.
- Kracalik, M.; Studenovský, M.; Mikesova, J.; Sikora, A.; Thomann, R.; Friedrich, C.; Fortelny, L.; Simonik, J. *J Appl Polym Sci* 2007, 106, 926.
- Kracalik, M.; Studenovský, M.; Mikesova, J.; Kovarova, J.; Sikora, A.; Thomann, R.; Friedrich, C. *J Appl Polym Sci* 2007, 106, 2092.
- Yu, Z. Z.; Yan, C.; Yang, M.; Mai, Y. W. *Polym Int* 2004, 53, 1093.
- Anand, K. A.; Agarwal, U. S.; Nisal, A.; Joseph, R. *Eur Polym J* 2007, 43, 2279.
- Vaia, R. A.; Jandt, K. D.; Kramer, E. J.; Giannelis, E. P. *Chem Mater* 1996, 8, 2628.
- Davis, C. H.; Mathias, L. J.; Gilman, J. W.; Schiraldi, D. A.; Shields, J. R.; Trulove, P.; Sutto, T. E.; Delong, H. C. *J Polym Sci Part B: Polym Phys* 2002, 40, 2661.
- Shon, K.; Chang, D.; White, J. L. *Int Polym Process* 1999, 14, 44.
- Laske, S.; Kracalik, M.; Feuchter, M.; Maier, G.; Pinter, G.; Langecker, G. R. Presented at the International Conference PPS-24, June 15–19, 2008, Salerno, Italy.
- Wang, Y.; Chen, F. B.; Li, Y. C.; Wu, K. C. *Compos B* 2004, 35, 111.
- Zhu, L.; Xanthos, M. *J Appl Polym Sci* 2004, 93, 1891.
- Lertwimolnun, W.; Vergnes, B. *Polymer* 2005, 46, 3462.
- Moad, G.; Dean, K.; Edmond, L.; Kukaleva, N.; Li, G.; Mayadunne, R. T. A.; Pfaendner, R.; Schneider, A.; Simon, G. P.; Wermter, H. *Macromol Mater Eng* 2006, 291, 37.

14. Dennis, H. R.; Hunter, D. L.; Chang, D.; Kim, S.; White, J. L.; Cho, J. W.; Paul, D. R. *Polymer* 2001, 42, 9513.
15. Ishibashi, J.; Kikutani, T. *Int Polym Process* 2005, 20, 388.
16. Ton-That, M. T.; Perrin-Sarazin, F.; Cole, K. C.; Bureau, M. N.; Denault, J. *Polym Eng Sci* 2004, 44, 1212.
17. Lertwimolnun, W.; Vergnes, B. *Polym Eng Sci* 2006, 46, 314.
18. Elkouss, P.; Bigio, D.; Raghavan, S. In *Proceedings of the International Conference ANTEC; Society of Plastics Engineers, USA, 2004*; p 113.
19. Peltola, P.; Välipakka, E.; Vuorinen, J.; Syrjälä, S.; Hanhi, K. *Polym Eng Sci* 2006, 46, 995.
20. Wang, Y.; Chen, F. B.; Wu, K. C. *J Appl Polym Sci* 2004, 93, 100.
21. Laske, S. MSc Thesis, University of Leoben, Leoben, Austria, 2005.
22. Gschweidl, M. MSc Thesis, University of Leoben, Leoben, Austria, 2007.
23. Laske, S.; Kracalik, M.; Gschweidl, M.; Langecker, G. R. In *Proceedings of the International Conference Polymermischungen; Haus-Joachim Rausch, Martin-Luther University Halle-Wittenberg, Germany; 2007*; p 20.
24. Kracalik, M.; Laske, S.; Gschweidl, M.; Feuchter, M.; Maier, G.; Pinter, G.; Friesenbichler, W.; Langecker, G. R. In *Proceedings of the International Conference NanoEurope; Olma Nessen, St. Gallen, Switzerland; 2007*; pp 13–14.
25. Laske, S.; Kracalik, M.; Gschweidl, M.; Feuchter, M.; Maier, G.; Pinter, G.; Thomann, R.; Friesenbichler, W.; Langecker, G. R. *J Appl Polym Sci* 2009, 111, 2253.
26. Göttfert Ltd., Germany. Available at: <http://www.goettfert.com>.
27. Wagener, R.; Reisinger, T. J. G. *Polymer* 2003, 44, 7513.

2.2.2 Manuscript 7

„FT-NIR as a determination method for reinforcement of polymer nanocomposites“

Laske, Stephan; Kracalik, Milan; Feuchter, Michael; Pinter, Gerald; Maier, Günther; Märzinger, Wolfgang et al. (2009): In: J. Appl. Polym. Sci. 114 (4), S. 2488–2496. DOI: 10.1002/app.30765.

This is the first manuscript describing possibility to use FT-NIR method for prediction of polymer nanocomposites properties. It was proved that using chemometrical evaluation of FT-NIR data enables prediction of rheological properties (melt strength level) in dependency on processing parameters (typical compounding process vs. inclusion of the melt pump, variations in screw speed and screw geometry). NIR spectroscopy was shown to be a qualitative and predominantly quantitative method for monitoring nanocomposite quality of all sample groups investigated, although the extruded sample material had to be cooled down, granulated and processed to plates for measurements with the off-line NIR system. As the unknown changes in the samples caused by these postprocessing procedures negatively affect the calculated chemometric models, it was decided to measure the quality of the nanocomposites in-line without any additional processing, to prevent any negative effect on the material structure or reinforcement level. Extensional rheometry and NIR measurements were intended to be done simultaneously on the extruder to collect spectral and mechanical data in samples with the same processing history.

FT-NIR as a Determination Method for Reinforcement of Polymer Nanocomposites

Stephan Laske,¹ Milan Krcalik,¹ Michael Feuchter,² Gerald Pinter,² Günther Maier,³ Wolfgang Märzinger,⁴ Michael Haberkorn,⁵ Günter Rüdiger Langecker¹

¹Institute of Plastics Processing, University of Leoben, 8700 Leoben, Austria

²Institute of Materials Science and Testing of Plastics, University of Leoben, 8700 Leoben, Austria

³Material Center Leoben, 8700 Leoben, Austria

⁴i-RED Infrarot Systeme GmbH, 4020 Linz, Austria

⁵Upper Austrian Research GmbH, 4020 Linz, Austria

Received 21 July 2008; accepted 16 May 2009

DOI 10.1002/app.30765

Published online 7 July 2009 in Wiley InterScience (www.interscience.wiley.com).

ABSTRACT: Layered silicates as nanoscale fillers have a great potential in improving polymer material properties. Depending on the composite structure (agglomerated, intercalated, or exfoliated) a significantly higher level of reinforcement of the virgin polymer can be achieved with a very small amount of filler. The morphology of the composites is usually characterized by XRD and microscopic methods (e.g., transmission electron microscopy). But the level of reinforcement of nanocomposites is not always proportional to morphology (delamination level of the silicate layers). A new approach for characterizing the material reinforcement level as a consequence of melt quality is to correlate the results of extensional rheometry (level of melt strength) with those of near infrared (NIR) spectroscopy. The advantage

of the NIR technique is the suitability for in-line implementation by using quartz based optics and optical fibers for the signal transfer from the measuring probe to the NIR spectrometer. The presented results show a direct correlation between the reinforcement level determined by rheotens measurements and the data analyzed from off-line NIR measurements. The results of the chemometric analysis of the NIR data shows that this in-line capable optical method provides quantitative information on the quality of the nanocomposite. © 2009 Wiley Periodicals, Inc. *J Appl Polym Sci* 114: 2488–2496, 2009

Key words: nanoparticles; polymer composite materials; FT-NIR spectroscopy

INTRODUCTION

Nanocomposites are modified polymers with particles, where at least one dimension is in the order of nanometers. Polymer material reinforced by nanoscale particles exhibit significantly higher performance, for example, higher elastic modulus, tensile strength, thermal resistance, lower gas and liquid permeability, reduced flammability, and enhanced rheological properties already for small amounts of the filler.^{1,2} For preparation of polymer nanocomposites, layered silicates (clay, especially montmorillonite, MMT) have been the most commonly used nanofillers due to the possibility to achieve aspect ratios ideally up to 1000. On the basis of MMT, nanocomposites containing polyamide, polyethers, polyesters, epoxides, polystyrene, and polypropylene have been prepared.^{2–16} Polymer/clay nanocomposites can generally be prepared by mixing during polymerization

(“*in situ*”), mixing in solvent and melt mixing.¹⁷ Additionally, possibilities of nanoparticle dispersion by application of electric fields,⁸ by ultrasonic mixing,¹⁸ or direct chemical bonding of polymer chains onto the surface of silicate platelets^{19–22} have been studied. Melt mixing (compounding) is the industrially most attractive method due to its technological simplicity (usage of common polymer processing machines in contrast to special equipment and procedures in chemical laboratories). According to the dispersion of MMT platelets in the polymer matrix, three composite structures (conventional composites, intercalated, and exfoliated nanocomposites) can be formed. In the first case, the MMT particles (tactoids) are dispersed in the polymer matrix in micrometer scale with the tactoids acting as a micro-filler. Intercalated (partially delaminated) systems show penetration of polymer chains into the interlayer gallery of silicate platelets whereas exfoliated (entirely delaminated) nanocomposites are characterized by homogeneous and uniform dispersion of silicate layers in the polymer. During the process, the structures, which are responsible for the reinforcement level, are formed by physical bonding between the hydrophilic clay, hydrophobic polymer matrix, and compatibilizer. The number and type of

Correspondence to: S. Laske (stephan.laske@unileoben.ac.at).

Journal of Applied Polymer Science, Vol. 114, 2488–2496 (2009)
© 2009 Wiley Periodicals, Inc.

interactions depend on the processing conditions and can be monitored by NIR spectroscopy.

Near infrared (NIR) spectroscopy is a non-destructive, optical method to determine information on the composition of samples. Like mid infrared (MIR) spectroscopy, the NIR method measures the absorbance of light due to excitation of molecular vibrations of the substance under investigation. However, MIR, which exploits radiation in the wavelength range of 2500 to 25000 nm, measures the fundamental molecular vibrations, whereas NIR, operating in the spectral range between 780 and 2500 nm, detects the overtones and combinations of these vibrations. By placing the sample in the light path, the substances present in the sample absorb NIR radiation at specific frequencies according to their molecular structure, resulting in NIR sample spectra. As the frequencies, at which the absorbances take place, are depending on the energy, a molecular structure requires to be stimulated, the position of the absorbance bands in the NIR spectrum provides the information for identification of substances and for the existence of specific chemical functionalities present in the sample. By evaluating the intensity of the features identifying a substance or chemical functionality, the amount/concentration of the respective analyte can be determined. In polymer industry, NIR spectroscopy is used for example for examination of polymerization or copolymerization, moisture content, crystallinity, molecular weight, intermolecular interactions, tacticity, orientation, dispersion and alteration of the particle size of fillers, and density of polyethylenes. As described earlier, NIR spectroscopy in principle determines the chemical composition of samples. However, it is also capable of providing information on mechanical properties as these properties are generally linked to the chemical state of the sample. For example, the strength of coatings often depends on the degree of polymerization of polymers, which again can be monitored by determining the remaining amount of monomer functionalities which have not been converted by the polymerization reaction. Furthermore, some parameters can be determined by NIR spectroscopy although neither a chemical conversion is the basis for the phenomenon nor does the analyte show any activity in the NIR. For example, ions dissolved in water can be determined to a certain degree although they are not IR active and do not cause any specific chemical reaction. The reason for this is the fact that the charged ions interact with the water molecules, influencing the strength of the O—H bond and thereby shifting the water's O—H absorbance peak. In polymer nanocomposites, the silicate platelets form different levels of 3D physical network. Generally, in the real nanocomposite systems, both the intercalated as well as exfoliated structure

exist. During the compounding process, both structures are formed by the physical bounds between the hydrophilic clay, hydrophobic polymer matrix, and compatibilizer. The number and type of interactions between polypropylene chains, organic modifier based on organoclay (quaternary ammonium salt presented in Nanofil 5), polypropylene grafted with maleic anhydride (compatibilizer), and free maleic anhydride molecules (up to 0.1% in compatibilizer) depend on the processing conditions and can be monitored with NIR spectroscopy. A few studies studying the usage of vibrational (FTIR or Raman) spectroscopy to detect the changes in physical characteristics of polymers have been published up to now.^{23–31} Some of these studies proposed an approach to analyze the deformation behavior in polymer-clay nanocomposites.^{32,33} However, no study dealing with NIR spectroscopy for the determination of the reinforcement in polymer nanocomposites have been found in available literature.

EXPERIMENTAL

Preparation of polymer nanocomposites

The used polymer matrix was an isotactic polypropylene homopolymer (HC600TF; MFI 2.8 g/10 min, 230°C/2.16 kg; Borealis/A, Linz, Austria). As a nanofiller, a layered silicate intercalated with dimethyl distearyl ammonium chloride (Nanofill5, Sud Chemie/D, Munich, Germany) and as a compatibilizer a PP grafted with maleic acid anhydride (PP-MA, Scona TPPP 2112 FA, Kometra/D, Schkopan, Germany) was used. For the compounding process, a co-rotating twin screw extruder Theysohn TSK30/40D, Korneuburg, Austria with a string die has been used. The feed rate was set at 10 kg/h with a screw speed variation, between 75 and 400 rpm. The extruder temperature profile has been set to 160–200°C from the hopper up to the die. The melt pump temperature has been kept at 200°C. As listed in Table I, different nanocomposite systems have been prepared. In the first sample group (No. 1–16), masterbatches containing 20 wt % of compatibilizer with the same amount of organoclay have been prepared under different processing conditions (with or without melt pump, varying screw speed and screw geometry). In this sample group, a variation in melt pump adjustment has been performed: For $\Delta p_{\text{maximal}}$, a maximal negative difference (up to –100 bar) between the input and outlet pressure of the melt pump has been set. In this way, melt accumulation up to the 9th extruder section (~ 40 cm before the melt pump) has been achieved. In the $\Delta p_{\text{neutral}}$ mode, the input and outlet pressure were kept constant (around 10 bar), while in $\Delta p_{\text{positive}}$ mode, a positive pressure difference (around 5 bar) was set. The

TABLE I
Description of Samples

No.	Indication	Note	Clay/PP-MA content (wt %)	Screw speed (rpm)	Geometry
1	Osp65	Without melt pump	20/20	75	1
2	MB4-65rpm	$\Delta p_{\text{maximal}}$			
3	MB5-65rpm	$\Delta p_{\text{neutral}}$			
4	MB6-65rpm	$\Delta p_{\text{positive}}$			
5	Osp100	Without melt pump	20/20	100	1
6	MB1-100rpm	$\Delta p_{\text{maximal}}$			
7	MB2-100rpm	$\Delta p_{\text{neutral}}$			
8	MB3-100rpm	$\Delta p_{\text{positive}}$			
9	Osp2_75	Without melt pump	20/20	75	2
10	MB10-75rpm	$\Delta p_{\text{maximal}}$			
11	MB11-75rpm	$\Delta p_{\text{neutral}}$			
12	MB12-75rpm	$\Delta p_{\text{positive}}$			
13	Osp2_100	Without melt pump	20/20	100	2
14	MB7-100rpm	$\Delta p_{\text{maximal}}$			
15	MB8-100rpm	$\Delta p_{\text{neutral}}$			
16	MB9-100rpm	$\Delta p_{\text{positive}}$			
17	MB16-75rpm	$\Delta p_{\text{maximal}}$	20/20	75	3
18	MB13-100rpm			100	
19	MB19-150rpm			150	
20	MB20-200rpm			200	
21	MB21-300rpm			300	
22	G3-75	$\Delta p_{\text{maximal}}$	5/5	75	3
23	G3-100			100	
24	G3-150			150	
25	G3-200			200	
26	G3-300			300	
27	G4-75	$\Delta p_{\text{maximal}}$	5/5	75	4
28	G4-100			100	
29	G4-150			150	
30	G4-200			200	
31	G4-300			300	
32	G4-400			400	

second sample group (No. 17–21) consists of masterbatches prepared at different screw speed and the $\Delta p_{\text{maximal}}$ mode. The third sample group (No. 22–32) contains nanocomposites prepared by dilution of appropriate masterbatches to 5 wt % organoclay concentration under the same processing conditions used for masterbatches.

For the Rheotens measurements, the primary granulate obtained from the extrusion process has been used. The samples for near infrared have been prepared using a hydraulic vacuum press.

Evaluation of testing methods for NIR calibration

As we have already presented elsewhere,³⁴ the level of real reinforcement in polypropylene nanocomposites is not only based on the delamination level (increase in interlayer distance) determined by the XRD method. The simple rule “a higher delamination leads to higher improvement in mechanical material properties” does not apply to all cases. The only way to find the ideal clay structure (e.g., type

and grade of mixture elements, degree of intercalation/exfoliation) in the polymer matrix for the best achievable material reinforcement is to combine the XRD and TEM technique with the characterization of mechanical properties. These methods require rather expensive scientific equipment and additional experimental time for the preparation of samples. Nevertheless, XRD, TEM, and tensile testing are the most approved methods for characterizing nanocomposites and can not be disclaimed when it comes to solid parts and their properties. But for monitoring the nanocomposite production and quality (e.g., melt homogeneity), it is necessary to examine the melt directly. We proved that the investigation of the melt strength level in compatibilized polypropylene nanocomposites using the Rheotens equipment enables to detect the material reinforcement level as a consequence of melt quality. A correlation between mechanical properties in the melt and solid state has been confirmed.³⁴ Concerning the suitability of the described methods for the polypropylene-nanocomposites characterization and the possibility for

Rheotens test being performed off- and on-line, we decided to correlate the results of Rheotens measurements (level of melt strength) with those of off-line near infrared spectroscopy to gain chemometric NIR calibration models.

Rheotens measurements

The advantage of Rheotens measurements consists in their simplicity without the need of expensive scientific equipment and additional time for sample preparation. The principle of the Rheotens measurement is shown in Figure 1. It is based on the elongation of the extruded string by two or four rotating wheels connected with a force transducer. The rotation speed is linearly increased up to the point when the molten string breaks. The tensile force applied to the wheels at a specific draw rate is the reference value for the melt strength level (stress at break). In our work, the Rheotens 71.97 equipment (Göttfert, Buchen, Germany) in combination with a capillary rheometer has been used. To compare the tensile force level of different nanocomposite systems (revealing different magnitudes of draw rate at break), the tensile force at a draw rate of 350 mm/s has been chosen as a comparative value. The data of at least three measurements for each sample with a measurement error of 2% was evaluated.

The silicate platelets form different levels of 3D physical network in the polymer matrix depending on their structure (intercalated or exfoliated). The different physical crosslinking and bonding between polymer chains and organoclay results in a diversity of viscoelastic response. Therefore, Rheotens measurements are used to identify changes of the elon-

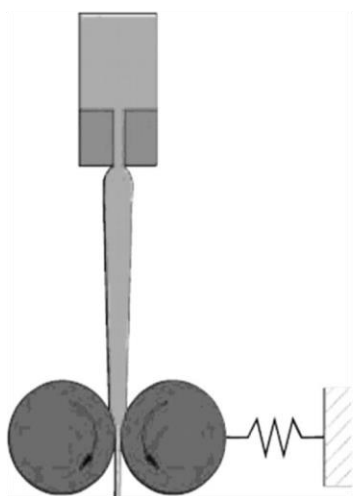


Figure 1 Principle of Rheotens measurements.³⁵

gational viscosity. Individual nanoparticles act as entanglement or crosslinking sites and raise the extensional stiffness of the composite. Depending on the degree of dispersion, this change is more or less pronounced compared to the polymer without filler.

Experimental setup for NIR measurements

The NIR spectra of the different samples were collected with the laboratory FT-NIR spectrometer Vertex 70 from Bruker Optics/D (Ettlingen, Germany). The samples were prepared as plates with a thickness of 0.8 mm and were measured in transmission by placing the plates in the optical path of the spectrometer in the sample chamber. All samples were measured three times at different lateral positions on the plate. The quantitative chemometric evaluation of the measured spectra was done with the software package OPUS from Bruker Optics/D. The measurement parameters for the acquisition of all spectra were:

- Detector: Extended InGaAs.
- Wavenumber range: 4000–10,000 cm^{-1} .
- Resolution: 8 cm^{-1} .
- Number of scans: 64.

Evaluation of NIR data

For the realization of efficient NIR spectroscopic process control applications, the extraction of process relevant information from the measured NIR spectra is essential. In the NIR region, typically, the spectral features of different species strongly overlap. This results in the need for more sophisticated evaluation methods.³⁶ In this case, the partial least squares (PLS 1) method was applied to extract quantitative information from NIR spectra and to evaluate the data for a desired parameter measured by NIR.

For example, NIR spectra are often used to estimate the amount of different chemical components in a sample. In this case, the so called “factors” are the wavelength specific measurements that comprise the spectrum. The parameters of interest, the so called “responses” are typically component amounts that the researcher wants to determine in future samples. In our case, the main response of interest is the level of reinforcement in the nanostructured materials produced by filling a polymer matrix with nanoparticles in different processing ways.

For evaluating NIR spectroscopy as a method capable of measuring a certain sample attribute (responses: e.g., reinforcement level) a straight forward approach was applied. Experimentally NIR spectra of samples with varying but known

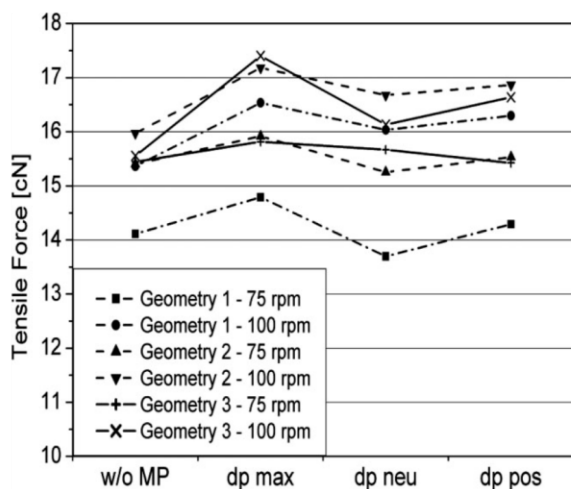


Figure 2 Melt strength of nanocomposite masterbatches prepared by different processing conditions.

responses were measured. Then PLS 1 was used to generate a linear calibration model for calculating the responses from the measured NIR data (factors).

By looking at correlation parameters [like correlation coefficient R^2 and root mean square error of cross validation (RMSECV)] of the resulting model, it is possible to evaluate whether the model shows sufficient predictive ability or not. R^2 and RMSECV are determined as follows with Y_k as the reference parameter value and Y_p as the predicted parameter value:

$$R^2 = \frac{\sum_{i=1}^n (Y_{pi} - \bar{Y}_k)^2}{\sum_{i=1}^n (Y_{ki} - \bar{Y}_k)^2}$$

$$\text{RMSECV} = \sqrt{\frac{\sum_{i=1}^n (Y_{ki} - Y_{pi})^2}{n}}$$

RESULTS AND DISCUSSION

Rheotens testing

As can be seen in Figure 2, nanocomposite masterbatches processed with screw geometry 2 (applying higher shear energy) as compared to those processed with screw geometry 1 (lower shear configuration) revealed a higher level of melt strength. The difference in screw speed shows a clear trend: a higher screw speed (generating higher shear rate) for a certain screw geometry results in a higher magnitude of tensile force (level of melt strength). Comparing

the tensile force level of masterbatches prepared using geometry 2 and 3, respectively, no significant difference occurred. This is attributed to the moderate diversity between both geometries, which differed only in the sequence of the identical screw elements.

The tensile force level of nanocomposites prepared by dilution of appropriate masterbatches using different screw geometries can be observed in Figure 3. It is obvious that for a certain screw geometry, a critical screw speed with optimal shear energy as well as residence time occurs. For geometry 4, this critical screw speed is shifted from 100 rpm (geometry 3) up to 150 rpm, because no kneading blocks in geometry 4 have been assembled and the shear rate acts proportionally to the screw speed. That means, with higher screw speed, higher shear energy is applied to the melt and a lower amount of kneading blocks is required.

The presented results show a direct relation between the melt strength level (reinforcement level) and the processing conditions (screw speed, geometry, etc.). This means that Rheotens equipment can be used for characterization of polymer nanocomposites in the molten state due to reflection of structural changes caused by different processing conditions. Furthermore, this technique can be applied on-line using a by-pass flow channel.

Near infrared spectroscopy

Sample group 1 (No. 1–16)

The samples discussed in this section were generated by running the extruder with different melt pump operation modes. Running the melt pump in

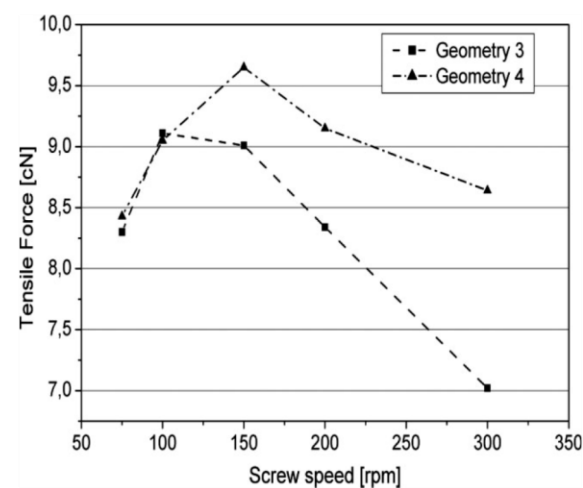


Figure 3 Melt strength of nanocomposites prepared by different processing conditions.

different operation modes enables a variation of residence time of the polymer and the nanomaterial in the extruder, and thus, results in a variation of the mechanical treatment of the material. The different degrees of mechanical treatment again result in different mechanical sample properties.

In the following figures (Figs. 4–7), the steps from the raw measurement to a calibration model are demonstrated. In Figure 4, raw measurement data is shown. As can be seen, the spectra are shifted by varying offset values. The differences are mainly caused by variations in transparency and light scattering properties from sample to sample.

Basically, a chemometric algorithm works in two steps:

Pretreatment: The spectra are pretreated to get rid of parasitic measurement effects like light straying, positioning variations or granularity, and to exclude spectral regions with irrelevant spectral information regarding the specific parameter of interest (response).

Evaluation: A scalar product of the pretreated spectrum vector with the regression coefficient (or loading) results in the numerical value of the parameter of interest (response).

Thus, the task of finding the best chemometric model for a specific measurement problem is the task of finding the best pretreatment method and regression coefficient. This can be done by testing different pretreatment methods applied to different wavenumber ranges and by searching for a model which gives the best correlation properties with the desired response.

For the first series of measurements, the response of interest is the tensile force value normally deter-

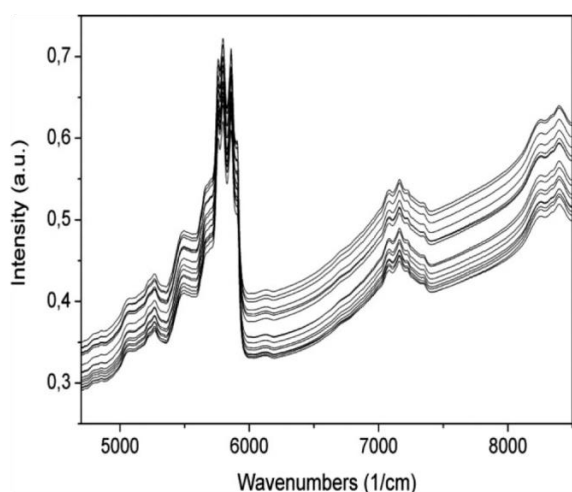


Figure 4 Absorbance data of samples 1–16. Spectra are shown as measured without any data treatment.

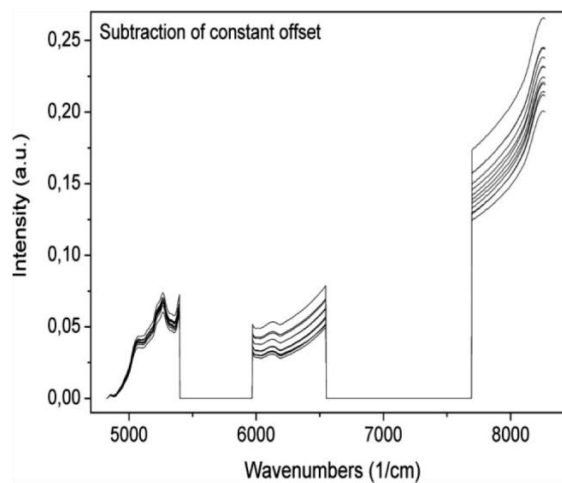


Figure 5 Selected regions of NIR absorbance spectra after subtraction of constant offset values.

mined by Rheotens measurement. In the following pictures, the final result of an iterative model optimization procedure is shown. The gained chemometric model should be near to the best model for the evaluation of the tensile force value from NIR measurements.

In Figure 5, the resulting spectral vectors after pretreatment are given. Optimization in terms of best correlation parameters led to the elimination of selected wavelength ranges and to the pretreatment method “subtraction of constant offset.” This means that the pretreatment method subtracts a constant value from each spectrum.

In Figure 6, the wavenumber dependent coefficients of regression are shown. The PLS 1 algorithm

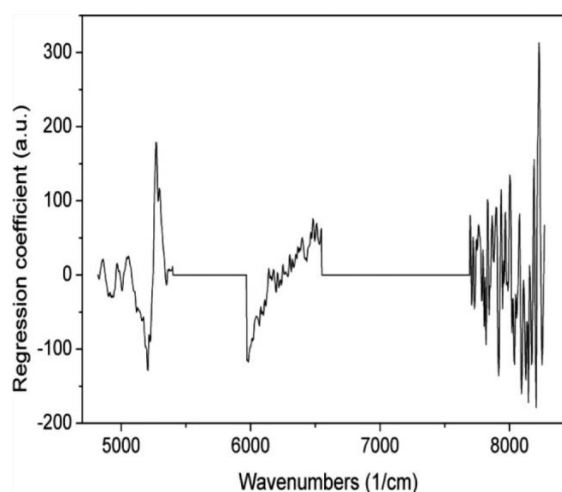


Figure 6 Wavelength dependent coefficient of regression calculated by PLS 1 algorithm.

TABLE II
Comparison of Drawing Force Values Evaluated by Rheotens Method and Calculated Values from the NIR Spectra for Sample Group 1 (Samples 1, 5, 9, and 13 Excluded Due to Different Processing Procedure as Explained in the Text)

No.	Indication	Note	Rheotens (cN)	NIR 1 (cN)	NIR 2 (cN)	NIR 3 (cN)	Average NIR (cN)
2	MB4-65rpm	$\Delta p_{\text{maximal}}$	16.54	16.52	16.41	16.46	16.46
3	MB5-65rpm	$\Delta p_{\text{neutral}}$	16.03	15.97	16.09	16.11	16.06
4	MB6-65rpm	$\Delta p_{\text{positive}}$	16.30	16.20	16.27	16.06	16.18
6	MB1-100rpm	$\Delta p_{\text{maximal}}$	14.90	14.92	15.14	14.63	14.90
7	MB2-100rpm	$\Delta p_{\text{neutral}}$	13.70	13.75	13.95	13.74	13.81
8	MB3-100rpm	$\Delta p_{\text{positive}}$	14.29	14.22	14.08	14.04	14.11
10	MB10-75rpm	$\Delta p_{\text{maximal}}$	17.18	16.98	16.92	17.19	17.03
11	MB11-75rpm	$\Delta p_{\text{neutral}}$	16.68	17.00	16.68	16.82	16.83
12	MB12-75rpm	$\Delta p_{\text{positive}}$	16.87	16.92	16.81	16.62	16.78
14	MB7-100rpm	$\Delta p_{\text{maximal}}$	15.92	15.90	15.40	15.72	15.67
15	MB8-100rpm	$\Delta p_{\text{neutral}}$	15.25	15.23	15.78	15.32	15.44
16	MB9-100rpm	$\Delta p_{\text{positive}}$	15.53	15.58	15.50	15.90	15.66

searches for linear correlations between spectral data (factors) and reference values (responses). The diagram shows the wavelength regions which are changing with the effect of interest as well as how these regions are changing. Positive values mean that the spectral value is increasing with increasing response value. Negative values mean that the spectral value is decreasing with increasing response value. The response value in this case is the tensile force.

Table II and Figure 7 give an overview of the resulting chemometric model. In Table II, the single measurement values and the corresponding average value of the NIR method are shown and can be compared with the Rheotens values. In Figure 7, the tensile force values evaluated by Rheotens method (horizontal axis) are plotted versus the calculated values from the NIR spectra (vertical axis). The quality of the chemometric model and thus the ability of the NIR spectroscopic method to measure the tensile force value can be quantified by the values R^2 and RMSECV. The correlation coefficient R^2 shows the correlation of the NIR data with the reference values of the investigated response parameter. Values of R^2 are between 0 and 100. Typically, models with R^2 values above 90 enable quantitative calculation of the response parameter of interest. Correlation coefficients above 70 allow qualitative evaluations. If R^2 lies below 70, the response is not well pronounced in the factors (the spectral data) and thus can not be evaluated with reasonable practical relevance.

The root mean square error of cross validation (RMSECV) is determined by calculating a predictive model by using all samples except for one. This model is applied to the sample left out for prediction of the desired response parameter. RMSECV is calculated by doing this procedure for every sample and by summing up the root mean square errors of the deviations of the calculation results from the assumed true reference values. This value is a mea-

sure for the error of the developed NIR measurement method.

The chemometric model given in Figure 7 shows a very good correlation with the Rheotens method and allows absolute quantification of tensile force values by the NIR method. It was necessary to exclude samples 1, 5, 9, and 13 due to their different processing procedure. Including these samples in the chemometric model design led to a chemometric model with R^2 value of 83. With this model, semi-quantitative evaluation of the tensile force parameter would still be possible. Samples 1, 5, 9, and 13 were produced without melt pump. In the experimental procedure, all other samples were produced first, then the melt pump was detached and samples 1, 5, 9, and 13 were extruded. It is assumed that the change in the experimental setup has caused not only changes in the mechanical treatment in the extruder

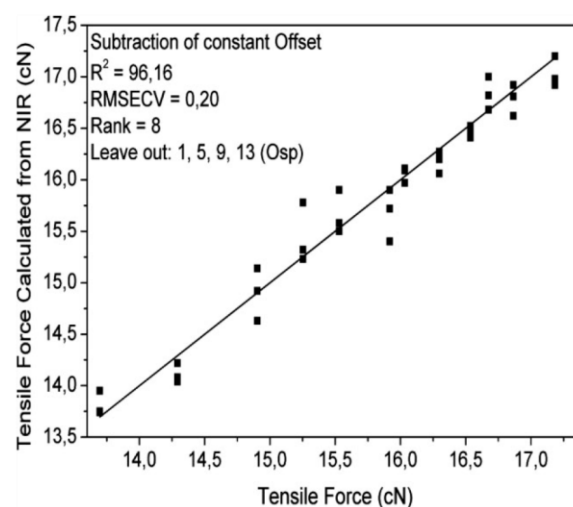


Figure 7 Drawing force values calculated versus measured for samples 1 to 16.

TABLE III
Drawing Force Values Calculated Versus Measured for Samples 17–21

No.	Indication	Note	Rheotens (cN)	NIR 1 (cN)	NIR 2 (cN)	NIR 3 (cN)	Average NIR (cN)
17	MB16-75rpm	$\Delta p_{\text{maximal}}$	17.40	17.37	17.44	17.07	17.29
18	MB13-100rpm		15.81	15.74	16.00	16.06	15.93
19	MB19-150rpm		17.14	16.56	17.33	16.76	16.88
20	MB20-200rpm		17.12	17.12	17.02	16.59	16.91
21	MB21-300rpm		12.90	13.63	13.28	13.74	13.55

but eventually also led to slight differences in chemical composition, transparency, or light stray properties of the samples.

The procedure shown in detail for samples 1 to 16 was also done with the other sample groups which are identical in chemical composition. For the other groups, only the final result, the comparison of the reference values and the values determined by NIR spectroscopy is shown.

Sample group 2 (No. 17–21)

In this sample group, the extruder was operated with the melt pump at maximal pressure difference. The PP-MA and organoclay content was constant at 20 wt % for all samples. Differences were achieved by changing the screw speed in the range from 75 to 300 rpm.

In Table III and Figure 8, the detailed results of the chemometric evaluation of this sample group are given. Very good correlation of Rheotens and NIR tensile force values can be achieved by designing an optimized chemometric model. The chosen spectral pretreatment method was "subtraction of constant

offset" as in sample group 1. Even though the coefficient of correlation R^2 is in the same region as in group 1, the results can not be judged with the same relevance, because of the low number of samples and because of the non-uniform distribution of the sample parameter values over the parameter interval (effectively only three really different tensile force values in sample set 2).

Sample group 3 (No. 22–32)

For the sample group 3, the extruder was operated with the melt pump at maximal pressure difference. The PP-MA and organoclay content was constant at 5 wt % for all samples. Differences were achieved by changing the screw speed in the range from 75 to 400 rpm and by changing the geometry of the extruder screw.

The results of the chemometric evaluation are shown in Table IV and Figure 9. The best spectral pretreatment method for this chemometric model for the determination of the tensile force values from NIR spectra, is "first derivative and multiplicative scatter correction (MSC)." The coefficient of correlation R^2 of 82 for this model is lower than for the models of the other sample groups but still enables qualitative evaluation. The chemometric model enables an evaluation of the mechanical properties of the samples generated with three different extruder

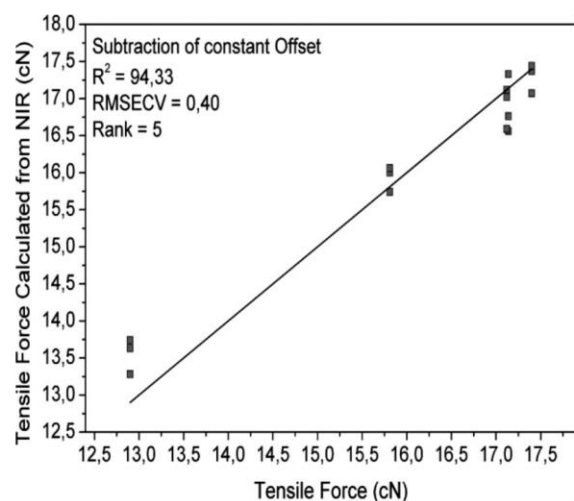


Figure 8 Drawing force values calculated versus measured for samples 17 to 21.

TABLE IV
Drawing Force Values Calculated Versus Measured for Samples 22–32

No.	Indication	Screw speed (rpm)	Rheotens (cN)	Average NIR (cN)
22	G3-75	75	8.30	8.84
23	G3-100	100	9.11	8.68
24	G3-150	150	9.01	9.15
25	G3-200	200	8.34	8.42
26	G3-300	300	7.02	6.84
27	G4-75	75	8.43	8.86
28	G4-100	100	9.05	8.67
29	G4-150	150	9.65	9.59
30	G4-200	200	9.15	9.31
31	G4-300	300	8.64	8.65
32	G4-400	400	7.66	7.66

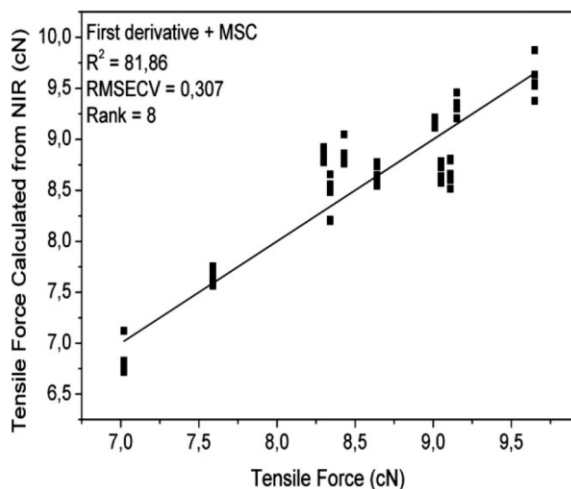


Figure 9 Drawing force values calculated versus measured for samples 22 to 32.

screw geometries. The chemometric model itself will improve significantly, when measurements are taken in-line at the extruder, without any postprocessing of the material.

CONCLUSION

It can be seen that the material reinforcement (level of melt strength) exhibits good correlation with NIR data analyzed by the partial least squares method. NIR spectroscopy was shown to be a qualitative and predominantly quantitative method for monitoring nanocomposite quality of all sample groups investigated, although the extruded sample material had to be cooled down, granulated, and processed to plates for measurements with the off-line NIR system. Therefore, it is crucial to measure the quality of the nanocomposites in-line without any additional processing, to prevent any negative effect on the material structure or reinforcement level. Unknown changes in the samples caused by these postprocessing procedures are negatively affecting the shown chemometric models. In-line-measurement of NIR data is technically possible for the extruder and would lead to a higher quality of the chemometric models due to omission of postprocessing steps. Rheotens and NIR measurements could be done simultaneously on the extruder if the NIR system is implemented in-line and the Rheotens measurements are done on-line through a bypass die system.

This work was done within the project Nano-comp—0901 PlaComp1 funded by the Austrian Nano Initiative. Parts of the FT-NIR research work were done within the FH Plus—Project AMiESP (Advanced Methods in Embedded Signal Processing).

References

- Gilman, J. W.; Kashiwagi, T.; Lichtenhan, J. D. *Sampe J* 1997, 33, 40.
- Ray, S. S.; Okamoto, M. *Progr Polym Sci* 2003, 28, 1539.
- Sanchez-Solis, A.; Garcia-Rejon, A.; Manero, O. *Macromol Symp* 2003, 192, 281.
- Sanchez-Solis, A.; Romero-Ibarra, I.; Estrada, M. R.; Calderas, F.; Manero, O. *Polym Eng Sci* 2004, 44, 1094.
- Ishida, H.; Cambell, S.; Blackwell, J. *Chem Mater* 2000, 12, 1260.
- Vaia, R. A.; Giannelis, E. P. *Macromolecules* 1997, 30, 8000.
- Pinnavaia, T. J.; Beall, G. W. *Polymer-Clay Nanocomposites*; New York, 2000.
- Kim, D. H.; Park, J. U.; Cho, K. S.; Ahn, K. H.; Lee, S. J. *Macromol Mater Eng* 2006, 291, 1127.
- Hasegawa, N.; Kawasumi, M.; Kato, M.; Usuki, M.; Okada, A. *J Appl Polym Sci* 1998, 87, 67.
- Maxfield, M.; Shacklette, L. W.; Baughman, R. H.; Christiani, B. R.; Eberly, D. E. *PCT Int Appl WO* 1993, 93, 04118.
- Lee, S. S.; Kim, J. *Polym Mater Sci Eng* 2003, 89, 370.
- Kracalik, M.; Mikesova, J.; Puffr, R.; Baldrian, J.; Thomann, R.; Friedrich, C. *Polym Bull* 2007, 58, 313.
- Kracalik, M.; Studenovský, M.; Mikesova, J.; Sikora, A.; Thomann, R.; Friedrich, C.; Fortelny, I.; Simonik, J. *J Appl Polym Sci* 2007, 106, 926.
- Kracalik, M.; Studenovský, M.; Mikesova, J.; Kovarova, J.; Sikora, A.; Thomann, R.; Friedrich, C. *J Appl Polym Sci* 2007, 106, 2092.
- Kracalik, M.; Pospisil, L.; Slouf, M.; Mikesova, J.; Sikora, A.; Simonik, J.; Fortelny, I. *Polym Compos* 2008, 29, 437.
- Kracalik, M.; Pospisil, L.; Slouf, M.; Mikesova, J.; Sikora, A.; Simonik, J.; Fortelny, I. *Polym Compos* 2008, 29, 915.
- Gilman, J. W.; Morgan, A. B.; Harris, R. H., Jr.; Trulove, P. C.; DeLong, H. C.; Sutto, T. E. *Polym Mater Sci Eng* 2000, 83, 59.
- Messersmith, P. B.; Giannelis, E. P. *Chem Mater* 1994, 6, 1719.
- Hoffmann, B.; Kressler, J.; Stöppelmann, G.; Friedrich, C.; Kim, G. M. *Colloid Polym Sci* 2000, 278, 629.
- Lepoittevin, B.; Pantoustier, N.; Devalckenaere, M.; Alexandre, M.; Kubies, D.; Calberg, D.; Jérôme, R.; Dubois, P. *Macromolecules* 2002, 35, 8385.
- Messersmith, P. B.; Giannelis, E. P. *Chem Mater* 1993, 5, 1064.
- Messersmith, P. B.; Giannelis, E. P. *J Polym Sci Polym Phys Ed* 1995, 33, 1047.
- Tashiro, K. *Vibr Spectr Polym* 2007, 143.
- Loo, L. S.; Gleason, K. K. *Macromolecules* 2003, 36, 6114.
- Sakurai, T.; Kasahara, T.; Yamaguchi, N.; Tashiro, K.; Amemiya, Y. *PMSE Preprints* 2003, 88, 352.
- Nakamoto, S.; Tashiro, K.; Matsumoto, A. *Macromolecules* 2003, 36, 109.
- Tashiro, K. *Sen'i Gakkaishi* 2002, 58, 253.
- Kitagawa, T.; Tashiro, K.; Yabuki, K. *J Polym Sci Part B: Polym Phys* 2002, 40, 1269.
- Wang, H.; Palmer, R. A.; Manning, C. *J Appl Spectrosc* 1997, 51, 1245.
- Sonoyama, M.; Shoda, K.; Katagiri, G.; Ishida, H. *Appl Spectrosc* 1997, 51, 346.
- Tashiro, K. *Korea Polymer J* 1996, 4, 166.
- Kalra, A.; Parks, D. M.; Rutledge, G. C. *Macromolecules* 2007, 40, 140.
- Loo, L. S.; Gleason, K. K. *Macromolecules* 2003, 36, 2587.
- Laske, S.; Kracalik, M.; Gschweilt, M.; Feuchter, M.; Maier, G.; Pinter, G.; Thomann, R.; Friesenbichler, W.; Langecker, G. R. *J Appl Polym Sci* 2009, 111, 2253.
- Goettfert Ltd. Buchen, Germany. Available at: <http://www.goettfert.com>.
- Brerenton, R. G. *Chemometrics Data Analysis for the Laboratory and Chemical Plant*, ISBNs: 0-471-48977-8 (HB); 0-471-48978-6 (PB), 2003.

2.2.3 Manuscript 8

“In-line characterization of polypropylene nanocomposites using FT-NIR”

Witschnigg, Andreas; Laske, Stephan; Kracalik, Milan; Feuchter, Michael; Pinter, Gerald; Maier, Günther et al. (2010): In: J. Appl. Polym. Sci. 8, n/a-n/a. DOI: 10.1002/app.32024.

Using the know-how from manuscript 7, chemometrical modelling was applied for prediction of rheological (melt strength level), structural (interlayer distance) and application (Young's modulus) properties. For the first time, in-line FT-NIR mit on-line rheometry was combined simultaneously for material characterization during compounding of polymer nanocomposites. The Young's Modulus, the interlayer distance and the tensile force exhibited good correlation with NIR data analyzed by PLS algorithm. It was proved that near infrared spectroscopy is a quantitative method for monitoring nanocomposite quality although the measurements were partially done at different aggregate states and samples with different processing history caused by sample preparation. Therefore important parameters like crystallization could not be considered by the NIR measurements. It was evident that the different aggregate states (melt state vs. semicrystalline solid state) and the postprocessing procedures (cooling down, heating up, molding and cooling down again) cause for example preferential orientations, affecting the chemometric models negatively. Nevertheless this work showed that it is possible to determine the Young's modulus, the interlayer distance and the tensile force with sufficient precision for quantitative evaluation with near infrared spectroscopy. Therefore NIR spectroscopy was found to be suitable for inline quality control and characterization of nanocomposites in real time and directly in the melt state during production, leading to a faster composite optimization process with reduced rejections and costs. This approach opened new opportunity to speed up development of tailor-made materials based on polymer nanocomposites.

In-Line Characterization of Polypropylene Nanocomposites Using FT-NIR

Andreas Witschnigg,¹ Stephan Laske,¹ Milan Kracalik,¹ Michael Feuchter,² Gerald Pinter,² Günther Maier,³ Wolfgang Märzinger,⁴ Michael Haberkorn,⁵ Günter Rüdiger Langecker,¹ Clemens Holzer¹

¹Institute of Plastics Processing, University of Leoben, Leoben 8700, Austria

²Institute of Materials Science and Testing of Plastics, University of Leoben, Leoben 8700, Austria

³Material Center Leoben, Leoben 8700, Austria

⁴i-RED Infrarot Systeme GmbH, Hafenstrasse 47-51, Linz 4020, Austria

⁵RECENDT GmbH, Hafenstrasse 47-51, Linz 4020, Austria

Received 22 October 2009; accepted 27 December 2009

DOI 10.1002/app.32024

Published online 29 April 2010 in Wiley InterScience (www.interscience.wiley.com).

ABSTRACT: The morphology of polymer nanocomposites is usually characterized by various methods like X-ray diffraction (XRD) or transmission electron microscopy (TEM). In this work, a new approach for characterizing nanocomposites is developed: the results of small angle x-ray scattering, on-line extensional rheometry (level of melt strength) and Young's modulus out of tensile test are correlated with those of near infrared (NIR) spectroscopy. The disadvantages of the common characterization methods are high costs and very time consuming sample preparation and testing. In contrast, NIR spectroscopy has the advantage to be measured in-line and in real time directly in the melt. The results were obtained for different aggregate states (NIR spectroscopy and

on-line rheotens test in melt state, tensile test, and XRD in solid state). Therefore, important factors like crystallization could not be considered. Nevertheless, this work demonstrates that the NIR-technology is perfectly suitable for quantitative in-line characterization. The results show that, by the installation of a NIR spectrometer on a nanocomposite-processing compounder, a powerful instrument for quality control and optimization of compounding process, in terms of increased and constant quality, is available. © 2010 Wiley Periodicals, Inc. *J Appl Polym Sci* 117: 3047–3053, 2010

Key words: nanoparticles; polymer composite materials; FTNIR spectroscopy

INTRODUCTION

The use of nanocomposites has developed rapidly over the last years. One reason is their great potential for improving material properties with only a small amount of filler. Nanocomposites are polymers filled with particles where at least one dimension is in the order of nanometers. There are several types of nanofillers, which are classified in three structures (spherical, laminar, or fibrous particles). Because of the high aspect ratio, which is linked with the ability to improve polymers, fibrous, and laminar particles are commonly used.

There are two reasons for the improvement of material properties by the application of nanofillers. The first reason is the enforcement of the polymer matrix by means of the particles (like it is the case

for other fillers). The second effect is the movement-restrictive effect on the polymer chains caused by the layered anorganic nanofillers. Therefore mainly layered silicates (most common montmorillonite) with an aspect ratio up to 1000 are used.

To reach best interactions between polymer matrix and nanofiller (especially layered silicates) a homogeneous dispersion is essential. Because of the technological simplicity, nanocomposites are preferably produced by using a twin screw extruder operating at high temperatures and pressures.^{1,2} Shearing forces, induced by the rotation of the screw and thermodynamical interactions between polymer chain and layered silicate clay are delaminating the layered silicate. During the process, the structures which are responsible for the level of reinforcement are formed by physical bonding between the hydrophilic clay, the hydrophobic polymer matrix and a compatibilizer.³

According to the dispersion and the homogeneity of the nanofiller conventional composites, intercalated nanocomposites and exfoliated nanocomposites can be formed. To determine the homogeneity of the material a variety of methods are commonly used. These include optical [scanning (SEM) and transmission (TEM) electron microscopy], mechanical (tensile

Correspondence to: S. Laske (stephan.laske@unileoben.ac.at).

Contract grant sponsor: Austrian Nano Initiative (project Nanocomp – 0901 PlaComp1).

Journal of Applied Polymer Science, Vol. 117, 3047–3053 (2010)
© 2010 Wiley Periodicals, Inc.

strength, extensional rheology) and light scattering methods (small angle (SAXS) and wide angle (WAXS) X-ray scattering). A new way to determine material homogeneity is the use of near infrared (NIR) spectroscopy. NIR spectroscopy is a nondestructive, optical method to obtain information about the composition of samples and interactions within the sample. Near- and mid-infrared methods (NIR, MIR) measure the absorbance of light due to excitation of molecular vibrations of the substance under investigation. Mid-infrared measurements (often referred to only as IR) are exploiting radiation in a spectral range between 2500 and 25,000 nm, detecting fundamental molecular vibrations, while NIR is operating in the spectral range between 780 and 2500 nm. Therefore NIR detects the overtones and combinations of the molecular vibrations. Although NIR signals are 100–1000 times weaker than IR signals, only the NIR technique is suitable for in-line implementation due to the use of quartz based optics and optical fibers for signal transfer from the measuring probe to the NIR spectrometer.

If light is transmitted through a sample, vibrations of the molecular bondings are excited, resulting in an energy absorbance at specific wavelengths depending on the type of molecule and molecular bondings, which can be detected by NIR spectroscopy. The wavelength position of the absorbance bands in the NIR spectrum provides the information for identification of substances and chemical functionalities. The prevailing conditions in the sample (chemical state, number, and type of interactions) are narrowly linked with the mechanical properties, which can therefore be determined by NIR spectroscopy.⁴

NIR measurements have a variety of successful applications in polymer science, such as the analysis of polymerization or copolymerization (mostly done by detecting the characteristically absorption caused by chemical groups as e.g., OH groups or vinyl acetate groups in ethylene vinyl acetate), crystallinity, molecular weight, anisotropy, intermolecular interactions, molar mass, porosity, specific surface area, tacticity, orientation, concentrations of flame retardants (e.g., melamine cyanurate), density measurements, and other chemical processes that appear during polymer processing.^{5–16}

In other studies, nanocomposites^{6,15–17} are analyzed regarding crystallization properties and particle size¹⁶ using NIR measurements.

The near infrared technique combined with stress-strain curves to evaluate filled rubbers (using SiO₂, TiO₂, layered silicate, and Nanotubes) with regard to changes in crystallization and degree of exfoliation under strain has also been investigated. A coherence between crystallization under strain and a shift in NIR spectra has been found.¹⁷

In addition, NIR spectroscopy has successfully been used to monitor the processing of pharmaceutical nanoparticles and to classify them by their particle size in a high solids dispersion.¹⁸

The analysis of the melt strength of a polypropylene (PP) nanocomposite with off-line NIR spectroscopy (correlated with off-line rheotens measurement) has already been achieved.⁴

EXPERIMENTAL

Materials

The isotactic PP homopolymer HC600TF (melt flow index (MFI) 2.8 g/10 min; 230°C/2.16 kg) was supplied by Borealis, Linz, Austria. The used nanofiller (montmorillonite intercalated with dimethyl distearyl ammonium chloride) with commercial indication Nanofil 5 was supplied by Sud-Chemie, Munich, Germany. The compatibilizer (Scona TPPP 2112 FA, MFI 14.8 g/10 min) was supplied by Kometra, Schkopau, Germany.

Preparation of polypropylene nanocomposites

For the compounding process, an intermeshing, corotating twin screw extruder Theysohn TSK30/40D (Theysohn Holding, Vienna, Austria) with a string die was used. The feed rate was set at 10 kg/h, with a screw speed from 100 to 300 rpm. The formulation of the nanocomposite was constant at 5 wt % organoclay, 5 wt % compatibilizer and 90 wt % polypropylene. A melt pump was used ($\Delta p \sim 100$ bar) to increase the residence time and shear rate and therefore improve the dispersion of the nanofiller. A bypass system was used to create a melt string for on-line rheotens measurement. Two different screw geometries, in the following referred to as geometry 1 and geometry 2, were used to produce nanocomposites with varying layer distance and mechanical properties. The main difference between these screw geometries is the number and position of kneading elements resulting in different values of induced shear energy and residence time. As can be seen in Figure 1, both geometries are identical until the side feeder. From this point, geometry 1 consists of a kneading block right after the side feeder followed by a short kneading block at the end of the screw for additional induced shear energy in the backpressure zone caused by the melt pump. In opposite to that, geometry 2 consists only of conveying blocks.

For structural and mechanical characterization, plates with a thickness of 2 mm and standard dog bone shaped specimens (150 mm length, 20 mm width, 4 mm thickness), respectively, were prepared using the hydraulic vacuum press machine (Collin

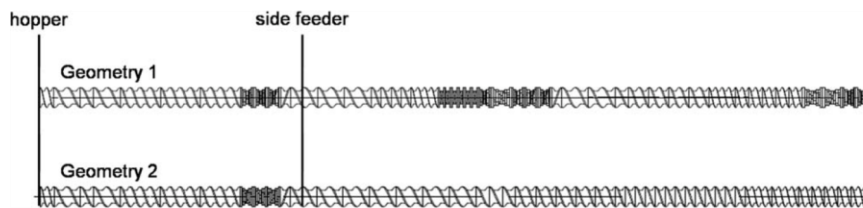


Figure 1 Schematically illustration of screw geometry 1 and 2.

200 PV, Dr. Collin, Ebersberg, Germany) and the injection molding machine (Engel ES330/80H, 800 KN closing force, Schwertberg, Austria).

Small angle x-ray scattering

X-ray measurements were performed using Bruker NanoSTAR (Bruker AXS, Karlsruhe, Germany) small angle X-ray scattering (SAXS) equipment. This system was equipped with a two dimensional X-ray detector. A wavelength of 0.154 nm ($\text{Cu-K}\alpha$) was used. The samples were measured in transmission at a temperature of 23°C. To avoid the influence of texture, all scattering measurements were performed on plate samples. The gallery period 1 of the nanofiller was determined on a powder sample. To avoid statistical effects, the scattering curves recorded at three different positions on the samples were averaged. To determine the gallery period, scattering curves were corrected for background scatter and a Lorenz correction was applied. The Lorenz correction was performed by multiplying the scattered intensity ($I(q)$) by q^2 , q being the magnitude of the scattering vector. For the determination of the peak position the data were fitted with a Pseudo-Voigt function.¹⁹ The interlayer distance is then calculated with the Bragg's law. The modulus of scattering vector q is defined as $q = (4\pi \sin\theta)/\lambda$ where λ is the wavelength of the used radiation and θ is the half of the scattering angle 2θ . The SAXS data evaluation was basically performed by applying a correlation function method according to Strobl and Schneider.²⁰

Mechanical properties - tensile test

A universal tensile testing machine (Type: Z010, Zwick and Co. KG, Ulm, Germany) was used to carry out the tensile tests according to ISO 527-1. All tests were carried out under standardized conditions ($23 \pm 2^\circ\text{C}/50 \pm 5\% \text{ r.H.}$). The data was evaluated using the testXpert II software (ZWICK, Ulm, Germany).

Rheotens measurements

The different physical crosslinking and bonding between polymer chains and organoclay results in a

diversity of viscoelastic response. Therefore rheotens measurements are used to identify changes of the elongational viscosity. Individual nanoparticles act as entanglement or crosslinking sites and raise the extensional stiffness of the composite.²¹

The Rheotens 71.97 equipment (Göttfert, Buchen, Germany) was used. The melt string was applied through a bypass system directly from the extruder to achieve on-line measurement. Two or four rotating wheels (linearly accelerated) are connected to a force transducer while drawing off the extruded string until it breaks. The drawing force applied to the wheels at a specific draw rate is the reference value for the melt strength level. To compare the draw force level of different nanocomposite systems, the drawing force at a draw rate of 150 mm/s has been chosen as a comparative value. The data of at least three measurements for each sample were evaluated.

In-line FTNIR measurements

For in-line measurement a Fourier transform near infrared (FTNIR) spectrometer of i-Red Infrared Systems (Linz, Austria) with a probe installed right before the die was used. The spectrometer is working at a spectral range of 12,000 – 3800 cm^{-1} (900–2600 nm) with a spectral resolution of 1.5 cm^{-1} . The probe was connected to the spectrometer using fiber optics. The spectral data was collected with near infrared process spectrometer software (NIPS). The chemometric evaluation of the measured spectra was done with the software package Thermo GRAMS/AI from Thermo Fisher Scientific.

For a single spectrum 50 scans (10 scans per second) were averaged. For each setting 100 spectra were used to create a chemometrical model. To avoid drift effects caused by environmental or other parasitic effects, the measurement settings were chosen randomly.

Evaluation of NIR data

For the realization of an adequate process monitoring it is essential to find relations between composition of the sample, particle size or mechanical properties. This procedure is extensive, because NIR

measurements detect combinations of vibrations and overlapping bands. Therefore statistics provides various algorithms that establish a relationship between spectral data and a chemometric model. The intricacy for building a chemometric model is the problem of finding the right algorithm, the right preprocessing method and the right wavelength range. NIR measurements are in need of reference investigations (for linking them with mechanical properties), which are providing the values used for correlation with the spectral data. It is of immense importance for the accurateness of the chemometric model that these values are as precise as possible.

The multivariate data applied by NIR spectra are more dimensional (n -dimensional space). Therefore it is necessary to project the data on a two dimensional plane. The emerging picture is changing if the data points are rotated in the n -dimensional space. The possibilities of such projections are infinite so it is essential to find the direction where the scatter along the axis reaches its maximum (maximum of information). If such a direction is found an axis orthogonal on the first axis is rotated until the scattering of data is reaching the maximum again. This approach is continued as all n -dimensions are considered. This procedure is defined mathematically as eigenvalue problem.

All performable evaluation methods, such as principal component analysis (PCA), principal component regression (PCR) or partial least squares (PLS 1 and PLS 2) are working basically on this approach.

It is of great advantage to exclude some regions with irrelevant spectral information. This can be done by calculating an absorption spectra out of two different spectra. This absorption spectra shows those wavelength regions with the highest difference and preferably low signal noise. This region can then be chosen to achieve good correlating chemometrical models.

Before the spectra are used for further calculation a preprocessing is often beneficial to get rid of parasitic effects like light straying caused by irregularities in the melt. One of the methods used is mean centering, which is calculating an average spectrum out of all used spectra and subtracts it from every single spectrum to get rid of offset effects. A way to achieve path length correction is to normalize the spectra to correct simple nonlinearities or to use algorithms such as standard normal variate transformation (SNV) or multiplicative scatter correction (MSC).

Experimentally NIR spectra of samples with varying but known responses were measured, pretreated and then the PLS 1 algorithm was used to generate a linear calibration model for calculating the responses from the measured NIR data using reference values. Then a cross validation was performed on the calculated chemometrical model. The principle of a cross

validation is always the same. The model data are separated in two excluding sets (one experimental adjustment is sequentially left out). The bigger set is called training set and is used to calculate the model. The second set (test-set) is used to affirm the model. This procedure is repeated for all experimental adjustments. The bigger the training set gets the better cross validation works, especially when extrapolation is needed. The quality and the predictive ability of the model is rated basically with the coefficient of determination R^2 and the root mean square error of cross validation RMSECV. R^2 (values between 0 and 100%) shows the correlation of the NIR data with the reference values of the response parameter. The coefficient of determination R^2 should lie above 90 for quantitative calculation and above 70 for qualitative calculation. All models with values below 70 can not be used reasonably. Additionally, a precise model has a RMSECV as low as possible. A good and stable model should also not consist of many eigenvectors (referred to as "factors"), because the more factors are used the more unsteady the chemometric model becomes. So it is clear that the number of factors used should always stay in relation to the problem investigated. In the case of the investigation of nanocomposites the number of factors should preferably not be higher than 8.

RMSECV and R^2 are calculated the following:

$$\text{RMSECV} = \sqrt{\frac{\sum_{i=1}^n (Y_{ki} - Y_{pi})^2}{n}}$$

$$R^2 = 1 - \frac{\sum_{i=1}^n (Y_{pi} - \bar{Y}_j)^2}{\sum_{i=1}^n (Y_{ki} - \bar{Y}_j)^2}$$

Y_k ... actual measurement value

Y_p ... predicted value

$\bar{Y}, \bar{\bar{Y}}$... mean value

RESULTS AND DISCUSSION

Near infrared spectroscopy with Young's modulus as reference value

For this measurement, the response of interest is the Young's Modulus. The gained chemometric model should be close to the best model for the evaluation of the Young's Modulus values from NIR measurements. Very good correlation of tensile test and NIR measurements can be achieved by designing an optimized chemometric model. The chosen spectral pretreatment methods were mean centering and SNV. A coefficient of determination $R^2 = 97.70\%$ (factors = 5) with an RMSECV of 30 MPa for screw geometry 1 and $R^2 = 90.55\%$ (factors = 4) with an RMSECV of 94 MPa

TABLE I
Sample Description, Actual Values and Values Predicted by NIR for the Young's Modulus

Geometry	Clay/PP-MA content (wt %)	Screw speed (rpm)	Young's modulus (MPa)	NIR (MPa)
G1	5/5	100	2220	2230
		150	2190	2195
		200	2220	2214
		250	2200	2197
		300	2010	2074
G2	5/5	100	2340	2199
		150	2280	2275
		200	2260	2295
		250	2280	2237
		300	2210	2356

TABLE II
Sample Description, Actual Values, and Values Predicted by NIR for the Layer Distance

Geometry	Clay/PP-MA content (wt %)	Screw speed (rpm)	Layer distance (mN)	NIR (nm)
G1	5/5	100	42.35	2.708
		150	37.42	2.637
		200	31.56	2.599
		250	23.77	2.621
		300	17.23	2.716
G2	5/5	100	50.35	2.765
		150	45.32	2.677
		200	40.88	2.658
		250	36.53	2.602
		300	28.66	2.554

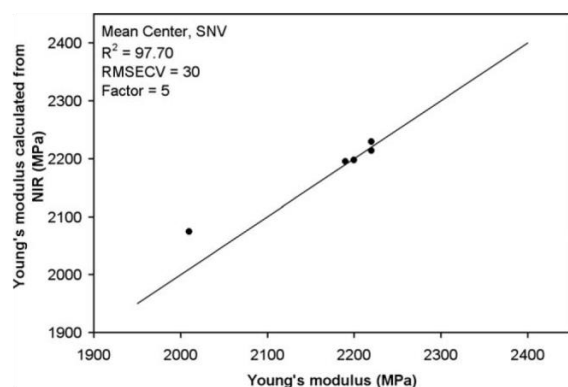


Figure 2 Young's modulus values calculated versus measured for geometry 1.

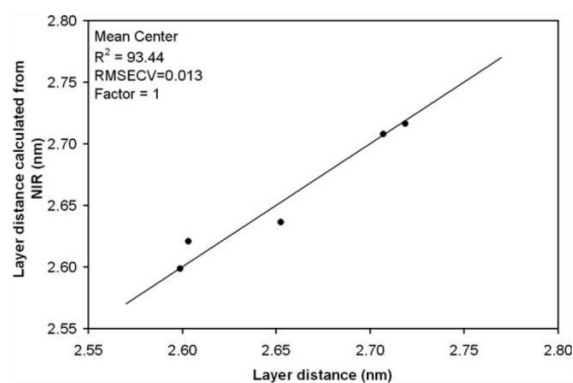


Figure 4 Layer distance calculated versus measured for geometry 1.

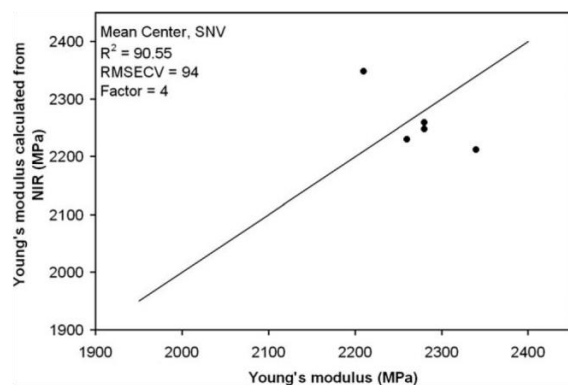


Figure 3 Young's modulus values calculated versus measured for geometry 2.

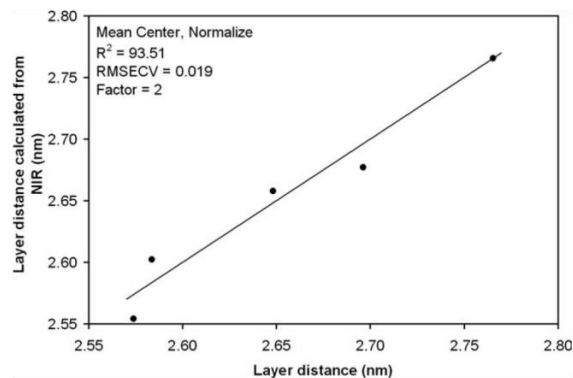


Figure 5 Layer distance calculated versus measured for geometry 2.

for screw geometry 2 could be achieved. Table I, Figures 2 and 3 show the results for both geometries.

The calculated Young's Moduli for geometry 1 are very close to the real values regarding that the performed tensile test has a mean standard deviation of 67 MPa.

The values for geometry 2 at screw speed 100 and 300 show greater deviations, which can be explained with the fact that cross validation is not always that efficient with extrapolation. Nevertheless, the values are quite precise regarding that the tensile test has a mean standard deviation of 166 MPa for geometry 2.

TABLE III
Sample Description, Actual Values, and Values Predicted by NIR for the Drawing Force

Geometry	Clay/PP-MA content (wt %)	Screw speed (rpm)	Drawing force (mN)	NIR (mN)
G1	5/5	100	42.35	40.30
		150	37.42	36.93
		200	31.56	29.39
		250	23.77	26.04
		300	17.23	12.83
G2	5/5	100	50.35	49.66
		150	45.32	43.39
		200	40.88	41.94
		250	36.53	37.68
		300	28.66	32.13

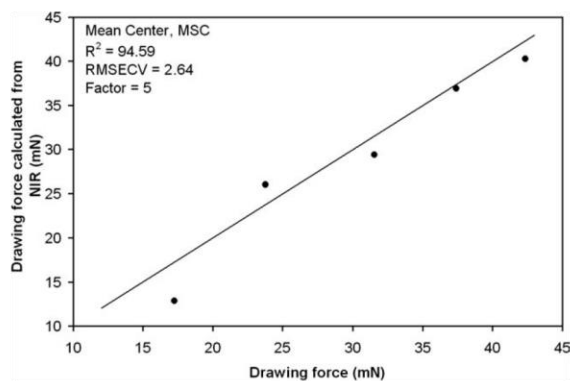


Figure 6 Drawing force calculated versus measured for geometry 1.

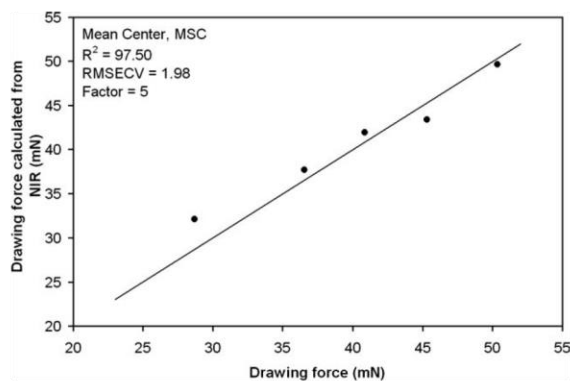


Figure 7 Drawing force calculated versus measured for geometry 2.

Near infrared spectroscopy with layer distance as reference value

The second response of interest is the interlayer distance gained by SAXS measurements. The interlayer distance is the spacing of one particle including the distance to the next particle. A very good correlation

is achieved when the chemometric model is optimized with mean centering and normalization (Fig. 5). The coefficient of determination R^2 calculated for screw geometry 1 was 93.44% (factors = 1) with an RMSECV of 0.013 and $R^2 = 93.51\%$ (factors = 2) with an RMSECV of 0.019 nm for screw geometry 2. Table II, Figures 4 and 5 show the values for the layer distance calculated with the chemometrical model.

Near infrared spectroscopy with drawing force as reference value

The third response of interest is the on-line measured drawing force. To gain good correlation the chemometric model is optimized with mean centering and Multiplicative Scatter Correction (MSC). A coefficient of determination $R^2 = 94.59\%$ (factors = 5) with an RMSECV of 2.64 mN for screw geometry 1 and $R^2 = 97.50\%$ (factors = 5) with an RMSECV of 1.98 mN for screw geometry 2 could be achieved. Table III, Figures 6 and 7 show the results measured and calculated for both geometries.

CONCLUSIONS

As shown in this work the Young's Modulus, the layer distance and the drawing force exhibit good correlation with NIR data analyzed by PLS 1 algorithm. It can be seen that near infrared spectroscopy is a quantitative method for monitoring nanocomposite quality although the measurements were done at different aggregate states and samples with different processing history caused by sample preparation. Therefore important parameters like crystallization could not be considered by the NIR measurements. It is evident that the different aggregate states (melt state vs. semicrystalline solid state) and the postprocessing procedures (cooling down, heating up, molding, and cooling down again) causing for example preferential orientations, are affecting the chemometric models negatively. Nevertheless this work shows that it is possible to determine the Young's modulus, the layer distance and the drawing force with sufficient precision for quantitative evaluation with near infrared spectroscopy. Therefore NIR spectroscopy is perfectly suitable for in-line quality control and characterization of nanocomposites in real time and directly in the melt during production, leading to a faster composite optimization process with reduced rejections and costs.

Parts of the FTNIR research work were done within the FH Plus - Project AMiESP (Advanced Methods in Embedded Signal Processing).

References

1. Vaia, R. A.; Jandt, K. D.; Kramer, E. J.; Giannelis, E. P. *Chem Mater* 1996, 8, 2628.
2. Davis, C. H.; Mathias, L. J.; Gilman, J. W.; Schiraldi, D. A.; Shields, J. R.; Trulove, P.; Sutto, T. E.; Delong, H. C. *J Polym Sci Part B: Polym Phys* 2002, 40, 2661.
3. Pinnavaia, T. J.; Beall, G. W. *Polymer-Clay Nanocomposites*; John Wiley & Sons: New York, 2000.
4. Laske, S.; Kracalik, M.; Feuchter, M.; Pinter, G.; Maier, G.; Märzinger, W.; Haberkorn, M.; Langecker, G. R. *J Appl Polym Sci* 2009, 114, 2488.
5. Heigl, N.; Petter, C. H.; Rainer, M.; Najam-Ul-Haq, M.; Vallant, R.; Bakry, R.; Bonn, G.; Huck, C. *J Near Infrared Spectrosc* 2007, 15, 269.
6. D. Fischer, I. Alig, J. Hutschenreuter, Presented at the 21st Annual Meeting of the Polymer Processing Society (PPS21), Leipzig, 2005.
7. Fischer, D.; Kirschner, U. *GIT* 2002, 11, 1267.
8. Barnes, S.; Sibley, M.; Brown, E.; Edwards, H.; Scowen, I.; Coates, P. *Annu Tech Conference* 2003, 3, 3311.
9. Fischer, D.; Sahre, K.; Abdelrhim, M.; Voit, B.; Sadhu, V.; Pionteck, J.; Komber, H.; Hutschenreuter, J. *CR Chimie* 2006, 9, 1419.
10. Barrès, C.; Bounor-Legaré, V.; Melis, F.; Michel, A. *Polym Eng Sci* 2006, 46, 1613.
11. Watari, M.; Ozaki, Y. *Appl Spectrosc* 2006, 60, 529.
12. Nagata, T.; Ohshima, M.; Tanigaki, M. *Polym Eng Sci* 2000, 40, 1107.
13. Barnes, S.; Brown, E.; Sibley, M.; Edwards, H.; Scowen, I.; Coates, P. *Appl Spectrosc* 2005, 59, 611.
14. Barnes, S.; Brown, E.; Sibley, M.; Edwards, H.; Coates, P. *Analyst* 2005, 130, 286.
15. Steinhoff, B.; Lellinger, D.; Pötschke, P.; Alig, I. Presented at the 21st Annual Meeting of the Polymer Processing Society (PPS21), Leipzig, 2005.
16. Asai, K.; Okamoto, M.; Tashiro, K. *Polymer* 2008, 49, 5186.
17. Bokobza, L.; Diop, A.; Fournier, V.; Minne, J.; Brunell, J. *Macromol Symp* 2005, 230, 87.
18. Higgins, J.; Arrivo, S.; Thurau, G.; Green, R.; Bowen, W.; Lange, A.; Templeton, A.; Thomas, D.; Reed, R. *Anal Chem* 2003, 75, 1777.
19. Balta-Calleja, F. J.; Vonk, C. G. *X-Ray Scattering of Synthetic Polymers*; Elsevier: New York, 1989.
20. Strobl, G. R.; Schneider, M. *J Polym Sci* 1980, 18, 1343.
21. Laske, S.; Kracalik, M.; Gschweil, M.; Feuchter, M.; Maier, G.; Pinter, G.; Thomann, R.; Friesenbichler, W.; Langecker, G. R. *J Appl Polym Sci* 2009, 111, 2253.

2.2.4 Manuscript 9

“Influence of induced shear work on the properties of polyolefine nanocomposite pipes”

Witschnigg, Andreas; Laske, Stephan; Kracalik, Milan; Holzer, Clemens (2012): In: Polym. Eng. Sci. 52 (5), S. 1155–1160. DOI: 10.1002/pen.22146.

In this work, a closer look to calculation of shear energy generated by different processing routes (single- vs. double-pass compounding, pipe extrusion) of polymer nanocomposites was done. An attempt was taken to calculate the shear energy for different processing techniques and make them comparable. It was shown that the shear energy generated during injection molding cannot be separated from the strain energy in the die and in the tool and, therefore, is present in the calculated energy values in high extent, which is compensating the effect of the extrusion processes. This was responsible for the incomparableness of the combined shear and strain energy from injection molding with the normalized shear energy values of single and twin screw extrusion. Nevertheless, the shear energy comparison between the two extrusion processes showed good compliance with the measured properties. This calculation supplemented previous rheological results, in which effect of shear energy and residence time on processing and application properties of nanocomposites was estimated using extensional rheometry.

Influence of Induced Shear Work on the Properties of Polyolefine Nanocomposite Pipes

Andreas Witschnigg, Stephan Laske, Milan Kracalik, Clemens Holzer

Chair of Polymer Processing, Department Polymer Engineering and Science, Montanuniversitaet Leoben, Otto Gloeckel-Strasse 2, 8700 Leoben, Austria

The use of layered silicates is steadily growing in polymer processing due to their great potential of enhancing material properties. Depending on the particle structure (agglomerated, intercalated, or exfoliated), a significantly higher level of improvement of the material properties can be achieved. The degree of exfoliation is exceedingly linked with the residence time and shear energy induced during processing. These processing parameters themselves are depending on the type of processing technique and conditions. The influence on exfoliation rate and the needed values for processing nanocomposites are not known precisely, but would be of major interest according to an optimization of mechanical and physical properties. In this work, the effect of different processing techniques (compounding, extrusion, and injection molding) on the dispersion of the nanofiller is investigated. A specific shear energy is calculated by the induced shear energy and the residence time regarding the mass throughput for better comparison. The differences in the degree of exfoliation according to dissimilarity of the chosen processing techniques are compared via various methods such as internal pressure creep rupture test, longitudinal shrinkage, and tensile test. It is shown that the calculated values are correlating with good precision, especially for the extrusion process. POLYM. ENG. SCI., 52:1155–1160, 2012. © 2012 Society of Plastics Engineers

INTRODUCTION

Layered silicates as nanoclays are the most common nanofiller used in polymer processing due to their great potential of enhancing material properties and the fact that they are less expensive compared to other nanofillers, like carbon nanotubes or fullerene.

There are two reasons for the improvement of material properties by the application of nanofillers. The first reason is the enforcement of the polymer matrix by means of the particles (like it is the case for other fillers). The second effect is the movement-restrictive effect on the polymer chains caused by the layered inorganic nano-

fillers. Therefore, mainly layered silicates (most common montmorillonite) with an aspect ratio up to 1000 are used.

To achieve best interactions between the polymer matrix and the filler, a homogeneous dispersion is essential. Because of the technological simplicity, nanocomposites are preferably produced by using a twin screw extruder operating at high temperatures and pressures [1, 2].

If processed adequate, layered silicate is able to enhance Young's modulus, elongation at break, barrier, and other mechanical or physical properties. Beside this, the size of the interface is also of great importance due to the fact that it is increasing with increasing exfoliation rate of the silicate layers in the polymer matrix leading to a good degree of dispersion. From the processing point of view, there are two main influencing factors: the induced shear energy and the residence time. Both should be preferably high to make sure the polymer chains penetrate between the silicate layers but always low enough to be sure that there is no thermal degradation of the material. These influences have to be concerned for all processing steps starting from the polymer pellets to the test specimen to make statements for the whole polymer-layered silicate system.

A lot of different experiments have been carried out to examine the influence of induced energy in various properties of polymer nanocomposites like (i) the effect of screw speed, which is linked with the induced shear energy, on the Young's modulus as well as oxygen permeation rate [3, 4], (ii) the effect of duration and the speed of mixing on a nanocomposites solute in glycerol on mechanical properties (Young's modulus) [5, 6], (iii) the influence of processing conditions on mechanical properties of polypropylene nanocomposites justified to different amounts of shear energy induced, though a calculation has not been achieved [7], (iv) the effect of processing technique on viscosity and photo-oxidative degradation of polyethylene nanocomposites [8], (v) the influence of different processing routes and therefore shear rate on the crystallization and crystallization kinetics of PPNC [9], (vi) the influence of shear rate, due to different injection molding processing techniques, on the impacts strength of PP-nanocomposites [10], and (vii) the effect of different processing parameters such as

Correspondence to: Stephan Laske; e-mail: stephan.laske@unileoben.ac.at
DOI 10.1002/pen.22146
Published online in Wiley Online Library (wileyonlinelibrary.com).
© 2012 Society of Plastics Engineers

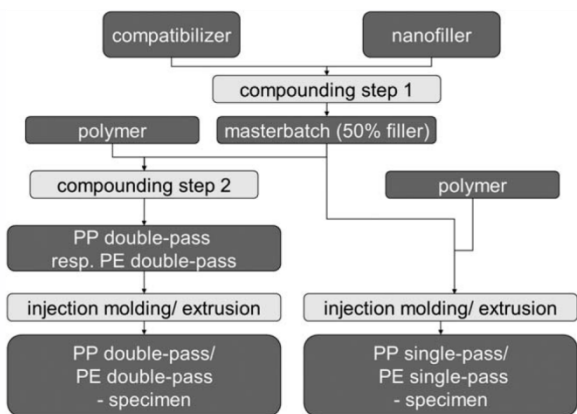


FIG. 1. Processing route for both nanocomposites.

temperature, residence time, and shear rate on mechanical, structural, and rheological as well as thermal properties on PPMC [11]. Nevertheless, the approach to calculate the induced shear energy, normalized with the mass and residence time and related with the achieved material properties for polymer nanocomposites is unique.

EXPERIMENTAL

Materials

Two polyolefins have been used for the investigations. On one hand, a polypropylene with a melt flow rate (MFR) of 0.3 g/10 min (230°C/2.16 kg) from Borealis has been used in combination with a specific compatibilizer.

On the other hand, a polyethylene with a MFR of 0.22 g/10 min (190°C/5 kg) has been used in combination with another compatibilizer to achieve a better dispersion. For homogenous dispersion, a modified nanofiller (montmorillonite intercalated with dimethyl distearyl ammonium chloride) was used in combination with a compatibilizer.

Production of Polyolefin Nanocomposites

For the compounding process, an intermeshing, co-rotating twin-screw extruder Theysohn TSK30/40D (Theysohn Holding, Vienna, Austria) was used. The two processing route can be seen in Fig. 1. One route is the one-step compounding (PP-single pass or PE-single pass). The other route is the two-step compounding (PE-double pass or PP-double pass). The difference between them is a second

TABLE 1. Residence time for twin screw extrusion.

Material	Residence time (s)
PP-masterbatch	385
PP-C	260
PE-masterbatch	365
PE-C	330

TABLE 2. Temperature profile for twin screw extrusion (cylinderzonelength = 120 mm).

Cylinderzones	Temperature (°C)
1	Cooling
2	160
3	180
4	190
5	200
6	200
7	200
8	200
9	200
10	200
Nozzle	200

compounding step to achieve the final composite and only one compounding step (PP-single pass und PE-double pass) with dilution directly in the form giving process. The residence time for the compounding steps can be seen in Table 1.

The feed rate was set at 6 kg/h for the masterbatch and 5 kg/h for both polyolefins nanocomposites with a screw speed of 100 rpm. The masterbatch formulation was 50 wt% compatibilizer and 50 wt% layered silicate. For the finally produced composite (referred to as PE-double pass and PE-single pass, respectively, PP-double pass and PP-single pass), the formulation was 90 wt% polyolefin, 5 wt% compatibilizer, and 5 wt% layered silicate. A melt pump, which induced a backpressure of 100 bar, was used to increase the residence time and shear rate and therefore improve the dispersion of the nanofiller. The temperature profile for the two compounding steps can be seen in Table 2.

As can be seen in Fig. 2, the screw geometry can be divided into three kneading and four conveying blocks. The first kneading block is positioned right before the side feeder. A short kneading block is arranged right before the screw tip for additional induced shear energy in the backpressure zone.

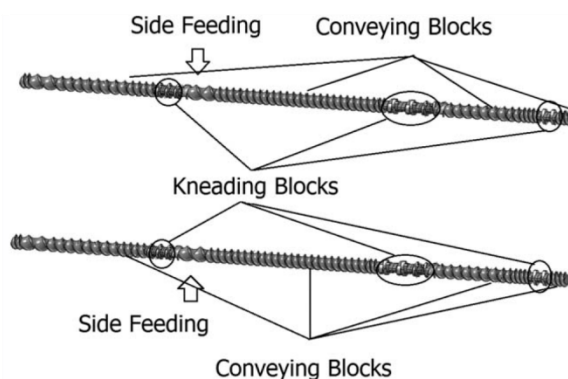


FIG. 2. Screw configuration for both compounding steps.

TABLE 3. Temperature profile for pipe production.

Cylinderzones	Temperature (°C)
1	175
2	200
3	205
4	220
5	225
Toolzone 1	225
Toolzone 2	225
Toolzone 3	230

Production of the Pipes

For the production of pipes, a single screw extruder Proton A 45-28G (Cincinnati Extrusion, Vienna, Austria) with a melt temperature of 230°C at the screw tip, and a screw speed of 40 rpm was used. A barrier screw with additional shear part to increase induced shear energy was applied. The pipes were produced with 1 m in length, a diameter of 50 mm, and a wall thickness of 3 mm. The residence time for the pipe production was measured with 200 s using a specific color-masterbatch. The temperature profile for pipe extrusion can be seen in Table 3.

Production of Tensile Specimen

For tensile tests, standard dog bone shaped specimens (150 mm length, 20 mm width, and 4 mm thickness) were prepared using an injection-molding machine (Engel ES330/80H, 800 KN closing force, Schwertberg, Austria). The melt temperature was set to 230°C with a tool temperature of 50°C. The temperature profile for the injection molding machine can be seen in Table 4.

Tensile Test

An universal tensile testing machine (Type: Z010, Zwick Co. KG, Ulm, Germany) was used to carry out the tensile tests according to ISO 527-1. All tests were carried out under standardized conditions (23°C ± 2°C 50% ± 5% r.H.). The data was evaluated using the testXpert II software (ZWICK, Ulm, Germany).

Internal Pressure Creep Rupture Test

The long-term stability tests were carried out with a pipe facility of IPT (Todtenweis, Germany). The test conditions have been set with 80°C and 5.3 MPa for PE and 4.2 MPa for PP test tension according to ÖNORM EN ISO 1167.

TABLE 4. Temperature profile for injection molding.

Cylinderzones	Temperature (°C)
1	215
2	220
3	225
4	230
Mold	50

Longitudinal Shrinkage

For measuring the longitudinal shrinkage pipe, pieces were given in a hot-air oven with a temperature of 150°C for 60 min. The differences between the length of the pipe pieces before and after the residence in the kiln are used to calculate the longitudinal shrinkage according to EN 743.

Transmission Electron Microscopy

The TEM experiments were performed using a Zeiss LEO 912 Omega transmission electron microscope (Carl Zeiss, Jena, Germany) using an acceleration voltage of 120 kV. The samples were prepared using a Leica Ultracut UCT ultramicrotome (Leica Microsystems, Wetzlar, Germany) equipped with a cryo chamber. Thin sections of about 50 nm were cut with a Diatome diamond knife at -120°C.

Calculation of the Shearing Force for Extrusion and Compounding

The energy balance for an extruder, following the first law of thermodynamics, is given with [12]:

$$P \pm H = \frac{dm}{dt} \cdot \Delta h + p \cdot \frac{dV}{dt} \quad (1)$$

where P is driving power, H the heating/cooling power, $\frac{dm}{dt} \cdot \Delta h$ the enthalpy change, and $p \cdot \frac{dV}{dt}$ the compression work.

Because of the fact that the heating power is very low and has for itself no influence on the shearing processes, it must not be considered. With the negligence of the heating power, the energy introduced into the system must be equal to the driving power minus the compression work and has to be transferred into shear energy (S).

$$\frac{dm}{dt} \cdot \Delta h = P - p \cdot \frac{dV}{dt} = S \quad (2)$$

With this equation, the shear energy introduced into the system for the twin-screw extruder and the single screw extruder can be calculated.

Because of the fact that a comparison between single and twin screw extruder is very difficult, the shear energy was normalized with the mass throughput and the residence time.

$$S_{\text{norm}} = \frac{S}{\dot{m} \cdot t} \quad (3)$$

Calculation of the Shearing Force for Injection Molding

The major part of shear exposure is composed of yielding in the injection die and in the tool. The shear energy

evolving while plastification has also been calculated, but compared to the shearing while injection it can be neglected (only 0.5%). The injection work that comprises the shear exposure in the injection tool can be calculated by integrating the injection pressure along the injection distance [13].

$$W_{inj} = A_S \cdot \int_{s_0}^{s_1} p_S(s) \cdot ds \quad (4)$$

where A_S is the screw area and p_S the injection pressure. The injection energy is then calculated with

$$S_{inj} = \frac{W_{inj}}{t_{inj}} \quad (5)$$

where t_{inj} is the injection time.

The injection energy comprises shear energy, compression energy, and strain energy. The compression energy can be calculated with Eq. 6:

$$S_{compress} = T \cdot \frac{1}{V_{spez}} \cdot \frac{\Delta V_{spez}}{\Delta T} \cdot \frac{\Delta p}{\Delta t} \cdot V \quad (6)$$

The combined shear and strain energy can then be calculated with

$$S_{comb} = S_{inj} - S_{compress} \quad (7)$$

This combined shear and strain energy cannot be directly compared with the shear energy of extruding processes, due to the fact that the strain energy part is very high and not neglectable as far as injection molding is considered. So, the calculated values appear higher than those for extrusion and compounding. Nevertheless, an attempt was started by normalizing the combined energy by considering the mass of the specimen (m).

$$S_{nom} = \frac{S_{comb}}{m} \quad (8)$$

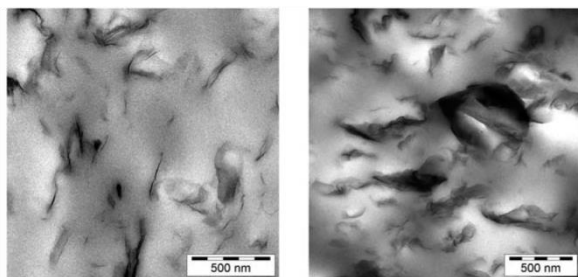


FIG. 3. TEM pictures of both PP-pipe samples.

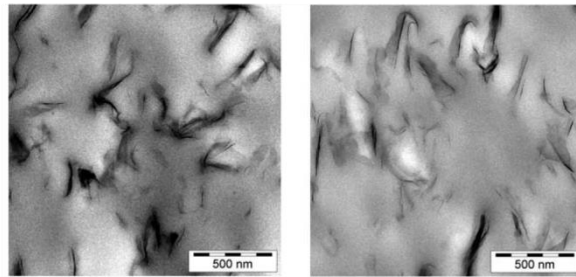


FIG. 4. TEM pictures of both PP-tensile specimen

RESULTS AND DISCUSSION

Results of Transmission Electron Microscopy

Figures 3 and 4 are showing transmission electron microscopy pictures for polypropylene. It can be seen (Fig. 3) that the silicate layers are separated from each other and very well dispersed for PP-double-pass pipe sample compared to the PP-single-pass pipe sample where the layers are still lying in stacks and are not well dispersed.

Figure 4 shows TEM pictures for PP-tensile specimen. It can be seen that the PP-double-pass samples are slightly better dispersed and exfoliated than the PP-single-pass samples.

TEM pictures for the PE samples were disclaimed due to the carbon black particles in the polymer.

Influence on Young's modulus and breaking strain

The shear energy generated in the compounding process and the combined shear and strain energy caused by injection molding during the production of a tensile test specimen can be seen in Figure 5 and Table 5. The Young's modulus and the breaking strain measured with tensile test for both materials are shown in Table 5.

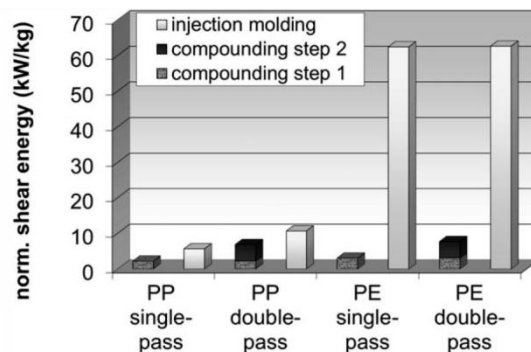


FIG. 5. Shear energy for compounding as well as combined shear and strain energy from injection molding.

TABLE 5. Values for Young's modulus and breaking strain for the different materials as well as normalized shear energy for compounding and combined shear and strain energy for injection molding.

Material	PP-single pass	PP-double pass	PE-single pass	PE-double pass
Young's modulus (MPa)	1780	1740	854	837
Breaking strain (%)	23	52	25	30
Norm. shear energy—compounding (kW/kg)	2.2	6.8	3.1	7.7
Norm. shear energy— injection molding (kW/kg)	5.7	10.7	62.4	62.6

It can be seen that compared to the single step compounding, the Young's modulus for PE–double-pass compounding as well as PP–double-pass compounding is slightly lower although the shear energy introduced during compounding is nearly twice as high. The reason for that is possibly the very high combined shear and strain energy generated during injection molding, which potentially flattens the effect of the second compounding step. Although the layered silicates should be better exfoliated, this does not lead to a material enhancement in the case of these two investigated polymers. On the other hand, a control measurement showed that if one of the unfilled polymers (PP or PE) is processed in the twin-screw extruder without any fillers, a small decrease in Young's modulus can be observed. This decrease is the same as observed between the single and double pass compounding nanocomposites.

Nevertheless, the second compounding step for the PP is leading to a significant increase for the breaking strain. This can be explained by the fact that a higher level of exfoliation and therefore smaller particles are better dispersed in the polymer matrix and are leading to, due to their high aspect ratio and therefore bigger surface, more points for physical bondings between the nanoscale filler and the polymer itself. The formed bondings are increasing the elongation at break.

Although this effect is not as strong for the PE–double-pass compounding, the same trend can be seen from the results in Table 5. A reason for that might be the fact that the used PE type is a carbon black-filled PE leaving a

possibility for other interactions. For example, it is possible that the carbon black particles due to their lower aspect ratio are influencing the crack initiation negatively. It is also possible that there are interactions between these two types of fillers that are influencing breaking strain negatively. Another reason might be the very high combined shear and strain energy during injection molding exposing the material more than the PP.

Influence on Internal Pressure Creep Time and Longitudinal Shrinkage

The shear energy generated in the compounding process and the extrusion process during the production of the pipe specimen is shown in Fig. 6. The internal pressure creep time and the longitudinal shrinkage measured on pipes for both materials can be seen in Table 6.

It is shown that the internal pressure creep time is increasing for the PP and the PE if the overall shear energy induced into the polymer system is increased. For the PP, the time is increasing from 77 to 92 h. As far as the PE is concerned, the time is increasing from 1117 to over 1500 h. The reason for this behavior lies in the fact that with more shear energy, the silicate layers are more exfoliated, and therefore the surface area becomes higher leading to more space for forming out a three-dimensional network between the filler and the polymer matrix. This result correlates well with the breaking strain out of the tensile test investigations.

As far as longitudinal shrinkage is considered, the increase of induced shear energy with the use of a second compounding step is decreasing the longitudinal shrinkage significantly for the PP and slightly for the PE. The

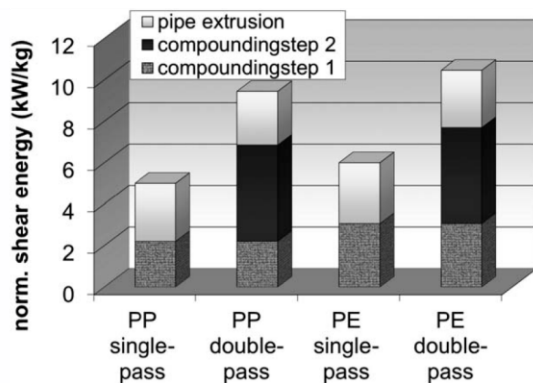


FIG. 6. Shear energy for compounding and pipe extrusion.

TABLE 6. Values for internal pressure creep time and longitudinal shrinkage for the different materials as well as norm shear energy.

Material	PP-single pass	PP-double pass	PE-single pass	PE-double pass
Internal pressure creep time (h)	77	92	1117	>1500
Longitudinal shrinkage (%)	0.84	0.67	1.63	1.57
Norm. shear energy (kW/kg)	5.0	9.4	6.0	10.5

results are showing that a higher level of exfoliation has a positive effect on the shrinkage of pipes, because the bonding strength of the formed 3D network between the nanofiller and the polymer matrix is lowering shrinkage affinity with only 5 wt% of filler. The explanation for the lower values for the PE materials is simply explained in the fact that the PE material is carbon black filled. The carbon black itself is lowering the longitudinal shrinkage itself; therefore, the effect of the layered silicate is not that high. On the other hand, undefined interactions between the silicate and the carbon black may also influence the properties negatively.

CONCLUSIONS

All investigations are showing indications that the amount of shear energy generated during processing is influencing mechanical properties. An attempt was taken to calculate the shear energy for different processing techniques and make them comparable. It is shown that the shear energy generated during injection molding cannot be separated from the strain energy in the die and in the tool and therefore is present in the calculated energy values in big extent, which is evening out the effect of the extrusion processes. This is responsible for the incomparableness of the combined shear and strain energy from injection molding with the normalized shear energy values of single and twin screw extrusion. Nevertheless, the shear energy comparison between the two extrusion processes shows good compliance with the measured properties.

It can also be seen that an increase of shear energy is leading to better results as far as longitudinal shrinkage, breaking strain and internal pressure creep time are concerned. For the Young's modulus, the values could not be increased with the use of a second compounding step in fact there was a slight decrease measurable.

Further investigations will lay emphasis on a step-by-step rising of the shear energy generated during production to find an energy plateau on which the property of interest is no longer improving. This is very important for the masterbatch processing industry, because then the amount of shear energy that has to be introduced into the masterbatch will be known exactly. Because of the fact that the whole production line is considered, it will be possible for the part producing industry (e.g., pipe industry) to determine the amount of normalized shear energy introduced into the nanocomposite during part production. Based on this in-

formation, the masterbatch producing industry can then determine the amount of normalized shear energy needed to achieve the mechanical or physical properties desired regarding nanocomposites. Therefore, a characteristic ratio would be calculated for a polymer–compatibilizer–nanofiller system to achieve good homogeneity and best mechanical and physical properties.

As far as injection molding is concerned, a new method of separating the shear energy from the strain energy should be used to make an addition of the shear energy directly with those of the extrusion processes.

REFERENCES

1. R.A. Vaia, K.D. Jandt, E.J. Kramer, and E.P. Giannelis, *Chem. Mater.*, **8**, 2628 (1996).
2. C.H. Davis, L.J. Mathias, J.W. Gilman, D.A. Schiraldi, J.R. Shields, P. Trulove, T.E. Sutto, and H.C. Delong, *J. Polym. Sci., Part B*, **40**, 2661 (2002).
3. A. Hasook, H. Muramatsu, S. Tanoue, Y. Iemoto, and T. Unryu, *Polym. Compos.*, **29**, 1 (2008).
4. C. Thellen, C. Orroth, D. Froio, D. Ziegler, J. Lucciarini, R. Farrell, N.A. D'Souza, and J.A. Ratto, *J. Membr. Sci.*, **340**, 45 (2009).
5. X. Wang, X. Zhang, H. Liu, and N. Wang, *Starch/Staerke*, **61**, 489 (2009).
6. N. Wang, X. Zhang, N. Han, and S. Bai, *Carbohydr. Polym.*, **76**, 68 (2009).
7. M. Modesti, A. Lorenzetti, D. Bon, and S. Besco, *Polymer*, **46**, 10237 (2005).
8. S. Aslanzadeh, M.H. Kish, and A. Katbab, *Polym. Degrad. Stab.*, **95**, 1800 (2010).
9. A. Rozanski, B. Monasse, E. Szkudlarek, A. Pawlak, E. Piorkowska, A. Galeski, and J.M. Haudin, *Eur. Polym. J.*, **45**, 88 (2009).
10. K. Wang, S. Liang, R. Du, Q. Zhang, and Q. Fu, *Polymer*, **45**, 7953 (2004).
11. R. Patel, H. Benkreira, A. Khan, P.D. Coates, Y. Shen, S. Xie, R. Zurayk, E. Harkin-Jones, T. McNally, and P. Hornsby, "Polypropylene–MMT clay nanocomposites: process and post-processing structuring" Proceedings of the 26th Annual Meeting of the Polymer Processing Society, Banff, Canada (2009).
12. H. Potente, *Verfahrenstechnische Auslegung von Plastifizier- und Schmelzeaggregaten*, Paderborn, Germany (1986).
13. F. Johannaber and W. Michaeli, *Handbuch Spritzgießen*, München, Germany (2004).

2.2.5 Manuscript 10

“Determining the ageing of polpropylene nanocomposites using rheological measurements”

Laske, Stephan; Witschnigg, Andreas; Mattausch, Hannelore; Kracalik, Milan; Pinter, Gerald; Feuchter, Michael et al. (2012): In: Applied Rheology 22 (2), 24590-1 - 24590-9. DOI: 10.3933/ApplRheol-22-24590.

In this manuscript, results of shear as well as extensional rheometry were used to describe the effect of ageing on polymer nanocomposites properties. It was shown that 36 months after production, melt viscosity, melt elasticity and melt strength were significantly reduced, due to photo-oxidative degradation of polypropylene matrix and due to re-agglomeration of the nanofiller. The deterioration in material properties was more pronounced in highly-filled systems (15 wt.% and 20 wt.% of organoclay, respectively) comparing to typical (5 wt.% of organoclay) nanocomposite. Generally, the long-term stability was massively influenced by the size of the reactive filler surface (interface) monitored by the clay content and the degree of exfoliation. With increasing clay content as well as a higher degree of exfoliation the possible interface to the polymer matrix is increasing, leading to a faster and higher material degradation. Additionally, the results of the rheological experiments revealed two degradation mechanisms. Firstly, the chain splitting caused by photo-oxidative degradation resulted to a loss in molecular weight shown by the decreased zero shear viscosity (Newtonian plateau). This chemical factor is mainly influenced by the interface between polymer and the particles. When using nanofillers, this effect is intensified because of the nanoscale particles and the resulting significantly increased interface. The second factor was the weakened 3D network displayed in the range of higher angular frequencies by a decrease of the complex viscosity (shear thinning range) as well as a higher loss in tensile force respectively melt strength. This physical factor can be explained by the reverse diffusion of the polymer chains out of the clay gallery and/or reagglomeration of the nanoparticles, when the distance between the layers is too small to overcome the interparticular forces. This can happen in intercalated as well as high-filled systems.

DETERMINING THE AGEING OF POLYPROPYLENE NANOCOMPOSITES USING RHEOLOGICAL MEASUREMENTS

STEPHAN LASKE^{1*}, ANDREAS WITSCHNIG¹, HANNELORE MATTAUSCH¹, MILAN KRACALIK¹,
GERALD PINTER², MICHAEL FEUCHTER², GUENTHER MAIER³, CLEMENS HOLZER¹

¹ Polymer Processing, Montanuniversitaet Leoben, Otto Gloeckel-Strasse 2, 8700 Leoben, Austria

² Materials Science and Testing of Plastics, Montanuniversitaet Leoben, Otto Gloeckel-Strasse 2,
8700 Leoben, Austria

³ Materials Center Leoben Forschung GmbH, Roseggerstrasse 12, Leoben 8700, Austria

* Corresponding author: stephan.laske@unileoben.ac.at
Fax: x43-3842-4023502

Received: 20.9.2011, Final version: 27.1.2012

ABSTRACT:

The principle of silicate layer reinforcement in a polymer matrix is known as the formation of a 3D network of single layers. Nevertheless there is still a lack of knowledge about the physical ageing of nanocomposites respectively the stability of this network over time. As most of the nanocomposite applications have a more or less long-term shelf life respectively storage time, the investigation of the storage-time dependent behavior of the layered 3D structure in a polymer matrix is of major interest. In this study, the rheological (shear and elongational) properties of different polypropylene nanocomposites were measured using a cone-plate rheometer and a Rheotens apparatus. To evaluate the structural stability over time, the samples were measured immediately after processing and after defined periods (18 and 36 months) stored under constant conditions. Furthermore the network structure was determined using XRD and TEM measurements. The results show, that, depending on the clay rate and especially the degree of exfoliation, the rheological properties are changing significantly. Thereby chain-splitting caused by photo-oxidative degradation, leading to a loss in molecular weight, as well as a weakened 3D network by reverse diffusion of the polymer chains out of the clay gallery and/or reagglomeration of the nanoparticles are the two main factors.

ZUSAMMENFASSUNG:

Das Prinzip der Aufbereitung von Polymeren mit Schichtsilikaten wird generell durch die Bildung eines 3D Netzwerkes der einzelnen Schichten erklärt. Diesbezüglich gibt es noch immer wenig Wissen über das physikalische Altern von Nanocomposites beziehungsweise über die Stabilität dieses Netzwerkes in Abhängigkeit von der Zeit. Da die meisten Nanocomposite-Anwendungen eine mehr oder minder lange Lebensdauer bzw. Lagerungszeit haben, ist das zeitabhängige Verhalten dieser 3D Schichtstruktur von großem Interesse. In dieser Studie wurden die (scher- und dehn-) rheologischen Eigenschaften von unterschiedlichen Polypropylen-Nanocomposites unter Verwendung eines Kegel-Platte-Rheometers und einer Rheotensapparatur gemessen. Um die Strukturstabilität in Abhängigkeit von der Zeit zu bestimmen, wurden Probestkörper unmittelbar nach der Herstellung und nach definierten Zeiträumen (18 beziehungsweise 36 Monate unter definierten Bedingungen) untersucht. Des Weiteren wurde die Struktur mittels XRD und TEM untersucht. Die Ergebnisse zeigen, dass abhängig von der Menge an Schichtsilikat und im Speziellen des Exfolierungsgrades die rheologischen Eigenschaften sich stark unterscheiden. Dabei sind sowohl Kettenspaltung durch photo-oxidativen Abbau, der zu einer Reduktion der Molmasse führt, als auch ein durch umgekehrte Diffusion der Ketten aus den Zwischenschichten beziehungsweise Reagglomeration geschwächtes 3D-Netzwerk die beiden wesentlichen Faktoren.

RÉSUMÉ:

Le principe du renforcement d'une matrice polymère par de la silice est connu comme la formation d'un réseau tridimensionnel de couches simples de silice. Néanmoins, il n'existe pas d'explication pour le vieillissement physique des nanocomposites, c-à-d pour la stabilité dans le temps du réseau. Comme la plupart des applications des nanocomposites contemple des durées de vie plus ou moins longues, l'étude du comportement de la structure tridimensionnelle au cours du temps de stockage est d'un intérêt majeur. Dans cette étude, les propriétés rhéologiques (en cisaillement et en élongation) de différents nanocomposites de polypropylène ont été mesurées en utilisant un rhéomètre cône-plan et un appareil Rheotens. Afin d'évaluer la stabilité structurelle au cours du temps, les échantillons ont été mesurés immédiatement après la mise en œuvre et après des périodes de stockage définies (18 et 38 mois) dans des conditions constantes. De plus, la structure du réseau a été déterminée à l'aide de la diffraction de RX et des mesures de TEM. Les résultats montrent que, en fonction de la vitesse et spécialement le degré d'exfoliation de l'argile, les propriétés rhéologiques changent de manière significative. Ainsi, la scission de chaîne causée par la dégradation photo-oxydative, qui conduit à une perte de la masse

© Appl. Rheol. 22 (2012) 24590

DOI: 10.3933/ApplRheol-22-24590

24590-1

Applied Rheology
Volume 22 · Issue 2

moléculaire, ainsi que l'affaiblissement du réseau tridimensionnel par la diffusion réversible des chaînes de polymère hors de la galerie d'argile et/ou la ré agglomération des nanoparticules sont les deux facteurs prépondérants.

KEY WORDS: nanocomposites, ageing, rheology, polypropylen, layered silicates, degradation

1 INTRODUCTION

Nanocomposites are modified polymers with particles, where at least one dimension is in the order of nanometers. Polymers reinforced by nanoscale particles exhibit significantly higher performance, for example higher elastic modulus, tensile strength, thermal resistance, lower gas and liquid permeability, reduced flammability and enhanced rheological properties (e.g. increased melt stiffness) already for small amounts of filler [1, 2]. There are two reasons for the improvement of material properties by the application of nanofillers. The first reason is the enforcement of the polymer matrix by means of the particles (like it is the case for other fillers) caused by the movement-restrictive effect on the polymer chains. The second reason are the nanoscale particles due to the substantially higher surface, the special particle shape as well as the high aspect ratio. Therefore mainly chemical modified, layered silicates (most common montmorillonite, MMT) with an aspect ratio up to 1000 are used. To reach best interactions between polymer matrix and nanofiller (especially layered silicates) a homogeneous dispersion is essential.

To disperse the hydrophilic clay in hydrophobic polypropylene (PP), a compatibilizer (mostly PP grafted with maleic acid anhydride, PP-g-MA) must be admixed to close the polarity gap. Nanocomposites are preferably produced by using a twin-screw extruder operating at high temperatures and pressures because of the technological simplicity [1, 2]. Shearing forces, induced by the rotation of the screw and thermodynamical interactions between polymer chain and layered silicate clay are delaminating the layered silicate depending on the residence time. During this process the structures, which are responsible for the reinforcement level, are formed by physical bonding between the hydrophilic clay, the hydrophobic polymer matrix and the compatibilizer. According to the dispersion of MMT platelets in the polymer matrix, three composite structures can be formed: conventional composites,

intercalated and exfoliated nanocomposites. In the case of highly dispersed systems, a 3D physical network is achieved, formed by the silicate platelets and the polymer chains.

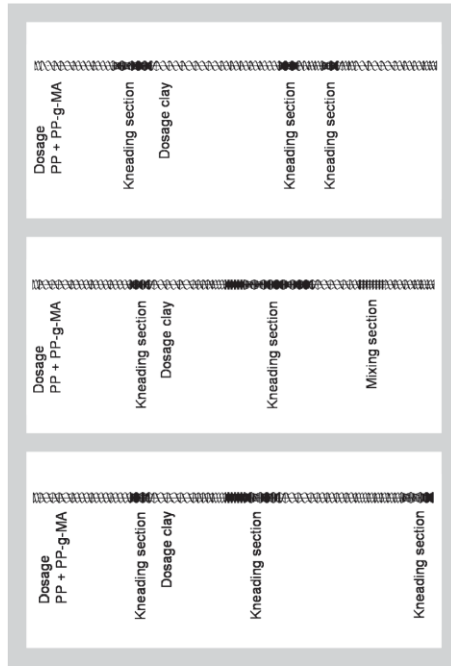
Rheological properties of polymer nanocomposites have been intensively studied over the years identifying this 3D network of single layers in the polymer matrix as the principle of reinforcement [3, 4]. Accordingly this phenomenon can be investigated by analyzing the composite using rotational rheometry [5–8]. In the range of small angular frequencies the complex viscosity is increasing because of a virtual chain extension caused by the single layers acting as physical net-points as well as the apparent viscosity increases caused by the additional shearing of the polymer chains in between the filler. In the range of higher frequencies, the physical 3D network is displayed by an increase of the complex viscosity with an unchanged slope. Another fast way to evaluate this network effect is using elongational rheometry [9, 10], which provides information about variations in melt strength caused by different extension of the physical network.

Although the processing and characterizing of polymer composites have been deeply investigated, there is still a lack of knowledge about the stability of this 3D network respectively the influence of the filler on the material ageing. As already published [11], common fillers like calcium carbonate or talc have a major influence on the rheological properties of polymer composites. Thereby the interactions between filler and polymer matrix are influenced by (i) particle surface area, (ii) particle surface functionality, (iii) hydrophilicity, (iv) thermal- and photosensitization properties, (v) transition metal ion content and (vi) the particle aspect ratio. In the case of nanofillers, the (photo-)oxidative degradation of polymers is accelerated, because of (i) a larger surface for interaction, (ii) more or less perfect distribution in exfoliated state, (iii) transition metals as impurities, (iv) degradation of the organic clay modification (Hofmann elimina-

Figure 1 (above):
G1 screw configuration.

Figure 2 (middle):
G2 screw configuration.

Figure 3 (below):
G3 screw configuration.



tion) and (v) the compatibilizer [12, 13]. Additionally a loss of the 3D network (which means loss of reinforcement) can occur, caused by a reverse diffusion of the polymer chains out of the layer gallery in the case of intercalated structures as well as reagglomeration of the silicates layers if the exfoliation is not homogeneous and the space in between is too small to overcome the interparticle forces [14, 15]. Therefore, the stability of the 3D network and a possible faster material degradation is of major interest, as most of the nanocomposite applications are supposed to have more or less a long-term shelf life.

Table 1 (left above):
Temperature profile in different extruder sections.

Table 2 (left below):
Nanocomposite formulation and process settings.

Table 3 (right):
Press profile.

Section	Feeding	2	3	4	5	6	7	8	9	Die
Temperature (°C)	cool	160	180	190	200	200	200	200	200	200

Nr.	Notation	Clay set (wt%)	Clay actual (wt%)	Compatibilizer (wt%)	Screw speed	Geometry	Ageing time (month)	Variation of
1	Comp5 new/aged	5	6.28	5	200	1	36	Compatibilizer content
2	Comp1 new/aged	5	5.75	15	200	1	36	Compatibilizer content
3	Screw100 new/aged	5	5.15	5	100	3	18	Screw speed
4	Screw300 new/aged	5	5.22	5	300	3	18	Screw speed
5	G1 new/aged	20	19.82	20	100	1	36	Geometry
6	G2 new/aged	20	20.78	20	100	2	36	Geometry
7	MMT20 new/aged	20	19.82	20	100	1	36	Clay content
8	MMT5 new/aged	5	6.14	5	100	1	36	Clay content

2 EXPERIMENTAL

2.1 MATERIALS

The isotactic PP homopolymer HC600TF (MFR 2.8 g/10 min; 230°C/2.16 kg) was supplied by Borealis, Inc., Linz, Austria. The used nanofiller (montmorillonite intercalated with dimethyl distearyl ammonium chloride) with commercial indication Nanofil 5 was supplied by Sud-Chemie Inc., Munich, Germany. The compatibilizer (Scona TPPP 2112, MFR 14.8 g/10 min, 230°C/2.16 kg) was supplied by Kometra, Ltd., Schkopau, Germany.

2.2 PREPARATION OF POLYPROPYLENE NANOCOMPOSITES

For the compounding process, an intermeshing, co-rotating twin-screw extruder Theysohn TSK30/40D (Theysohn Holding Ltd, Vienna, Austria) with a string die was used. The feed rate was 10 kg/h and the temperature profile can be seen in Table 1. For processing different nanocomposites the clay and compatibilizer content as well as the screw speed and geometry were varied. The different formulations and process settings can be seen in Table 2. The main difference between the screw geometries, in the following referred to as geometry 1 to geometry 3, is the number and position of kneading elements resulting in different values of induced shear energy and residence time and can be seen in Figures 1 to 3. For the Rheotens measurements, the primary granulate obtained from the extrusion process was used. For rotational rheometry, round-shaped plates with a thickness of 2 mm and a diameter of 25 mm were prepared using the hydraulic vacuum press (Collin 200 PV, Dr. Collin Ltd., Ebersberg, Germany). The press profile with a total press time of 44 minutes is given in Table 3.

2.3 TRANSMISSION ELECTRON MICROSCOPY

The TEM experiments were performed using a Zeiss LEO 912 Omega transmission electron

Temperature (°C)	200	200	200	200	50
Pressure (bar)	1	20	1	100	150
Time (min)	20	5	5	7	7

microscope (Carl Zeiss Inc., Jena, Germany) using an acceleration voltage of 120 kV. The samples were prepared using a Leica Ultracut UCT ultramicrotome (Leica Microsystems Ltd, Wetzlar, Germany) equipped with a cryo chamber. Thin sections of about 50 nm were cut with a Diatome diamond knife at - 120°C.

2.4 SMALL ANGLE X-RAY SCATTERING

X-ray measurements were performed using Bruker NanoSTAR (Bruker AXS, Karlsruhe, Germany) small angle X-ray scattering (SAXS) equipment. This system was equipped with a two-dimensional X-ray detector. A wavelength of 0.154 nm (CuKa) was used. The samples were measured in transmission. To avoid the influence of texture, all scattering measurements were performed on plate samples. The gallery period of the nanofiller was determined on a powder sample. To avoid statistical effects, the scattering curves recorded at three different positions on the samples were averaged. To determine the gallery period, scattering curves were corrected for background scatter and the Lorenz correction was applied. The Lorenz correction was performed by multiplying the scattered intensity $I(q)$ by q^2 , q being the magnitude of the scattering vector. The position of the gallery peak was then determined by fitting with a Lorenz function.

2.5 EXTENSIONAL AND ROTATIONAL MELT RHEOLOGY

The silicate platelets form different levels of 3D physical network in the polymer matrix depending on their level of delamination. Higher delamination results in a higher extent of physical network (correlating higher material reinforcement) and therefore in different particle - particle and polymer - particle physical interactions respectively in variations in viscoelastic response. Depending on the degree of delamination and in this case the ageing occurrence, this transformation is obvious compared with the unfilled polymer [3, 4].

As stated in the introduction, two methods of reinforcement assessment can be used in the molten state in polymer nanocomposites: analysis of the melt elasticity using rotational rheometry and melt strength evaluation (e.g. using Göttfert equipment). The principle of Rheotens measurements can be seen in Figure 4. It is based

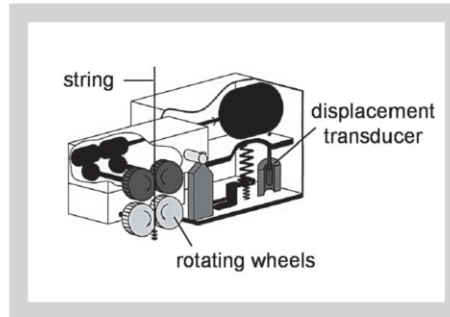


Figure 4: Principle of Rheotens measurement using the Göttfert equipment.

Table 4: Capillary rheometer testing specification.

on the elongation of an extruded string by two or four rotating wheels connected with a displacement transducer. The rotation speed is linearly increased until the molten string breaks. The drawing force applied to the wheels at a specific draw rate is the reference value for the melt strength level. We used the Rheotens 71.97 (Goettfert Ltd., Buchen, Germany) in combination with a capillary rheometer. The measuring conditions for capillary rheometer are listed in Table 4. The Rheotens equipment has been set to a wheel acceleration of 60 mm/s² and gap between wheels of 0.6 mm. To compare the melt strength level of different nanocomposite systems, the tensile force at a draw rate of 150 mm/s was chosen for comparison. The data of at least nine measurements for each sample were evaluated.

Rheological properties in the shear flow were studied using a Physica MCR 501 rheometer (Anton Paar Ltd., Graz, Austria) with the cone-plate geometry of 25 mm diameter and automatically controlled gap of 50 μm. The samples thickness was 0.7 mm. Experiments were performed at 210°C under nitrogen to prevent degradation of samples. The following types of rheological measurements were carried out: 1) dynamic strain sweep test (at angular frequency of 6.28 rad/s) to confirm the linearity of viscoelastic region and 2) dynamic frequency sweep test over a frequency range of 0.1–100 rad/s, at the strain of 12 %. The data have been evaluated from at least 3 measurements for each sample and then average data have been plotted.

2.6 TEST PROCEDURE

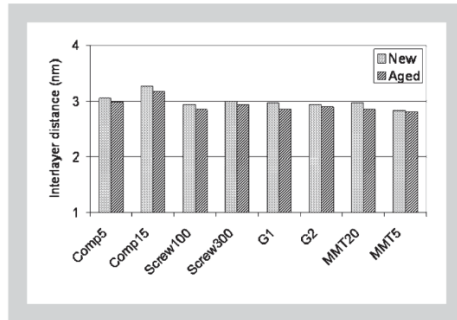
The different materials were examined right after production as well as after 18 respectively

Cylinder diameter	12 mm
Die (length/diameter)	30/2 mm
Temperature	210°C
Piston speed	1.9 mm/s
Shear rate	273.6 1/s

Figure 5 (left): XRD results of the nanocomposites.

Figure 6: TEM images of the materials with different compatibilizer content.

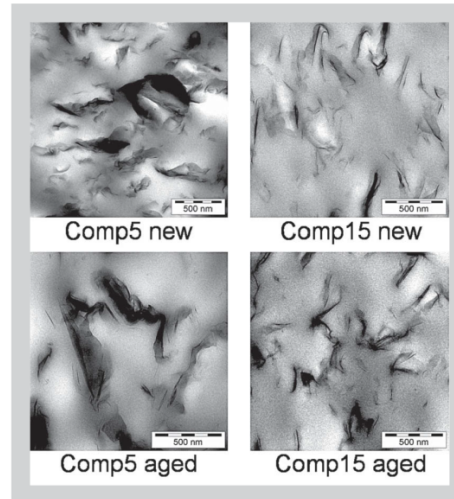
Table 5: Numerical results of the rotational rheometry measurements.



36 months. During shelf life, all the materials were light protected stored under the same conditions (20°C, 60 rel% humidity) avoiding UV radiation.

3 RESULTS AND DISCUSSION

As reference material neat polypropylene was stored under the same conditions (light protected) as the nanocomposites. The measurements showed that, because of the storage conditions (no UV-light influence) and the polymer stabilization, there is no change in rheological properties and the results before and after storage are congruent. Therefore, degradation of pure polypropylene can be eliminated. The results of the XRD (all samples) and TEM (compatibilizer content samples as example) measurements, shown in Figures 5 and 6, illustrate the structure of the silicate layers in the polymer matrix and therefore the degree of exfoliation right after production and after storing for 18 and 36 months. It can easily be seen, that the structures are changing significantly over time resulting in a decreased degree of exfoliation. Regarding the silicate lay-



ers, (i) a larger surface area for interaction, (ii) a higher aspect ratio, (iii) a higher degree of exfoliation and (iv) the chemical modification leads to a faster and higher polymer degradation and therefore loss in material properties.

3.1 ROTATIONAL RHEOMETRY

Generally, the ageing of polypropylene nanocomposites is displayed by two factors. At first a chemical ageing caused by photo-oxidative degradation leading to a loss in molecular weight and therefore complex viscosity in the range of low angular frequencies respectively the Newtonian plateau and changes of the moduli in the polymer dominated high frequency region (e.g. chain scission [17–19]). Secondly, a physical ageing (weakened 3D network) occurs due to reagglomeration of the silicate layers as well as migration of the polymer chains out of the clay gallery (abolished 3D percolation network). This can be seen by a decrease in complex viscosity in the range of higher angular frequencies respectively the shear thinning region with an unchanged slope of the curve respectively parallel shift as already mentioned by Fordiani et al. [15] and changes of the moduli in the low frequency region (e.g. increase of G' caused by the pseudo solid-like behavior [16–18]). Table 5 shows the numerical results of the rotational rheometry results of all samples.

Figure 7 A and B show the results of the materials with different MMT content evaluated right after respectively 36 months after production. First of all, the results show clearly the effect of different clay content on the rheological behavior of polypropylene nanocomposites by an increased complex viscosity over the whole frequency as well as a major shift of the Newtonian plateau to lower angular frequencies and therefore an expanded shear thinning region.

rad/s	MT20 (Pa·s)			MT5 (Pa·s)		
	new	aged	- %	new	aged	- %
0.1	139000	62400	55.1	10730	10714	0.1
100	2350	1260	46.4	984	753	23.5
	Comp15 (Pa·s)			Comp5 (Pa·s)		
	new	aged	- %	new	aged	- %
0.1	10600	10600	0.0	10600	8870	16.3
100	934	771	17.5	968	769	20.6
	Comp15 (Pa·s)			Screw100 (Pa·s)		
	new	aged	- %	new	aged	- %
0.1	8710	7220	17.1	15300	12700	17.0
100	958	697	27.2	1058	816	22.9
	Geometry 2 (Pa·s)			Geometry 1 (Pa·s)		
	new	aged	- %	new	aged	- %
0.1	187000	79300	57.6	139000	62700	54.9
100	2661	1300	51.1	2374	1260	46.9

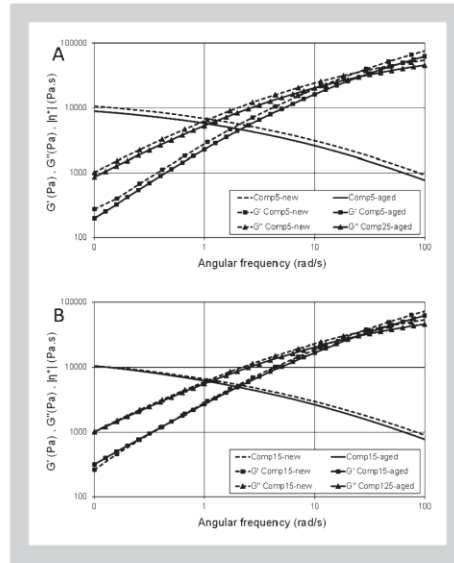
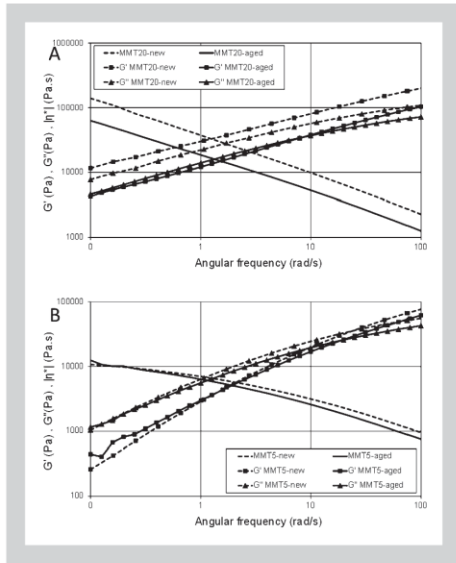


Figure 7 A and B (left): Results of the materials with different MMT content.

Figure 8 A and B: Results of the materials (5 wt% MMT) with different compatibilizer content (5 and 15 wt%).

Furthermore the content of MMT has a major influence on the ageing effect. The decrease of the viscosity of the 20 wt% clay nanocomposite (MMT20) is significantly higher than the 5 wt% nanocomposite (MMT5). Additionally the large difference in the shear thinning region may expect also large decrease in zero shear viscosity resulting from polymer chain splitting. This can be seen at MMT20-aged in the beginning of the transition zone between Newtonian plateau and shear thinning at ca. 1.0 rad/s. Additionally, the earlier starting transition zone of MMT20-aged in contrast to MMT20-new shows the weakened 3D network of the aged sample. Regarding the moduli, there is a constant increase in moduli values at all frequencies with a frequency independent behavior which is characteristic for pseudo-solidlike behavior [16]. It can be observed, that the magnitude of G' and G'' is affected significantly but not the material characteristics [17].

In opposite, the MMT5 nanocomposite complex viscosity only differs in the range of higher frequencies (shear thinning region) which can be interpreted as abolished 3D network (reduced virtual chain enhancement, caused by the layers). For the moduli the low frequency region is an indication for aggregates or percolation structures whereas at the high frequency region the polymer matrix is the dominating factor [18]. The results for G' and G'' as well show a reduced percolation network (low frequencies) and slightly changes within the polymer matrix (high frequencies) which promotes chain scission. As polymers are generally sensitive to material degradation (e.g. oxidation), especially when they are filled with minerals, the enhanced surface of the nanoscale particles of the MMT are

additional enforcing degradation. As the deterioration is acceptable with MMT5, nanocomposites containing higher amounts of MMT (e.g. masterbatches containing > 20 wt% clay) are not suitable of being stored for longer time. As most of the nanocomposites are stored and delivered in form of a high-filled masterbatch (better handling and cost effectiveness) this must be considered.

In Figure 8 the results of the materials with different compatibilizer content evaluated right after respectively 36 months after production can be seen. It is obvious, that the amount of compatibilizer has no significant influence on the complex viscosity or moduli of the aged nanocomposites. As the compatibilizer is a maleic acid anhydride (MAH) grafted polypropylene with a graft-grade of only 0.001 wt% it can be expected, that this small amount of MAH has no effect. Generally spoken, there is a straight coherence between material properties respectively degree of exfoliation and clay/compatibilizer ratio. A higher compatibilizer content leads to a higher degree of exfoliation and therefore a faster and higher degradation. Nevertheless the more influencing factor is the clay content which is very low in that case and leads to only minor changes in the rheological properties and furthermore has no influence on the storing capability. This confirms, that nanocomposites can be long-term stored or utilized below a certain clay content (in this case 5 wt%) independent of the compatibilizer content.

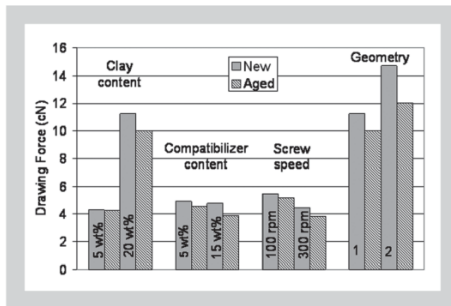
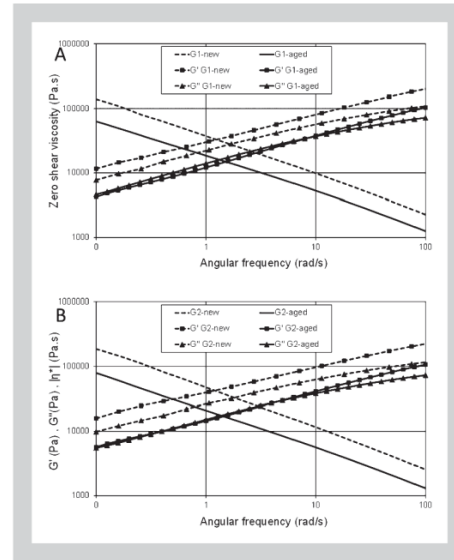
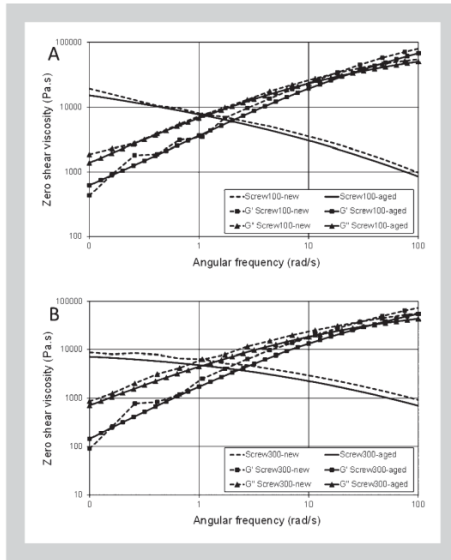
Figure 9 and table 5 show the results of the aged nanocomposites, processed at different screwspeeds. As the induced shear energy as well as residence time differs with varying screw speeds, the rate of exfoliation is diverse. As

Figure 9 A and B (left): Results of the materials processed at different screw speeds.

Figure 10 A and B (right above): Results of the materials with different geometries.

Figure 11 (left below): Results of the elongation measurements.

Table 6: Numeric results of the elongation measurements.



already said, a higher exfoliation rate ensures higher surface area, aspect ratio and therefore more interaction prospects. Following this, the better the clay is exfoliated (screw speed 300 rpm) the more sensitive the nanocomposite is to chemical as well as physical degradation, which is displayed by higher changes in complex viscosity, G' and G'' at all frequencies. Another interesting fact is that the degradation runs very fast, as there is almost no change between 18 month and 36 month of ageing (Comp5 in Figure 8a versus Screw100 in Figure 9a). Figure 10 and table 5 show the results of the nanocomposites processed with two different screw geometries.

As already mentioned the influence of the clay on the physical and chemical ageing of the

polymer matrix is increasing with increasing degree of exfoliation. This is obvious as the surface is growing likewise. Inducing more shear energy with a sharper geometry leads to a more exfoliated structure and therefore a higher chemical degradation. Overall, the results of the materials processed with different screw speeds are corresponding with the results of different screw geometries, as the mechanism and therefore the degradation incidents are similar.

3.2 ELONGATIONAL RHEOMETRY

The evaluation of polymer matrices with rheotens equipment has already been published by Bachelli [20], Burghilea et al. [21] or White et al. [22]. According to our previous investigations [3, 4, 9] the level of reinforcement in PP nanocomposites can be estimated with analysis of the melt strength as well. The silicate platelets form different levels of 3D physical network in the polymer matrix depending on their level of delamination. Higher delamination results in higher extent of physical network (higher material reinforcement) and therefore in an increase of melt strength. Different particle – particle and polymer – particle physical interactions result in variations in viscoelastic response. It is possible to use extensional rheometry to identify changes in the melt elongational behavior. Individual silicate platelets form a nanoscale network (cardhouse structure) and raise the melt strength of the composite. In return, a weakened 3D structure, caused by for example reagglomeration or reverse diffusion of the polymer chains out of the clay gallery, leads to a decrease of the melt strength displayed by a lower drawing force.

Clay Content		Screw Speed	
5 wt% New	4.28 cN	20 wt% New	11.25 cN
5 wt% Aged	4.27 cN	20 wt% Aged	9.99 cN
	0.20%		11.20%
Compatibilizer Content		Geometry	
5 wt% New	4.92 cN	1 New	11.25 cN
5 wt% Aged	4.54 cN	1 Aged	9.99 cN
	7.70%		11.20%
		2 New	14.70 cN
		2 Aged	12.05 cN
			18.00%

Figure 11 and table 6 show the results of the elongation tests right after and 18 and 36 month after production. The results of the elongation measurements reflect the same trend as the results from the rotational rheometer. Depending on the degree of exfoliation and the clay content the drawing force is decreasing more or less. The most exfoliated structures (e.g. 300 rpm or 15 wt% compatibilizer or geometry 2) show the highest level of 3D physical network and after storage the largest decrease in drawing force. The same can be seen with the clay content, as the sample with 20 wt% clay has a larger loss in drawing force, than that with 5 wt%. Generally spoken, the more the 3D network is established, the more sensitive it reacts on ageing respectively the easier it is damaged.

4 CONCLUSIONS

In this work the rheological (shear as well as elongational) properties of different nanocomposites (varying formulation and process conditions) where measured right after respectively 18 and 36 months after production. The results show clearly, that the long-term stability is massively influenced by the size of the reactive filler surface (interface) monitored by the clay content and the degree of exfoliation. With increasing clay content as well as a higher degree of exfoliation the possible interface to the polymer matrix is increasing, leading to a faster and higher material degradation. Additionally, the results of the rheological experiments show clearly the two factor degradation mechanism. Firstly, the chain splitting caused by photo-oxidative degradation leading to a loss in molecular weight shown by the decreased zero shear viscosity (Newtonian plateau). This well known chemical factor is mainly influenced by the interface between polymer and the particles. When using nanofillers, this effect is multiplied because of the nanoscale particles and the resulting massively increased interface.

The second factor is the weakened 3D network displayed in the range of higher angular frequencies by a decrease of the complex viscosity (shear thinning range) as well as a higher loss in drawing force respectively melt strength. This physical factor can be explained by the reverse diffusion of the polymer chains out of the clay gallery and/or reagglomeration of the nanopar-

ticles, when the distance between the layers is too small to overcome the interparticular forces. This can happen in intercalated as well as high-filled systems. The grafted compatibilizer with very low graft grades has only minor influence itself but is a major factor to achieve a high exfoliated nanocomposite. The degradation incidents are occurring very fast, as no difference could be seen in the 18 months respectively 36 months samples. Therefore also a short-term storage or shelf-life is affected.

REFERENCES

- [1] Gilman JW, Kashiwagi T, Lichtenhan JD: Nanocomposites: A revolutionary new flame retardant approach, *Sampe J.* 33 (1997) 40.
- [2] Ray SS, Okamoto M: Polymer/layered silicate nanocomposites: a review from preparation to processing, *Progr. Polym. Sci.* 28 (2003) 1539.
- [3] Witschnigg A, Laske S, Kracalik M, Feuchter M, Pinter G, Maier G, Märzinger W, Haberkorn M, Langecker GR, Holzer C: In-line characterization of polypropylene nanocomposites using FT-NIR, *J. Appl. Polym. Sci.*, 117 (2010) 3047.
- [4] Laske S, Kracalik M, Feuchter M, Pinter G, Maier G, Märzinger W, Haberkorn M, Langecker GR: FT-NIR as a determination method for reinforcement of polymer nanocomposites, *J. Appl. Polym. Sci.* 114 (2009) 2488.
- [5] Ray SS, Yamada K, Okamoto M, Ueda K: New polylactide-layered silicate nanocomposites. 2. Concurrent improvements of material properties, biodegradability and melt rheology, *Polymer* 44 (2003) 857.
- [6] Krishnamoorti R, Giannelis EP: Rheology of End-Tethered Polymer Layered Silicate Nanocomposites, *Macromolecules* 30 (1997) 4097.
- [7] Wagener R, Reisinger TJG: A rheological method to compare the degree of exfoliation of nanocomposites, *Polymer* 44 (2003) 7513.
- [8] Laske S, Kracalik M, Gschweidl M, Langecker GR: Abhängigkeit des Exfolierungsgrades von Silikatschichten in einer Polymermatrix vom Compatibilizer – Nanoclay Mischungsverhältnisses, *Proceedings, International Conference Polymermischungen, Bad Lauchstaedt, Germany* (2007).
- [9] Laske S: Verbesserung der rheologischen Eigenschaften von unverzweigtem Polypropylen mit Nanofüllstoffen im Hinblick auf das Extrusionsschäumen, *M.Sc. Thesis, University of Leoben* (2005).
- [10] Cabedo L, Plackett D, Gimenez E, Lagaron J M: Studying the degradation of polyhydroxybutyrate-co-valerate during processing with clay-based nanofillers, *J. Appl. Polym. Sci.* 112 (2009) 3669

- [11] Pfaendner R: Additives to Enhance Manufacturing and Long-term Performance of Nanocomposites, *Proceedings NanoEurope 2009*.
- [12] Lewicki JP, Liggat JJ, Pethrick RA, Patel M, Rhoney I: Investigating the ageing behavior of polysiloxane nanocomposites by degradative thermal analysis, *Polym. Degr. Stab.* 93 (2008) 158.
- [13] Li J, Yang R, Yu J, Liu Y: Natural photo-aging degradation of polypropylene nanocomposites, *Polym. Degr. Stab.* 93 (2008) 84.
- [14] Vlasveld DPN, Bersee HEN, Picken SJ: Creep and physical aging behaviour of PA6 nanocomposites, *Polymer* 46 (2005) 12539.
- [15] Fordiani F, Aubry T, Grohens Y: Structural changes evidenced by rheology in PPGMA nanocomposites during oxidative ageing, *J. Appl. Polym. Sci.* 114 (2009) 4011.
- [16] Ren J, Silva SS, Krishnamoorti R: Linear Viscoelasticity of Disordered Polystyrene–Polyisoprene Block Copolymer Based Layered-Silicate Nanocomposites, *Macromolecules* 33 (2000) 3739.
- [17] Solomon MJ, Almusallam AS, Seefeldt KF, Somwangthanaroj A, Varadan P: Rheology of Polypropylene/Clay Hybrid Materials, *Macromolecules* 34 (2001) 1864.
- [18] Vermant J, Ceccia S, Dolgovskij MK, Maffettone PL, Macosko CW: Quantifying dispersion of layered nanocomposites via melt rheology, *J. Rheol.* 51 (2007) 429.
- [19] Galindo-Rosales FJ, Moldenaers P, Vermant J: Assessment of the Dispersion Quality in Polymer Nanocomposites by Rheological Methods, *Macromol. Mater. Eng.* 296 (2011) 331.
- [20] Bachelli F: A Rheotens-based setup for the constant strain rate uniaxial extension of uncured elastomers, *Rheol. Acta*, 46 (2007) 1223.
- [21] Burghelca TI, Griess HJ, Münstedt H: Comparative investigations of surface instabilities (“sharkskin”) of a linear and a long-chain branched polyethylene, *J. Non-Newtonian Fluid Mech.* 165 (2010) 1093.
- [22] White JL, Yamane H: A collaborative study of the stability of extrusion, melt spinning and tubular film extrusion of some high-, low- and linear-low density polyethylene samples, *Pure App. Chem.* 59 (1987) 193.



2.3 Characterization of polymer nanocomposites

In this chapter (manuscripts 11 – 17), new structural and rheological analysis approaches for characterization of typical as well as complex polymer nanocomposites are presented. It was proved that shear as well as extensional rheometry can be used for fast assessment of reinforcement in polymer-clay nanocomposites. Concerning the fact that rheological experiments can be performed on-line in the compounding process, an interesting way to gain first information about material performance in dependency on mixture composition and processing protocol was introduced. Furthermore, establishment of new rheological parameter (cumulative storage factor) enabled characterization of reinforcement in polymer matrix taking into account possible chemical and physical interactions during the processing. Regarding structural analysis, average agglomerate size was introduced as new parameter gained from SAXS measurement.

2.3.1 Manuscript 11

„ Effect of organoclay chemistry and morphology on properties of poly(lactic acid) nanocomposites “

Kracalik, Milan (2017): In: *Plastics, Rubber and Composites*, 2017, 46 (9), 389-395, <https://doi.org/10.1080/14658011.2017.1373489>.

In this paper, new parameter, average agglomerate size, could be gained from SAXS measurement. This structural parameter complementary to the interlayer distance, provides with quantitative information about dispersion state. In this way, the nanocomposite structure is completely characterized and some other usually used techniques like transmission electron microscopy (TEM) or scanning electron microscopy (SEM) do not have to be applied as they generate only qualitative information not allowing reliable comparison of dispersion state.

Effect of organoclay chemistry and morphology on properties of poly(lactic acid) nanocomposites

Milan Kracalik 

Institute of Polymer Science, Johannes Kepler University Linz, Linz, Austria

ABSTRACT

Poly(lactic acid) (PLA) nanocomposites with different layered organoclays (variation in the surface treatment of silicate) and one special nanofiller (mixed mineral thixotrope) were melt-compounded using a semi-industrial co-rotating twin-screw extruder. Effects of the silicate surface treatment and shape on the structure as well on processing and utility properties in PLA matrix were investigated. The structural changes in polymer matrix were evaluated from dynamic experiments in the shear flow using low-amplitude oscillatory measurements. Moreover, new approach for morphological investigation of nanocomposites using small-angle X-ray scattering was presented. Concerning utility properties, tests of mechanical and barrier properties were performed to compare enhancement of PLA matrix due to incorporation of different nanoparticles. Surprisingly, filling the PLA matrix with mixed mineral thixotrope resulted into very high material performance (in particular, significant improvement in barrier properties) compared to filling with commercial layered silicates. In this way, new type of nanofiller for PLA applications has been successfully tested.

ARTICLE HISTORY

Received 10 February 2017
Revised 18 July 2017
Accepted 25 August 2017

KEYWORDS

Polymer nanocomposites;
poly(lactic acid); clay;
rheology; structure;
mechanical properties;
permeability

Introduction

Recently, both increasing price of petrochemical products as well as responsibility for sustainable production facilitated industrial applications of bio-based polymers. Actual developments focus on bio-based technical polymers possessing similar property profile as their fossil equivalents. Using different additives and fillers enables optimisation of application properties (e.g. life-time, temperature stability) of bio-based polymers. Nano-scaled fillers have high potential to optimise processing as well as utility properties due to high specific surface area and low interfacial tension as compared to conventional fillers like glass or basalt fibers [1–7].

The primary particle shape of different nanofillers can be sphere, needle or a plate. High aspect ratio (particle length/thickness) of filler facilitates high reinforcement of polymer. Therefore, layered and needle-formed fillers have been widely used for enhancement of polymer property profile. Montmorillonite belongs to the group of layered silicates and theoretically it is possible to reach aspect ratio of 1000 by proper dispersion of this mineral in polymer matrix. Montmorillonite is a three-layer-silicate where the primary layer consists of one octahedral sheet surrounded by two tetrahedral sheets. Na⁺ or Ca²⁺ ions in the interlayer area have been usually replaced by long alkylammonium ions to increase interlayer space and, consequently, to facilitate dispersion in polymer melt during the melt-compounding process. Nanocomposites using different

polymer matrices and layered silicates have been intensively investigated because of the improvements in their processing and use properties. Consequently, it is possible to prepare new, tailored, materials or to use nanofillers in polymer recycling [1–3,6–11].

Concerning PLA nanocomposites, different types of nanoparticles have been tested [1,2,8,12–14]. However, no mention of effect of mixed mineral thixotrope on PLA structure, processing and utility properties, has been found in the relevant literature. In this work, both Na⁺ (Cloisite)- and Ca²⁺ (Nanofil)-based montmorillonite with different surface modifications were used. Furthermore, special nanofiller (mixed mineral thixotrope) with commercial name Garamite has been compounded with PLA matrix and analysed using structural as well as thermo-mechanical methods.

Experimental

Materials

PLA with commercial indication Ingeo 2003D used for the preparation of nanocomposites has been supplied by NatureWorks LLC, Minnetonka, MN, U.S.A. The used nanofillers (Table 1) have been supplied by Rockwood Clay Additives Ltd., Moosburg, Germany. Na⁺-based (commercially indicated as Cloisite) and Ca²⁺-based (commercially indicated as Nanofil) organoclays have been denoted as C and N following by characteristic number and letter, respectively, to keep

Table 1. Characteristics of organoclays.

Organoclay	Organic modifier*	Modifier concentration [mequiv/100 g clay]	Moisture [%]	Weight loss on ignition [%]	d_{001} [Å]
Nanofil 3010	2M2HT	110	<2	41	36
Cloisite 15A	2M2HT	125	<2	43	31.5
Cloisite 20A	2M2HT	95	<2	38	24.2
Cloisite 10A	2MBHT	125	<2	39	19.2
Cloisite 30B	MT2EtOH	90	<2	30	18.5

*Quaternary ammonium chlorides: dialkyldimethyl-(2M2HT), alkyl(benzyl)dimethyl-(2MBHT), alkyl(2-ethylhexyl)dimethyl-(2MHTL8), alkylbis(2-hydroxyethyl)-methyl-(MT2EtOH). Alkyls are a mixture of 65% C18, 30% C16 and 5% C14, derived from hydrogenated tallow.

transparency in the plotted figures. In addition to layered silicates, special nanofiller (mixed mineral thixotrope, in this case mixture of organically modified layered and needle-formed silicates) commercially named Garamite was tested.

Compounding process and samples preparation

For the compounding process, a co-rotating intermeshing twin screw extruder Werner & Pfleiderer ZSK-25 (Coperion GmbH, Stuttgart, Deutschland) using six heating zones and a string die has been employed. The feed rate was set at 6 kg/h with a screw speed of 100 rev min⁻¹. The temperature profile is described in Table 2. For subsequent characterisation, plates and films, respectively, with different thicknesses were prepared using the hydraulic vacuum press machine (Collin 200 PV, Dr. Collin Ltd, Ebersberg, Germany).

Rotational rheometry

Rheological properties in the shear flow were studied using a Physica MCR 501 rheometer (Anton Paar Ltd., Graz, Austria) with the cone-plate geometry of 25 mm diameter and automatically controlled gap of 50 µm. The samples thickness was 1 mm. Experiments were performed at 180°C under nitrogen to prevent degradation of samples. The following types of rheological measurements were carried out: (1) dynamic strain sweep test (at angular frequency of 6.28 rad s⁻¹) to confirm the linearity of viscoelastic region, (2) dynamic frequency sweep test over a frequency range of 0.1–500 rad s⁻¹, at the strain 0.01%. The data were evaluated from at least three measurements for each sample and then average data was plotted.

Mechanical testing

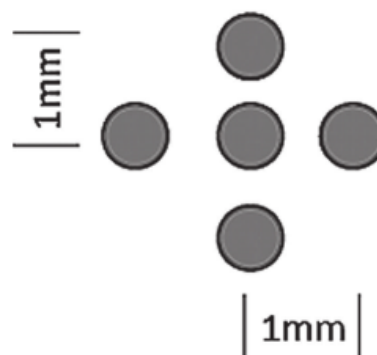
A universal tensile testing machine (Type: Z010, Zwick Ltd & Co. KG, Ulm, Germany) was used to carry out the tensile tests according to ISO 527-1. All tests were

carried out under standard conditions (23 ± 2°C/50 ± 5% RH). The data were evaluated using the testXpert II software (ZWICK, Ulm, Germany).

Small-angle X-ray scattering (SAXS)

Scattering patterns were recorded in a Bruker NanoStar small-angle X-ray scattering (SAXS) device (Bruker AXS, Karlsruhe, Germany). This system was equipped with X-ray Microsource and Montel optics (both from Incoatec, Geesthacht, Germany) providing monochromatic X-rays with a wavelengths of 0.154 nm (Cu Kα). A Vantec 2000 2D Detector system (Bruker AXS, Karlsruhe, Germany) was used to record the scattering patterns. For the measurements two sheets of the polymer and polymer composites were fixed together and measured on five individual points with 1 mm distance in-between them according to Figure 1 in transmission. The footprint of the circular shaped X-ray beam on the sample was approximately 550 µm in diameter.

Sample transmission was determined for each individual measuring point using glassy carbon (GC) as secondary standard. For the determination of morphological parameters, isotropic SAXS patterns $I(q, \psi)$ were radially averaged with respect to ψ , yielding the $I(q)$ scattering curves, q being the magnitude of the scattering vector. The individual scattering curves were corrected for background scatter and averaged resulting in one scattering curve per sample. To perform deeper structural analysis, the PLA nanocomposites were analysed using the SCATTER software [15,16]. For all samples a linear background was

**Figure 1.** Measurement strategy for SAXS analysis.**Table 2.** Compounding temperature profile.

Section	1	2	3	4	5	6
Temperature (°C)	160	170	180	190	200	200

chosen. Using SCATTER evaluation, the data were analysed assuming lamellar structure factor and cylindrical, coin like form factor. The domain sizes are calculated using paracrystalline interaction (damping) model as described in references [15,16]. Morphological parameters like bending of crystals, interlayers from organic compounds on crystals and filler and other side effects were neglected.

Measurement of barrier properties

For the permeability tests, MOCON[®]OX-TRANS MH 2/20 equipment was used. Measurements on thin films were performed according to ASTM F 1927-07 standard at $23 \pm 0.5^\circ\text{C}/1\%$ RH. Nitrogen throughput of 10 mL min^{-1} through the sample with an area of 50 cm^2 was set. The time of ca. $8 \pm 4 \text{ h}$ for the samples conditioning as well for getting stable diffusion conditions after oxygen treatment was chosen.

Transmission electron microscopy

The transmission electron microscopy (TEM) experiments were performed with a Zeiss LEO 912 Omega transmission electron microscope using an acceleration voltage of 120 keV. The samples were prepared using a Leica Ultracut UCT ultramicrotome equipped with a cryo-chamber. Thin sections of about 50 nm were cut with a Diatome diamond knife at -120°C .

Results and discussion

Rheological properties

The nanocomposites structure can be assessed by analysis of viscosity curve (shear-thinning behaviour) in combination with evaluation of the storage modulus curve (G' secondary plateau) [1–4,6–11]. In comparison with the unfilled matrix, complex viscosity of nanocomposites significantly increased in the range of low frequencies, as shown in Figure 2. The power-law

dependence at low frequencies, which is characteristic of neat PLA, is absent in the nanocomposites. The systems filled with Cloisite 10A and Cloisite 20A revealed pronounced shear thinning phenomenon, which is caused first by disruption of network structures and later on by orientation of filler particles in flow direction.

The internal structural changes in nanocomposites during shear flow can be also analysed in frequency dependency of the storage (G') modulus (Figure 3). The dependence of $G'(\omega)$ in nanocomposites filled with Cloisite 10A and Cloisite 20A becomes nearly invariable ('rubber-like behavior'). This 'secondary' plateau indicates the formation of a 3D-network structure (card-house structure) of silicate layers in nanocomposites [17–35].

The strong physical network formed in nanocomposites containing Cloisite 10A can be explained by high modifier concentration of Cloisite 10A, where the benzyl group on each surface modifier molecule will give a degree of polarisability due to the delocalised pi-electrons in the phenyl ring of the benzyl group. The highest magnitude of shear viscosity and storage modulus in the range of higher frequencies revealed system filled with Cloisite 30B. This could be explained that higher shear rates and residence time, respectively, result to strong interactions between hydroxyl groups (presented on basic sheets as well as surface modifier) of Cloisite 30B and carbonyl groups of PLA chains based on hydrogen bonding [1,2,8,36,37]. The mixture filled with Garamite revealed enhanced viscosity with rather lower shear-thinning phenomenon and tendency to 'rubber-like behavior' at low frequencies, which is a sign of stable dispersion, homogeneous particles distribution and high interfacial adhesion between filler and polymer matrix.

Generally, it can be clearly seen that in all prepared nanocomposites (except of mixture filled with Nanofil 116) magnitude of storage modulus (level of melt elasticity) has been significantly increased, as compared to unfilled matrix in the range of lower frequencies, which

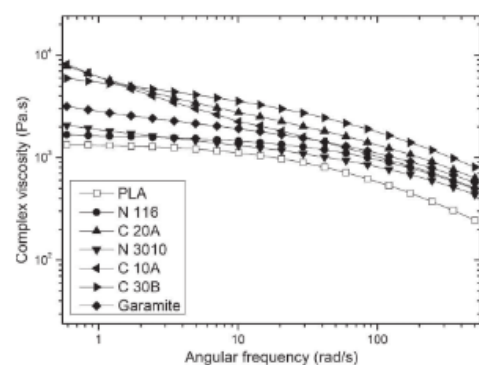


Figure 2. Complex viscosity of PLA nanocomposites.

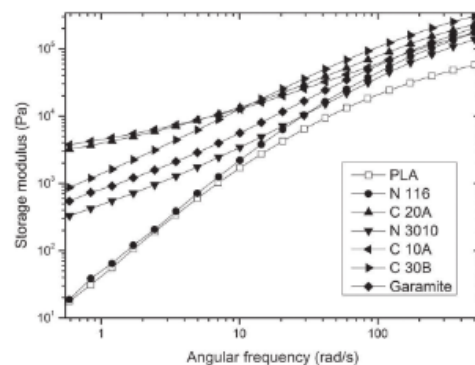


Figure 3. Storage modulus of PLA nanocomposites.

reflects formation of physical network between filler particles and PLA matrix. The highest melt elasticity revealed systems filled with Cloisite 10A and Cloisite 20A at lower frequencies and PLA/Cloisite 30B at higher frequencies. Filling with Nanofil 116 led to increased melt elasticity only in the range of higher frequencies indicating rather weak incorporation of filler into polymer matrix.

Mechanical properties

The highest magnitudes of tensile strength revealed systems filled with Nanofil 116 (Ca^{2+} natural montmorillonite without surface modification) and Garamite (Figure 4). In these nanocomposites, high level of 3D network structure between silicate layers and polymer chains has been achieved. In PLA-Garamite, this effect can be explained by formation of stronger network between PLA, platelets and needles of the silicate, respectively, coming from high spatial mobility of mixed mineral thixotrope. In the case of Nanofil 116 filled compound, calcium-based montmorillonite seems to match spatial configuration of the used PLA by given processing conditions as well and, consequently, homogeneous dispersion of clay in polymer can be reached.

Concerning the stiffness of prepared nanocomposites, all the systems revealed increase in tensile modulus (Figure 5) comparing to the unfilled PLA matrix. The highest magnitude of tensile modulus was observed in nanocomposites filled with Cloisite 10A, Cloisite 30B and Garamite, which can be associated with polarisability of organic modifiers used in Cloisite 10A/Cloisite 30B and with high spatial mobility of Garamite, respectively, resulting into strong reinforcement of PLA.

Morphological analysis

The measured d_{001} distance as typical SAXS result is plotted in Figure 6. It is obvious that similar magnitude

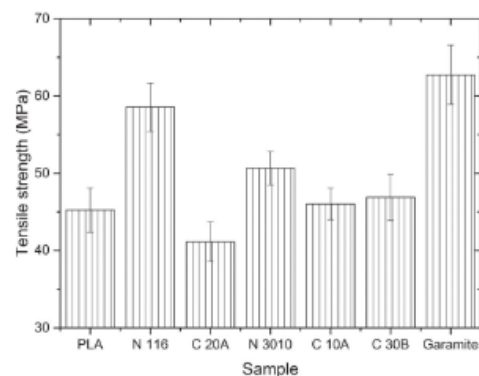


Figure 4. Tensile strength of PLA nanocomposites.

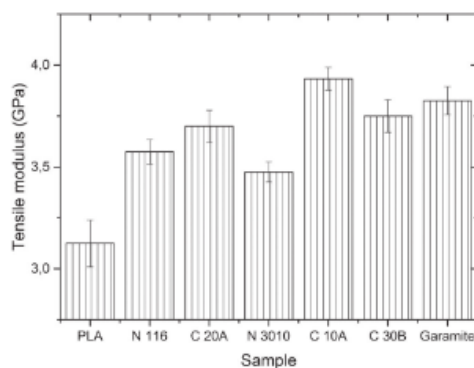


Figure 5. Young's modulus of PLA nanocomposites.

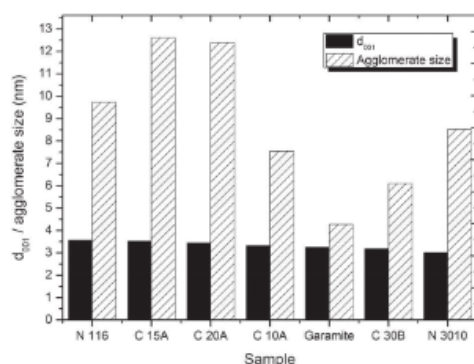


Figure 6. Delamination parameters of PLA nanocomposites.

of the interlayer distance was achieved in all the prepared nanocomposites. However, using deeper analysis of results as described in section 'Small-angle X-ray scattering (SAXS)', a closer look into nanocomposite structure could be achieved and new parameter, average tactoid thickness, could be gained from SAXS measurement. This structural parameter complementary to the interlayer distance, provide us with quantitative information about dispersion state. In this way, the nanocomposite structure is completely characterised and some other usually used techniques like TEM or scanning electron microscopy do not have to be applied as they generate only qualitative information not allowing reliable comparison of dispersion state. As can be seen from Figure 6, different values of average tactoid thickness were observed comparing all the prepared systems. The lowest average tactoid thickness revealed mixtures filled with Garamite, Cloisite 30B and Cloisite 10A, which is in a good agreement with previously described measurements. In the case of PLA-Garamite nanocomposite, this result can be explained by inherence of needle-formed particles, which facilitates dispersion level in PLA matrix and acts against re-agglomeration. The tendency towards

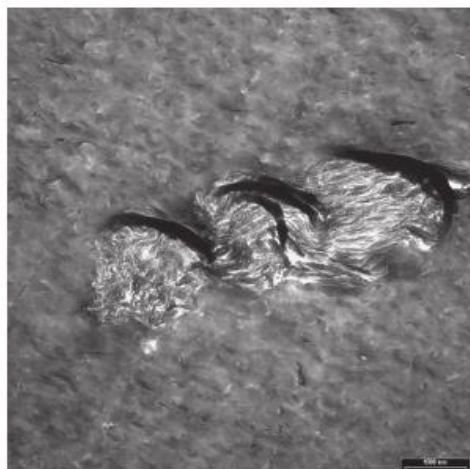


Figure 7. Transmission electron micrograph of PLA/Cloisite 20A (1000 nm).

re-agglomeration of layered silicates during melt mixing has been described previously [8]. In this work, TEM micrographs of nanocomposites with highest and lowest average tactoid thickness have been performed. The re-agglomeration tendency can be seen in nanocomposite with Cloisite 20A (Figure 7), which is not the case in nanocomposite with Garamite (Figure 8) revealing rather homogeneous dispersion state.

Barrier properties

In Figure 9, oxygen permeability ($\text{cm}^3/\text{m}^2/\text{day}$) of different PLA nanocomposites is plotted. The lowest value of oxygen permeability (33% lower permeability

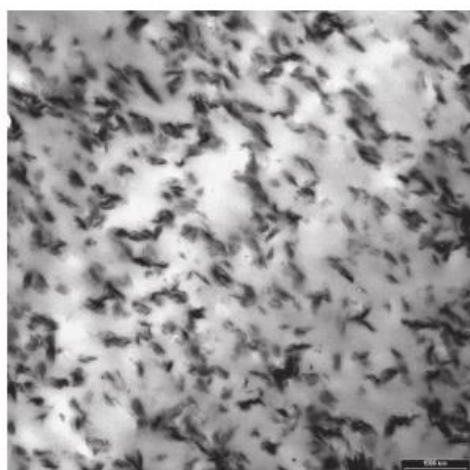


Figure 8. Transmission electron micrograph of PLA/Garamite (1000 nm).

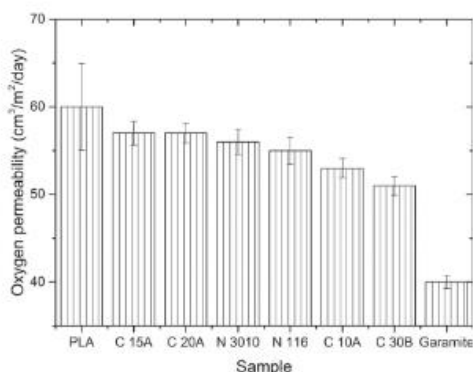


Figure 9. Barrier properties of PLA nanocomposites.

as compared to pure PLA) has been achieved in compound filled with Garamite, which can be again explained by very homogeneous spatial distribution of dispersed clay platelets and needles in PLA matrix. Furthermore, nanocomposites filled with Cloisite 30B and Cloisite 10A revealed also significant reduction (15 and 12% reduction, respectively) in oxygen permeability, which can be assigned to polarisability of the mentioned clays matching the polarisability of PLA.

Conclusions

PLA nanocomposites were prepared using the melt mixing method. Different sodium as well as calcium type organophilic montmorillonites and special mixture of layered and needle formed clay (Garamite) were tested. Their effect on morphology, processing, mechanical and barrier properties was investigated. Surprisingly, nanocomposite filled with Garamite revealed very interesting property profile with low permeability, high mechanical performance as well as enhanced rheological properties associated with the lowest average tactoid thickness as compared to other nanocomposites. In this way, new type of clay filler was successfully tested for polymer applications and new morphological parameter for quantitative description of dispersion grade in polymer nanocomposites has been introduced.

Acknowledgement

Livia Chitu and Günther Maier from Materials Center Leoben Forschung GmbH, Austria for X-ray scattering measurements, Ralf Thomann from Freiburg Materials Research Center, University of Freiburg, Germany for TEM measurements, Peter Zaucher from Chair of Construction in Polymers and Polymer Composites, Department Polymer Engineering and Science, Montanuniversitaet Leoben, Austria for mechanical testing, Martin Hirschenauer from ofi Technologie & Innovation GmbH, Austria for measurement of barrier properties and Clemens Holzer from Chair of Polymer Processing, Department Polymer Engineering and

Science, Montanuniversitaet Leoben, Austria for enabling material compounding and rheological measurements are gratefully acknowledged.

Disclosure statement

No potential conflict of interest was reported by the author.

Funding

This research was supported by the research platform AKTION Czech Republic – Austria, project Nr. 63p24: Development of effective technology for production of biodegradable polymer nanocomposite films with advanced properties.

ORCID

Milan Krcalik  <http://orcid.org/0000-0001-7398-0394>

References

- [1] Araújo A, Botelho G, Oliveira M, et al. Influence of clay organic modifier on the thermal-stability of PLA based nanocomposites. *Appl Clay Sci.* 2014;144:88–89.
- [2] Lai S-M, Wu S-H, Lin G-G, et al. Unusual mechanical properties of melt-blended poly(lactic acid) (PLA)/clay nanocomposites. *Eur Polym J.* 2014;52:193–206.
- [3] Laske S, Krcalik M, Feuchter M, et al. FT-NIR as a determination method for reinforcement of polymer nanocomposites. *J Appl Polym Sci.* 2009;114(4):2488–2496.
- [4] Yu ZZ, Yan C, Yang M, et al. Mechanical and dynamic mechanical properties of nylon 66/montmorillonite nanocomposites fabricated by melt compounding. *Polym Int.* 2004;53(8):1093–1098.
- [5] Anand KA, Agarwal US, Nisal A, et al. PET-SWNT nanocomposites through ultrasound assisted dissolution-evaporation. *Eur Polym J.* 2007;43(6):2279–2285.
- [6] Krcalik M, Pospisil L, Slouf M, et al. Effect of glass fibers on rheology, thermal and mechanical properties of recycled PET. *Polym Compos.* 2008;29(8):915–921.
- [7] Krcalik M, Pospisil L, Slouf M, et al. Recycled poly(ethylene terephthalate) reinforced with basalt fibres: rheology, structure, and utility properties. *Polym Compos.* 2008;29(4):437–442.
- [8] Ray SS, Okamoto M. Polymer/layered silicate nanocomposites: a review from preparation to processing. *Progr Polym Sci.* 2003;28:1539–1641.
- [9] Krcalik M, Laske S, Gschweilt M, et al. Advanced compounding: extrusion of polypropylene nanocomposites using the melt pump. *J Appl Polym Sci.* 2009;113(3):1422–1428.
- [10] Krcalik M, Laske S, Witschnigg A, et al. Elongational and shear flow in polymer-clay nanocomposites measured by on-line extensional and off-line shear rheometry. *Rheol Acta.* 2011;50:937–944.
- [11] Laske S, Witschnigg A, Mattausch H, et al. Determining the ageing of polypropylene nanocomposites using rheological measurements. *Appl Rheol.* 2012;22(2):24590.
- [12] Raquez JM, Habibi Y, Murariu M, et al. Polylactide (PLA)-based nanocomposites. *Progr Polym Sci.* 2013;38:1504–1542.
- [13] Fukushima K, Fina A, Geobaldo F, et al. Properties of poly(lactic acid) nanocomposites based on montmorillonite, sepiolite and zirconium phosphonate. *eXPRESS Polym Lett.* 2012;6:914–926.
- [14] Chow WS, Lok SK. Thermal properties of poly(lactic acid)/organo-montmorillonite nanocomposites. *J Therm Anal Calorim.* 2009;95:627–632.
- [15] Förster S, Burger C. Scattering functions of polymeric core-shell structures and excluded volume chains. *Macromolecules.* 1998;31:879–891.
- [16] Förster S, Timmann A, Konrad M, et al. Scattering curves of ordered mesoscopic materials. *Phys Chem B.* 2005;109:1347–1360.
- [17] Krishnamoorti R, Giannelis EP. Rheology of end-tethered polymer layered silicate nanocomposites. *Macromolecules.* 1997;30:4097–4102.
- [18] Khan SA, Prudhomme RK, et al. Melt rheology of filled thermoplastics. *Rev Chem Eng.* 1987;4:205.
- [19] Krishnamoorti R, Vaia RA, Giannelis EP. Structure and dynamics of polymer-layered silicate nanocomposites. *Chem Mater.* 1996;8:1728–1734.
- [20] Hoffmann B, Dietrich C, Thomann R, et al. Morphology and rheology of polystyrene nanocomposites based upon organoclay. *Macromol Rapid Commun.* 2000;21:57–61.
- [21] Hoffmann B, Kressler J, Stöppelmann G, et al. Rheology of nanocomposites based on layered silicates and polyamide-12. *Colloid Polym Sci.* 2000;278:629–636.
- [22] Lee KM, Han CD. Rheology of organoclay nanocomposites: effects of polymer matrix/organoclay compatibility and the gallery distance of organoclay. *Macromolecules.* 2003;36:7165–7178.
- [23] Sanchez-Solis A, Garcia-Rejon A, Manero O. Production of nanocomposites of PET-montmorillonite clay by an extrusion process. *Macromol Symp.* 2003;192:281–292.
- [24] Sanchez-Solis A, Romero-Ibarra I, Estrada MR, et al. Mechanical and rheological studies on polyethylene terephthalate-montmorillonite nanocomposites. *Polym Eng Sci.* 2004;44:1094–1102.
- [25] Solomon MJ, Almusallam AS, Seefeldt KF, et al. Rheology of polypropylene/clay hybrid materials. *Macromolecules.* 2001;34:1864–1872.
- [26] Hyun YH, Lim ST, Choi HJ, et al. Rheology of poly(ethylene oxide)/organoclay nanocomposites. *Macromolecules.* 2001;34:8084–8093.
- [27] Ray SS, Yamada K, Okamoto M, et al. New polylactide-layered silicate nanocomposites. 2. Concurrent improvements of material properties, biodegradability and melt rheology. *Polymer (Guildf).* 2003;44:857–866.
- [28] Incarnato L, Scarfato P, Scatteia L, et al. Rheological behavior of new melt compounded copolyamide nanocomposites. *Polymer (Guildf).* 2004;45:3487–3496.
- [29] Lepoittevin B, Devalckenaere M, Pantoustier N, et al. Poly(ϵ -caprolactone)/clay nanocomposites prepared by melt intercalation: mechanical, thermal and rheological properties. *Polymer (Guildf).* 2002;43:4017–4023.
- [30] Lee KM, Han CD. Effect of hydrogen bonding on the rheology of polycarbonate/organoclay nanocomposites. *Polymer (Guildf).* 2003;44:4573–4588.
- [31] Kotsilkova R, et al. Rheology-structure relationship of polymer/layered silicate hybrids. *Mechanics Time-Dependent Mater.* 2002;6:283–300.
- [32] Kim TH, Jang LW, Lee DC, et al. Synthesis and rheology of intercalated polystyrene/Na⁺-montmorillonite nanocomposites. *Macromol Rapid Commun.* 2002;23:191–195.

- [33] Gelfer M, Song HH, Liu L, et al. Manipulating the microstructure and rheology in polymer-organoclay composites. *Polym Eng Sci.* 2002;42:1841–1851.
- [34] Wagener R, Reisinger TJG. A rheological method to compare the degree of exfoliation of nanocomposites. *Polymer (Guildf).* 2003;44:7513–7518.
- [35] Lim ST, Hyun YH, Choi HJ, et al. Polyester/Montmorillonite Nanocomposites. *Polym Prepr.* 2001;42(1):640.
- [36] Pluta M, Galeski A, Alexandre M, et al. Polylactide/montmorillonite nanocomposites and microcomposites prepared by melt blending: structure and some physical properties. *J Appl Polym Sci.* 2002;86:1497.
- [37] Fukushima K, Tabuani D, Camino G. Nanocomposites of PLA and PCL based on montmorillonite and sepiolite. *Mater Sci Eng C.* 2009;29:1433–1441.

2.3.2 Manuscript 12

„Estimation of reinforcement in compatibilized polypropylene nanocomposites by extensional rheology“

Laske, Stephan; Kracalik, Milan; Gschweidl, Michael; Feuchter, Michael; Maier, Günther; Pinter, Gerald et al. (2009): In: J. Appl. Polym. Sci. 111 (5), S. 2253–2259. DOI: 10.1002/app.29163.

This is the first manuscript describing material reinforcement of complex polymer nanocomposites by elongational rheology. For polypropylene-clay nanocomposites it was shown that higher admixture of compatibilizer results in higher dispersion grade (interlayer distance measured by SAXS, optical comparison by TEM), but this trend was not valid for rheological and mechanical properties, where too high compatibilizer admixture led to lowering the rheological/mechanical performance. The reason was in molecular weight of the compatibilizer (maleic acid grafted PP), which was significantly lower than that of PP matrix – therefore, with too high compatibilizer admixture, the effect of reinforcement coming from higher dispersion grade was lower than effect of average molecular weight decrease coming from compatibilizer. In this way, extensional rheometry was proved to be fast method for analysis of effective material reinforcement taking into account both the dispersion grade of nanofiller as well as possible changes in average molecular weight of polymer matrix.

Estimation of Reinforcement in Compatibilized Polypropylene Nanocomposites by Extensional Rheology

Stephan Laske,¹ Milan Kracalik,¹ Michael Gschweidl,¹ Michael Feuchter,² Günther Maier,³ Gerald Pinter,² Ralf Thomann,⁴ Walter Friesenbichler,¹ Günter Rüdiger Langecker¹

¹Institute of Plastics Processing, University of Leoben, Leoben 8700, Austria

²Institute of Materials Science and Testing of Plastics, University of Leoben, Leoben 8700, Austria

³Materials Center Leoben Forschung GmbH, Roseggerstrasse 12, Leoben 8700, Austria

⁴Freiburg Materials Research Center, University of Freiburg, Freiburg 79104, Germany

Received 23 April 2008; accepted 9 August 2008

DOI 10.1002/app.29163

Published online 13 November 2008 in Wiley InterScience (www.interscience.wiley.com).

ABSTRACT: Structural characterization in polymer nanocomposites is usually performed using X-ray scattering and microscopic techniques, whereas the improvements in processing and mechanical properties are commonly investigated by rotational rheometry and tensile testing. However, all of these techniques are time consuming and require quite expensive scientific equipment. It has been shown that a fast and efficient way of estimating the level of reinforcement in polymer nanocomposites can be performed by melt extensional rheology, because it is possible to correlate the level of melt strength with mechanical properties, which reflect both

the 3D network formed by the clay platelets/polymer chains as well as final molecular structure in the filled system. The physical network made of silicate filler and polymer matrix has been evaluated by X-ray diffraction and transmission electron microscopy. Extensional rheometry and tensile testing have been used to measure efficiency of the compatibilizer amount in a polypropylene-nanoclay system. © 2008 Wiley Periodicals, Inc. *J Appl Polym Sci* 111: 2253–2259, 2009

Key words: nanocomposites; melt compounding; melt strength

INTRODUCTION

Nanocomposites using different polymer matrices and layered silicates have been intensively investigated because of the improvements in their processing and use properties. Consequently, it is possible to prepare new, tailored, materials¹ or to use nanofillers in polymer recycling.^{2–4} The improvement in material properties due to nanoclay addition has usually been evaluated using a combination of transmission electron microscopy (TEM) and morphological (X-ray diffraction (XRD), mechanical (tensile testing), and sometimes also rheological (rotational rheometry) analyses. However, these conventional methods require quite expensive scientific equipment and long sample preparation and characterization times. Generally, intercalated and delaminated (partially exfoliated) polymer nanocomposites reveal significant enhancements in their properties: higher elastic modulus, tensile strength, thermal resistivity,

lower gas and liquid permeability, reduced flammability,⁵ and improved rheological properties (e.g., higher melt strength) compared with the unfilled polymer matrix.¹ The high level of possible reinforcement due to the addition of the layered silicates results from their large active surface area (in the case of montmorillonite 700–800 m²/g).⁶ In the case of highly dispersed systems, a 3D physical network is achieved, formed by the silicate platelets and the polymer chains. This phenomenon can be investigated by analyzing the melt elasticity using rotational rheometry.^{1–4,6–22} A fast way to evaluate this network effect is using elongational rheometry,^{23–26} which provides information about the melt strength.

To disperse the clay in hydrophobic polypropylene (PP), a compatibilizer (mostly PP grafted with maleic acid anhydride (MA)) must be admixed. However, the molecular weight of the compatibilizer is usually lower than that of the PP matrix due to the grafting reaction and the presence of free MA molecules.²⁷

We have already presented^{23,24} that the effective level of reinforcement in PP nanocomposites cannot be based solely on an evaluation of the delamination level (increase in interlayer distance) determined by X-ray scattering. In the PP-PPMA-nanoclay system, the simple rule “higher delamination leads to an improvement in material properties” is not always

Correspondence to: M. Kracalik (Milan.Kracalik@mu-leoben.at).

Contract grant sponsor: PlaComp1 Project (NanoComp research project cluster founded by the Austrian Nanoinitiative).

Journal of Applied Polymer Science, Vol. 111, 2253–2259 (2009)
© 2008 Wiley Periodicals, Inc.

TABLE I
Temperature profile in different extruder sections

Section	1	2	3	4	5	6	7	8	9	10
Temperature (°C)	cool	160	180	190	200	200	200	200	200	200

valid because of the influences of the grafted PP on the material properties. With a higher compatibilizer addition, the final delamination increases but the average molecular weight decreases. This means that there is an optimal compatibilizer admixture at which physical reinforcement caused by silicate delamination is still higher than the deterioration in mechanical properties due to decreasing molecular weight and combination of the interfacial area able to be generated.

A fast and accurate method to find this optimal compatibilizer admixture in different PP nanocomposites is to compare the material reinforcement in the systems using extensional rheometry. A further advantage of elongational experiments is the use of primary granulates: no preparation of samples is necessary. To date, a few articles have dealt with the possibility of using extensional rheometry for the characterization of elongational viscosity in polymer nanocomposites.^{28,29} However, no correlation between the melt strength and the mechanical properties with respect to nano-structural details has yet been published. The goal of this article is to present a fast, qualitative method of reinforcement evaluation based on extensional rheology in polymer nanocomposites with a view to speed up the industrial application of the systems investigated.

EXPERIMENTAL

Materials

The isotactic PP homopolymer HC600TF (MFI 2.8 g/10 min; 230°C/2.16 kg) was supplied by Borealis, Inc., Linz, Austria. Used nanofiller (montmorillonite intercalated with dimethyl distearyl ammonium chloride) with commercial indication Nanofil 5 was supplied by Süd-Chemie Inc., Munich, Germany. The compatibilizer (Scona TPPP 2112 FA, MFI 14.8 g/10 min) was supplied by Kometra, Ltd., Schkopau, Germany.

TABLE II
Press profile

Temperature (°C)	200	200	200	200	50
Pressure (bar)	1	20	1	100	150
Time (min)	20	5	5	7	7

Preparation of nanocomposites

For the compounding process, an intermeshing, corotating twin screw extruder Theysohn TSK30/40D (Theysohn Holding Ltd, Vienna, Austria) with a string die was used. The feed rate was set at 20 and 7 kg/h, with a screw speed of 200 rpm. The temperature profile is described in Table I. The compatibilizer admixture content relative to the organoclay content (5 wt %) was chosen at ratios (clay : compatibilizer) from 1 : 0 to 1 : 3.

For the Rheotens measurements, the primary granulate obtained from the extrusion process was used. For structural (X-ray diffraction, transmission electron microscopy) and mechanical characterization, plates with a thickness of 2 mm and standard dog-bone shaped specimens (150 mm length, 20 mm width, 4 mm thickness), respectively, were prepared using the hydraulic vacuum press machine (Collin 200 PV, Dr. Collin Ltd., Ebersberg, Germany). The press profile is given in Table II.

Extensional melt rheology

As stated in the introduction, two methods of reinforcement assessment can be used in the molten state in polymer nanocomposites: analysis of the melt elasticity using rotational rheometry or melt strength evaluation, e.g., using Rheotens equipment. The advantage of Rheotens measurements consists in their simplicity without the need for expensive scientific equipment and additional time for sample preparation. The principle of Rheotens measurements can be seen in Figure 1. It is based on the

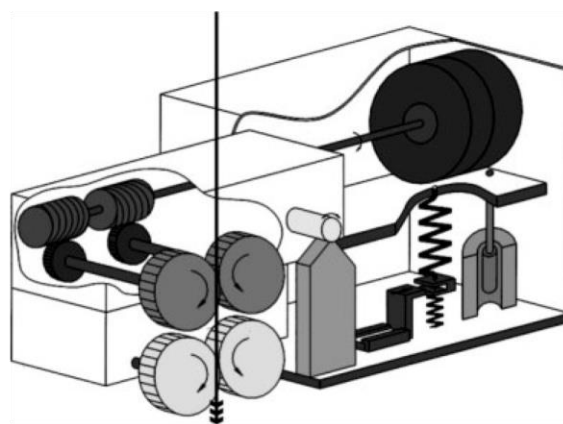


Figure 1 Principle of Rheotens measurement.³⁰

TABLE III
Capillary rheometer testing specification

Cylinder diameter	12 mm
Die (length/diameter)	30/2 mm
Temperature	210°C
Piston speed	1.9 mm/s
Shear rate	273.6 s ⁻¹

elongation of an extruded string by two or four rotating wheels connected with a force transducer. The rotation speed is linearly increased until the molten string breaks. The tensile force applied to the wheels and the draw rate at break allows the calculation of the melt strength (stress at break)³¹:

$$\sigma_b = F_b v_b / A_0 v_0,$$

σ_b —stress at break (Pa),

F_b —tensile force at break (N),

v_b —draw rate at break (mm s⁻¹),

A_0 —initial cross section of molten string (at the die outlet) (m²),

v_0 —extrusion speed of molten string (piston speed) (mm s⁻¹).

We used the Rheotens 71.97 (Göttfert Ltd., Buchen, Germany) in a combination with a capillary rheometer. The measuring conditions for capillary rheometer are listed in Table III. The rheotens equipment has been set applying wheel acceleration of 60 mm/s² and gap between wheels of 0.6 mm. To compare the melt strength level of different nanocomposite systems (revealing different magnitudes of v_b), the tensile force at a draw rate of 320 mm/s was chosen for comparison (Fig. 2).

The silicate platelets form different levels of 3D physical network in the polymer matrix depending on their level of delamination.^{1–4} Higher delamination results in a higher extent of physical network (higher material reinforcement) and, therefore, in an increase in melt strength. Different particle–particle and polymer–particle physical interactions result in variations in viscoelastic response. Therefore, Rheotens measurements are used to identify changes in the melt elongational behavior. Individual silicate platelets form nanoscale network (cardhouse structure)²¹ and raise the melt strength of the composite. Depending on the degree of delamination, this transformation is obvious compared with the unfilled polymer.

Small angle X-ray scattering

X-ray measurements were performed using Bruker NanoSTAR (Bruker AXS, Karlsruhe, Germany) small angle X-ray scattering (SAXS) equipment. This sys-

tem was equipped with a two-dimensional X-ray detector. A wavelength of 0.154 nm (CuK α) was used. The samples were measured in transmission.

To avoid the influence of texture, all scattering measurements were performed on plate samples. The gallery period¹ of the nanofiller was determined on a powder sample. To avoid statistical effects, the scattering curves recorded at three different positions on the samples were averaged. To determine the gallery period, scattering curves were corrected for background scatter and the Lorenz correction was applied.³² The Lorenz correction was performed by multiplying the scattered intensity ($I(q)$) by q^2 , q being the magnitude of the scattering vector. The position of the gallery peak was then determined by fitting with a Lorenz function.

Transmission electron microscopy

The TEM experiments were performed using a Zeiss LEO 912 Omega transmission electron microscope (Carl Zeiss Inc., Jena, Germany) using an acceleration voltage of 120 kV. The samples were prepared using a Leica Ultracut UCT ultramicrotome (Leica Microsystems Ltd, Wetzlar, Germany) equipped with a cryo chamber. Thin sections of about 50 nm were cut with a Diatome diamond knife at –120°C.

Mechanical properties

A universal tensile testing machine (Type: Z010, Zwick Ltd and Co. KG, Ulm, Germany) was used to carry out the tensile tests according to ISO 527-1. All tests were carried out under standardized conditions (23 \pm 2°C/50 \pm 5% r.H.). The data was evaluated using the testXpert II software (ZWICK, Ulm, Germany).

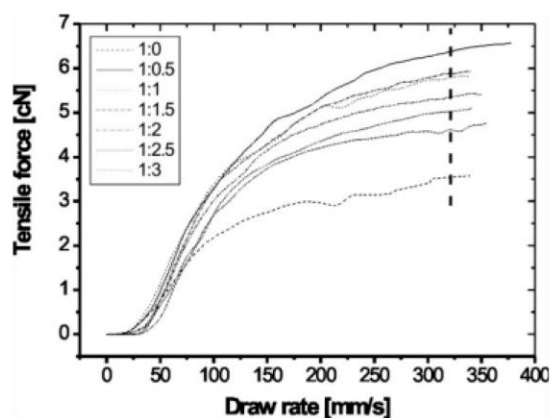


Figure 2 Melt strength level comparison.

Journal of Applied Polymer Science DOI 10.1002/app

RESULTS AND DISCUSSION

Extensional melt rheology

The elongational behavior of nanocomposite masterbatches prepared using different compatibilizer admixtures at two throughput rates is shown in Figure 3. It is obvious that the compatibilizer content as well as the effect of the feed rate on material properties can be analyzed by evaluating the melt strength. As stated in the Introduction section, determination of the optimum compatibilizer admixture in polyolefine nanocomposites is essential to reach the maximal reinforcement using layered silicates. We have shown^{23,24} that the MFI difference in PP matrices results in different optimum compatibilizer admixtures. The lower the MFI, the lower the compatibilizer content needed. The high molecular weight of the HC600TF matrix leads to high shear forces in the compounder and, therefore, facilitates delamination of silicate platelets. A lower quantity of compatibilizer is, therefore, required. Using the HC600TF matrix led to higher level of material reinforcement due to requiring two to four times less compatibilizer compared with other lower molecular weight PP matrices.^{23,24} It is obvious that the exact determination of the optimum compatibilizer admixture is a key factor in both maximizing the level of polymer reinforcement and minimizing compatibilizer costs. For the effect of the feed rate (at a constant screw speed) on the optimum compatibilizer content, an opposite trend was found to that for MFI. A lower throughput rate leads to a higher need for compatibilizer, which is explained by the lower fill factor in the screw segments. A higher feed rate leads to a higher fill factor and, subsequently, to higher shear forces applied on silicate tactoids to be delaminated. Therefore, it is necessary to evaluate the optimum compatibilizer admixture for PP matrices with different molecular structures or by varying the process-

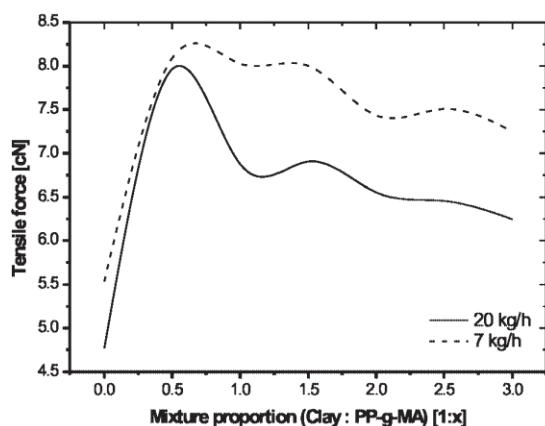


Figure 3 Melt strength level of nanocomposites.

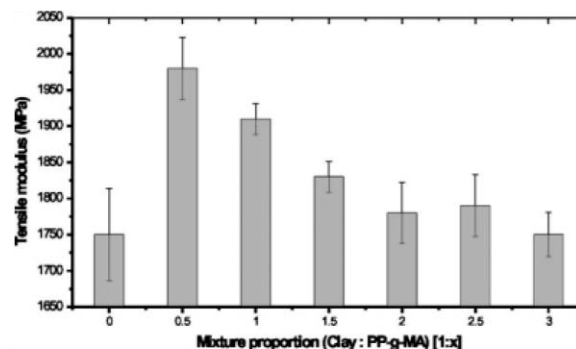


Figure 4 Tensile modulus in nanocomposites with different compatibilizer admixture.

ing conditions such as throughput rate. To our knowledge, this important aspect in the preparation of PP-organoclay nanocomposites has not been discussed in depth so far.

Mechanical properties

The results of mechanical testing in the solid state reflect those in the melt state. In Figure 4, the Young's modulus is plotted for the nanocomposites with differing compatibilizer admixtures. The same trend can be observed as for the extensional behavior. The highest increase in stiffness was found in the system filled with 2.5 wt % of compatibilizer. A further increase in the compatibilizer admixture leads to a decline in the tensile modulus. At 15 wt % compatibilizer the mean value of modulus reaches approximately the same value as for the mixture without compatibilizer. This result is in agreement with that published by Paul et al.,³³ where the mechanical properties of PP nanocomposites with different compatibilizer admixtures (1 : 0 to 1 : 2 PP-g-MA to organoclay ratio) were investigated. However, supposedly due to the high melt flow index of the matrix used (37 g/10 min, 230°C), an increase in

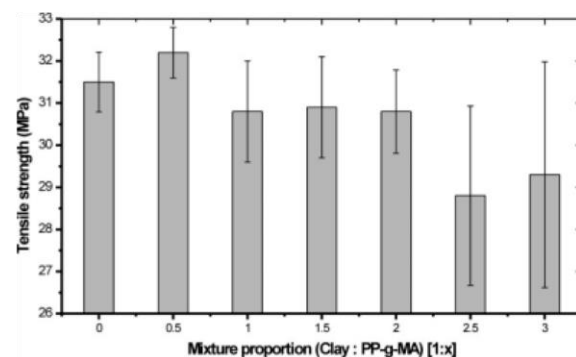


Figure 5 Tensile strength in nanocomposites with different compatibilizer admixture.

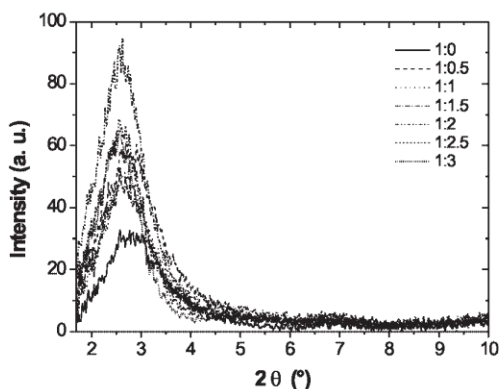


Figure 6 X-ray diffraction patterns of nanocomposites.

the compatibilizer content (1 : 0.5 up to 1 : 2 PP-g-MA to organoclay ratio) reported by Paul et al. did not result in a significant decrease in tensile modulus. As we already reported,^{23,24} molecular structure (in particular molecular weight) of PP matrix has significant influence on the optimum compatibilizer admixture and compatibilizing efficiency. The polymer matrix with the highest molecular weight possible to process with other composite components is favored to ensure maximal shear forces during compounding. Results for tensile strength (Fig. 5) reveal a similar trend as for melt strength and tensile modulus. The highest mean value of tensile strength was reached at a compatibilizer admixture of 2.5 wt %, while higher amounts resulted in a decline in tensile strength. The highest level of polymer-filler interfacial shear strength in the system, using 2.5 wt % of compatibilizer, is reflected in the high magnitudes of both melt and tensile strength. Therefore, it is possible to correlate the reinforcement level in the melt state with that in the solid state. In this way, extensional rheology can be used in terms of estimating the prior routes in the development of nanocompo-

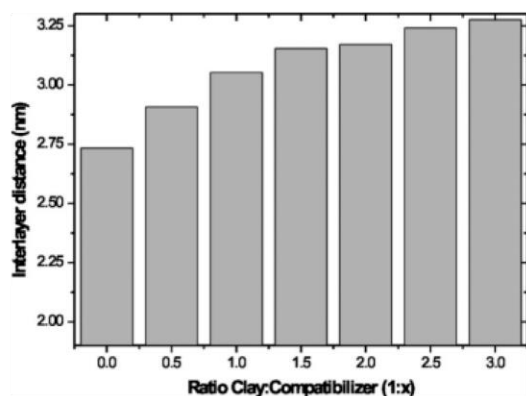


Figure 7 Gallery periodicity as a function of compatibilizer content.

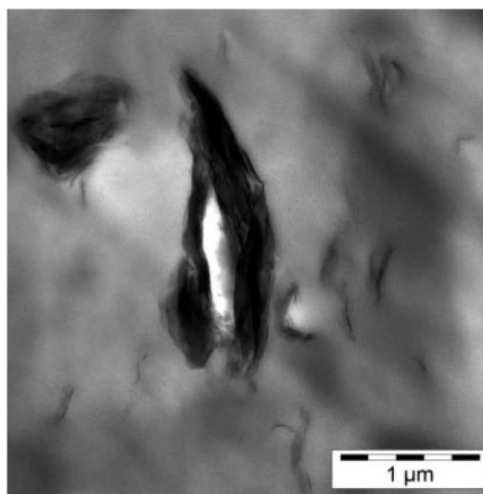


Figure 8 TEM of nanocomposite with 1 : 0 compatibilizer ratio.

sites and, presumably, any other filled systems based on polymer matrix.

Delamination of organoclay in polypropylene

The morphological analysis revealed a clear trend in delamination and homogeneity of silicate platelets in PP nanocomposites. In Figure 6, X-ray diffraction patterns of all investigated systems can be observed. The highest intensity peak was revealed in the system filled with 10 wt % of compatibilizer. On the other hand, the lowest peak can be seen in nanocomposite without compatibilizer. Calculated interlayer distance of organoclay is plotted in Figure 7 (relative to pure organoclay). It is obvious that the increase in

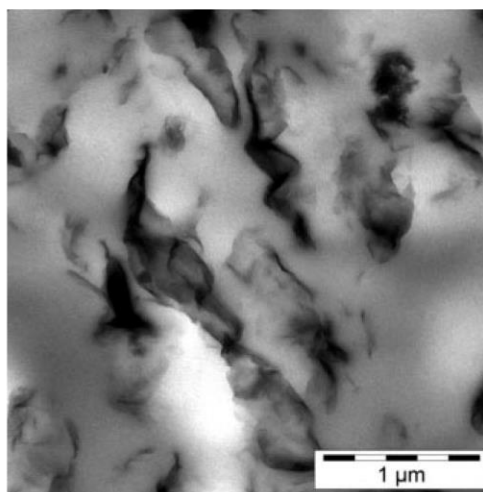


Figure 9 TEM of nanocomposite with 1 : 0.5 compatibilizer ratio.

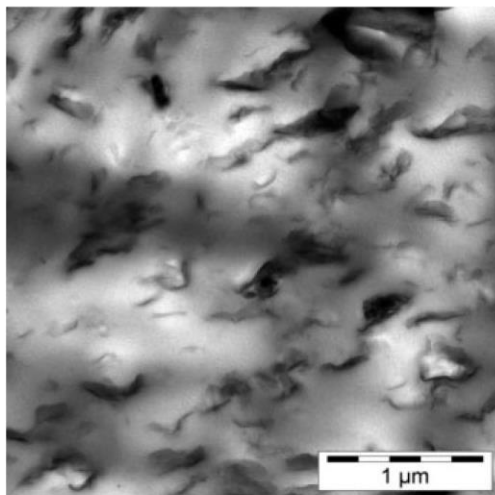


Figure 10 TEM of nanocomposite with 1 : 1 compatibilizer ratio.

compatibilizer admixture leads to a higher interlayer distance of montmorillonite in the nanocomposite system. The same trend was observed concerning the homogeneity of the prepared systems, as can be seen in Figure 8–12. The nanocomposite without compatibilizer revealed a stacking of silicate platelets rather than delamination behavior. On the other hand, a significantly higher level of homogeneity occurs in the 2.5 wt % compatibilizer admixture (Fig. 9), with a maximum at 15 wt % compatibilizer (Fig. 12). It can be clearly seen that results of structural measurements revealed completely other trend when compared with the mechanical and rheological testing. Therefore, grade of delamination in compatibilized PP nanocomposites cannot possess informa-

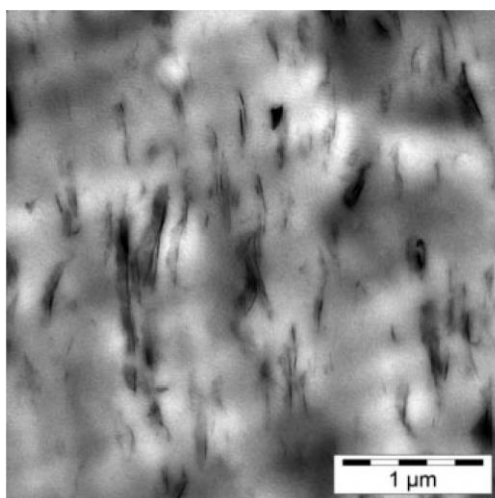


Figure 11 TEM of nanocomposite with 1 : 2.5 compatibilizer ratio.

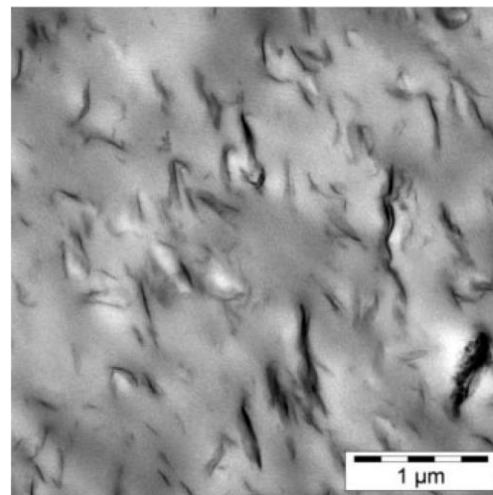


Figure 12 TEM of nanocomposite with 1 : 3 compatibilizer ratio.

tion on the level of polymer reinforcement, as in the case of systems without compatibilizers.^{2–4} Nevertheless, extensional rheology cannot replace conventional measuring techniques and is introduced in this paper only as a possibility of fast reinforcement estimation in the filled polymer systems.

CONCLUSIONS

The PP-PPMA-nanoclay system was investigated to find the optimum amount of compatibilizer. Although X-ray scattering and TEM revealed an increase in silicate dispersion with an increase in compatibilizer content, the mechanical and rheological properties of the material reached an optimum at significantly lower amounts of compatibilizer. Therefore, the effective reinforcement in PP-layered silicate nanocomposites cannot be evaluated successfully using only structural characterization methods. It was shown that the results of melt extensional rheometry can be correlated with those of tensile tests in a solid state. In this context, the method could be used as a fast, accurate, and cheap way to estimate the reinforcement in polymer nanocomposites. From industrial point of view, extensional rheometry could be employed on-line in the processing line and, subsequently, control and dose composite components in the adequate proportion directly during compounding. In the case of PP nanocomposites, an optimum compatibilizer content can also be assessed by this technique. However, it is necessary to measure this optimum each time by variation in PP, compatibilizer or filler type.

The authors thank Dr. Tung Pham, Borealis, Inc., Linz, for cooperation within the Nanocomp cluster.

References

1. Ray, S. S.; Okamoto, M. *Prog Polym Sci* 2003, 28, 1539.
2. Kracalik, M.; Mikesova, J.; Puffr, R.; Baldrian, J.; Thomann, R.; Friedrich, C. *Polym Bull* 2007, 58, 313.
3. Kracalik, M.; Studenovskiy, M.; Mikesova, J.; Sikora, A.; Thomann, R.; Friedrich, C.; Fortelny, I.; Simonik J. J. *Appl Polym Sci* 2007, 106, 926.
4. Kracalik, M.; Studenovskiy, M.; Mikesova, J.; Kovarova, J.; Sikora, A.; Thomann, R.; Friedrich, C. *J Appl Polym Sci* 2007, 106, 2092.
5. Gilman, J. W.; Kashiwagi, T.; Lichtenhan, J. D. *SAMPE J* 1997, 33, 40.
6. Lee, K. M.; Han, C. D. *Macromolecules* 2003, 36, 7165.
7. Hoffmann, B.; Dietrich, C.; Thomann, R.; Friedrich, C.; Mühlhaupt, R. *Macromol Rapid Commun* 2000, 21, 57.
8. Hoffmann, B.; Kressler, J.; Stöppelmann, G.; Friedrich, C.; Kim, G. M. *Colloid Polym Sci* 2000, 278, 629.
9. Sanchez-Solis, A.; Garcia-Rejon, A.; Manero, O. *Macromol Symp* 2003, 192, 281.
10. Sanchez-Solis, A.; Romero-Ibarra, I.; Estrada, M. R.; Calderas, F.; Manero, O. *Polym Eng Sci* 2004, 44, 1094.
11. Solomon, M. J.; Almusallam, A. S.; Seefeldt, K. F.; Somwangth-anaroj, A.; Varadan, P. *Macromolecules* 2001, 34, 1864.
12. Hyun, Y. H.; Lim, S. T.; Choi, H. J.; Jhon, M. S. *Macromolecules* 2001, 34, 8084.
13. Ray, S. S.; Yamada, K.; Okamoto, M.; Ueda, K. *Polymer* 2003, 44, 857.
14. Incarnato, L.; Scarfato, P.; Scatteia, L.; Acierno, D. *Polymer* 2004, 45, 3487.
15. Lepoittevin, B.; Devalckenaere, M.; Pantoustier, N.; Alexandre, M.; Kubies, D.; Calberg, C.; Jérôme, R.; Dubois, P. *Polymer* 2002, 43, 4017.
16. Lee, K. M.; Han, C. D. *Polymer* 2003, 44, 4573.
17. Kotsilkova, R. *Mechanics Time-Dependent Mater* 2002, 6, 283.
18. Krishnamoorti, R.; Giannelis, E. P. *Macromolecules* 1997, 30, 4097.
19. Kim, T. H.; Jang, L. W.; Lee, D. C.; Choi, H. J.; Jhon, M. W. *Macromol Rapid Commun* 2002, 23, 191.
20. Gelfer, M.; Song, H. H.; Liu, L.; Avila-Orta, C.; Yang, L.; Si, M.; Hsiao, B. S.; Chu, B.; Rafailovich, M.; Tsou, A. H. *Polym Eng Sci* 2002, 42, 1841.
21. Wagener, R.; Reisinger, T. J. G. *Polymer* 2003, 44, 7513.
22. Lim, S. T.; Hyun, Y. H.; Choi, H. J.; Jhon, M. S. *Polym Prepr* 2001, 42, 640.
23. Laske, S.; Kracalik, M.; Gschweidl, M.; Langecker, G. R. *International Conference Polymermischungen 2007*, March 28–29, Bad Lauchstädt, Germany, 2007, Proceed; p 20.
24. Kracalik, M.; Laske, S.; Gschweidl, M.; Feuchter, M.; Maier, G.; Pinter, G.; Friesenbichler, W.; Langecker, G. R. *International Conference NanoEurope 2007*, September 11–13, 2007, St. Gallen, Switzerland, Proceed; p 13–14.
25. Laske, S. *Improvement of the Rheological Properties of Unbranched Polypropylene with Nano-Particles with Regard to Foam Extrusion*, M.Sc. Thesis, University of Leoben, 2005.
26. Gschweidl, M. *Assembling and Implementing a Line for Producing Exfoliated Nanocomposites*, M.Sc. Thesis, University of Leoben, 2007.
27. Tong, G. S.; Liu, T.; Hu, G. H.; Hoppe, S.; Zhao, L.; Yuan, W. K. *Chem Eng Sci* 2007, 62, 5290.
28. Koo, C. M.; Kim, J. H.; Wang, K. H.; Chung, I. J. *J Polym Sci Part B: Polym Phys* 2005, 43, 158.
29. Wang, K. H.; Xu, M.; Choi, Y. S.; Chung, I. J. *Polym Bull* 2001, 46, 499.
30. Göttfert Ltd. Buchen, Germany. Available at: <http://www.goettfert.com>.
31. Rheotens 71.97. Technical Documentation; Göttfert Ltd.: Germany, 1998.
32. Balta-Calleja, F. J.; Vonk, C. G. *X-ray Cattering of Synthetic Polymers*; Elsevier: Amsterdam, 1989.
33. Kim, D. H.; Fasulo, P. D.; Rodgers, W. R.; Paul, D. R. *Polymer* 2007, 48, 5308.

2.3.3 Manuscript 13

“Effect of the Mixture Composition on Shear and Extensional Rheology of Recycled PET and ABS Nanocomposites”

Kracalik, Milan; Laske, Stephan; Witschnigg, Andreas; Holzer, Clemens (2012): In: *Macromol. Symp.* 311 (1), S. 33–40. DOI: 10.1002/masy.201000122.

Using knowledge from manuscript 12 (correlation between extensional rheometry and mechanical testing), different analyses of data from rotational rheometry were presented and compared with data obtained from extensional rheometry for ABS and PET nanocomposites. Evaluation of viscoelastic damping behaviour revealed that the 3D silicate network in polymer melt is very sensitive to shear deformation and after reaching the angular frequency of about 1 rad/s, the original polymer-clay structure in the ABS-R nanocomposite melt persist no more. In the PET-R nanocomposites both, the delamination effect (formation of 3D structure) as well as degradation phenomenon (chain scission, generation of low-molecular products) have been detected by dynamic rheological experiments. Using extensional rheometry, effect of organoclay surface treatment on the melt strength level of different ABS-R as well as PET-R nanocomposites has been investigated. It was shown for ABS nanocomposites that despite very small differences visible in data from rotational rheometry, it was possible to make clear comparison between different samples using data from extensional rheometry. In addition to PP nanocomposites (manuscript 13), suitability of extensional rheometry for reinforcement characterization was further proved for ABS and PET nanocomposites.

Effect of the Mixture Composition on Shear and Extensional Rheology of Recycled PET and ABS Nanocomposites

Milan Kracalik,* Stephan Laske, Andreas Witschnigg, Clemens Holzer

Summary: Recycled PET as well as ABS - organomodified montmorillonite nanocomposites were prepared via melt compounding in a counter-rotating twin screw extruder. The topological changes in polymer matrices as dependency on clay modification have been evaluated from dynamic experiments in the shear flow using low amplitude oscillatory measurements. Flow characteristics of all studied organoclay nanocomposites showed shear-thinning behavior at low frequencies. Filling of PET with some organoclays led to degradation reactions, which were reflected by lower magnitudes of viscosity and storage modulus in the range of higher frequencies as compared to unfilled polymer matrix. On the contrary, no degradation during the processing of different organoclays with recycled ABS has been observed.

Keywords: acrylonitrilbutadienestyren; elongation flow; nanocomposites; polyethyleneterephthalate; rheology; shear flow

Introduction

Nanotechnology was introduced as a new method of improvement of polymer properties in 1995. The technology involves not only incorporation of nanosized particles into the polymer but, more importantly, investigation of interactions between the polymer matrix and the enormously large nanofiller surface.^[1] Especially for polymer/clay nanocomposites, the surface effects are responsible for improvement of barrier, mechanical and rheological properties, dimensional stability, heat, flame and oxidative resistance. In comparison with traditional fillers (20–40 wt. % loading), 2–5 wt. % filling of layered clays is sufficient to achieve analogous material improvement.^[2,3] Addition of nanoscaled fillers to recycled polymers represents a promising possibility of properties

enhancement.^[4–6] Generally, three methods of polymer/clay nanocomposites preparation are used: in situ polymerization, solution mixing and melt mixing.^[7,8] The melt mixing process is technologically much more interesting; nevertheless, satisfactory results with polyethyleneterephthalate matrix have not been achieved. Despite sensitivity of melt rheology to changes in structure of the dispersed nanoparticles in the matrix, rheological experiments have been so far rarely used in investigation and characterization of polymer nanocomposites as compared e.g. to morphological, thermal and mechanical testing. The published rheological studies of polymer/clay systems, concerning mostly nanocomposites with polyamides, confirm the pronounced shear thinning behavior associated with clay loading in the region of low shear rates. The relation between the level of delamination of silicate platelets and formation of a physical network, indicated by secondary G' and G'' plateaus^[1,2] was also published. In our previous work, we established extensional rheology as a fast

Institute of Polymer Processing, Montanuniversitaet Leoben, Otto Gloeckel-Str. 2, 8700 Leoben, Austria
Fax: +43 3842 402 3502;
E-mail: Milan.Kracalik@unileoben.ac.at

method for reinforcement characterization in polymer nanocomposites.^[9,10] We also published that it is possible to correlate data of extensional rheometry with those of shear rheometry.^[11] In this contribution, recycled polyethyleneterephthalate (PET-R) and acrylonitrile-butadiene-styrene (ABS-R) have been chosen from the group of polar polymers in order to study effect of differently modified commercial organoclays on rheological properties of PET-R and ABS-R, respectively. Further motivation for this study was to investigate topological changes (in dependency on filler modification) and their impact on material properties (e.g. melt elasticity, melt strength) of the recycled polymer matrices.

Experimental Part

Preparation of Nanocomposites

Colour-sorted recycled PET (PET-R) as well as recycled ABS (ABS-R) has been used as matrix. Organically modified layered silicates with 6 different surface treatments have been indicated as OST_1–OST_6. For the compounding process, a counter-rotating twin screw extruder Brabender Plasticorder PL2000 using a string die with consequent granulation using a water bath has been employed. The prepared nanocomposites containing 5 wt.% of organoclay were indicated in the same way as the organoclay used.

Preparation of Samples

For the extensional rheometry, the primary granulate obtained from the compounding process has been used. The samples for rotational rheometry have been prepared using the hydraulic vacuum press Collin 200 PV.

Rotational Rheometry

Rheological properties in the shear flow were studied using a Rheometrics RMS-800 rheometer with the cone-plate geometry of 25 mm diameter and controlled gap of 50 μm . Experiments were performed at

180 °C (ABS-R nanocomposites) and 260 °C (PET-R nanocomposites), respectively, under nitrogen (liquid N₂ source) to prevent degradation of samples. The following types of rheological measurements were carried out: (1) dynamic strain sweep test (at angular frequency of 6.28 rad/s) to confirm the linearity of viscoelastic region, (2) dynamic frequency sweep test over a frequency range of 0.1–100 rad/s at the strain 0.01%.

Extensional Rheometry

We have already presented the advantages of polymer nanocomposites reinforcement assessment by melt strength evaluation using Rheotens equipment.^[9,10] The main benefit of Rheotens measurement consists in its simplicity without need of expensive scientific equipment and additional time for specimens preparation (primary granulate obtained from the extrusion process can be used). The principle of this measurement is based on elongation of an extruded string by two or four rotating wheels connected with a displacement sensor. The rotation speed is linearly increased up to when the molten string breaks. In our work, the Göttfert Rheotens 71.97 equipment in a combination with a capillary rheometer has been used.

Results and Discussion

The nanocomposites structure can be assessed by analysis of viscosity curve (shear-thinning effect) in combination with evaluation of the storage modulus curve (G' secondary plateau).^[4–6] In Figure 1-2, complex viscosity magnitudes of ABS-R as well as PET-R nanocomposites in dependency on angular frequency have been plotted. The efficiency of the organoclay filling manifests itself as a significant increase in melt viscosity in the range of low shear rates. At higher frequencies, the complex viscosity of some PET-R nanocomposites decreased below the value of the unfilled matrix with the same processing history as the nanocomposites. It was

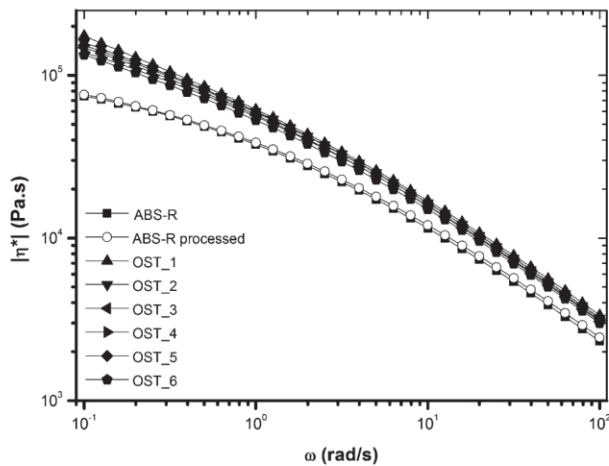


Figure 1.
Complex viscosity of ABS-R nanocomposites.

already found that the most significant degradation during the processing of recycled PET and organoclay is attributed to chemical reactions between the functional groups of organic modifiers, free water of silicate and the polymer chains.^[4] These reactions lead to a decrease in molecular weight, which explains lower viscosity values in nanocomposites at higher shear rates. The level of the mentioned degradation reactions can be

assessed by viscosity decrease of the processed PET-R as compared to original PET-R before processing. On the contrary, no degradation during the processing of ABS-R nanocomposites was detected because of identical viscosity curves of primary ABS-R and processed ABS-R, respectively.

The melt elasticity is reflected by storage modulus curves (Figure 3, 4). Compared to the unfilled polymer matrices, all nano-

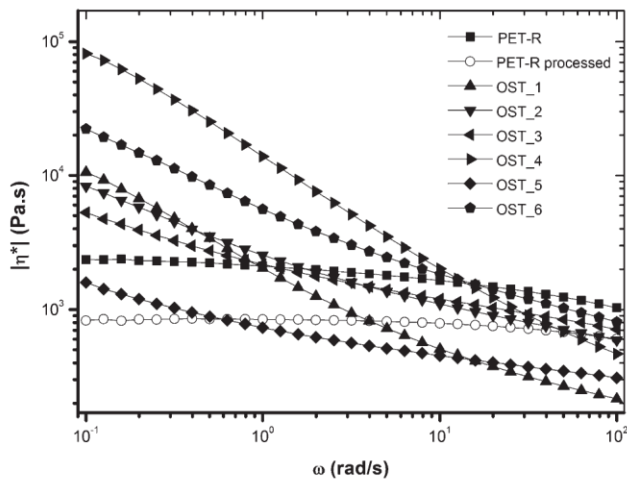


Figure 2.
Complex viscosity of PET-R nanocomposites.

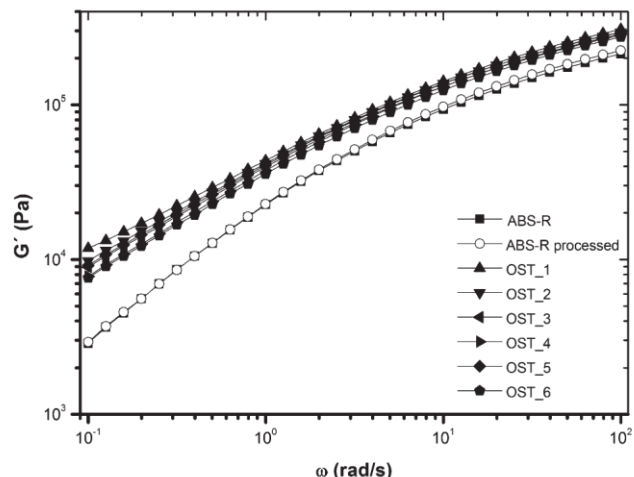


Figure 3.
Storage modulus of ABS-R nanocomposites.

composites show significant increase in melt elasticity at lower frequencies. In the range of higher shear rates, the melt elasticity of some PET-R nanocomposites decreased below the value of the unfilled PET-R matrix due to degradation mechanism described hereinbefore. The OST_1 nanocomposite with ABS-R matrix as well as all PET-R nanocomposites revealed a moderate rubber-like behavior which is indicated as G' secondary plateau in the

range of low frequencies. This secondary plateau indicates the formation of a network structure (delamination) of silicate layers in nanocomposites.^[12-14] The van Gurp-Palmen (vGP) plot as a typical dependency of loss angle δ on complex modulus $|G^*|$ has been used in order to evaluate the topological structures of polymers (Figure 5, 6). The vGP plot is temperature invariant and provides a method to check for the time temperature

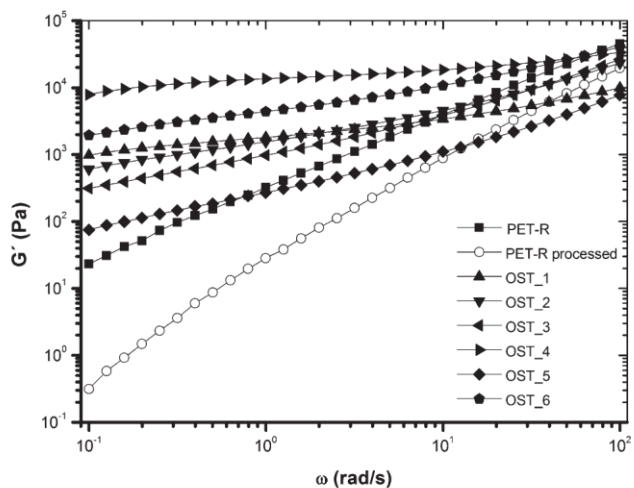


Figure 4.
Storage modulus of PET-R nanocomposites.

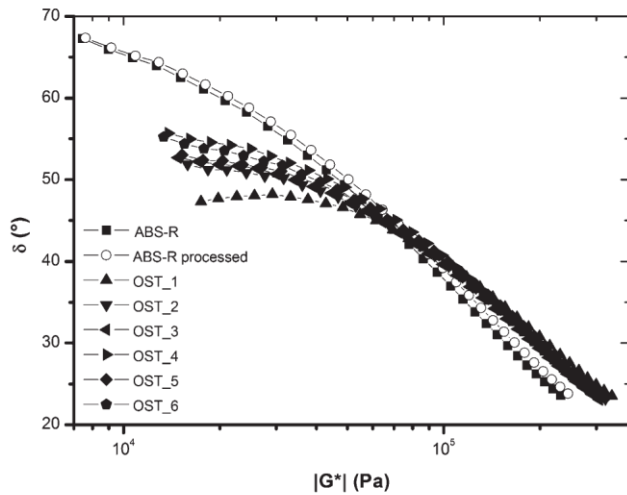


Figure 5. Van Gorp-Palmen plot of ABS-R nanocomposites.

superposition principle.^[15-17] In Figure 5-6, this type of dependency is plotted for nanocomposites prepared using ABS-R and PET-R, respectively. All the prepared nanocomposites show significant topological deviation from “ideal behavior” represented by unfilled polymer matrices. The ABS-R/OST_1 and PET-R/OST_4 nanocomposites showed the highest structural deviations from those of unfilled matrices,

which can be attributed to highest level of silicate delamination as compared to mixtures using other surface treatments.

In order to describe the viscoelastic damping behaviour of the prepared nanocomposites, phase shift δ in dependency on angular frequency has been plotted (Figure 7, 8). The curves of ABS-R nanocomposites are similar to those of vGP and confirm formation of differently

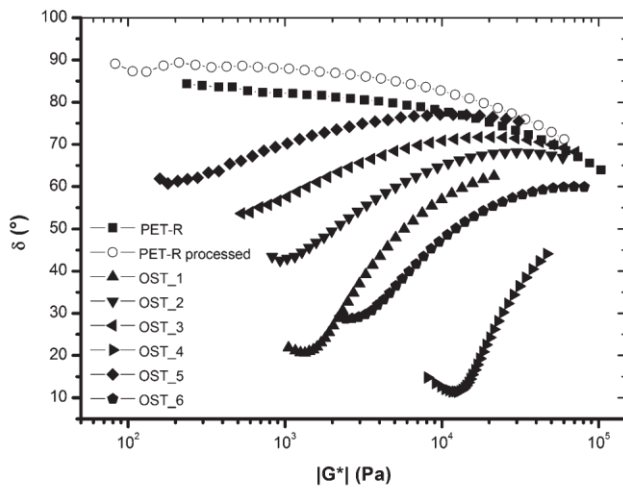


Figure 6. Van Gorp-Palmen plot of PET-R nanocomposites.

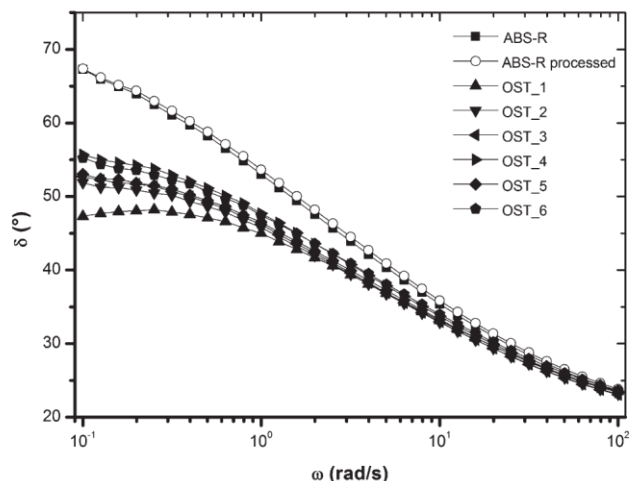


Figure 7.
Phase shift of ABS-R nanocomposites.

organized structures (specific combination of agglomerated, delaminated and exfoliated structure) depending on surface modification of organoclay. It can be clearly seen that the 3D silicate network is very sensitive to shear deformation and after reaching the angular frequency of about 1 rad/s, the original spatial structure in the ABS-R nanocomposite melt persist no more. In the range of higher frequencies, the 3D disordered structure is going to disrupt and alignment of silicate layers in the flow direction occurs. Considering

damping characteristics of the PET-R nanocomposites, a complex behavior in the whole range of applied frequencies was revealed because both delamination effect (formation of 3D structure) as well as degradation phenomenon (chain scission, generation of low-molecular products) is reflected by the values of phase angle.

In Figures 9, 10, the melt strength level of different nanocomposites in dependency on surface treatment is plotted. The 3D physical network made of silicate platelets and polymer matrix depends on the level of clay

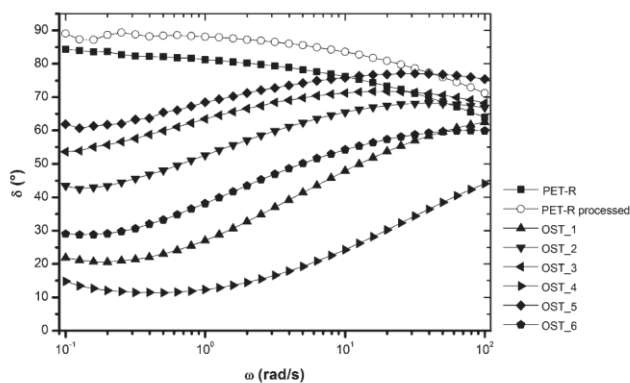


Figure 8.
Phase shift of PET-R nanocomposites.

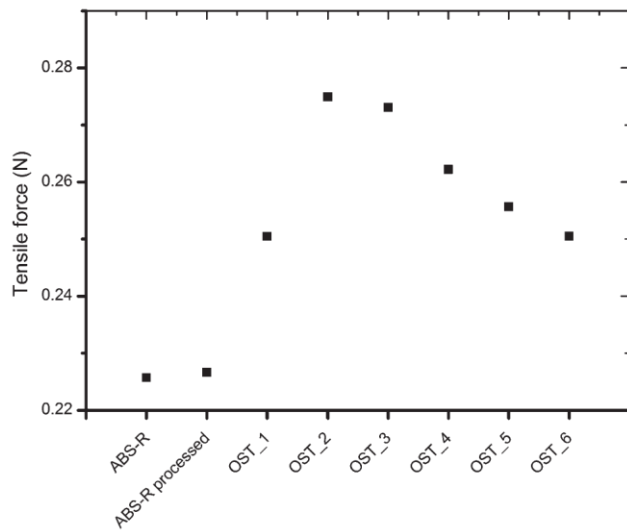


Figure 9.
Melt strength level of ABS-R nanocomposites.

delamination.^[12-14] High delamination level together with rigid 3D-physical network results in high material reinforcement reflected by an increase in melt strength. It is obvious that all the prepared nanocomposites revealed significant increase in the melt strength as compared to unfilled polymer

matrices. The highest reinforcement in ABS-R as well as PET-R nanocomposites has been achieved with the OST_2 and OST_3 organoclays, respectively. On the other hand, no significant differences in melt strength level between original and processed polymer matrices have been found.

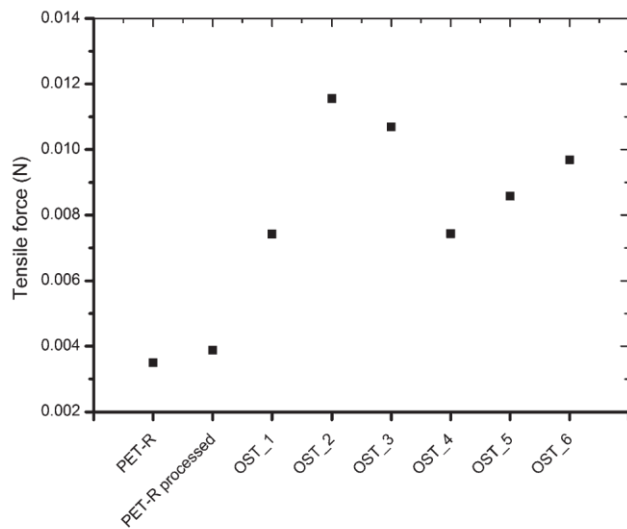


Figure 10.
Melt strength level of PET-R nanocomposites.

Conclusion

ABS-R as well as PET-R nanocomposites have been prepared using different organic surface modifications of layered silicate and tested by shear as well as extensional rheometry. Evaluation of viscoelastic damping behaviour revealed that the 3D silicate network in polymer melt is very sensitive to shear deformation and after reaching the angular frequency of about 1 rad/s, the original polymer-clay structure in the ABS-R nanocomposite melt persists no more. In the PET-R nanocomposites both, the delamination effect (formation of 3D structure) as well as degradation phenomenon (chain scission, generation of low-molecular products) have been detected by dynamic rheological experiments. Using Rheotens equipment, effect of organoclay surface treatment on the melt strength level of different ABS-R as well as PET-R nanocomposites has been investigated. In order to verify the formation of specific spatial structures in dependency on different organoclay surface treatment conventional morphological methods (e.g. X-ray diffraction, electron microscopy) will be employed in the future work.

- [1] K. M. Lee, C. D. Han, *Macromolecules* **2003**, 36, 7165.
 [2] S. S. Ray, M. Okamoto, *Prog. Polym. Sci.* **2003**, 28, 1539.

- [3] H. Olphen, *Clay Colloid Chemistry*, New York Wiley, **1977**.
 [4] M. Kracalik, J. Mikesova, R. Puffr, J. Baldrian, R. Thomann, C. Friedrich, *Polym. Bull.* **2007**, 58, 313.
 [5] M. Kracalik, M. Studenovsky, J. Mikesova, A. Sikora, R. Thomann, C. Friedrich, I. Fortelny, J. Simonik, *J. Appl. Polym. Sci.* **2007**, 106(2), 926.
 [6] M. Kracalik, M. Studenovsky, J. Mikesova, J. Kovarova, A. Sikora, R. Thomann, C. Friedrich, *J. Appl. Polym. Sci.* **2007**, 106(3), 2092.
 [7] J. F. Lee, M. M. Mortland, C. T. Chiou, D. E. Kile, S. A. Boyd, *Clays Clay Miner.* **1990**, 38, 113.
 [8] J. W. Gilman, A. B. Morgan, R. H. Harris, P. C. Trulove, H. C. DeLong, T. E. Sutto, *Polym. Mater. Sci. Eng.* **2000**, 83, 59.
 [9] S. Laske, M. Kracalik, M. Gschweidl, M. Feuchter, G. Maier, G. Pinter, R. Thomann, W. Friesenbichler, G. R. Langecker, *J. Appl. Polym. Sci.*, **2009**, 111, 2253.
 [10] M. Kracalik, S. Laske, M. Gschweidl, W. Friesenbichler, G. R. Langecker, *J. Appl. Polym. Sci.*, **2009**, 113, 1422.
 [11] M. Kracalik, S. Laske, A. Witschnigg, C. Holzer, *Elongational and shear flow in polymer-clay nanocomposites measured by on-line extensional and off-line shear rheometry*, AERC 2010, Annual European Rheology Conference, Gothenburg, Sweden, April 7–9 **2010**.
 [12] R. Krishnamoorti, E. P. Giannelis, *Macromolecules*, **1997**, 30, 4097.
 [13] S. A. Khan, R. K. Prud'homme, *Rev. Chem. Eng.*, **1987**, 4, 205.
 [14] R. Krishnamoorti, R. A. Vaia, E. P. Giannelis, *Chem. Mater.*, **1996**, 8, 1728.
 [15] M. Van Gurp, J. Palmen, *Rheol. Bull.*, **1998**, 67, 5.
 [16] S. Trinkle, C. Friedrich, *Rheol. Acta*, **2001**, 40, 322.
 [17] S. Trinkle, P. Walter, C. Friedrich, *Rheol. Acta*, **2002**, 41, 103.

2.3.4 Manuscript 14

“Elongational and shear flow in polymer-clay nanocomposites measured by on-line extensional and off-line shear rheometry”

Kracalik, Milan; Laske, Stephan; Witschnigg, Andreas; Holzer, Clemens (2011): In: Rheol Acta 50 (11-12), S. 937–944. DOI: 10.1007/s00397-011-0545-2.

Using knowledge from manuscripts 12 and 13, different attempts for correlation between data of shear and extensional rheometry were tested. It was found out that inverse parameter to loss factor ($\tan \delta$) measured by rotational rheometry can be effectively used for description of reinforcement in polymer nanocomposites, similarly to melt strength level measured by extensional rheometry. In order to reduce the values of $\cot \delta$ to one representative magnitude for one nanocomposite sample (cumulative storage factor, CSF), G' as well as G'' values of each sample were integrated over the specific frequency range as follows:

$$CSF = \frac{\int_{0.1 \text{ rad/s}}^{628 \text{ rad/s}} G' / \int_{0.1 \text{ rad/s}}^{628 \text{ rad/s}} G''$$

Plotting the CSF values together with melt strength level of nanocomposites in dependency on screw speed, the same trends for results of extensional as well as shear rheometry have been found. In this way, it was shown that CSF can be correlated with values of melt strength level, i.e. that 3D physical network in polymer nanocomposites is reflected in the same way in both shear as well as elongational flow.

Elongational and shear flow in polymer-clay nanocomposites measured by on-line extensional and off-line shear rheometry

Milan Kracalik · Stephan Laske ·
Andreas Witschnigg · Clemens Holzer

Received: 25 June 2010 / Revised: 15 December 2010 / Accepted: 14 March 2011 / Published online: 17 May 2011
© Springer-Verlag 2011

Abstract Rheological behaviour of polymer nanocomposites has been usually characterized by rotational as well as capillary rheometry, which are both time and cost consuming. We have already published that reinforcement in polymer-clay nanocomposites can be estimated very fast using extensional rheometer in combination with a capillary rheometer. It has been proven that the magnitude of melt strength can be correlated with that of tensile strength, i.e. 3D physical network made of layered silicate and polymer matrix, which is responsible for material reinforcement, can be monitored directly using extensional rheometry. Therefore, additional time for samples preparation by press or injection moulding as well for long measurements by tensile testing is not required any more. In this contribution, results of extensional rheometry measured directly during compounding process are presented. In this manner, further reduction in time required for material characterization has been achieved. The samples have been prepared by advanced compounding using a melt pump and special screw geometries. With the use of on-line extensional rheometry and off-line rotational rheometry, different nanocomposites have been tested and the effect of processing conditions (screw speed and geometry in the twin-screw extruder) on elongational and viscoelastic properties has been investigated. It has been found that the level of melt strength mea-

asured by extensional rheometry correlates with a high accuracy with dynamic rheological data measured by rotational rheometry. It was hereby confirmed that the network structure made of silicate platelets in polymer melt is reflected in both elongational and shear flow in the same way.

Keywords Nanocomposites · Compounding · Elongation flow · Shear flow · Polymer · Clay

Introduction

Polymer-clay nanocomposites have been intensively investigated because of the improvements in processing as well as use properties. Consequently, tailored materials (Ray and Okamoto 2003; Ray et al. 2003) based on virgin as well as recycled polymers can be prepared (Kracalik et al. 2007a, b, c, d). The improvement in material properties due to nanoclay addition has usually been evaluated using a combination of morphological (X-ray diffraction [XRD], transmission electron microscopy), mechanical (tensile testing) and sometimes also rheological (rotational rheometry) analyses. However, these conventional methods require expensive scientific instruments as well as additional sample preparation and characterization times. Generally, intercalated and delaminated (partially exfoliated) polymer nanocomposites reveal significant enhancements in their properties—higher elastic modulus, tensile strength, thermal resistivity, lower gas and liquid permeability, reduced flammability (Gilman et al. 1997) and improved rheological properties (e.g. higher melt strength)—compared to the unfilled polymer matrix (Ray et al. 2003). High level of reinforcement due to

This paper was presented at the Annual European Rheology Conference, April 7–9 2010, in Göteborg, Sweden.

M. Kracalik (✉) · S. Laske · A. Witschnigg · C. Holzer
Institute of Polymer Processing, Montanuniversitaet
Leoben, Otto Gloeckel-Str. 2, 8700 Leoben, Austria
e-mail: Milan.Kracalik@unileoben.ac.at

the addition of the layered silicates results from their large active surface area (in the case of montmorillonite 700–800 m²/g) (Lee and Han 2003a, b). In the case of highly dispersed systems, a 3D physical network is achieved, formed by the silicate platelets and the polymer chains. This phenomenon can be investigated by analyzing the melt elasticity using rotational rheometry (Ray et al. 2003; Kracalik et al. 2007a, b, c, d; Hoffmann et al. 2000a, b; Sanchez-Solis et al. 2003, 2004; Solomon et al. 2001; Hyun et al. 2001; Incarnato et al. 2004; Lee and Han 2003a, b; Kotsilkova 2002; Krishnamoorti and Giannelis 1997; Kim et al. 2002; Gelfer et al. 2002; Wagener and Reisinger 2003). A fast way to evaluate this network effect is using elongational rheometry (Laske et al. 2009; Kracalik et al. 2007a, b, c, d; 2009; Göttfert Ltd., Buchen, Germany, <http://www.goettfert.com>), which provides information about the melt strength.

As we have already presented (Laske et al. 2009; Kracalik et al. 2007a, b, c, d), the effective level of reinforcement in polypropylene nanocomposites cannot be based solely on an evaluation of the delamination level (increase in interlayer distance) determined by XRD. The simple rule “higher delamination leads to an improvement in material properties” is not always valid because of different influence of dispersion grade on different material properties. For example, to improve barrier and flame properties a high delamination level is favoured. On the other hand, rather intercalated structure is preferred to achieve the highest improvement in mechanical properties. In the real polymer-clay system, intercalated as well as delaminated structure is present. The final combination of these structures is responsible for the material reinforcement in the polymer matrix and can be monitored by extensional rheometry (Laske et al. 2009). Further advantage of elongational experiments is usage of primary granulate: no preparation of additional samples is necessary. In this paper, we extended elongational rheology on polymer nanocomposites to be performed on-line during the compounding process using a by-pass die. Therefore, this fast method of reinforcement evaluation can now be applied industrially. In order to investigate complex rheological behaviour in polymer nanocomposites, extensional as well as rotational rheometry has been applied and results of different evaluation approaches have been discussed.

Materials

The isotactic polypropylene homopolymer HC600TF (MFR 2.8 g/10 min; 230°C/2.16 kg) used for the prepa-

ration of nanocomposites was supplied by Borealis Inc., Linz, Austria. The used nanofiller (montmorillonite intercalated with dimethyl distearyl ammonium chloride) with the commercial name of Nanofil 5 was supplied by Rockwood Clay Additives Ltd., Moosburg, Germany. The compatibilizer Scona TPPP 2112 FA (polypropylene grafted with 1 wt.% of maleic acid anhydride, MFR 14.8 g/10 min; 230°C/2.16 kg) was supplied by Kometra Ltd., Schkopau, Germany.

Experimental

Preparation of nanocomposites

For the compounding process, a co-rotating twin screw extruder Theysohn TSK30/40D (Theysohn Extrusionstechnik Ltd., Korneuburg, Austria) using 10 barrel segments and a string die has been employed. The feed rate was set at 10 kg/h with the screw speed variation between 75 and 300 rpm. The temperature profile is described in Table 1.

As listed in Table 2, different nanocomposite systems have been prepared by advanced compounding (Kracalik et al. 2009) using the Extrex SP gear pump (Pump Systems Textron Inc., Oberglatt, Switzerland). The melt pump has been adjusted to negative pressure gradient (Δp negative, $p_{\text{outlet}} - p_{\text{inlet}} = -100$ bar). In this way, a back pressure of polymer melt up to the ninth extruder segment (approximately 30–40 cm before the melt pump) has been achieved. The organoclay as well as compatibilizer content has been fixed to 5 wt.% according to our previous investigation (Laske et al. 2009). High as well as low shear screw geometries (indicated as G1 and G2, respectively) have been applied.

Preparation of samples

For the extensional rheometry, the primary granulate obtained from the compounding process has been used. The samples for rotational rheometry have been prepared using the hydraulic vacuum press Collin 200 PV (Dr. Collin Ltd., Ebersberg, Germany). The optimal press profile (Table 3) has been chosen according to light microscope analysis of samples pressed at

Table 1 Temperature profile in different extruder sections

Section	1	2	3	4	5	6	7	8	9	10
Temperature (°C)	Cool	160	180	190	200	200	200	200	200	200

Table 2 Samples' description

Melt pump adjustment	Screw speed (rpm)	Screw geometry: $D = 30 \text{ mm}$, $L/D = 40$
Δp negative	75	G1 (high shear)
	100	
	150	
	200	
	300	
	75	G2 (low shear)
	100	
	150	
	200	
	300	

different temperature, pressure and time conditions. This procedure has been performed in order to ensure homogeneous melting of granulate in the press mould.

Extensional rheometry

We have already presented the advantages of polymer nanocomposite reinforcement assessment by melt strength evaluation using Rheotens equipment (Laske et al. 2009; Göttfert Ltd., Buchen, Germany, <http://www.goettfert.com>). The main benefit of Rheotens measurement consists in its simplicity without the need for expensive scientific equipment and additional time for specimens' preparation (primary granulate obtained from the extrusion process can be used). The principle of this measurement is shown in Fig. 1. It is based on elongation of an extruded string by two or four rotating wheels connected to a displacement sensor. The rotation speed is linearly increased up to the time when the molten string breaks. In our work, the Rheotens 71.97 equipment (Göttfert Ltd., Buchen, Germany) has been used. The Rheotens equipment has been set by applying wheel acceleration of 60 mm/s^2 and gap between wheels of 0.6 mm . In order to compare the melt strength level of different nanocomposites (revealing different magnitudes of v_b), the tensile force at a draw rate of 300 mm/s has been chosen as a comparative value. The data have been evaluated from at least three measurements for each sample and then average data have been plotted.

Table 3 Press profile

Temperature ($^{\circ}\text{C}$)	200	200	200	200	50
Pressure (bar)	1	20	1	100	150
Time (min)	20	5	5	7	7

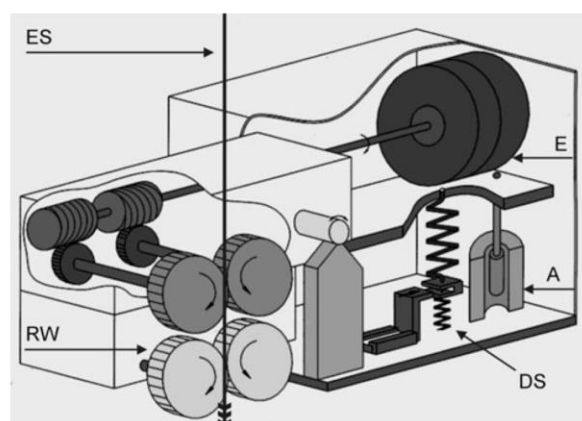


Fig. 1 Principle of Rheotens measurement. *ES* extruded string, *RW* rotating wheels, *E* engine, *A* attenuator, *DS* displacement sensor. (Adapted from Göttfert Ltd., Buchen, Germany, <http://www.goettfert.com>)

Rotational rheometry

Rheological properties in the shear flow were studied using a Physica MCR 501 rheometer (Anton Paar Ltd., Graz, Austria) with a cone–plate geometry of 25 mm in diameter and automatically controlled gap of $50 \mu\text{m}$. The samples' thickness was 0.7 mm . Experiments were performed at 210°C under nitrogen to prevent degradation of the samples. The following types of rheological measurements were carried out: (1) dynamic strain sweep test (at angular frequency of 6.28 rad/s) to confirm the linearity of the viscoelastic region, and (2) dynamic frequency sweep test over a frequency range of $0.1\text{--}500 \text{ rad/s}$, at a strain of 0.01% . The data have been evaluated from at least three measurements for each sample and then average data have been plotted.

Results and discussion

The silicate platelets form different levels of 3D physical network in the polymer matrix depending on their structure (intercalated or exfoliated). The different physical crosslinking and bonding between polymer chains and organoclay result in a diversity of viscoelastic response. In the case of PP-g-MA compatibilized nanocomposites, chemical reactions between quaternary ammonium cations and maleic acid anhydride take place and facilitate silicate delamination (Dintcheva et al. 2009). Therefore, individual nanoparticles act as entanglement or crosslinking sites and raise the extensional stiffness of the composite. Depending on the degree of dispersion, this change is more or less pronounced compared to the unfilled polymer and can be

monitored by elongational rheology (Laske et al. 2009). In Fig. 2, the melt strength level of different nanocomposites in dependence on screw speed and screw geometry is plotted. It is obvious that, for a specific screw geometry, a critical screw speed with optimal shear rate as well as residence time occurs. For G2 geometry, this critical screw speed is shifted from 100 rpm (G1) up to 150 rpm, because no kneading blocks in G2 geometry have been assembled and the shear rate acts proportionally to the screw speed. That means, with higher screw speed higher shear energy is applied to the melt and a lower amount of kneading blocks is required. As a consequence of increased screw speed, the residence time is shortened. This explains generally reduction in melt strength when applying screw speed higher than 100 rpm (G1) and 150 rpm (G2), respectively, because silicate dispersion in polymer melt is a diffusion process as well and appropriate residence time is required. Comparison of the shear energy applied during compounding showed that nanocomposites prepared using low-shear screw geometry had higher level of the melt strength than those prepared with high-shear screw geometry.

With the aim to correlate extensional rheology with the results of shear rheometry, crossover moduli (G_c : $G' = G''$) of different nanocomposites have been compared. As Zeichner et al. (Zeichner and Patel 1981; Zeichner and Macosko 1982) published for polypropylene melt, the weight average molecular weight (M_w) as well as molecular weight distribution (MWD) and polydispersity index (M_w/M_n) can be evaluated from the shift of crossover modulus G_c . However, no similar empirical correlations could be found in rheological analysis of the prepared nanocomposites.

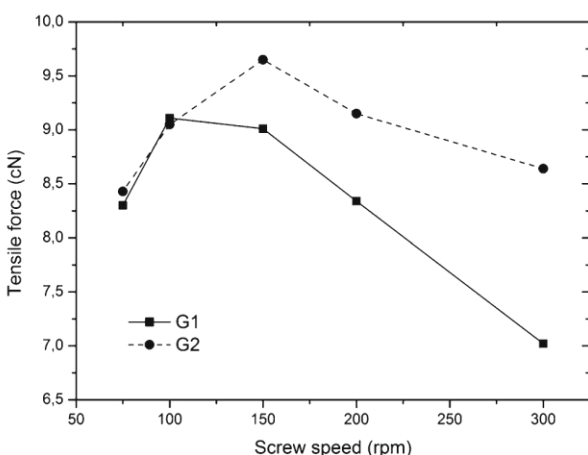


Fig. 2 Melt strength level of nanocomposites prepared by different processing conditions

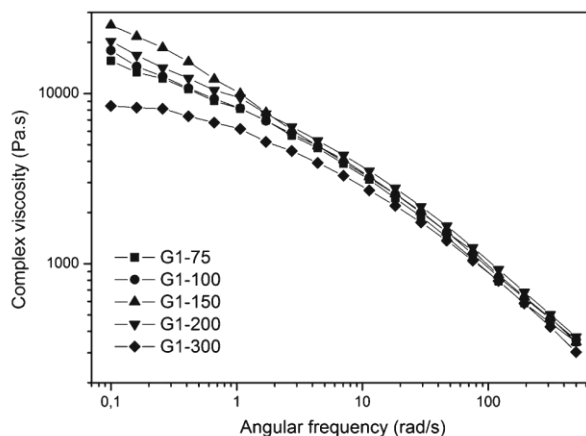


Fig. 3 Complex viscosity of nanocomposites prepared using high-shear screw geometry

The nanocomposite structure can be assessed by analysis of the viscosity curve (shear-thinning effect) in combination with evaluation of the storage modulus curve (G' secondary plateau; Kracalik et al. 2007a, b, c, d). In Figs. 3, 4, 5 and 6, magnitudes of complex viscosity as well as storage modulus in dependence on angular frequency have been plotted. As can be seen from Fig. 3, the systems prepared with high-shear screw geometry revealed pronounced shear-thinning behaviour except for nanocomposites prepared using a screw speed of 300 rpm. This nanocomposite revealed the lowest level of melt strength (Fig. 2) as well. However, the G1-100 system exhibiting the highest melt strength level in the G1 sample group did not show the highest values of complex viscosity. The remaining samples in

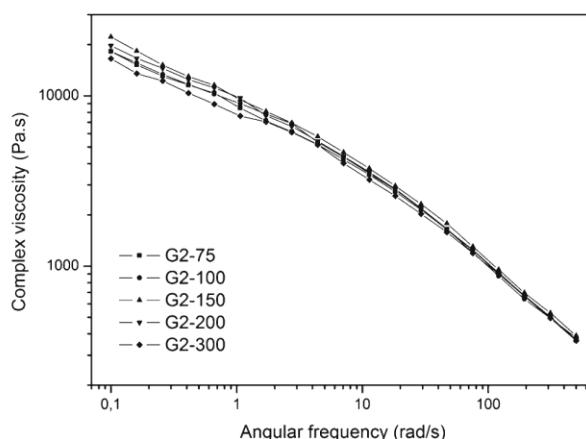


Fig. 4 Complex viscosity of nanocomposites prepared using low-shear screw geometry

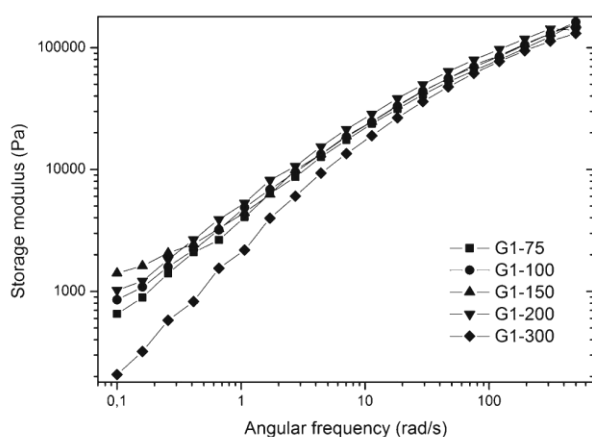


Fig. 5 Storage modulus of nanocomposites prepared using high-shear screw geometry

the G1 group show no correlation between elongational and shear data either. Analogically, the values of storage moduli (Fig. 5) of the G1 samples revealed indication of a G' secondary plateau except for the G1-300 sample. This can be assumed to be a delaminated (partially exfoliated) structure in the G1-75 to G1-200 samples and rather low level of silicate delamination in the G1-300 sample (Kracalik et al. 2007a, b, c, d). In the G2 sample group, the highest values of melt strength level, complex viscosity and storage modulus were exhibited in the G2-150 system, while the lowest values have been found in the G2-300 sample. However, the differences in complex viscosity and storage modulus values within the G2 sample group are not pronounced enough to ensure reliable interpretation. Furthermore,

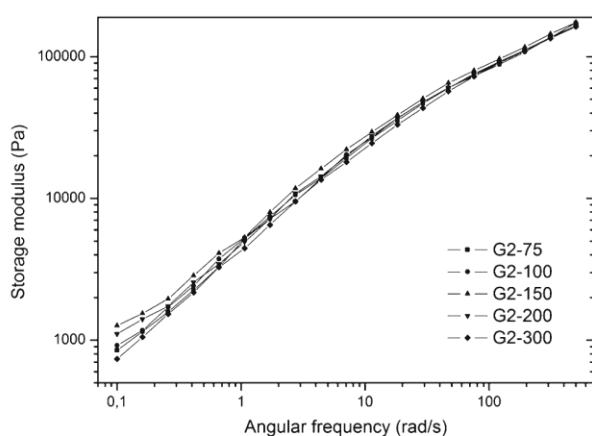


Fig. 6 Storage modulus of nanocomposites prepared using low-shear screw geometry

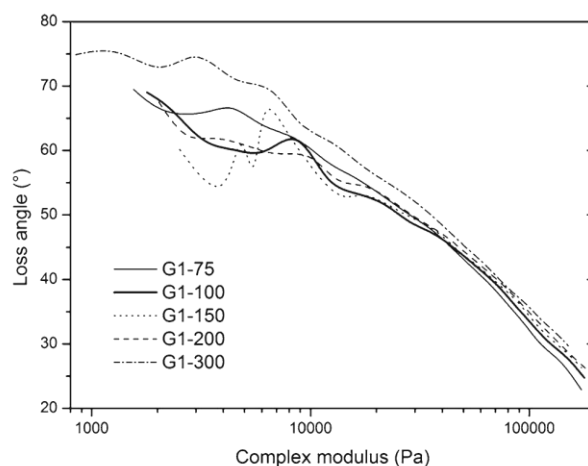


Fig. 7 Van Gorp–Palmen plot of nanocomposites prepared using high-shear screw geometry

it is not possible to correlate elongational data with shear data for the G2-75, G2-100 and G2-200 samples.

The Van Gorp–Palmen (vGP) plot as a typical dependency of loss angle δ on complex modulus $|G^*|$ has been used in order to evaluate the topological structures of polymers. The vGP plot is temperature invariant and provides a method to check for the time temperature superposition principle (Lohse et al. 2002; Schulze et al. 2003; Trinkle and Friedrich 2001; Trinkle et al. 2002; Van Gorp and Palmen 1998). In Fig. 7 and Fig. 8, this type of dependency is plotted for nanocomposites prepared with high and low shear screw geometry, respectively. For the polymer samples with linear chain structure, a typical “V”-shaped

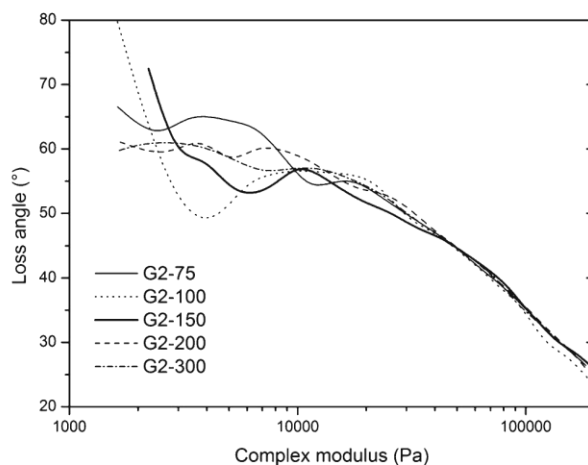


Fig. 8 Van Gorp–Palmen plot of nanocomposites prepared using low-shear screw geometry

curve has been published. With decreasing complex modulus, the values of phase angle reached the minimum followed by further increase until reaching a plateau at 90°. On the contrary, long-chain branched (LCB) polymers exhibited a more or less developed bump between the $|G^*|$ minimum and the 90° plateau (Trinkle et al. 2002). As can be seen in Figs. 7 and 8, all the prepared nanocomposites show a topological structure similar to mentioned LCB polymers with even two or three bumps or peaks, indicating a complex 3D structure made of silicate layers and polymer chains. The curves of systems revealing the highest values of melt strength level (G1–100, G2–150) are highlighted. However, it is difficult to find any direct correlation between elongational data and vGP curves.

In order to describe the viscoelastic damping behaviour of the prepared nanocomposites, phase shift δ in dependence on angular frequency has been plotted (Figs. 9 and 10). The curves are similar to those of vGP and confirm the formation of differently organized structures (specific combination of agglomerated, delaminated and exfoliated structure) depending on variation of screw speed as well as screw geometry. It can be clearly seen that the 3D silicate network is very sensitive to shear deformation and after reaching the angular frequency of about 10 rad/s, the original spatial structure in the nanocomposite melt persists no more.

As the conventional approaches have not resulted in a successful correlation between data of shear and extensional rheology, we have tried a new way to analyse the data of the shear flow. The storage modulus G' reflects the elastic part, while the loss modulus gives information about the viscous part of the dynamic shear

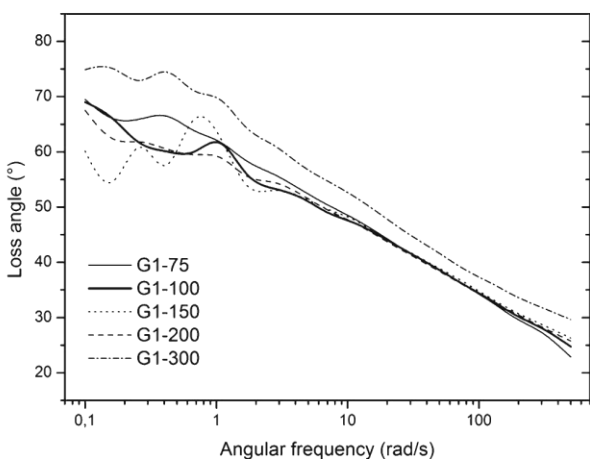


Fig. 9 Phase shift of nanocomposites prepared using high-shear screw geometry

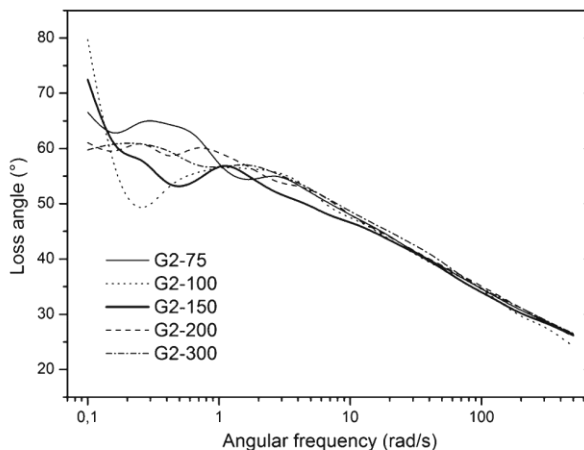


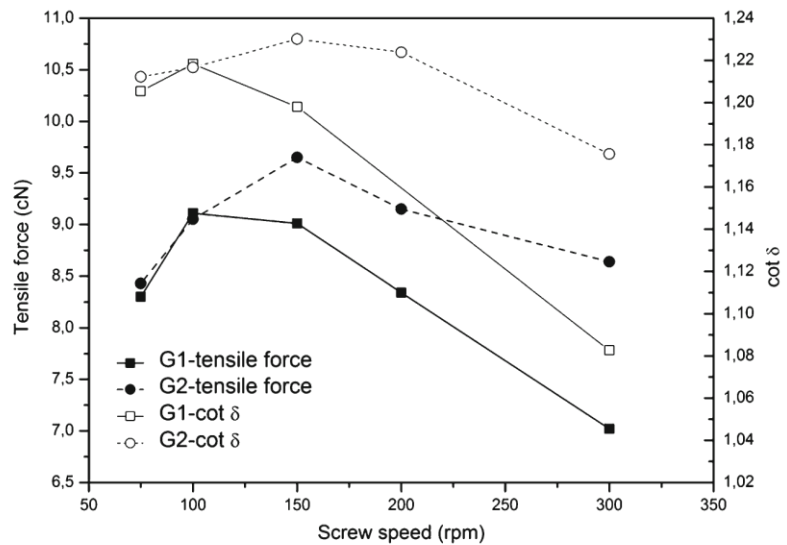
Fig. 10 Phase shift of nanocomposites prepared using low-shear screw geometry

flow. The relation of G''/G' is defined as $\tan \delta$ and describes the damping behaviour of the polymer system. On the contrary, to our knowledge, the G'/G'' ratio ($\cot \delta$) has not been used for rheological evaluation of nanocomposites up to now. Compared to $\tan \delta$, $\cot \delta$ reflects melt rigidity, which can be associated with reinforcement effect of nanostructured filler (combination of chain elasticity with silicate layers' rigidity in the polymer melt). Therefore, it should be possible to correlate the melt strength level (tensile force from extensional rheometry) with melt rigidity ($\cot \delta$). In order to reduce the values of $\cot \delta$ to one representative magnitude for one nanocomposite sample, G' as well as G'' curves have been integrated over the frequency range of 10–100 rad/s (Eq. 1) in order to use only reliable results with a minimal scattering for the evaluation and to neglect the structural changes that occur during the samples' preparation by press moulding. These changes affect rheological results particularly in the range of lower frequencies.

$$\cot \delta = \frac{\int_{10 \text{ rad/s}}^{100 \text{ rad/s}} G'}{\int_{10 \text{ rad/s}}^{100 \text{ rad/s}} G''} \quad (1)$$

As can be seen from Fig. 11, the same trends for tensile force and $\cot \delta$ have been found within the G1 as well as the G2 sample group in the whole range of screw speeds tested. Even the slight differences between the G1–100 and G2–100 samples are reflected by magnitudes of tensile force and $\cot \delta$ in the same way. This is a proof of possibility to correlate tensile strength level measured by extensional rheometry with melt

Fig. 11 Comparison of extensional with shear flow rheology



rigidity measured by shear rheometry. Because of the opportunity to measure extensional rheometry on-line, this method could be extended to provide information about melt strength in elongational flow as well as about melt rigidity in the shear flow directly during the compounding process. This evaluation approach will be tested on higher sample amount (difference in polymer morphology, filler type, processing conditions, etc.) in a future work.

Conclusion

Polypropylene–clay nanocomposites have been prepared using different processing conditions (screw speed and screw geometry) and tested by extensional as well as shear rheometry. Evaluation of viscoelastic damping behaviour revealed that the 3D silicate network in polymer melt is very sensitive to shear deformation and after reaching the angular frequency of about 10 rad/s, the original polymer–clay structure in the nanocomposite melt persists no more. With the use of conventional rheological analysis, no direct correlation between the shear and elongational data has been found. However, the G'/G'' ratio ($\cot \delta$) has been calculated for each nanocomposite sample by integration of storage and loss moduli over the specific frequency range. A plot of the $\cot \delta$ values together with the melt strength level of nanocomposites in dependence on screw speed shows the same trends for results of extensional as well as shear rheometry. In this way, fast assessment of the melt strength in the elongational flow as well as melt rigidity in shear flow could be

performed on-line during the compounding process. In order to verify the new evaluation approach, measurements on a broader sample range (different polymer morphologies, filler type, processing conditions, etc.) will be performed in a future work.

Acknowledgements This research has been supported by the NanoComp–0901 PlaComp1 Project, which is part of the NanoComp research project cluster founded by Austrian Nanoinitiative.

References

- Dintcheva NTZ, Al-Malaika S, La Mantia FP (2009) Effect of extrusion and photo-oxidation on polyethylene/clay nanocomposites. *Polym Degrad Stab* 94(9):1571–1588
- Gelfer M, Song HH, Liu L, Avila-Orta C, Yang L, Si M, Hsiao BS, Chu B, Rafailovich M, Tsou AH (2002) Manipulating the microstructure and rheology in polymer–organoclay composites. *Polym Eng Sci* 42:1841–1851
- Gilman J, Kashiwagi T, Lichtenhan J (1997) Nanocomposites: a revolutionary new flame retardant approach. *Sampe J* 33: 40–46
- Hoffmann B, Dietrich C, Thomann R, Friedrich C, Mülhaupt R (2000a) Morphology and rheology of polystyrene nanocomposites based upon organoclay. *Macromol Rapid Commun* 21:57–61
- Hoffmann B, Kressler J, Stöppelmann G, Friedrich C, Kim GM (2000b) Rheology of nanocomposites based on layered silicates and polyamide-12. *Colloid Polym Sci* 278:629–636
- Hyun YH, Lim ST, Choi HJ, Jhon MS (2001) Rheology of poly(ethylene oxide)/organoclay nanocomposites. *Macromolecules* 34:8084–8093
- Incamato L, Scarfato P, Scatteia L, Acierno D (2004) Rheological behavior of new melt compounded copolyamide nanocomposites. *Polymer* 45:3487–3496
- Kim TH, Jang LW, Lee DC, Choi HJ, Jhon MW (2002) Synthesis and rheology of intercalated polystyrene/Na⁺-

- montmorillonite nanocomposites. *Macromol Rapid Commun* 23:191–195
- Kracalik M, Mikesova J, Puffr R, Baldrian J, Thomann R, Friedrich C (2007a) Effect of 3D structures on recycled PET/organoclay nanocomposites. *Polym Bull* 58:313–319
- Kracalik M, Studenovský M, Mikesova J, Sikora A, Thomann R, Friedrich C, Fortelny I, Simonik J (2007b) Recycled PET nanocomposites improved by silanization of organoclays. *J Appl Polym Sci* 106(2):926–937
- Kracalik M, Studenovský M, Mikesova J, Kovarova J, Sikora A, Thomann R, Friedrich C (2007c) Recycled PET-organoclay nanocomposites with enhanced processing properties and thermal stability. *J Appl Polym Sci* 106(3):2092–2100
- Kracalik M, Laske S, Gschweidl M, Feuchter M, Maier G, Pinter G, Friesenbichler W, Langecker GR (2007d) Invited lecture at international conference NanoEurope 2007, St. Gallen, Switzerland, September 11–13, 2007, Proceed, pp 13–14
- Kracalik M, Laske S, Gschweidl M, Friesenbichler W, Langecker GR (2009) Advanced compounding: extrusion of polypropylene nanocomposites using the melt pump. *J Appl Polym Sci* 113(3): 1422–1428
- Krishnamoorti R, Giannelis EP (1997) Rheology of end-tethered polymer layered silicate nanocomposites. *Macromolecules* 30:4097–4102
- Kotsilkova R (2002) Rheology–structure relationship of polymer/layered silicate hybrids. *Mechanics Time-Dependent Mater* 6:283–300
- Laske S, Kracalik M, Gschweidl M, Feuchter M, Maier G, Pinter G, Thomann R, Friesenbichler W, Langecker GR (2009) Estimation of reinforcement in compatibilized polypropylene nanocomposites by extensional rheology. *J Appl Polym Sci* 111(5):2253–2259
- Lee KM, Han CD (2003a) Rheology of organoclay nanocomposites: effects of polymer matrix/organoclay compatibility and the gallery distance of organoclay. *Macromolecules* 36:7165–7178
- Lee KM, Han CD (2003b) Effect of hydrogen bonding on the rheology of polycarbonate/organoclay nanocomposites. *Polymer* 44:4573–4588
- Lohse DJ, Milner ST, Fetters LJ, Xenidou M, Hadjichristidis N, Mendelson RA, Garcia-Franco CA, Lyon MK (2002) Well-defined, model long chain branched polyethylene: 2. Melt rheological behaviour. *Macromolecules* 35:3066–3075
- Ray SS, Okamoto M (2003) Polymer/layered silicate nanocomposites: a review from preparation to processing. *Progr Polym Sci* 28:1539–1641
- Ray SS, Yamada K, Okamoto M, Ueda K (2003) New polylactide-layered silicate nanocomposites: 2. Concurrent improvements of material properties, biodegradability and melt rheology. *Polymer* 44:857–866
- Sanchez-Solis A, Garcia-Rejon A, Manero O (2003) Production of nanocomposites of PET-montmorillonite clay by an extrusion process. *Macromol Symp* 192:281–292
- Sanchez-Solis A, Romero-Ibarra I, Estrada MR, Calderas F, Manero O (2004) Mechanical and rheological studies on polyethylene terephthalate–montmorillonite nanocomposites. *Polym Eng Sci* 44:1094–1102
- Schulze D, Trinkle S, Mulhaupt R, Friedrich C (2003) Rheological evidence of modifications of polypropylene by β -irradiation. *Rheol Acta* 42:251–258
- Solomon MJ, Almusallam AS, Seefeldt KF, Somwangthanaroj A, Varadan P (2001) Rheology of polypropylene/clay hybrid materials. *Macromolecules* 34:1864–1872
- Trinkle S, Friedrich C (2001) Van Gorp–Palmen plot: a way to characterize polydispersity of linear polymers. *Rheol Acta* 40:322–328
- Trinkle S, Walter P, Friedrich C (2002) Van Gorp–Palmen plot II — classification of long chain branched polymers by their topology. *Rheol Acta* 41:103–113
- Van Gorp M, Palmen J (1998) Time–temperature superposition for polymeric blends. *Rheol Bull* 67:5–8
- Wagener R, Reisinger TJG (2003) A rheological method to compare the degree of exfoliation of nanocomposites. *Polymer* 44:7513–7518
- Zeichner GR, Patel PD (1981) A comprehensive evaluation of polypropylene melt rheology. In: *Proc 2nd world congr chem engng, Montreal*
- Zeichner GR, Macosko CW (1982) On-line viscoelastic measurements for polymer melt processes, vol 28. *SPE ANTEC Tech. Papers*, p 79

2.3.5 Manuscript 15

“Rheology of multiphase polymer systems using novel “melt rigidity” evaluation approach”

Kracalik, Milan (2015): In: AIP Conference Proceedings (1662). DOI: 10.1063/1.4918890.

Continuing the work from manuscript 14, complex LDPE nanocomposites with nanoclay, nano-scaled TiO₂ and compatibilizer were tested by novel rheological analysis approach. The values of $\cot \delta$ were called as storage factor (analogically to commonly used loss factor $\tan \delta$) and the integrated values of $\cot \delta$ were called as cumulative storage factor. Then, further cumulative parameters were calculated (e.g. cumulative complex viscosity, cumulative complex modulus) in order to test different evaluation approaches. The cumulative storage factor plotted over cumulative complex viscosity exhibited high linear dependency and could be directly correlated with trends of storage modulus and complex viscosity curves in terms of dispersion grade association. This was not the case for the plot of cumulative storage factor in dependency on cumulative complex modulus, exhibiting rather lower coefficient of linear regression together with some discrepancies concerning correlation with trends of storage modulus and complex viscosity curves. The cumulative storage modulus in dependency on cumulative complex viscosity revealed high coefficient of linear regression but some discrepancies concerning correlation with trends of storage modulus and complex viscosity curves. However, plot of cumulative storage modulus in dependency on cumulative complex modulus exhibited both high coefficient of linear regression as well as high correlation with trends of storage modulus and complex viscosity curves in terms of dispersion grade association.

Rheology of Multiphase Polymer Systems using Novel “Melt Rigidity” Evaluation Approach

Milan Kracalik^{1, a)}

¹Johannes Kepler University Linz, Institute of Polymer Science, Altenberger Str. 69, 4040 Linz, Austria

^{a)}Corresponding author: Milan.Kracalik@jku.at

Abstract. Multiphase polymer systems like blends, composites and nanocomposites exhibit complex rheological behaviour due to physical and also possibly chemical interactions between individual phases. Up to now, rheology of heterogeneous polymer systems has been usually described by evaluation of viscosity curve (shear thinning phenomenon), storage modulus curve (formation of secondary plateau) or plotting information about damping behaviour (e.g. Van Gurp-Palmen-plot). On the contrary to evaluation of damping behaviour, “melt rigidity” approach has been introduced for description of physical network of rigid particles in polymer matrix as relation of $\int G'/G''$ over specific frequency range. This approach has been experimentally proved for polymer nanocomposites in order to compare shear flow characteristics with elongational flow field. In this contribution, LDPE-clay nanocomposites with different dispersion grades (physical networks) have been prepared and characterized by both conventional as well as novel “melt rigidity” approach.

INTRODUCTION

Polymer-clay nanocomposites have been intensively investigated because of the improvements in processing as well as application properties. Consequently, tailored materials [1] based on virgin as well as recycled polymers can be prepared [2-4]. The improvement in material properties due to nanoclay addition has usually been evaluated using a combination of morphological (X-ray diffraction (XRD), transmission electron microscopy (TEM)), mechanical (tensile testing) and sometimes also rheological (rotational rheometry) analyses. For the industrial applications, in-line near infrared spectroscopy has been introduced as one of interesting methods for assessment of dispersion grade directly during the mixing process [5, 6]. Generally, intercalated and delaminated (partially exfoliated) polymer nanocomposites reveal significant enhancements in their properties: higher elastic modulus, tensile strength, thermal resistivity, lower gas and liquid permeability, reduced flammability [7] and improved rheological properties (e.g. higher melt strength) compared to the unfilled polymer matrix [8]. High level of reinforcement due to the addition of the layered silicates results from their large active surface area (in the case of montmorillonite $700-800 \text{ m}^2 \cdot \text{g}^{-1}$) [9]. In the case of highly dispersed systems, a 3D physical network is achieved, formed by the silicate platelets and the polymer chains. This phenomenon can be investigated by rotational or elongational rheometry, according to analysis of melt elasticity or melt strength, respectively [10, 11].

In order to correlate the data between rotational and elongational rheometry, “melt rigidity” evaluation approach has been introduced. This includes using of factor G'/G'' , which could be assigned as “storage factor” ($\cot \delta$) associated with melt rigidity comparing to loss factor ($\tan \delta$) describing damping behavior of the viscoelastic system. For the comparison of this storage factor in shear flow with melt strength in elongational flow field, data of G' and G'' have been integrated over the specific frequency range and, consequently, cumulative storage factor $\int G'/G''$ has been calculated. It has been proved that this cumulative storage factor correlates with values of melt strength measured for polymer-clay nanocomposites with different dispersion grades [11]. In this work, cumulative storage factor for different multiphase polymer systems (LDPE-clay nanocomposites with compatibilizer and nano-scaled TiO_2 , respectively) has been determined for the extended range of frequencies. Moreover, further cumulative

Novel Trends in Rheology VI

AIP Conf. Proc. 1662, 040002-1–040002-6; doi: 10.1063/1.4918890

© 2015 AIP Publishing LLC 978-0-7354-1306-1/\$30.00

040002-1

parameter from dynamic rheological data have been calculated and their possibility for evaluation of multiphase polymer systems comparing to conventional approaches has been discussed.

EXPERIMENTAL

CA9150 low-density polyethylene for extrusion coating has been used for the preparation of nanocomposites (supplied by Borealis Inc., Linz, Austria). The used nanoclays (Cloisite Na⁺, Cloisite 20) as well as compatibilizer (Scona TSPE 1112 GALL) and masterbatch with nano-scaled TiO₂ were supplied by BYK-Chemie Ltd, Wesel, Germany / POLYchem Ltd, Markt Allhau, Austria, respectively. Samples have been prepared using laboratory compounder MiniLab II Haake Rheomex CTW5 (Thermo Fisher Scientific, Germany). Performance of six different compositions (5wt.% of nanoclay and in some mixtures further addition of 5wt.% of compatibilizer or TiO₂) have been compared with the neat LDPE matrix. Rheological properties in the shear flow were studied using a Physica MCR 502 rheometer (Anton Paar Ltd., Graz, Austria) with the cone-plate geometry of 25 mm diameter and automatically controlled gap of 43 μm.

RESULTS AND DISCUSSION

The nanocomposites structure can be assessed by analysis of viscosity curve (shear-thinning effect) in combination with evaluation of the storage modulus curve (G' secondary plateau). In Figs. 1 and 2, magnitudes of complex viscosity as well as storage modulus in dependency on angular frequency have been plotted. As can be seen from both figures, the system prepared with Cloisite 20/TiO₂ revealed the most pronounced shear-thinning behaviour and G' secondary plateau, respectively. This effect can be associated with high dispersion grade of nanoclay in the polymer matrix due to surface modification of the clay and interfacial interactions between nanoclay and nano-scaled TiO₂. Surprisingly, nano-scaled TiO₂ revealed higher compatibilization effect at the interface polymer-clay as the Scona compatibilizer, which is obvious from the rheological data in the range of lower frequencies. Nanocomposites filled with Cloisite 20 or Cloisite Na⁺/Scona revealed similar dispersion grade as the system filled with Cloisite 20/Scona. On the other hand, nanocomposites with Cloisite Na⁺ or Cloisite Na⁺/TiO₂, respectively, revealed rather low level of clay dispersion in polymer matrix.

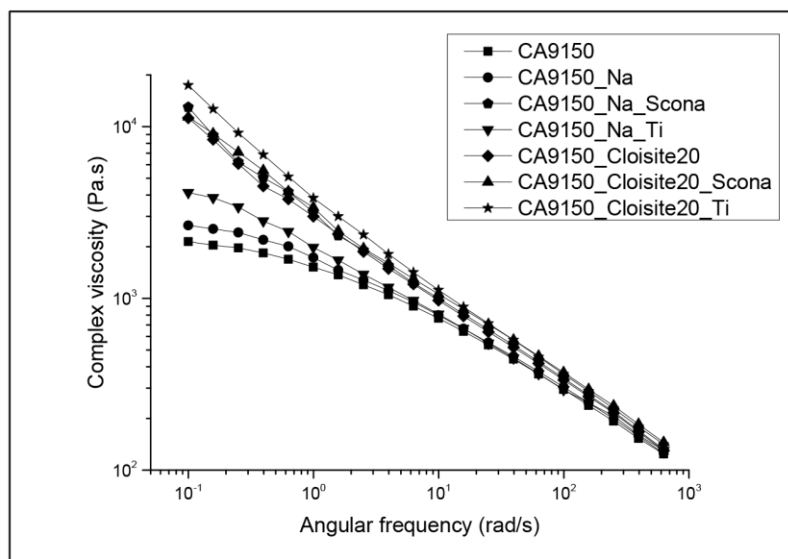


FIGURE 1. Complex viscosity in dependency on angular frequency.

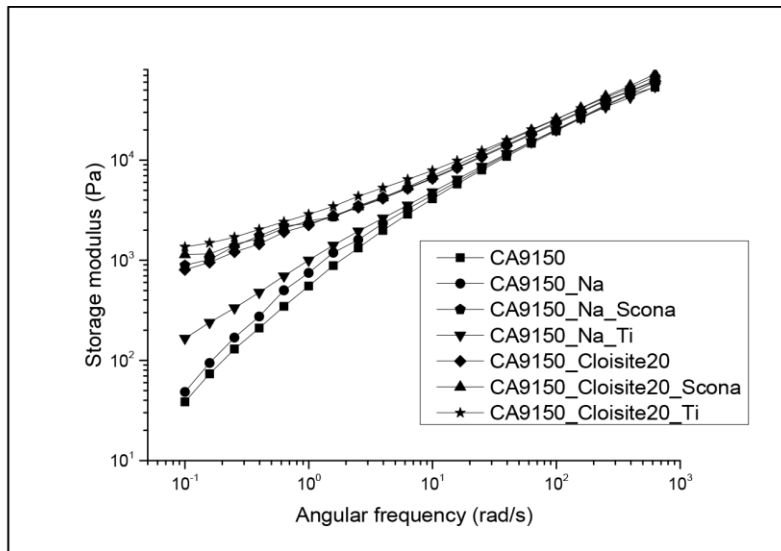


FIGURE 2. Storage modulus in dependency on angular frequency.

The van Gurp-Palmen (vGP) plot as a typical dependency of loss angle δ on complex modulus $|G^*|$ has been used in order to evaluate the topological structures of polymers. The vGP plot is temperature invariant and provides a method to check for the time temperature superposition principle [12]. In Fig. 3, this type of dependency is plotted for all the nanocomposites as well for neat LDPE matrix, respectively. For the polymer samples with linear chain structure, a typical “V” shaped curve has been published. With decreasing complex modulus, the values of phase angle reached the minimum followed by further increase until reaching plateau at 90° . On the contrary, long chain branched (LCB) polymers exhibited a more or less developed bump between the $|G^*|$ minimum and the 90° plateau [13]. As can be seen in Fig. 3, comparing to the unfilled LDPE matrix, all the prepared nanocomposites show topological structure similar to mentioned LCB polymers indicating complex 3D structure made of silicate layers, TiO_2 particles and polymer chains. However, it is difficult to find correlation between dispersion grade and vGP curves.

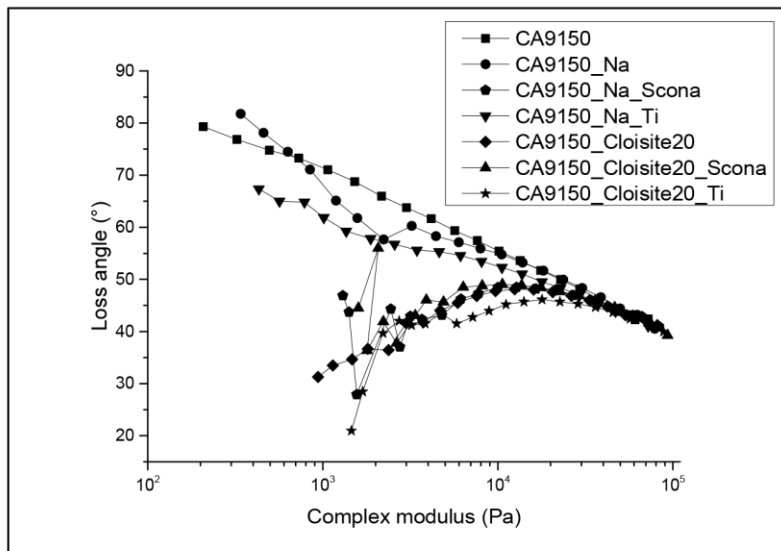


FIGURE 3. Van Gurp-Palmen plot.

In Figs. 4 and 5, cumulative storage factor (calculated over the whole measured frequency range of 0,1-628 rad.s⁻¹) for all the nanocomposites as well for neat LDPE matrix is plotted in dependency on cumulative complex viscosity and cumulative complex modulus, respectively, calculated also over the frequency range of 0,1-628 rad.s⁻¹. It can be seen that cumulative storage factor plotted over cumulative complex viscosity (Fig. 4) exhibits high linear dependency and can be directly correlated with trends of storage modulus and complex viscosity curves (Figs. 1 and 2) in terms of dispersion grade association. This is not the case for the plot of cumulative storage factor in dependency on cumulative complex modulus (Fig. 5), exhibiting rather lower coefficient of linear regression together with some discrepancies concerning correlation with trends of storage modulus and complex viscosity curves.

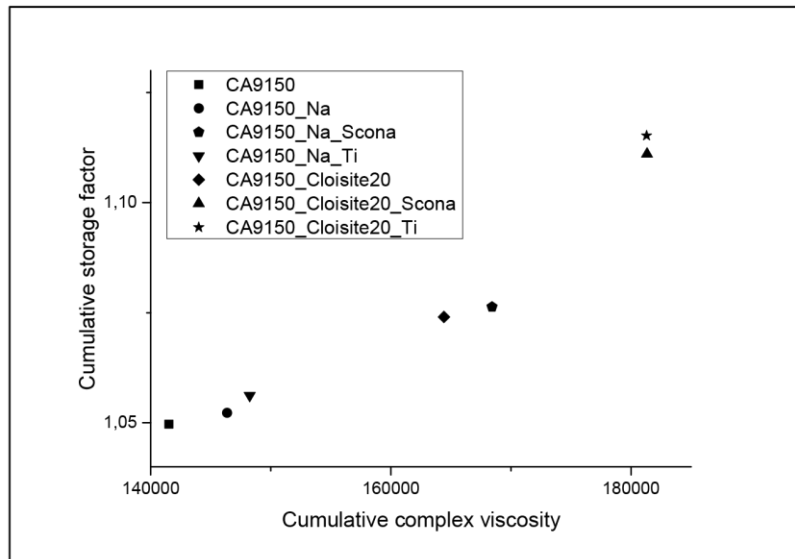


FIGURE 4. Cumulative storage factor in dependency on cumulative complex viscosity ($y = 2.10^{-6}x + 0,8194$, $R^2 = 0,9409$).

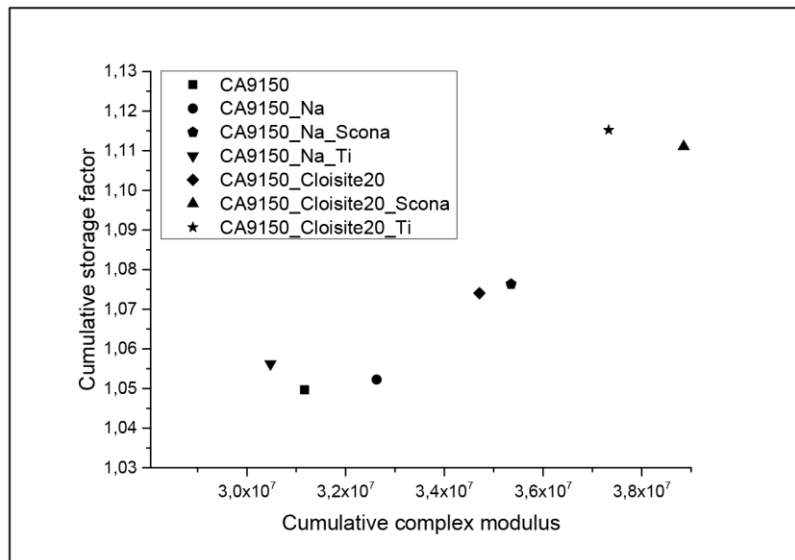


FIGURE 5. Cumulative storage factor in dependency on cumulative complex modulus ($y = 8.10^{-9}x + 0,7963$, $R^2 = 0,8773$).

Additionally to the mentioned cumulative rheological parameters, plots of cumulative storage modulus for the nanocomposites and neat LDPE matrix in dependency on cumulative complex viscosity and cumulative complex modulus, respectively (Figs. 6 and 7), have been analyzed. Figure 6 shows that cumulative storage modulus in dependency on cumulative complex viscosity reveals high coefficient of linear regression but some discrepancies concerning correlation with trends of storage modulus and complex viscosity curves. However, plot of cumulative storage modulus in dependency on cumulative complex modulus exhibits both high coefficient of linear regression as well as high correlation with trends of storage modulus and complex viscosity curves (Figs. 1 and 2) in terms of dispersion grade association.

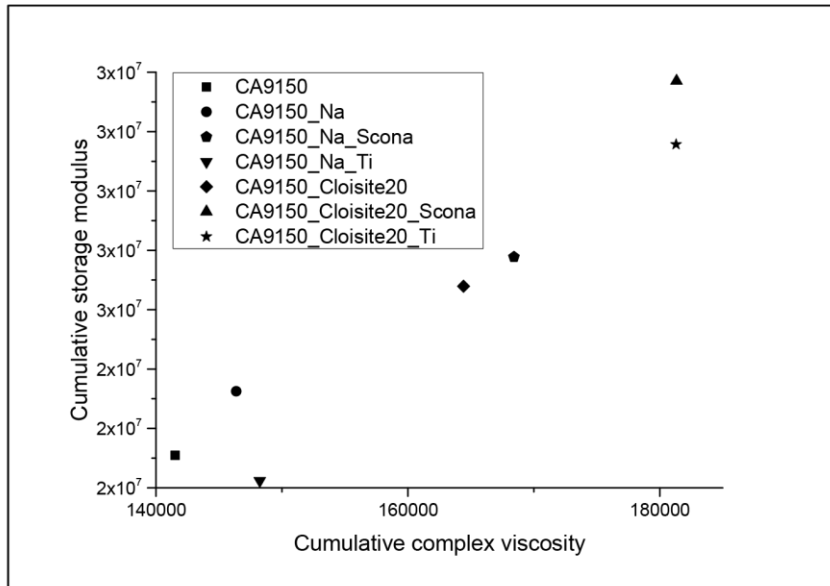


FIGURE 6. Cumulative storage modulus in dependency on cumulative complex viscosity ($y = 149,92x + 937584$, $R^2 = 0,935$).

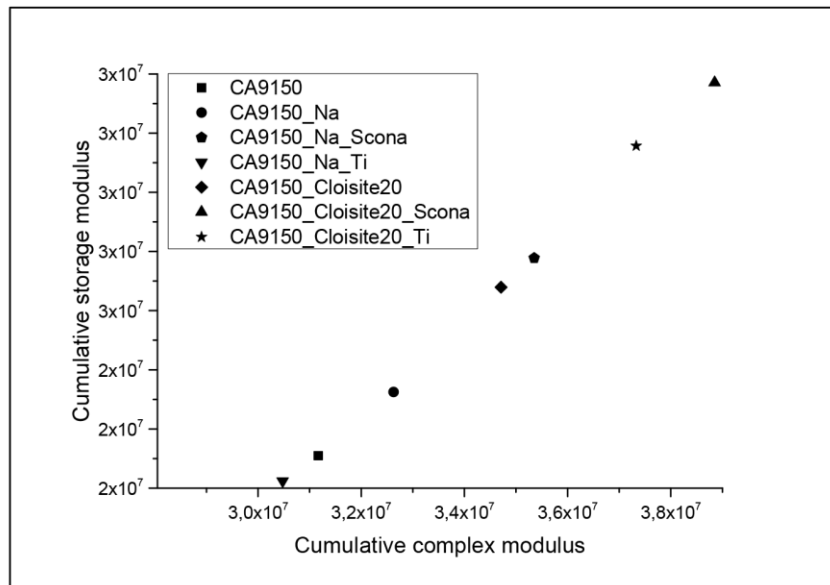


FIGURE 7. Cumulative storage modulus in dependency on cumulative complex modulus ($y = 0,8225x - 3.10^6$, $R^2 = 0,9981$).

CONCLUSION

Using novel “melt rigidity” evaluation approach, specific cumulative rheological parameters have been analyzed and compared with conventional approach like shear-thinning or G' secondary plateau evaluation in order to estimate dispersion grade in multiphase polymeric systems. It has been proved that cumulative storage factor plotted over cumulative complex viscosity and cumulative storage modulus plotted over cumulative complex modulus, respectively, exhibit high linear dependency and can be compared with trends of storage modulus and complex viscosity curves in terms of dispersion grade estimation.

REFERENCES

1. S. S. Ray and M. Okamoto, *Prog. Polym. Sci.* **28**, 1539-1641 (2003).
2. M. Kracalik, L. Pospisil, M. Slouf, J. Mikesova, A. Sikora, J. Simonik and I. Fortelny, *Polym. Compos.* **29** (4), 437-442 (2008).
3. M. Kracalik, L. Pospisil, M. Slouf, J. Mikesova, A. Sikora, J. Simonik and I. Fortelny, *Polym. Compos.* **29** (8), 915-921 (2008).
4. M. Kracalik, S. Laske, M. Gschweidl, W. Friesenbichler and G. R. Langecker, *J. Appl. Polym. Sci.* **113** (3), 1422-1428 (2009).
5. S. Laske, M. Kracalik, M. Feuchter, G. Pinter, G. Maier, W. Märzinger, M. Haberkorn and G. R. Langecker. *J. Appl. Polym. Sci.* **114** (4), 2488-2496 (2009).
6. A. Witschnigg, S. Laske, M. Kracalik, M. Feuchter, G. Pinter, G. Maier, W. Märzinger, M. Haberkorn, G. R. Langecker and C. Holzer. *J. Appl. Polym. Sci.* **117** (5), 3047-3053 (2010).
7. J. Gilman, T. Kashiwagi, J. Lichtenhan, *Sampe J.* **33**, 40-46 (1997).
8. S. S. Ray, K. Yamada, M. Okamoto, K. Ueda, *Polymer* **44**, 857-866 (2003).
9. K. M. Lee, C. D. Han, *Macromolecules* **36**, 7165-7178 (2003).
10. S. Laske, M. Kracalik, M. Gschweidl, M. Feuchter, G. Maier, G. Pinter, R. Thomann, W. Friesenbichler and G. R. Langecker. *J. Appl. Polym. Sci.* **111** (5), 2253-2259 (2009).
11. M. Kracalik, S. Laske, A. Witschnigg and C. Holzer, *Rheol. Acta* **50** (11-12), 937-944 (2011).
12. M. Van Gurp, J. Palmen, *Rheol. Bull* **67**, 5-8 (1998).
13. S. Trinkle, P. Walter, C. Friedrich, *Rheol. Acta* **41**, 103-113 (2002).

2.3.6 Manuscript 16

“Assessment of reinforcement in polymer nanocomposites using cumulative rheological parameters”

Kracalik, Milan (2017): In: Epitoanyag – Journal of Silicate Based and Composite Materials 69 (4), S. 116–120. DOI: 10.14382/epitoanyag-jsbcm.2017.21.

In this manuscript, new analysis method based on cumulative rheological parameters was tested for nanocomposites with LDPE, nanoclay and nano-scaled ZnO. The cumulative storage factor (CSF) plotted over cumulative complex viscosity (CCV) showed clearly other trend as trends obtained from conventional rheological analysis. For CA9150 matrix it could be seen that viscosity value is high, but reinforcement level represented by CSF (comparing to all nanocomposites) is low. Comparing to CA9150, the nanocomposite with 5% of ZnO revealed lower value of viscosity, but higher value of reinforcement, followed by nanocomposite with 2.5/2.5 wt.% of Cloisite20/ZnO and finally followed by nanocomposite with 5wt.% of Cloisite20 showing the highest reinforcement and approximately same level of viscosity. In this way, it was possible to separate contribution of “internal reinforcement” coming from internal friction (high molecular weight and viscosity values, respectively) – represented by viscosity values – and “external reinforcement” coming from 3D physical network between polymer chains and nanofiller particles – represented by CSF values. This separation was not possible to analyze using conventional evaluation methods based on damping behaviour. If only polymer nanocomposites were compared, there was high correlation between CSF and CCV values, giving possibility to compare previously described “external reinforcement” not only for cases of nanocomposites using one polymer matrix, but also for cases of nanocomposites based on polymer blends.

Assessment of reinforcement in polymer nanocomposites using cumulative rheological parameters

MILAN KRACALIK • Institute of Polymer Science, Johannes Kepler University • Milan.Kracalik@jku.at
 Érkezett: 2017. 10. 26. • Received: 26. 10. 2017. • <https://doi.org/10.14382/epitoanyag.jsbcm.2017.21>

Abstract

Multiphase polymer systems, like polymer nanocomposites, exhibit complex rheological behaviour due to physical and also possibly chemical interactions between individual phases. Up to now, rheology of dispersive polymer systems has been usually described by evaluation of viscosity curve (shear thinning phenomenon), storage modulus curve (formation of secondary plateau) or plotting information about dumping behaviour (e.g. Van Gorp-Palmen-plot, comparison of loss factor $\tan \delta$). On the contrary to evaluation of damping behaviour, values of $\cot \delta$ were calculated and called as „storage factor“, analogically to loss factor. Then values of storage factor were integrated over specific frequency range and called as “cumulative storage factor”. In this contribution, LDPE-ZnO-clay nanocomposites with different dispersion grades (physical networks) have been prepared and characterized by both conventional as well as novel analysis approach. Next to cumulative storage factor, further cumulative rheological parameters like cumulative complex viscosity, cumulative complex modulus or cumulative storage modulus have been introduced.

Keywords: shear flow, oscillatory shear, polymer, clay, nanocomposites

Kulcsszavak: nyírási folyás, oszcilláló nyírás, polimer, agyag, nanokompozit

Prof. Dr. Milan KRACALIK is assistant professor at the Institute of Polymer Science, Johannes Kepler University Linz. His field of expertise covers in particular polymer rheology, polymer composites and nanocomposites, polymer recycling, study of structure-properties relationship in polymer materials and management associated with technological processes and products. He studied Technology & Management at the Brno University of Technology, Czech Republic (MSc.: 2000), at Tomas Bata University in Zlin and Institute of Macromolecular Chemistry, Academy of Sciences of the Czech Republic (Ph.D.: 2006) associated with praxis in marketing department of Podravka-Lagris Inc., Czech Republic. Between 2006 and 2012 he was post-doc researcher & project leader at the Department of Polymer Engineering and Science of the University of Leoben, Austria. Between 2012 and 2014 he was research manager at the Department Research and Development of the ISOVOLTAIC AG, Austria. He has also lectured on Technology & Management at several European universities such as Albert Ludwigs University Freiburg, Budapest University of Technology and Economics, Chemical Research Centre / Hungarian Academy of Sciences, University of Zagreb and Department of Technical Sciences / Croatian Academy of Sciences and Art.

1. Introduction

Polymer nanocomposites using organically modified clays have been intensively investigated due to enhancement of processing as well as utility properties. Using nanoparticles is an interesting way for preparation of polymer tailored materials. The enhancement of material properties because of nanoparticles addition has usually been analysed using a combination of morphological (X-ray diffraction (XRD), transmission electron microscopy (TEM)), mechanical (tensile testing) and possibly rheological (rotational rheometry) measurements [1-17]. Using 2-5% of clay, significant improvement of material properties can be reached: high elastic modulus, tensile strength, thermal resistivity, low gas and liquid permeability, reduced flammability [18] and improved rheological properties compared to the unfilled polymer matrix [1-17]. High reinforcement due to addition of the layered silicates results from their large surface area (specific surface of montmorillonite is about 700-800 m²/g) [19, 20]. In the case of highly dispersed systems, a three dimensional physical network is achieved, formed due to interactions between silicate platelets and the polymer chains. This phenomenon can be investigated by analysis of the melt elasticity using rotational rheometry [1-40]. These studies are mainly based on evaluation of viscosity curve shape (shear thinning phenomenon), storage modulus curve at low frequencies (formation of secondary plateau), phase homogeneity (Cole-Cole plot) or plotting information about dumping behaviour (e.g. Van Gorp-Palmen-plot, comparison of loss factor $\tan \delta$). In order to enable simple comparison of nanocomposites reinforcement in the shear flow, new way to analyze data of the shear flow has been tested [31, 32]. The storage modulus G' describes the elastic part while the loss modulus provides us with information about the

viscous part of the shear flow. The relation G''/G' is defined as $\tan \delta$ and reflects damping behaviour in the polymer system. According available literature, the G''/G' ratio ($\cot \delta$) has not been used for rheological evaluation of nanocomposites up to now. Compared to $\tan \delta$ (loss factor), $\cot \delta$ (called as storage factor, SF) reflects melt rigidity, which can be associated with reinforcement effect in polymer (combination of chain elasticity with silicate layers rigidity in the polymer melt). In order to reduce the magnitudes of storage factor to one representative value for one sample, G' as well as G'' curves have been integrated over the measured frequency range as following:

$$CSF = \frac{\int_{0.1 \text{ rad/s}}^{628 \text{ rad/s}} G' / \int_{0.1 \text{ rad/s}}^{628 \text{ rad/s}} G'' \quad (1)$$

In this way, cumulative storage factor (CSF) and some further cumulative rheological parameters (e.g. cumulative complex viscosity CCV, cumulative complex modulus CCM, cumulative storage modulus CSM) were introduced [31]. It was proven that values of CSF can be correlated with values of melt strength, i.e. the reinforcement in polymer nanocomposites can be assessed and compared in both, shear as well in elongational flow [32]. In this paper, LDPE-ZnO-clay nanocomposites with different dispersion grades (physical networks) are reported. It is shown that nano-scaled ZnO can be used not only as UV stabilizer but also as reinforcement and dispersion agent, respectively. The obtained data is analysed in this paper using typical rheological approaches as well as cumulative rheological parameters like CSF or CCV.

2. Materials and Method

CA9150 low-density polyethylene for extrusion coating has been used for the preparation of nanocomposites (supplied by Borealis Inc., Linz, Austria). The used nanoclay Cloisite 20 (Cl20) as well as LDPE masterbatch with 30% nano-scaled ZnO (Nanobyk) were supplied by BYK-Chemie Ltd, Wesel, Germany / POLYchem Ltd, Markt Allhau, Austria, respectively.

Mixtures have been prepared using laboratory compounder MiniLab II Haake Rheomex CTW5 (Thermo Fisher Scientific, Germany). Performance of four different compositions (pure PE matrix, 5wt.% of Cl20, 5wt.% of ZnO, 2.5/2.5 wt.% of Cl20/ZnO) have been compared. Rheological properties in the shear flow were studied using a Physica MCR 502 rheometer (Anton Paar Ltd., Graz, Austria) with the cone-plate geometry of 25 mm diameter and measuring gap of 43 μm.

3. Results & Discussion

The nanocomposites dispersion grade and effect of matrix molecular weight on final morphology can be evaluated using analysis of viscosity curve (shear-thinning effect) in combination with information obtained from the storage modulus curve (G' secondary plateau; [33]). In Figs. 1 and 2, magnitudes of complex viscosity as well as storage modulus in dependency on angular frequency were plotted. As can be seen from Fig. 1, the systems prepared with Cl20 and Cl20/ZnO revealed pronounced shear-thinning behavior, as result of disruption of network structures and, consequently, by orientation of filler particles in flow. On the other hand, CA9150 matrix as well as nanocomposite only with ZnO showed typical liquid viscoelastic behaviour. The lower viscosity values of nanocomposite only with ZnO comparing with pure CA9150 matrix can be explained by significantly lower viscosity of LDPE matrix used for preparation of ZnO masterbatch. Therefore, higher admixture of ZnO masterbatch to CA9150 matrix results to higher "dilution" of CA9150 matrix, i.e. the average molecular weight in such polymer blend will be lowered.

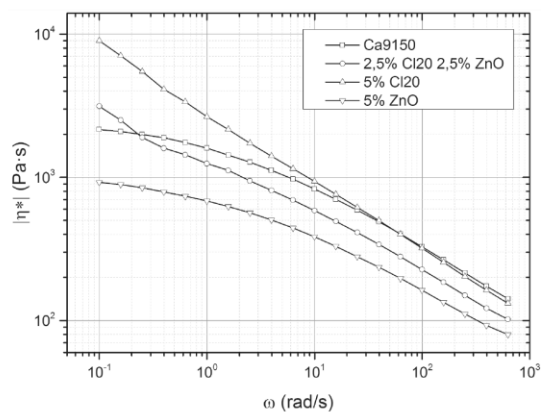


Fig. 1. Complex viscosity of nanocomposites
1. ábra Nanokompozitok komplex viszkozitása

For systems with high dispersion grade, the dependence of $G'(\omega)$ becomes almost invariable at low frequencies. Such "secondary" plateau indicates the formation of a network structure ("rubber-like" behavior) reflecting the exfoliation of silicate layers in nanocomposites [34, 47, 48]. As can be seen in Fig. 2, systems prepared with Cl20 and Cl20/ZnO showed "rubber-like" behaviour i.e. high dispersion grade, while pure CA9150 matrix as well as nanocomposite with ZnO exhibited typical viscoelastic behaviour. It means, in 2.5 Cl20/2.5 ZnO nanocomposite, two physical interactions are acting simultaneously: on one hand, melt elasticity is increased by formation of 3D-physical network between polymer chains and silicate platelets, and, on the other hand melt elasticity is decreased due to decrease in polymer average molecular weight. As can be seen from Figs. 1 and 2, the decrease in polymer average molecular weight is dominating in 5% ZnO nanocomposite system comparing to pure CA9150 matrix.

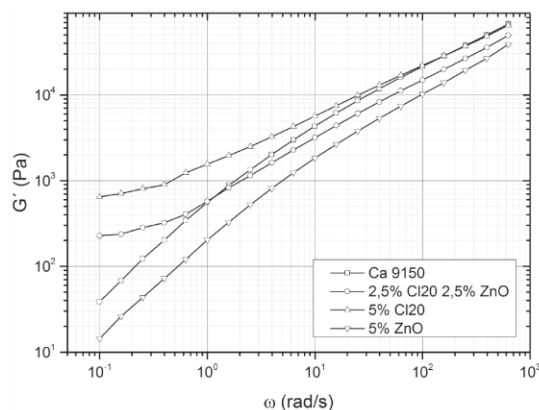


Fig. 2. Storage modulus of nanocomposites
2. ábra Nanokompozitok tárolási modulusa

The van Gorp-Palmen (vGP) plot as a dependency of loss angle δ on complex modulus $|G^*|$ can be used to analyze the spatial structures of polymers [41-45]. In Fig. 3, vGP plot is shown for prepared samples. For the polymer samples with rather linear chain structure, a continuous shaped curve has been published. On the contrary, long chain branched (LCB) polymers showed a developed bump between the $|G^*|$ minimum and the 90° plateau [44]. As can be seen in Fig. 3, systems prepared with Cl20 and Cl20/ZnO show spatial structure similar to mentioned LCB polymers with even two bumps or peaks (Cl20), indicating complex 3D structure made of filler and polymer chains [49]. The CA9150 matrix and nanocomposite with ZnO exhibit behaviour connected with linear chain structure. In order to get additional information about viscoelastic damping behaviour of the prepared samples, phase shift δ in dependency on angular frequency has been plotted (Fig. 4). The curves are similar to those of vGP and confirm formation of differently organized structures (combination of agglomerated, delaminated and exfoliated structure) depending on achieved 3D network.

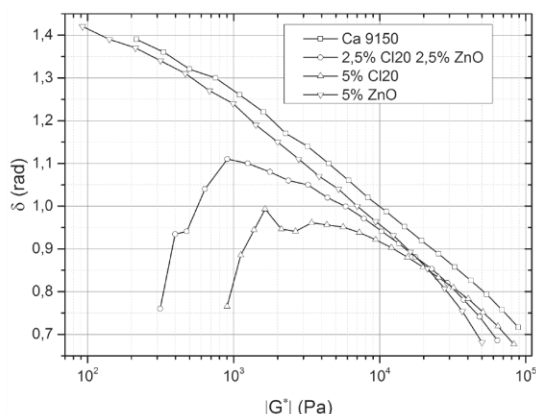


Fig. 3. Van Gorp-Palmen plot of nanocomposites
3. ábra Nanokompozitok Van Gorp-Palmen diagramja

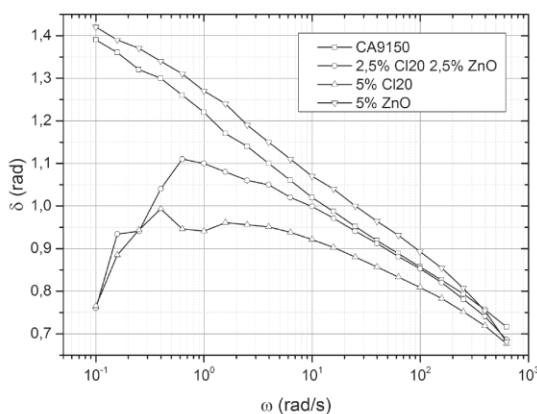


Fig. 4. Phase shift in dependency on angular frequency
4. ábra Fáziseltolódás a szögfrekvencia függvényében

Another approach for description of viscoelastic damping behaviour is so called “Cole-Cole” figure, in which imaginary part of complex viscosity over the real part is plotted. This figure has been widely used to assess miscibility/homogeneity of polymer blends and composites in the way that a smooth, semi-circular shape can be interpreted by better compatibility and homogeneity, respectively [23,46]. As shown in Fig. 5 the CA9150 matrix and nanocomposite with ZnO showed semi-circle shapes, reflecting high homogeneity of the system. However, for the analysis of polymer nanocomposites performance, not only homogeneity but also reinforcement should be addressed. Using Cole-Cole plot, it can be said, that systems prepared with Cl20 and Cl20/ZnO revealed deviation from semi-circle shape and, therefore, are rather not homogeneous. Nevertheless, no information about reinforcement level can be obtained from this figure and this problem is actually concomitant with each previously described rheological analysis based on damping behaviour.

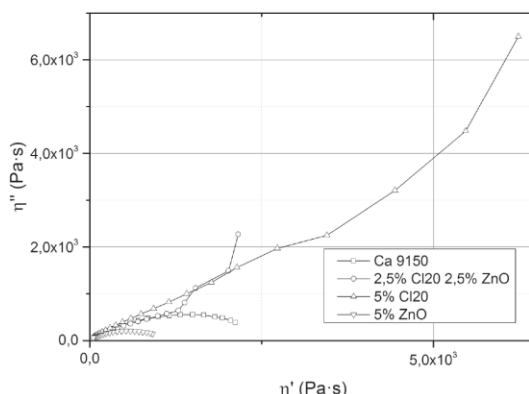


Fig. 5. Cole-Cole plot
5. ábra Cole-Cole diagram

Using previously introduced analysis based on “rigidity” behaviour [31, 32], there is possibility to analyze reinforcement level as result of 3D physical network between polymer chains and filler particles and, consequently, to obtain some information hidden in analysis based on damping behaviour.

The CSF plotted over CCV in Fig. 6 shows clearly other trend as trends obtained from figures analyzed previously in this paper. For CA9150 matrix it can be seen that viscosity value is high, but reinforcement level represented by CSF (comparing to all nanocomposites) is low. Comparing to CA9150, the nanocomposite with 5% of ZnO revealed lower value of viscosity, but higher value of reinforcement, followed by nanocomposite with 2.5/2.5 wt.% of Cl20/ZnO and finally followed by nanocomposite with 5wt.% of Cl20 showing the highest reinforcement and approximately same level of viscosity. In this way, it was possible to divide contribution of “internal reinforcement” coming from internal friction (high molecular weight and viscosity values, respectively) – represented by viscosity values – and “external reinforcement” coming from 3D physical network between polymer chains and nanofiller particles – represented by CSF values. This division was not possible to analyze using evaluation methods based on damping behaviour.

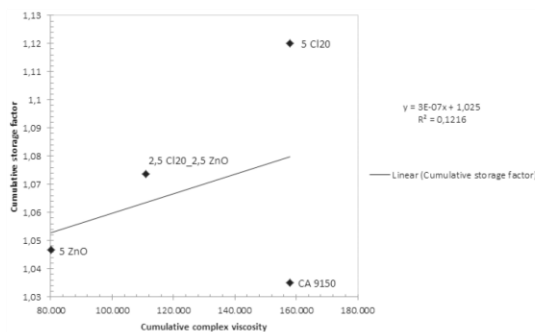


Fig. 6. Cumulative storage factor
6. ábra Kumulatív tárolási tényező

Comparing to Fig. 6, coefficient of linear regression in Fig. 7 is very high. It means, if only polymer nanocomposites are compared, there is high correlation between CSF and CCV values, giving possibility to compare previously described “external reinforcement” not only in cases of nanocomposites using one polymer matrix, but also in cases of nanocomposites based on polymer blends. This result will be proved in further work using not only polymer matrices with different molecular weight but also with different chemical compositions.

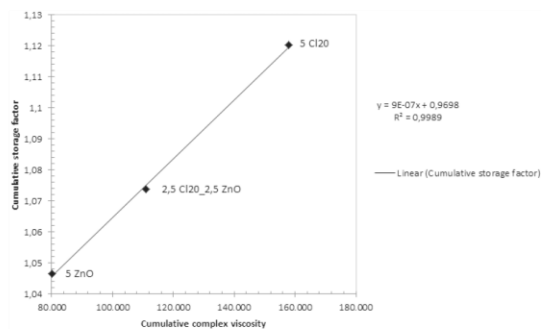


Fig. 7. Cumulative storage factor of nanocomposites without neat matrix
7. ábra Nanokompozitok kumulatív tárolási tényezője ágyazóanyag nélkül

4. Conclusions

Complex polymer nanocomposites with different molecular weight polyethylenes and clay/ZnO nanoparticles were prepared and analyzed by conventional as well by new rheological approach. Using novel approach based on melt rigidity analysis the reinforcement caused by 3D physical network between polymer chains and nanofiller particles could be divided from that coming from internal friction (polymer molecular weight). In this way, new inside into performance characterization of polymer nanocomposites has been introduced and will be tested on nanocomposites based on different polymer blends in future work.

References

[1] Ray S. S. – Okamoto M. (2003): Polymer/layered silicate nanocomposites: a review from preparation to processing. *Progress in Polymer Science*, 28:1539-1641. <https://doi.org/10.1016/j.progpolymsci.2003.08.002>

[2] Ray S. S. – Yamada K. – Okamoto M. – Ueda K. (2003): New polylactide-layered silicate nanocomposites. 2. *Concurrent improvements of material properties, biodegradability and melt rheology*. *Polymer*, 44:857-866. [https://doi.org/10.1016/S0032-3861\(02\)00818-2](https://doi.org/10.1016/S0032-3861(02)00818-2)

[3] Laske S. – Witschnigg A. – Mattausch H. – Krcalik M. – Pinter G. – Feuchter M. – Maier G. – Holzer C. (2012): Determining the ageing of polypropylene nanocomposites using rheological measurements. *Applied Rheology*, 22 (2), 24590 – 24599. <https://doi.org/10.3933/AppIRheol-22-24590>

[4] Abdel-Goad M. (2011): Rheological characterization of melt compounded polypropylene/clay nanocomposites. *Composites Part B*, 42: 1044–1047. <https://doi.org/10.1016/j.compositesb.2011.03.025>

[5] Aghjeh M. R. – Asadi V. – Mehdijabbar P. et al. (2015): Application of linear rheology in determination of nanoclay localization in PLA/EVA/Clay nanocomposites: Correlation with microstructure and thermal properties. *Composites Part B*, 86: 273–284. <https://doi.org/10.1016/j.compositesb.2015.09.064>

[6] Ahmed J. – Auras R. – Kijchavengkul T. et al. (2012): Rheological, thermal and structural behavior of pol (ε-caprolactone) and nanoclay blended films. *Journal of Food Engineering*, 111: 580–589. <https://doi.org/10.1016/j.jfoodeng.2012.03.014>

[7] Filippone G. – Carroccio S. C. – Curcuruto G. et al. (2015): Time-resolved rheology as a tool to monitor the progress of polymer degradation in the melt state e Part II: Thermal and thermo-oxidative degradation of polyamide 11/organo-clay nanocomposites. *Polymer*, 73: 102–110. <https://doi.org/10.1016/j.polymer.2015.07.042>

[8] Mishra J. K. – Hwang K.-J. – Ha C.-S. (2005): Preparation, mechanical and rheological properties of a thermoplastic polyolefin (TPO)/organoclay nanocomposite with reference to the effect of maleic anhydride modified polypropylene as a compatibilizer. *Polymer*, 46: 1995–2002. <https://doi.org/10.1016/j.polymer.2004.12.044>

[9] Nobile M. R. – Simon G. P. – Valentino O. et al. (2007): Rheological and Structure Investigation of Melt Mixed Multi-Walled Carbon Nanotube/PE Composites. *Macromolecular Symposia 247*: 78–87. <https://doi.org/10.1002/masy.200750110>

[10] Sadeghipour H. – Ebadi-Dehaghani H. – Ashouri D. et al. (2013): Effects of modified and non-modified clay on the rheological of high density polyethylene. *Composites: Part B*, 52: 164–171. <https://doi.org/10.1016/j.compositesb.2013.04.010>

[11] Samyn F. – Bourbigot S. – Jama C. et al. (2008): Crossed characterisation of polymer-layered silicate (PLS) nanocomposite morphology: TEM, X-ray diffraction, rheology and solid-state nuclear magnetic resonance measurements. *European Polymer Journal 44*: 1642–1653. <https://doi.org/10.1016/j.eurpolymj.2008.03.021>

[12] Wagener R. – Reisinger T. J. G. (2003): A rheological method to compare the degree of exfoliation of nanocomposites. *Polymer*, 2003(44): 7513–7518. <https://doi.org/10.1016/j.polymer.2003.01.001>

[13] Wang M. – Fan X. – Thitsartarn W. et al. (2014): Rheological and mechanical properties of epoxy/clay nanocomposites with enhanced tensile and fracture toughnesses. *Polymer*, 58: 43–52. <https://doi.org/10.1016/j.polymer.2014.12.042>

[14] Zhang X. – Yang G. – Lin J. (2006): Synthesis, Rheology, and Morphology of Nylon-11/Layered Silicate Nanocomposite. *Journal of Polymer Science: Part B: Polymer Physics*, 44: 2161–2172. <https://doi.org/10.1002/polb.20881>

[15] Zhao J. – Morgan A. B. – Harris J. D. (2005): Rheological characterization of polystyrene-clay nanocomposites to compare the degree of exfoliation and dispersion. *Polymer*, 2005(46): 8641–8660. <https://doi.org/10.1016/j.polymer.2005.04.038>

[16] Zhao Y. – Huang H.-X. (2008): Dynamic rheology and microstructure of polypropylene/clay nanocomposites prepared under Sc-CO₂ by melt compounding. *Polymer Testing*, 27: 129–134. <https://doi.org/10.1016/j.polymertesting.2007.11.006>

[17] Zhong Y. – Zhu Z. – Wang S.-Q. (2005): Synthesis and rheological properties of polystyrene/layered silicate nanocomposite. *Polymer*, 46 (3006-3013). <https://doi.org/10.1016/j.polymer.2005.02.014>

[18] Gilman J. – Kashiwagi T. – Lichtenhan J. (1997): Nanocomposites: A revolutionary new flame retardant approach. *Sampe Journal*, 33:40–46.

[19] Lee K. M., Han C. D. (2003): Rheology of Organoclay Nanocomposites: Effects of Polymer Matrix/Organoclay Compatibility and the Gallery Distance of Organoclay. *Macromolecules*, 36:7165-7178. <https://doi.org/10.1021/ma030302w>

[20] Lee K. M. – Han C. D. (2003): Effect of hydrogen bonding on the rheology of polycarbonate/organoclay nanocomposites. *Polymer*, 44:4573-4588. [https://doi.org/10.1016/S0032-3861\(03\)00444-0](https://doi.org/10.1016/S0032-3861(03)00444-0)

[21] Ahmed J. – Varhney S. K. – Auras R. – Hwang S. W. (2010): Thermal and rheological properties of L-poly(lactide)/poly(ethylene glycol)/silicate nanocomposites films. *Journal of Food Science*, 75: N97–N108. <https://doi.org/10.1111/j.1750-3841.2010.01809.x>

[22] Ahmed J. – Auras R. – Kijchavengkul T. – Varshney S. K. (2012): Rheological, thermal and structural behavior of poly(ε-caprolactone) and nanoclay blended films. *Journal of Food Engineering*, 111: 580–589. <https://doi.org/10.1016/j.jfoodeng.2012.03.014>

[23] Aklonis J. J. – Macknight W. J. (1983): Introduction to viscoelasticity. *New York: Wiley*; 1983.

- [24] Gelfer M. – Song H. H. – Liu L. – Avila-Orta C. – Yang L. – Si M. – Hsiao B. S. – Chu B. – Rafailovich M. – Tsou A. H. (2002): Manipulating the microstructure and rheology in polymer-organoclay composites. *Polymer Engineering and Science*, 42:1841-1851. <https://doi.org/10.1002/pen.11077>
- [25] Hoffmann B. – Dietrich C. – Thomann R. – Friedrich C. – Mülhaupt R. (2000): Morphology and rheology of polystyrene nanocomposites based upon organoclay. *Macromolecular Rapid Communications*, 21:57-61. [https://doi.org/10.1002/\(SICI\)1521-3927\(20001012\)21:1<57::AID-MARC57>3.0.CO;2-E](https://doi.org/10.1002/(SICI)1521-3927(20001012)21:1<57::AID-MARC57>3.0.CO;2-E)
- [26] Hoffmann B. – Kressler J. – Stöppelmann G. – Friedrich C. – Kim G. M. (2000): Rheology of nanocomposites based on layered silicates and polyamide-12. *Colloid and Polymer Science*, 278:629-636. <https://doi.org/10.1007/s003960000294>
- [27] Hyun Y. H. – Lim S. T. – Choi H. J. – Jhon M. S. (2001): Rheology of Poly(ethylene oxide)/Organoclay Nanocomposites. *Macromolecules*, 34:8084-8093. <https://doi.org/10.1021/ma002191w>
- [28] Incarnato L. – Scarfato P. – Scatteia L. – Acierno D. (2004): Rheological behavior of new melt compounded copolyamide nanocomposites. *Polymer*, 45:3487-3496. <https://doi.org/10.1016/j.polymer.2004.03.005>
- [29] Kim T. H. – Jang L. W. – Lee D. C. – Choi H. J. – Jhon M. W. (2002): Synthesis and Rheology of Intercalated Polystyrene/Na⁺-Montmorillonite Nanocomposites. *Macromolecular Rapid Communications*, 23:191-195. [https://doi.org/10.1002/1521-3927\(20020201\)23:3<191::AID-MARC191>3.0.CO;2-H](https://doi.org/10.1002/1521-3927(20020201)23:3<191::AID-MARC191>3.0.CO;2-H)
- [30] Kotsilkova R. (2002): Rheology-Structure Relationship of Polymer/Layered Silicate Hybrids. *Mechanics of Time-Dependent Materials*, 6:283-300. <https://doi.org/10.1023/A:101622618991>
- [31] Kracalik M. (2015): Rheology of Multiphase Polymer Systems using Novel „Melt Rigidity” Evaluation Approach. *AIP Conference Proceedings*, 1662: 040002-1 – 040002-6. <https://doi.org/10.1063/1.4918890>
- [32] Kracalik M. – Laske S. – Witschnigg A. – Holzer C. (2011): Elongational and shear flow in polymer-clay nanocomposites measured by on-line extensional and off-line shear rheometry. *Rheologica Acta*, 50 (11-12): 937-944. <https://doi.org/10.1007/s00397-011-0545-2>
- [33] Kracalik M. – Mikesova J. – Puffr R. – Baldrian J. – Thomann R. – Friedrich C. (2007): Effect of 3D Structures on Recycled PET/Organoclay Nanocomposites. *Polymer Bulletin*, 58:313-319. <https://doi.org/10.1007/s00289-006-0592-5>
- [34] Krishnamoorti R. – Giannelis E. P. (1997): Rheology of End-Tethered Polymer Layered Silicate Nanocomposites. *Macromolecules*, 30:4097-4102. <https://doi.org/10.1021/ma960550a>
- [35] Mohagheghian M. – Ebadi-Dehaghani H. – Ashouri D. – Mousavian S. (2011): A Study on the effect of nano-ZnO on rheological and dynamic mechanical properties of polypropylene: experiments and models. *Composites: Part B*, 42:1987-93. <https://doi.org/10.1016/j.compositesb.2011.04.043>
- [36] Sadeghipour H. – Ebadi-Dehaghani H. – Ashouri D. – Mousavian S. – Hashemi-Fesharaki M. – Gahruei M. S. (2013): Effects of modified and non-modified clay on the rheological behaviour of high density polyethylene. *Composites: Part B*, 52: 164-171. <https://doi.org/10.1016/j.compositesb.2013.04.010>
- [37] Sanchez-Solis A. – Garcia-Rejon A. – Manero O. (2003): Production of nanocomposites of PET-montmorillonite clay by an extrusion process. *Macromolecular Symposia*, 192:281-292. <https://doi.org/10.1002/masy.200390038>
- [38] Sanchez-Solis A. – Romero-Ibarra I. – Estrada M. R. – Calderas F. – Manero O. (2004): Mechanical and rheological studies on polyethylene terephthalate-montmorillonite nanocomposites. *Polymer Engineering and Science*, 44:1094-1102. <https://doi.org/10.1002/pen.20102>
- [39] Solomon M. J. – Almusallam A. S. – Seefeldt K. F. – Somwangthanaroj A. – Varadan P. (2001): Rheology of Polypropylene/Clay Hybrid Materials. *Macromolecules*, 34:1864-1872. <https://doi.org/10.1021/ma001122e>
- [40] Wagener R. – Reisinger T. J. G. (2003): A rheological method to compare the degree of exfoliation of nanocomposites. *Polymer*, 44:7513-7518. <https://doi.org/10.1016/j.polymer.2003.01.001>
- [41] Lohse D. J. – Milner S. T. – Fetters L. J. – Xenidou M. – Hadjichristidis N. – Mendelson R. A. – Garcia-Franco C. A. – Lyon M. K. (2002): Well-defined, model long chain branched polyethylene. 2. melt rheological behaviour. *Macromolecules*, 35:3066-3075. <https://doi.org/10.1021/ma0117559>
- [42] Schulze D. – Trinkle S. – Mulhaupt R. – Friedrich C. (2003): Rheological evidence of modifications of polypropylene by β -irradiation. *Rheologica Acta*, 42:251-258. <https://doi.org/10.1007/s00397-002-0282-7>
- [43] Trinkle S. – Friedrich C. (2001): Van Gorp-Palmen plot: a way to characterize polydispersity of linear polymers. *Rheologica Acta*, 40:322-328. <https://doi.org/10.1007/s003970000137>
- [44] Trinkle S. – Walter P. – Friedrich C. (2002): Van Gorp-Palmen plot II – classification of long chain branched polymers by their topology. *Rheologica Acta*, 41:103-113. <https://doi.org/10.1007/s003970200010>
- [45] Van Gorp M. – Palmen J. (1998): Time-temperature superposition for polymeric blends. *Rheology Bulletin*, 67:5-8.
- [46] Utracki L. A. (1999): Polymer blends handbook. *Netherlands: Kluwer Academic Publishers*
- [47] Khan, S. A. – Prudhomme, R. K. (1987): Melt Rheology of Filled Thermoplastics. *Reviews in Chemical Engineering*, 1987, 4, 205. <https://doi.org/10.1515/REVCE.1987.4.3-4.205>
- [48] Krishnamoorti, R. – Vaia, R. A. – Giannelis, E. P. (1996): Structure and Dynamics of Polymer-Layered Silicate Nanocomposites. *Chemistry of Materials*, 1996, 8, 1728. <https://doi.org/10.1021/cm960127g>
- [49] Chevallier C. – Becquart F. – Taha M. (2013): Polystyrene/polycarbonate blends compatibilization: Morphology, rheological and mechanical properties. *Materials Chemistry and Physics*, 139: 616-622. <https://doi.org/10.1016/j.matchemphys.2013.02.006>

Ref:

Kracalik, Milan: Assessment of reinforcement in polymer nanocomposites using cumulative rheological parameters
 Építőanyag – Journal of Silicate Based and Composite Materials,
 Vol. 69, No. 3 (2017), 116-120. p.
<https://doi.org/10.14382/epitoanyag-jsbcm.2017.21>



2.3.7 Manuscript 17

“Recycled clay/PET nanocomposites evaluated by novel rheological analysis approach”

Kracalik, Milan (2017): In: Applied Clay Science, 2018, 166, 181-184, <https://doi.org/10.1016/j.clay.2018.09.007>.

This manuscript proved the application of cumulative storage factor for reinforcement characterization in complex polymer nanocomposites (e.g. with PET), where the material improvement is dependent on both, clay dispersion grade as well as extent of degradation reactions during the processing. The CSF plotted over cumulative complex viscosity (CCV) shows clearly differences in material reinforcement using various organoclays. It can be seen that CSF values can be divided into three groups: CSF of the neat polymer matrix, CPNs with lower CSF values (10A, 30B) and CPNs with higher CSF values (6A, Na+). It means that effective material reinforcement was reached only in systems using 6A and Na+. This is result of complex physical and chemical reactions, which occur during the processing.



Note

Recycled clay/PET nanocomposites evaluated by novel rheological analysis approach



Milan Krcalik

Institute of Polymer Science, Johannes Kepler University Linz, Altenberger Str. 69, 4040 Linz, Austria

ARTICLE INFO

Keywords:
Rheology
Recycled PET
Shear flow
Oscillatory shear
Polymer
Clay
Nanocomposites

ABSTRACT

Clay-polymer nanocomposites exhibit complex rheological behavior due to physical and also possibly chemical interactions between individual phases. Up to now, rheology of clay-polymer nanocomposites has been usually described by evaluation of complex viscosity curve (shear thinning phenomenon), storage modulus curve (G' secondary plateau) or plotting parameters characterizing damping behavior (e.g. Van Gurp-Palmen-plot, Cole-Cole plot). On the contrary to evaluation of damping behavior, new approach – based on evaluation of rigidity behavior – was tested, where the values of $\cot \delta$ were calculated and called as „storage factor“, analogically to broadly used loss factor. Afterwards, values of storage factor were integrated over measured frequency range and called as “cumulative storage factor”. In this contribution, clay-PET nanocomposites with different organoclays have been prepared and characterized by both conventional as well as novel analysis approach. Rheological results have been supported by AFM micrographs.

1. Introduction

Nanotechnology was already introduced as a new method of improvement of polymer properties in 1995. The technology involves not only incorporation of nanosized particles into the polymer but, more importantly, investigation of interactions between the polymer matrix and the enormously large nanofiller surface. Especially for clay/polymer nanocomposites (CPNs), the surface effects are responsible for improvement of barrier, mechanical and rheological properties, dimensional stability, heat, flame and oxidative resistance. In comparison with traditional fillers (20–40 wt% loading), 2–5 wt% filling of clay minerals is sufficient to achieve analogous material improvement. Generally, the primary particle shape of different nanofillers can be sphere, needle or a plate. High aspect ratio (particle length/thickness) of filler facilitates high reinforcement of polymer. Therefore, layered and needle-formed fillers have been widely used for enhancement of polymer property profile. Montmorillonite belongs to the group of phyllosilicates and theoretically it is possible to reach aspect ratio of 1000 by proper dispersion of this mineral in polymer matrix. Montmorillonite is a three-sheet-silicate where the primary layer consists of one octahedral sheet surrounded by two tetrahedral sheets. Na^+ or Ca^{2+} ions in the interlayer space have been usually replaced by long alkylammonium ions in order to increase interlayer space and, consequently, to facilitate dispersion in polymer melt during melt-compounding process. Nanocomposites using different polymer matrices

and clay minerals have been intensively investigated because of the improvements in their processing and use properties. Consequently, it is possible to prepare new, tailored, materials or to use nanofillers in polymer recycling (Ghanbari et al., 2013; Cassagnau, 2008; Laske et al., 2012; Paul and Robeson, 2008; Ray et al., 2002; Százdí et al., 2006). Especially using nanoparticles for enhancement of recycled PET (Banda-Cruz et al., 2017; Gao, 2012; Liang et al., 2015; Majdzadeh-Ardakani et al., 2017; Mallakpour and Javadpour, 2016; Rosnan and Arsad, 2013; Krcalik et al., 2005) is of great interest due to broad potential applications.

The enhancement of material properties because of nanoparticles addition has usually been analyzed using a combination of morphological (X-ray diffraction (XRD), transmission electron microscopy (TEM)), mechanical (tensile testing) and rheological (rotational rheometry) measurements. In the case of highly dispersed systems, a three dimensional physical network is achieved, formed due to interactions between clay mineral layers and the polymer chains. This phenomenon can be investigated by analysis of the melt elasticity using rotational rheometry. Such studies are mainly based on evaluation of viscosity curve shape (shear thinning phenomenon), storage modulus curve at low frequencies (formation of secondary plateau), phase homogeneity (Cole-Cole plot) or plotting information about damping behavior (e.g. Van Gurp-Palmen-plot, comparison of loss factor $\tan \delta$). In order to enable simple comparison of nanocomposites reinforcement in the shear flow, new way to analyze data of the shear flow has been tested

E-mail address: Milan.Krcalik@jku.at.

<https://doi.org/10.1016/j.clay.2018.09.007>

Received 15 May 2018; Received in revised form 10 August 2018; Accepted 5 September 2018

Available online 27 September 2018

0169-1317/ © 2018 Elsevier B.V. All rights reserved.

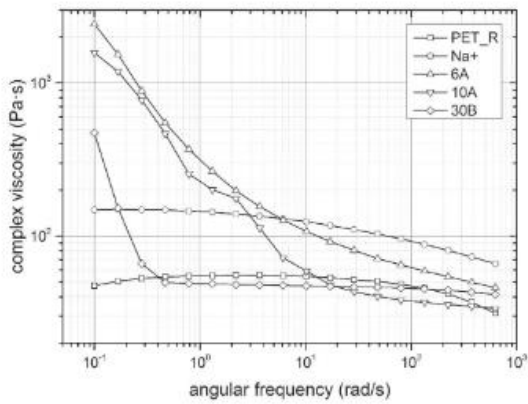


Fig. 1. Complex viscosity of nanocomposites.

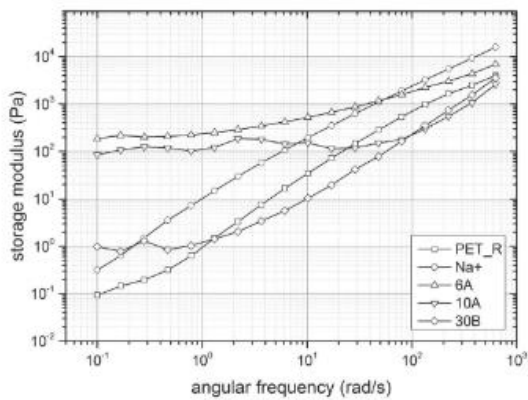


Fig. 2. Storage modulus of nanocomposites.

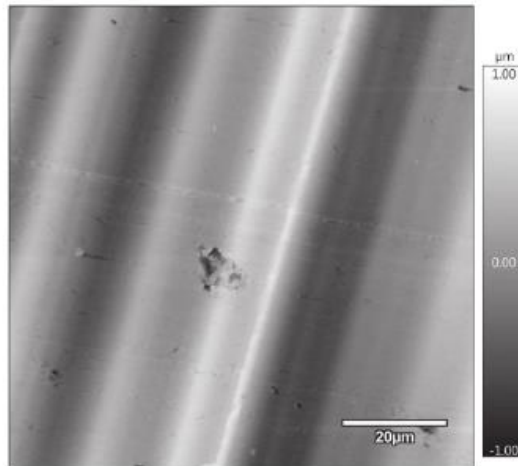


Fig. 4. AFM micrograph of PET/Cloisite 30B.

(Krcalik, 2015; Krcalik et al., 2011). The storage modulus G' reflects the elastic part while the loss modulus gives information about the viscous part of the dynamic shear flow. The relation of G''/G' is defined as $\tan \delta$ and describes damping behavior of the polymer system. On the contrary, the G'/G'' ratio ($\cot \delta$) has not been used for rheological evaluation of nanocomposites up to now. Compared to $\tan \delta$ (loss factor), $\cot \delta$ (named as storage factor, SF) reflects melt rigidity, which can be associated with reinforcement effect of nanostructured filler (combination of chain elasticity with clay layers rigidity in the polymer melt). In order to reduce the values of storage factor to one representative magnitude for one nanocomposite sample, G' as well as G'' curves have been integrated over the measured frequency range as following:

$$CSF = \int_{0.1 \text{ rad/s}}^{628 \text{ rad/s}} G' / \int_{0.1 \text{ rad/s}}^{628 \text{ rad/s}} G'' \quad (1)$$

In this way, cumulative storage factor (CSF) and some further cumulative rheological parameters (e.g. cumulative complex viscosity CCV, cumulative complex modulus CCM, cumulative storage modulus

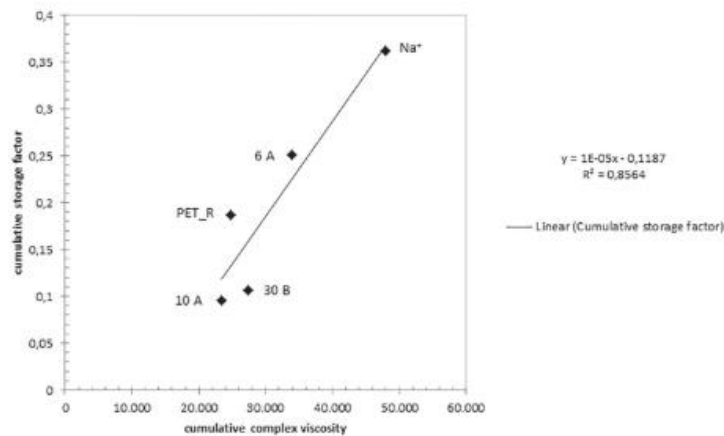


Fig. 3. Cumulative storage factor.

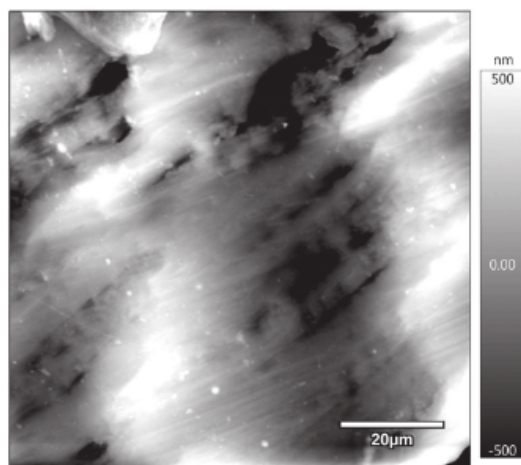


Fig. 5. AFM micrograph of PET/Cloisite Na⁺.

CSM) were introduced (Kracalik, 2015). It was proven that values of CSF can be correlated with values of melt strength, i.e. the reinforcement in polymer nanocomposites can be assessed and compared in both, shear as well in elongational flow (Kracalik et al., 2011). In this paper, recycled clay-PET nanocomposites with different dispersion grades (physical networks) are reported. The obtained data is analyzed in this paper using typical rheological approaches as well as cumulative rheological parameters like CSF or CCV.

2. Experimental

2.1. Materials

The used clay minerals Cloisite Na⁺ (Na⁺), Cloisite 6A (6A), Cloisite 10A (10A) and Cloisite 30B (30B) were supplied by BYK-Chemie Ltd., Wesel, Germany / POLYchem Ltd., Markt Allhau, Austria, respectively. Colour-sorted recycled poly(ethylene)terephthalate (PET_R), with the intrinsic viscosity 0.73 dl/g (dilution in phenol/tetrachloroethane 1:3), supplied by Polymer Institute Brno, Ltd. was used as matrix.

2.2. Methods

Mixtures & samples have been prepared using laboratory compounder MiniLab II Haake Rheomex CTW5 in combination with Haake MiniJet Pro (Thermo Fisher Scientific, Germany). Performance of five different compositions (pure PET_R matrix, 5 wt% of different clay minerals in PET_R) have been compared. Rheological properties in the shear flow were studied using a Physica MCR 502 rheometer (Anton Paar Ltd., Graz, Austria) with the cone-plate geometry of 25 mm diameter and measuring gap of 43 µm. Morphology of nanocomposites has been checked using atomic force microscope MFP-3D AFM (Oxford Instruments Asylum Research, Inc., Santa Barbara, CA).

3. Results and discussion

The nanocomposites dispersion grade and effect of matrix molar mass on final morphology can be evaluated using analysis of viscosity curve (shear-thinning effect) in combination with information obtained from the storage modulus curve (G' secondary plateau; (Kracalik et al., 2005). In Fig. 1–2, magnitudes of complex viscosity as well as storage

modulus in dependency on angular frequency are plotted. As can be seen from Fig. 1, the CPN systems prepared with 6A and 10A revealed pronounced shear-thinning behavior, as result of disruption of network structures and, consequently, by orientation of filler particles in flow. On the other hand, PET_R matrix as well as nanocomposite with Na⁺ showed typical liquid viscoelastic behavior. CPN with 30B showed shear-thinning behavior only in a very short range of low frequencies. Concerning the range of high frequencies, the complex viscosity of CPN systems using 30B and 10A was lower than that of pure PET_R matrix, which reflects strong degradation reactions occurring during the processing, described more in detail in previous work (Kracalik et al., 2005).

For CPN systems with high dispersion grade, the dependence of $G'(\omega)$ becomes almost invariable at low frequencies. Such “secondary” plateau indicates the formation of a network structure (“rubber-like” behavior) reflecting the exfoliation of clay layers in CPN (Cassagnau, 2008; Kracalik et al., 2011; Krishnamoorti et al., 2010; Pötschke et al., 2002; Ray et al., 2002; Százdí et al., 2006; Thomas et al., 2016; Vermant et al., 2007; Wagener and Reisinger, 2003; Wang et al., 2014; Wood-Adams et al., 2000). As can be seen in Fig. 2, CPN systems prepared with 6A, 10A and 30B showed “rubber-like” behavior i.e. high dispersion grade, while pure PET_R matrix as well as CPN nanocomposite with Na⁺ exhibited typical viscoelastic behavior.

Using previously introduced analysis based on “rigidity” behavior (Kracalik, 2015; Kracalik et al., 2011), there is possibility to analyze reinforcement level as result of 3D physical network between polymer chains and filler particles and, consequently, to obtain some information hidden in analysis based on damping behavior.

The CSF plotted over CCV in Fig. 3 shows clearly differences in material reinforcement between various CPNs. It can be seen that CSF values can be divided into three groups: CSF of the neat polymer matrix, CPNs with lower CSF values (10A, 30B) and CPNs with higher CSF values (6A, Na⁺). It means that effective material reinforcement was reached only in CPN systems using 6A and Na⁺. This is result of complex physical and chemical reactions, which occur during the processing. On one side, physical interactions based on electrostatic forces between polymer and clay mineral result into formation of differently organized structures (combination of agglomerated, delaminated and exfoliated structure) depending on achieved 3D network. On the other side, processing of PET CPNs is concomitant with different chemical reactions (e.g. chain scission, Hofmann elimination (Kracalik et al., 2005)) that lower CPN mechanical performance. Using cumulative storage factor, it can be clearly said which organoclays leads to effective material reinforcement (effect of 3D physical network is higher than effect of chemical degradation) and vice versa.

In order to get morphological information, atomic force microscopy has been employed and micrographs of CPNs with highest (30B) and lowest (Na⁺) dispersion grade have been compared. As expected, organoclay with highest polar surface modification (30B) led to highest dispersion level (only a few small agglomerates visible in Fig. 4) comparing to very low dispersion level using clay without surface modification (Na⁺) in Fig. 5.

4. Conclusions

PET CPNs with natural and organically modified clays were prepared and analyzed by conventional as well by new rheological approach. Using novel approach based on melt rigidity analysis the effective material reinforcement (caused by 3D physical network between polymer chains and nanofiller particles) could be analyzed taking in account material deterioration (caused by chemical reactions during the processing). In this way, new insight into performance characterization of CPNs has been introduced and will be tested on CPNs based on different polymers and polymer blends in future work.

Acknowledgement

Lisa Maria Uiberlacker from VTA Austria GmbH, Rottenbach, Austria for AFM measurements is gratefully acknowledged.

References

- Banda-Cruz, Ernestina Elizabeth, Flores-Gallardo, Sergio Gabriel, Rivera-Armenta, José Luis, 2017. Study of the dispersion of Cloisite 10A in recycled polyethylene terephthalate by extrusion. *DYNA* 84 (200), S. 107–111. <https://doi.org/10.15446/dyna.v84n200.52720>.
- Cassagnau, Ph., 2008. Melt rheology of organoclay and fumed silica nanocomposites. *Polymer* 49 (9), S. 2183–2196. <https://doi.org/10.1016/j.polymer.2007.12.035>.
- Gao, Fengge, (Hg.), 2012. *Advances in Polymer Nanocomposites*. Woodhead Pub (Woodhead Publishing in materials), Cambridge, UK Online verfügbar unter: <http://proquest.tech.safaribooksline.de/9781845699406>.
- Ghanbari, Abbas, Heuzey, Marie-Claude, Carreau, Pierre J., Ton-That, Minh-Tan, 2013. Morphological and rheological properties of PET/clay nanocomposites. *Rheol Acta* 52, S. 59–74.
- Kracalik, Milan, 2015. Rheology of multiphase polymer systems using novel "melt rigidity" evaluation approach. In: *Novel Trends in Rheology VI*. AIP Publishing LLC (AIP Conference Proceedings), Zlín, Czech Republic, pp. S. 40002 28–29 July 2015.
- Kracalik, Milan, Mikesowa, Jana, Puffr, Rudolf, Friedrich, Christian, 2005. Effect of 3D PET/organoclay nanocomposites. *Polymer Bull.* 58, S. 313–319.
- Kracalik, Milan, Laske, Stephan, Witschnigg, Andreas, Holzer, Clemens, 2011. Elongational and shear flow in polymer-clay nanocomposites measured by on-line extensional and off-line shear rheometry. *Rheologica Acta* 50, S. 937–944.
- Krishnamoorti, Ramanan, Banik, Indranil, Xu, Liang, 2010. Rheology and processing of polymer nanocomposites. *Rev. Chem. Eng.* 26 (1–2), S. 354. <https://doi.org/10.1515/REVCE.2010.003>.
- Laske, Stephan, Witschnigg, Andreas, Mattausch, Hannelore, Kracalik, Milan, Pinter, Gerald, Feuchter, Michael, et al., 2012. Determining the ageing of polypropylene nanocomposites using rheological measurements. *Appl. Rheol.* 22.
- Liang, Mong, Visakh, P.M., (Hg.), 2015. *Poly(Ethylene Terephthalate) Based Blends, Composites and Nanocomposites*. William Andrew (Plastics Design Library. PDL Handbook series), Waltham, MA Online verfügbar unter: <http://www.sciencedirect.com/science/book/9780323313063>.
- Majdzadeh-Ardakani, Kazem, Zekriardehani, Shahab, Coleman, Maria R., Jabarin, Saleh A., 2017. A novel approach to improve the barrier properties of PET/clay nanocomposites. *Int. J. Polymer Sci.* 2017, S. 1–10. <https://doi.org/10.1155/2017/7625906>.
- Mallakpour, Shadpour, Javadpour, Mashal, 2016. The potential use of recycled PET bottle in nanocomposites manufacturing with modified ZnO nanoparticles capped with citric acid. Preparation, thermal, and morphological characterization. *RSC Adv.* 6 (18), S. 15039–15047. <https://doi.org/10.1039/C5RA27631D>.
- Paul, D.R., Robeson, L.M., 2008. *Polymer nanotechnology. Nanocomposites*. *Polymer* 49 (15), S. 3187–3204. <https://doi.org/10.1016/j.polymer.2008.04.017>.
- Pötschke, Petra, Fornes, T.D., Paul, D.R., 2002. Rheological behavior of multiwalled carbon nanotube/polycarbonate composites. *Polymer* 43 (11), S. 3247–3255. [https://doi.org/10.1016/S0032-3861\(02\)00151-9](https://doi.org/10.1016/S0032-3861(02)00151-9).
- Ray, Suprakas Sinha, Okamoto, Kazuaki, Maiti, Pralay, Okamoto, Masami, 2002. New poly(butylene succinate)/layered silicate nanocomposites. preparation and mechanical properties. *J. Nanosci. Nanotechnol.* 2 (2), S. 171–176. <https://doi.org/10.1166/jnn.2002.086>.
- Rosnan, Rizuan Mohd, Arsad, Agus, 2013. Effect of MMT concentrations as reinforcement on the properties of recycled PET/HDPE nanocomposites. *J. Polym. Eng.* 33 (7). <https://doi.org/10.1515/polyeng-2013-0107>.
- Százdi, László, Ábrányi, Ágnes, Pukánszky, Béla, Vancso, Julius G., 2006. Morphology characterization of PP/clay nanocomposites across the length scales of the structural architecture. *Macromol. Mater. Eng.* 291 (7), S. 858–868. <https://doi.org/10.1002/mame.200600026>.
- Thomas, Sabu, Muller, Rene, Abraham, Jiji, 2016. *Rheology and processing of polymer nanocomposites*. John Wiley & Sons, Inc., Hoboken, NJ, USA.
- Vermant, J., Ceccia, S., Dolgovskij, M.K., Maffettone, P.L., Macosko, C.W., 2007. Quantifying dispersion of layered nanocomposites via melt rheology. *J. Rheol.* 51 (3), S. 429–450. <https://doi.org/10.1122/1.2516399>.
- Wagener, Reinhard, Reisinger, Thomas J.G., 2003. A rheological method to compare the degree of exfoliation of nanocomposites. *Polymer* 44, S. 7513–7518.
- Wang, M., Fan, X., Thitsartarn, W., He, C., 2014. Rheological and mechanical properties of epoxy/clay nanocomposites with enhanced tensile and fracture toughnesses. *Polymer* 58, S. 43–52.
- Wood-Adams, Paula M., Dealy, John M., deGroot, A. Willem, Redwine, O. David, 2000. Effect of molecular structure on the linear viscoelastic behavior of polyethylene. *Macromolecules* 33 (20), S. 7489–7499. <https://doi.org/10.1021/ma991533z>.

3. Summary

Research in this thesis concludes three aspects: polymer nanocomposites preparation, processing and characterization, where rotational as well as extensional rheometry is used for comparison with other measuring techniques.

The first aspect is focused on usage of conventional approaches in rheology for description of 3D physical network generated in polymer nanocomposites and for investigation of physical and chemical interactions during the processing. For this reason, new approaches for thermal stability increase of nanofillers as well as methods for structural investigation and filler/additives combinations were tested. The most important results in this part are development of new thermally stable organoclays for applications in polymers with melt temperature above 250°C, establishment of new structural parameter (average tactoid size) from SAXS data and detection of synergic effects of fillers and nanofillers combination on formation of 3D physical network on composites/nanocomposites.

The second aspect is devoted to relationships between rheology and processing parameters in compounding of polymer nanocomposites. Therefore, new technological approaches for compounding and on-line as well as in-line process characterization methods in combination with melt rheology were investigated. The main results in this part are establishment of new compounding technology for nanocomposites production (possibility to increase shear rate and residence time simultaneously), establishment of extensional rheometry (on-line) and FR-NIR spectroscopy (in-line) for real-time monitoring of dispersion grade and material properties during compounding process of nanocomposites and contributions to analyses of shear rate/residence time and material ageing on nanocomposite performance.

The third aspect describes the development of novel rheological analysis approach for separation of different physically-chemical interactions, which can take place simultaneously in processing of complex polymer nanocomposites, where more nano-scaled fillers or/and more polymer matrices are presented. The most important results in this part are establishment of extensional rheometry for fast characterization of reinforcement in polymer nanocomposites, creation of correlations between rheological parameters in shear and elongational flow, which were consequently used for

development of new rheological parameter (cumulative storage factor) for description of reinforcement in complex polymer nanocomposites.

Combination of all presented research aspects can be generally used for better understanding of dispersion process in multiphase polymer systems and, consequently, for faster development of new functional materials based on polymer composites and blends. Especially the research part dealing with development of thermally stable organoclays and real-time monitoring of dispersion process will be used for future work, because the kinetics of dispersion process in polymer-clay nanocomposites including all relevant thermo-mechanical aspects and physical/chemical interactions has not still been completely understood.